UNIVERSITY OF SOUTHAMPTON

Reactive Power-based Voltage Support for The Low Voltage Ride Through Capability of The Distributed Energy Resource

by

Akbar Swandaru

A thesis submitted for the degree of Doctor of Philosophy

in the
Faculty of Physical Sciences and Engineering
Electronics and Computer Science

January 2020

Abstract

UNIVERSITY OF SOUTHAMPTON

FACULTY OF PHYSICAL SCIENCES AND ENGINEERING

DEPARTMENT OF ELECTRONICS AND COMPUTER SCIENCE

Doctor of Philosophy

Reactive Power-based Voltage Support for The Low Voltage Ride Through Capability of The Distributed Energy Resource

By Akbar Swandaru

The increasing demand for energy is a trend that will continue in the foreseeable future. In the event the need to decommissioning old coal and gas plants as a means to reduce the global warming emissions, renewable-based energy resource may rise into taking the places of the power suppliers. Most renewable-based energy resource will be likely accommodated by, most notably, the inverter-based sources, e.g. photovoltaics (PVs) and wind turbines. It is expected that a large number of distributed energy resources (DER) will be connected via inverters within the distribution grid at the low voltage (LV) level.

Most of the grid codes require the wind and the PV park to remain connected during short-circuit grid faults and also provide reactive power-based voltage support. Meanwhile, a growing number of DERs will be connected onto the LV distribution system, which is mostly attributed by the introduction of the rooftop PVs. It is possible the LV-connected DER has to provide voltage support as well. Studies have shown that the voltage support may be affected by the low *X/R* ratio of the distribution grid. However, currently, the discussions could not demonstrate why the voltage support effectiveness is highly dependent on the *X/R* ratio of the grid. Further, the currently available studies could not substantiate clear understanding regarding the impeding effect of low *X/R* ratio to the voltage support in improving voltage sag. Even more, the currently available LVRT voltage support in some grid codes, do not cover these trends and hence do not consider the voltage support of the DER on low voltage connections.

The investigation of the reactive power-based voltage support on LV-connected DER can be done through Root-Mean-Square (RMS) simulation. However, constructing DER through RMS simulation modelling always requires an extensive modelling effort and data availability. On the other hand, modelling using an oversimplification may lead to a result that does not represent well the problem that needs to be solved. Defining the best compromise between model accuracy and simplicity when modelling power systems elements is not an easy task. Normally the evaluation of the effectiveness of the voltage support through the RMS simulation can be done when two following aspect can be obtained. First, the information on

how-to-construct the modelling; such as: how to model the DER in the simulation environment, how to appropriately design the bulk of the load systems, how to model the aggregate the transmission and the distribution line, and so on. Second, the data needed to simulate the modelling; such as the parameter design of the DER, the connection line, and loads, and so on, is obtainable. When these two requirements are met, the investigation can be done. On many occasions, the information needed is incomplete, and hence the construction of the modelling is done through approximations; still, extensive work and knowledge to construct the modelling are required. Grid planners are often challenged with the grid data restrictions and simulation modelling. As such, a more straightforward approach to do the estimation may help the task at hand.

This study aims to investigate the impact of the DER connection to the DER's reactive power-based voltage support performance, through simulation studies that are made based on the proposed methodology of the author's research. The proposed methodology provides a suitable compromise between the modelling accuracy and the modelling simplicity, so as to provide the solution for the grid data inadequacy and more straightforward construction of the DER's voltage support evaluation.

The realisation of the research work produces three main contributions. First, the proof of the effectiveness of DER's reactive power-based voltage support on improving voltage sag. The task provides an insight into how the voltage sag could be improved through the reactive power-based voltage support. Second, a proposed methodology is presented that can support distribution system operators (DSOs), or a DER grid planner in the event they need to justify effective grid support requirements for LVRT voltage support. The proposed methodology is made to answer the challenge upon compromising the accuracy and simplicity of the simulation modelling to account for grid data limitations and the simpler construction of the DER simulation modelling. Third, the impact of low voltage distribution grid characteristics on the performance of the DER's LVRT reactive power-based voltage support is investigated. This helps to clearly illustrate why the effectiveness of the reactive power-based LVRT voltage support is highly dependent on the *X/R* nature of the grid.

Contents

List of Figures

List of Tables

Declaration of Authorship

I, Akbar Swandaru, declare that this thesis entitled "*Reactive Power-based Voltage Support for The Low Voltage Ride Through Capability of The Distributed Energy Resource*" and the work presented in it are my own and has been generated by me as the result of my own original research.

I confirm that:

1. This work was done wholly or mainly while in candidature for a research degree at this University;
2. Where any part of this thesis has previously been submitted for a degree or any other qualification at this University or any other institution, this has been clearly stated;
3. Where I have consulted the published work of others, this is always clearly attributed;
4. Where I have quoted from the work of others, the source is always given. With the exception of such quotations, this thesis is entirely my own work;
5. I have acknowledged all main sources of help;
6. Where the thesis is based on work done by myself jointly with others, I have made clear exactly what was done by others and what I have contributed myself;
7. Parts of this work have been made into:

   International Conference publications;

   1. A. Swandaru, M. D. Rotaru and J. K. Sykulski, "Intelligence-based coordination of large scale grid-connected photovoltaic systems," *2016 51st International Universities Power Engineering Conference (UPEC)*, Coimbra, Portugal.
   2. A. Swandaru, M. D. Rotaru, and J. K. Sykulski, "The effectiveness of additional reactive current injection from a distributed energy resource unit to mitigate short voltage instability during extreme low voltage ride through," *2017 International Conference on Modern Power Systems (MPS)*, Cluj-Napoca, Romania.

   Journal publications;

   1. A. Swandaru, M. D. Rotaru and J. K. Sykulski, "A Simple Method for Estimating the Effectiveness of Reactive Power-based Low Voltage Ride-through Support of the Distributed Energy Resources," *IET Renewable Power Generation (to be submitted)*.
   2. A. Swandaru, M. D. Rotaru, and J. K. Sykulski, "Distributed Energy Resources Reactive Power-based Voltage Support for Low Voltage Ride Through on a Weak Distribution Grid," *IET Renewable Power Generation (to be submitted).*

Signed: .....

Date: .....

Abbreviations and Definitions

Abbreviations	Definitions
aACI	additional Active Current Injection
AEMC	The Australian Energy Market Commission
AEMO	The Australian Energy Market Operator
APD	Active Power Dependent
aRACI	additional Active Reactive Current Injection
aRCI	additional Reactive Current Injection
B/C ratio	Benefit/Cost Ratio
BESS	Battery Energy Storage Systems
BM	Blocking Mode, a DER's automatic disconnection following transient voltage sag
CDGU	Controllable Distributed Generating Unit
CDGU	Controllable Distributed Generating Unit
CHP Systems	Combined Heat and Power System
CPPM	Controllable Power Park Module
DER	Distributed Energy Resources
DFIG	Doubly-Fed Induction Generator
DG	Distributed Generator
DSO	Distribution System Operator
EDSO	European Distribution System Operators
EirGrid Grid Code	the grid code approved by the state-owned electric power transmission operator in Ireland
ENTSO-E	European Network of Transmission System Operators for Electricity
EXIM System	Export-Import Metering System
GCR	Grid Code Requirement
GTO Thyristor	Gate Turn-Off Thyristor
HIL	Hardware-In-the-Loop
HUT	Hardware-Under-Test
HVRT	High Voltage Ride Through
IGBT	Insulated-Gate Bipolar Transistor
ISP	Integrated System Plan
ITC	Investment Tax Credit

LV connected DER	Low voltage connected DER
LVRT	Low Voltage Ride Through
MOSFET	Metal Oxide Semiconductor Field Effect Transistor
MPPT	Maximum Power Point Tracking
MV connected DER	Medium voltage connected DER
NCDGU	Non-Controllable Distributed Generating Unit
NCPPM	Non-Controllable Power Park Module
NER	National Electricity Rules
PCC	Point-of-Common-Coupling
PLL	Phase-Locked-Loop
PPM	Power Park Module
PSA	Power System Analysis
pu	per unit
PV	Photovoltaic
PWM	Pulse Width Modulation
RMS Simulation	Root Mean Square Simulation
SONI Grid Code	System Operator for Northern Ireland (SONI) Grid Code
STATCOM	Static Synchronous Compensator
SVC	Static-VAR Compensator
TSO	Transmission System Operator
WAMS	Wide Area Measurement System
X/R Ratio	The ratio of the Reactance (X) / Resistance (R) of the impedance

Acknowledgements

I would like to thank to Allah for giving me health and blessing in completing this report. Without His blessing, I would never manage to complete this report.

I wish to express my gratitude to my supervisor, Dr Mihai Rotaru and Prof Jan Sykulski, who gave me helpful advice, invaluable encouragement, and extraordinary patience in guiding me throughout my study. I am also very grateful to them for allowing me to carry out my education at the University of Southampton. I am deeply thankful for the moral and technical support they have given, without which this project would not have been possible to be made.

I wish to express my gratitude to my examiner Dr James Pilgrim and Dr Thomas Andritsch for the helpful advice about my research in my nine month and transfer reports.

I wish to express my special thanks to my colleague Zhida Deng for his encouragement and discussions during my time spent working on this PhD study. Special thanks also to Donny Nurmayady for being a great friend throughout the years of my research.

I am most grateful for and honoured to be awarded, a scholarship from the Indonesian Endowment Fund for Education (LPDP) for covering all my need throughout my study.

I would like to express my thanks to all my friends for their encouragement.

Last but not least my gratitude goes to my parents and family members for their love, moral support and understanding.

Chapter 1 Introduction

1.1 Introduction

Electrical power systems are being revolutionised. The increasing number of inverter-based distributed energy resource (DER), which primarily comes in the forms of wind turbines and photovoltaics, has already changed the way in which the power systems are organised and managed. The electric grid is being revolutionised from vertically-designed systems with unidirectional transmission to distribution power flows to horizontally-designed systems with bidirectional power flows between all voltage levels [1]. Distribution systems are turning from 'passive' into 'active' distribution systems [1]. Conventional power plants for decades has produced vast amounts of power centrally and deliver it through a high voltage transmission system. While in the present and the near future, conventional (thermal) power plants (synchronous-based generators) are gradually being replaced by renewable-based energy generator that is connected to the lower voltage distributed grid, most of which are inverter-based generators. DERs are generally much smaller regarding their capacity, and many more DER units are needed in order to compensate the ongoing retirement plan of the conventional power plants.

The connections of these smaller capacity sources are commonly installed along the grid at medium voltage (MV) or low voltage (LV) level [2]–[5]. Such electric power sources directly connected to the distribution network or on the customer side of the meter [6]. The DER in some studies can be termed as well as Distributed Generator (DG) [6]. However, DG is a loose definition and not particularly for popular photovoltaic (PV) and wind power systems. The definition of DG can also be applied to, for instance, combined heat and power (CHP) systems that are usually based on a rotating synchronous machine. However, this study focuses only on the impact of the inverter-based power source to the power system stability; therefore, to avoid misunderstanding, DER in this study are inverter-based distributed energy resources.

1.2 Some Trends Relating to The Increased DER Penetrations

Over the decades the number of DERs units has been increasingly connected to the grid. This trends have been driven by international government policy to reduce greenhouse gas emittance and conserve fossil fuels and has been long-term driven by economic developments and energy market deregulations. Many DER units size is small, and many of are connected to the distribution grid, whereas most of the large percentage of the resources are connected to the grid via power electronic inverters. It is noted that although this size definition does not define the rated capacity of the generation source, the following categories are generally used

for defining the capacity of DER: micro DER (up to 5 kW), small DER (from 5 kW to 5 MW), medium DER (from 5 MW to 50 MW) and large DER (from 50 MW to 300 MW) [6].

The introduction of DER has been revolutionising the operation styles of the electrical power system. Since in the past, the conventional electrical power system is characterised by a power flow from a relatively small number of large power plants to a large number of dispersed end-users.

The percentage of renewables in the overall generation mix has increased considerably over the years. The increasing number of the renewable generation, like wind turbines and photovoltaic (PV), usually comes in the form of inverter-based DER. Their characteristic nature as an inverter-based generator, however, raise some particular concerns. It is reported that the increasing number of the DERs causes the grid to suffer from inertia reduction [7], [8]. Further, the increasing number of these power sources, especially when it is in urban/residenial areas, causes unwanted steady-state voltage rise of the grid [9]–[11]. Moreover, many studies reported that their presence in the grid is often linked with the emerging numbers of reverse power flow issue [4], [12], [13]. However, the implementation of the DER in the grid has also been associated with the great potential as the source for voltage support as well. The DER's capability to regulate their active and reactive power which allows them to provide voltage support has been in the discussion in many research [3], [4], [14], [15].

In the emerging applications of the DER in the grid, it is best to understand its presence leads to some important trends:

1. The connections of DER units are mainly in the medium- and the low-level voltage grid. However, it is likely that most of their connections are closely located in the distribution grid [16], [17]. This phenomenon introduces generators in the distribution grid, which in the past only contained loads. Thus some power sources are connected on lower level voltage [15], [18], whereas such power sources connected to the Point of Common Couplings (PCCs) with relatively low *X/R* ratio (the ratio of the inductive reactance and the resistive element of the grid) [19], [18]. A study mentioned the *X/R* ratio of the distribution grid with 22kV could be as low as 0.3 [20], while in other study *X/R* ratio of the distribution grid could (11kV) be between 0.5 and 1.3 [21].

2. Most DER units behave as 'negative loads' and do not participate in the conventional control of the network. Though, there are emerging ideas that the ancillary service which is usually provided by the conventional generators has to be gradually covered fully or partially by the DERs. To the date, the DER's transient ancillary service on low voltage ride through (LVRT) has been discussed and studied in many research studies. [10], [22]–[30]. The LVRT is the ability of a wind turbine or other generator to stay connected during voltage sags while the

DER's transient ancillary service on LVRT defines DER's voltage support for transient voltage sag improvement [31].

3. A large number of the DER units are connected to the grid via electronic power inverters, which have a behaviour that is fundamentally different from the behaviour of the conventional synchronous machine-based generators. Many DER replacing the conventional generators, such as the rooftop DER (LV-connected DER) [3], [4], have smaller power capacity than the large synchronous machines.

1.3 Potential Problems Relating to The Increased DER Penetrations

Due to the emerging presence of the trends mentioned earlier, an attempt to improve grid regulation, particularly in the distribution grid, has been shown [32]–[37]. Improvement on DER requirements has been in effect since the data exchange initiative as the collaboration between the Transmission System Operators (TSOs) and Distribution System Operators (DSOs) system operators to ensure the safety of the interoperation between the pre-existing system and the planned distributed generations [38], [39]. Recently, the DERs are required to remain connected during the fault, and some are required to provide transient LVRT ancillary service [40]. As a result, this trend leads many electrical TSOs and DSOs, through organisations such as ENTSO-E, and EDSO [41], [42], working together to formulate appropriate DER's transient LVRT ancillary service.

Essentially, the objective of transient LVRT ancillary service is to provide voltage control during fault by maintaining the RMS value of the voltage within specified limits. The large power plants mainly regulate conventional voltage control in the high-voltage transmission grid while tap changes regulate voltage control on distribution grid on distribution-side transformers. Voltage control through tap changing on distribution-side transformers is relatively slow and is usually for handling steady-state voltage drop along the distribution line. With the emerging presence of the DERs, voltage control from DER's reactive power regulation will allow DER to contribute voltage control not only in mitigating steady-state voltage drop, but also voltage sag mitigation from fault. DER transient LVRT ancillary service through voltage control comes into several varieties. The voltage control can be done through either additional reactive current injection (aRCI)-, additional active current injection (aACI)-, or additional active reactive current injection (aRACI) [1].

In this study, the investigation of the aRCI-based LVRT voltage support is the focus of the research. It will be shown in the following section 1.3.1 the background of the need to investigate the recent requirement of the aRCI-based LVRT voltage support. The challenge upon addressing the investigation through simulation is also presented in section 1.3.2, in order to explain in detail the challenge of evaluating aRCI-based LVRT voltage support.

1.3.1 Problems with The aRCI-based LVRT Voltage Support

The transient LVRT ancillary service through reactive power regulation, as many have suggested (sometimes it is termed as the additional reactive current injection (aRCI)-based LVRT ancillary service, or aRCI-based LVRT voltage support, to avoid confusion), has been implemented, and also has been discussed in many studies [43], [44]. As such, many wind and park and solar park nowadays are equipped with the inverter that capable of providing reactive power regulation which allows them to contribute ancillary service in the event of unwanted voltage deviations [3], [4]. However, the current practice in places such as Germany, reveals that only 10 percent of Medium Voltage (MV) connected DER are required to provide transient LVRT ancillary service through reactive power regulation, whereas a blocking mode (BM), DER's automatic disconnection following a fault, is used by the remaining MV connected DERs [4].

In Germany, for instance, around 90 percent of the grid-connected DER is rooftop PVs [4]. With the continuing growth in DER, it is possible that Low Voltage (LV) connected DER has to provide transient LVRT ancillary service as well. The implementation of aRCI-based LVRT voltage support on LV connected DER as transient LVRT ancillary service may potentially lead to some concerns. It has been reported that transient LVRT ancillary service through reactive power-based voltage support may be potentially affected by the low *X/R* nature of the distribution grid [3]–[5], [43], [44]. Though many studies could claim this evidence through simulation-assisted investigations, the discussions could not illustrate clearly as to why the effectiveness of the reactive power regulation is highly dependent to the *X/R* nature of the grid [27], [45]–[49]. To date, it was found that the aRCI-based LVRT voltage support tends to be less effective on low *X/R* ratio grid [28], [29], [50]. However, the studies could not provide a clear explanation regarding the impeding effect of low *X/R* ratio to the effectiveness of the aRCI in improving the LVRT voltage sag. Even more, the currently available aRCI-based LVRT voltage requirement that has been already adopted in some grid codes [32]–[35], do not cover this trend and hence do not consider the aRCI-based LVRT voltage support of the DER closely located in the urban/residential area. As such an attempt to investigate the effectiveness of the aRCI-based LVRT voltage support on LV connected DER (DER in the distribution grid level) is necessary.

1.3.2 Difficulty in Evaluating The Effectiveness of LVRT Voltage Supports

Investigating the effectiveness of the aRCI-based LVRT voltage support on LV connected DER can be done through RMS simulation. However, using a detailed dynamic representation of a large number of DERs at distribution level in the simulation tool, that has been attempted in

many studies [3], [4], [27], [28], [43]–[45], [47], will increase the complexity of the models in terms of computational effort and data availability. On the other hand, modelling power systems elements through an oversimplification may result in a solution that does not represent well the problem that needs to be solved.

Defining the best compromise between model accuracy and simplicity on modelling power systems elements is not an easy task. As such, designing LVRT voltage support that will meet the desired needs, such as the minimum voltage sag magnitude, and the permitted duration of the lowest voltage sag should be met when using the voltage support, is highly influenced by the accuracy of the DER modelling of the corresponding grid, and the required data availability [3], [4], [14], [23], [51], [52].

Upon building a simulation environment of the DER modelling along with its LVRT support, one should understand the mechanism of the investigated LVRT voltage support should be made, and the information regarding the criterion of the minimum voltage sag that should be withstood, and the voltage sag improvement that should be made of that particular grid. Estimating the effectiveness of the DER's LVRT voltage support through typical positive-sequence-RMS simulation can be achieved when first, the required knowledge, and second, the data needed to construct the simulation modelling is obtainable [53]. When all previously mentioned information is available, the estimation can be done through the RMS simulation. As such, a laborious task is required for estimating the effectiveness of the voltage support. Furthermore, even though often happening on many occasions, the information needed is incomplete and hence the construction of the grid modelling is done through approximations; still, extensive work and knowledge to construct the modelling are remain required.

Grid planners often face difficulties with the lack of availability of grid data (often due to manufacturers confidentiality) and challenges relating to the construction of the DER modelling [1]. A more straightforward approach to do the estimation may help the task required.

1.4 Research Motivation

To address the potential problems presented in section 1.3, the purpose of the study is to investigate the effectiveness of DER's LVRT support in the distribution grid. The simulation studies are made by considering the challenges on formulating strategy that could compromising the accuracy and simplicity of the simulation modelling. The purpose of the study presented requires attention to the following aspects:

1. The operation of the DER's aRCI-based LVRT voltage support in improving voltage sag.

2. Some challenges needed to be considered on the strategy of investigating DER's voltage

regulation that capable to compromise the accuracy and simplicity of the simulation modelling.

3. What impact of distribution grid characteristics has on the performance of the DER's aRCI-based LVRT voltage support.

1.5 Research Aim and Objectives

The research aim of the study is to understand the impact of the DER connection to the DER's aRCI-based LVRT voltage support performance, through simulation studies, in which the simulation effort is demonstrated based on the proposed methodology of the author's research. The proposed methodology is made suitable for compromising both simulation modelling accuracy and its simplicity to tackle inadequacy of the grid data and simplify the required information to build the DER connection modelling. The proposed methodology is made suitable for grid planner in the event of grid data and the modelling inadequacies upon DER's LVRT voltage support evaluation.

The realisation of the research aim produces the research objectives that are required to accomplish:

1. To examine how the DER's aRCI-based LVRT voltage support can improve voltage sag.

2. Build a simpler modelling strategy/methodology, with improved compromise between model accuracy and simplicity, that can be used to evaluate DER's LVRT voltage support more simply. This will help to tackle grid data and the modelling inadequacies.

3. To investigate the impact of distribution grid characteristics on the performance of the DER's aRCI-based LVRT voltage support.

1.6 Research Contributions

Through achieving the aim and the objectives of the research, contributions from this work are successfully made and summarised as follows:

1. The proof of the effectiveness of DER's aRCI-based LVRT voltage support on improving voltage sag. The task will provide an understanding of how the voltage sag could be improved through aRCI-based LVRT voltage support, which is presented in section 3.5 to 3.7. The first contribution has been made into the first and second conference publications as described in section 1.7.

2. A proposed methodology that can support distribution system operators (DSOs), or a DER grid planner in the event they need to justify effective grid support requirements for LVRT voltage support on a distribution network. The proposed methodology is made to answer the challenge upon compromising the accuracy and simplicity of the simulation modelling in the event of inadequacy of the grid data (due to the confidentiality matters) and the need of a more

straightforward approach to constructing the DER connection modelling. The proposed methodology can be found in section 3.8, and the accuracy of the proposed methodology is presented in section 3.9. The second contribution has been made into the first journal manuscript as described in section 1.7

3. The investigation of the DER's reactive power-based voltage support for LVRT on a distribution grid is presented. The work is made to investigate the dependency of the voltage support effectiveness to the *X/R* ratio of the grid, and to illustrate clearly as to why the voltage support is highly dependent to the *X/R* nature of the grid The work is presented in detail in chapter 5. The third contribution has been made into the second journal manuscript, as described in section 1.7.

1.7 Publications Resulting from The Research

The works in the thesis have contributed to the following publications.

International Conference publications;

1. A. Swandaru, M. D. Rotaru and J. K. Sykulski, "Intelligence-based coordination of large scale grid-connected photovoltaic systems," *2016 51st International Universities Power Engineering Conference (UPEC)*, Coimbra, 2016, pp. 1-6.
   doi: 10.1109/UPEC.2016.8114135

2. A. Swandaru, M. D. Rotaru, and J. K. Sykulski, "The effectiveness of additional reactive current injection from a distributed energy resource unit to mitigate short voltage instability during extreme low voltage ride through," *2017 International Conference on Modern Power Systems (MPS)*, Cluj-Napoca, 2017, pp. 1-6.
   doi: 10.1109/MPS.2017.7974384

Journal publications;

1. A. Swandaru, M. D. Rotaru and J. K. Sykulski, "A Simple Method for Estimating the Effectiveness of Reactive Power-based Low Voltage Ride-through Support of the Distributed Energy Resources," *IET Renewable Power Generation (to be submitted)*.

2. A. Swandaru, M. D. Rotaru, and J. K. Sykulski, "Distributed Energy Resources Reactive Power-based Voltage Support for Low Voltage Ride Through on a Weak Distribution Grid," *IET Renewable Power Generation (to be submitted).*

1.8 Report Organisation

The thesis consists of six chapters as described in the following paragraphs.

Chapter 2 reviews the recent issues related to the effects of the increasing penetration rate of

inverter-based DER to a grid (such as reverse power flow causing the unwanted steady-state voltage rise). Aspects related to the LVRT voltage control strategies are reviewed. Further, the Grid requirements on DER's reactive power regulations, DER's voltage control, and DER's Fault Ride Through are also reviewed.

Chapter 3 presents a simple methodology for estimating the effectiveness of the additional reactive current injection (aRCI)-based DER's LVRT voltage support. The proposed methodology is built based on 'static analysis' approach (typical static short circuit analysis but with some extensions as for evaluating effectiveness of DER's reactive power LVRT support) that simplifies dynamic aspects that are usually accounted by typical dynamic RMS simulations, while being able to capture fairly accurate the behaviour of the system. The advantage of the proposed methodology is on the computing process needed, which is much simpler since the construction of the dynamic DER modelling is not needed, and the evaluation of the effectiveness can be gained even under the condition of grid data and the modelling inadequacies. The novel methodology is made for easier evaluation of the influence of the network characteristics on the effectiveness of the DER's reactive power LVRT support in mitigating voltage sag. The chapter details essential information related to the representation adequacy of the modelled system (for example: how the external grid should be represented, how typical distribution load should be modelled, and how the system elements should be aggregated).

Chapter 4 focuses on aspects relating to the DER dynamic modelling on the power system grid. The LVRT voltage support modelling that is made based on the reactive power regulation standard as previously presented in section 2.7.1 is also provided. The purpose of chapter 4 is to present modelling of the DER, along with the proposed modelling of the aRCI-based voltage support that is made to understand the dynamic response of the system better - the voltage response following LVRT, the voltage improvement sag with respect to the amount of the additional reactive current being given, and so on.

Chapter 5 presents the study on the impact of grid characteristic on the effectiveness of DER's aRCI-based LVRT voltage support. With the help from the DER dynamic modelling as presented in chapter 4, the effectiveness of investigated voltage support under different grid characteristic is evaluated.

Chapter 6 presents a summary of the work presented in the thesis. The main contributions of this research are also discussed. Additionally, the outlines of proposed future work are presented.

Chapter 2 Reviews on The Implications of DER Connections to the Grid

2.1 Introduction

Most of the grid codes generally require the Distributed Energy Resources (DERs) to remain connected throughout short-circuit grid faults and also provide the grid voltage support during the Low Voltage Ride Through (LVRT). It is found that the *X/R* ratio of the DER connection affects the effectiveness of the voltage support in improving the voltage sags. As a means to help the study, four essential aspects relating to the impacts of the presence of the grid-connected DER to the grid are presented.

The first aspect will be about the impact of the DER connections to the steady-state voltage rise of the grid. It will be presented later that *X/R* ratio of the grid determines the magnitude level of the steady-state voltage rise. The presented review will provide valuable insight on understanding the way the impact of the DER connection to the steady-state voltage increment of the grid, through mathematical analyses based on the previous researchers. The mathematical analyses that are made by underlying the assumptions help the thesis author to construct the perspective on how the DERs are impacting the steady-state voltage profile of the grid. The aforementioned perspective helps the thesis author to develop the proposed methodology for estimating the effectiveness of reactive power-based Low Voltage Ride-Through support of the DER. The first aspect is presented in section 2.5.

The second aspect will be about reviews on some of the reported strategies to prevent the unwanted steady-state voltage rise on DER-connected grid. The review summarised three approaches to mitigate the unwanted steady-state voltage rise; through DER's reactive power regulation, DER's active power capping, and lastly using energy storage. It will be shown according to the likeliest trends that reactive power regulation is the most preferable. The presented review will give insight on the relevancy of the reactive power regulation method as the likeliest preference for the unwanted steady-state voltage rise mitigation, with the method for the LVRT voltage support. The reviewed aspect is made to support the argument for the need to focus the reactive power-based LVRT voltage support. The second aspect is presented in section 2.6.

The third aspect will be about the DER regulation strategies for LVRT voltage support. The review presents the three common methods as means for the voltage support; the reactive power-, the active power-, and the combinational active and reactive power-based LVRT voltage support. It will be shown in the discussion through some of the presented evidence;

DER reactive power-based voltage support is the best preference for improving voltage sag during LVRT. The third aspect is presented in section 2.7.

The fourth aspect will be about the grid code requirement on DER connection, DER Fault-Ride-Through, and its voltage support strategies. The attempt so far to provide better grid regulation by considering the DER penetrations are presented. Different standard on the DER LVRT requirement from different countries is evaluated. The fourth aspect is presented in section 2.8. The current state of some grid code's favoured preference means for their LVRT voltage support will be reviewed. Further, the evaluation of the readiness of some grid codes to consider the need for DER LVRT voltage support strategies on distribution levels is presented in section 2.8.4. The evaluation which is given in section 2.8.4 is made to help the author on constructing the potential research gap as presented in the summary (section 2.9).

The summary as in section 2.9 presents a brief overview of the presented literature review. It will be shown a short view on the current general state of the DER LVRT requirements. It will also point out in the following the need for paying attention to the trends of the DER growth are likely closely located in the urban/residential area. This reveals the potential research gap filled by the thesis - the need for investigating the potential impact of the *X/R* ratio of the distribution grid to the effectiveness of the DER LVRT voltage support. Further it will be shown as well the author's view about how useful is the extensive studies presented from previous research; the impact of *X/R* ratio to the increased steady-state voltage of DER-connected grid; in helping the author on constructing the evaluation strategy of the effectiveness of the DER LVRT voltage support which is presented in chapter 3.

Section 2.2, 2.3, and 2.4 are introductory sections which assist the reader in better understanding the rest of the literature review.

2.2 Background

The impact of DER generation has become a significant concern especially when a high penetration of DER is considered. It is well known that synchronous generator based conventional power plants could handle faults without being disconnected and at the same time injecting short-circuit currents during voltage sag. This characteristic property of the synchronous generators is crucial in a power system by raising the voltage around the location of the fault [5]. Initially, DER's implementations and its impact relating to the grid faults was not critical. Hence as a means of protecting the electronic component of the DERs, these inverter-based generating units were disconnected during grid faults. This disconnection mechanism can be achieved by using under-voltage protection. However, with increasing penetrations of DER, this disconnection mechanism has become counterproductive. Typically when a grid fault occurs the fault impact can be sensed in a wide area surrounding the fault, as

it propagates away from the fault site throughout the power system [3]. Consecutively this can lead to several DER units to automatically trip. In turn, disconnection in series of DER groups translates into a considerable cascading loss of electricity generation. Therefore, to avoid the above-mentioned problems, with the ongoing plan for increasing DER units, the DER has to remain connected during the fault. During fault ride through (FRT), as the requirement is defined, the DER has to provide transient voltage support to improve the LVRT voltage sag as well.

2.3 The Objective of The Voltage Support

The objective of voltage support is to regulate and maintain the RMS (root-mean-square) value of the voltage level within specified limits, irrespective of the trends of the generation and load [14]. Conventional voltage support in the high-voltage transmission network is mainly provided by the large synchronous machine generators. On distribution grid, however, voltage support is made by tap changing on distribution transformers. Voltage support through transformer tap changing is relatively slow as compared to the voltage support provided by the large power plants (that is usually via automatic voltage regulator - AVR). As such the tap changer can compensate the steady-state voltage drop along the distribution feeder. Voltage regulation via changing transformer tap is made on the basis that the voltage variation at the distribution level is only influenced by the load trends. However, with the introduction of DER units in the distribution grid, there is a possibility to employ voltage regulation by the DERs to solve not only the steady-state voltage drop but potentially also the transient voltage sag during a fault. As such, the introduction of DER units in the distribution grid can affect the way of the operating style of the traditional voltage regulation schemes (such as transformer tap changing) that already exist.

The voltage variations are primarily affected by the load trends and the transformer tap changing. The presence of the DERs at the distribution level may add another factor that influences the voltage variation of the distribution grid. Further, it is even reported that DER in some place, such as in Germany, has to be disconnected when the voltage variation reaches below 0.8 pu [4]. The disconnection scheme is initially employed as a means to minimises the risk of DER's internal failure. However, DER automatic disconnection may become undesirable, when a large number of DER units is connected to the network since it will result in a further unwanted disturbance, such as black-out. Moreover, the large number of DER automatic disconnections can result in no small power generation deficit which may cause power loss that could be even higher than the amount of power reserve needed for the reference incident (the worst incident that can be managed by primary reserve) [3]. As such, many grid codes require DER to have LVRT capability.

2.4 Challenges on Investigating The DER's LVRT Voltage Support

The prevalence of the DERs with LVRT capability allows them to sustain their connection in the event of voltage sags. As such, some DER requirements enforce the DER to provide LVRT voltage support as well. The LVRT voltage support allows the DER to provide transient voltage regulation which helps to improve LVRT voltage sag. Investigating DER's transient voltage regulation is challenging since there are factors that might need to be considered upon implementing voltage support. The consideration may come in the aspect of, for instance, the LVRT voltage support strategies. Generally, the DER's LVRT voltage support strategy comes into three types; through the DER's reactive power regulation, the active power regulation, and the combinational active and reactive power regulation [3]–[5]. Another factor is the steady-state voltage regulation strategies. It is revealed that increased DER penetrations may increase the steady-state voltage of the hosting grid [10], [54]. As such, to prevent unwanted steady-state voltage rise, the steady-state voltage regulation is often used. It will be shown that several considerations may arise due to the chosen steady-state voltage regulation to the effectiveness of the selected LVRT voltage support strategy. Lastly, it will be presented as well the *X/R* ratio of the DER-connected grid adding up the challenges on studying the DER's LVRT voltage support.

It has been discovered that *X/R* ratio of the DER connection affects the effectiveness of the voltage support in improving the voltage sags [3], [4], [23], [28]. Further, it has been claimed that smaller *X/R* ratio of the distribution line as compared to transmission line may impede the effectiveness of DER's transient voltage regulation via additional reactive current injection (aRCI) [4]. DER's transient voltage support via additional active current injection (aACI) [3], as a counterpart to the aRCI, may be promising. However, since aACI requires actively ready active power reserve, the method seems not economically favourable since the DER has been operated under sub-optimum condition - a condition that is not advantageous for long-term of DER usage [55]. The usability of aACI seems promising when the employment of active power curtailment [56] is also applied, and hence its active power reserve could be used to employ aACI.

However, noting the fact that active power curtailment may be employed when only the unwanted steady-state voltage rise is in effect [57], then the usability of aACI may seem not possible for all time, as compared to the flexibility offered by the aRCI. Without needing to take active power reserve from the active power curtailment mechanism, the aRCI usage seems more reliable since many DER's owners prefer to maximise their DERs active power generations. With the recent development and with the recent grid code relating LVRT requirement, aRCI may be preferred since the DER's inverter can be operated on a leading

power factor for a short time so that it could allow the function of transient voltage regulation via aRCI [32], [33], [36], [58].

It has been claimed as well that on the steady-state condition, more DER connection on a grid will increase the steady-state grid voltage. The increment rate of the steady-state voltages on low *X/R* ratio DER-connected grid, such as on distribution grid, will be higher than the increment rate of the steady-state voltages on a DER-connected grid with high *X/R* ratio, such as DER which connected at long medium voltage feeder [15]. Thus, by considering in the following aspects; such as economical, the feasibility for long-term usability, and the essential factor of the implementation; unwanted steady-state voltage mitigations on grid-connected DER through reactive power regulation can be a solution, better than 'active power capping'. As such, it is understandable that some researchers proposed the idea of DER's on under-excited operation [9]–[11] as an alternative to the active power curtailment method as means to prevent the unwanted steady-state voltage rise.

The solution by employing energy storage, such as a battery, to minimise unwanted steady-state voltage increment by storing some of the power generated by the DERs and act as voltage support by temporarily injecting power may potentially offer the best solution. However, it is shown with the introduction of DER's *feed-in tariff* scheme, which allows the DER's owner to benefit DER's energy export to the grid, DER's owner 'sees' battery implementation as a less preferable option. With the recent standard on DER connection that requires all DER to have reactive power regulation capability in order to increase the number of DERs with transient voltage support, the use to DER's reactive power regulation could be potentially advantaging as well for unwanted steady-state voltage mitigations.

The overview spans from discussing the steady-state voltage stability of the DER-integrated grid to the implications of the trends to the grid operator, in which they regulate the grid standard to responding it. It will be shown the usefulness of the understanding of some of the reported strategies to mitigate the unwanted DER-connected grid steady-state voltage rise problems for the formulation of the LVRT voltage support method investigated in the study. The readiness of the DER LVRT requirements in some grid codes will be reviewed, so that the reader could understand the problem standpoint and hence the urgency the need of the author's research.

2.5 Steady-state Voltage Rise on The DER Connected Grid

Though this study is focused on the DER's transient voltage regulation, it is best to describe some issues mentioned in the previous paragraph as the essential element needed before the investigation about the effectiveness of transient voltage support via reactive power regulation is taking place. How do factors, such as the unwanted steady-state voltage rise (that define the

pre-fault voltage state on transient simulation), the *X/R* ratio of the DER connections, typical of the faults, affect the performance of the DER's transient voltage regulation?

In the following, the discussion relating the steady-state voltage rise due to DER connections on the grid is introduced (Section 2.5.1 to 2.6.6).

2.5.1 Theoretical Analysis

To understand the steady-state voltage rise on the DER-connected grid, Canova et al. [59] explain how this may happen.

Suppose a distribution grid, with its distribution line impedances and the load profiles, through impedance transformation, is transformed into an equivalent Thevenin model as shown in Figure 2-1. From there, it provides the representation for the network-load-PV set-up (in this reference, DER is represented by PV). Suppose from the observed distribution grid and external grid that is set as 'external power source', has voltage magnitude along with its phase of E_g. The Thevenin line impedance then can be represented as Z_g whereas the Thevenin load can be represented as Z_{load}. From this on, then E_{pv} and I_{pv} can be set to represent the voltage and the current of the photovoltaic. The voltage at the Thevenin load, which can be represented as the Point of Common Coupling (PCC) of the PV, can be calculated using equation (2.1). So, on a system without PV, then it can be done by applying $I_{pv} = 0$.

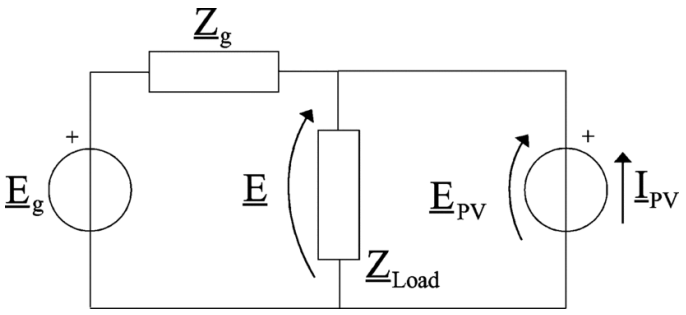

Figure 2-1 Circuital representation of the network–load–DER system [59]

$$\underline{E} = \frac{\underline{Z}_{load}}{\underline{Z}_g + \underline{Z}_{load}} \left(\underline{E}_g + \underline{Z}_g \underline{I}_{pv}\right) \tag{2.1}$$

By considering the constant element of all impedances (Z_{load} and Z_g), from equation (2.1), it can be noted that the voltage at the PCC of the PV, E, will be likely to increase when I_{pv} exist. For a constant E_g, it can be observed that the increment of E is linearly proportional to the increment of $Z_g I_{pv}$. Canova et al. [59] also mentioned that the steady-state voltage rise of the PCC of the PV is likely characterised by Z_g. The phase angle of Z_g which can be obtained

from $tan^{-1}(\frac{x_g}{r_g})$, where x_g and r_g represent the reactance and the resistance part of the Z_g, affects the steady-state voltage rise rate of the PCC bus, and is vital to the effectiveness of DER's transient voltage support.

Further, it can be observed that I_{pv} is also determining the steady-state voltage rise rate of the PCC bus as well. This can be explained in a clear manner by representing I_{pv} in the form of the active and reactive component, P_{PV} and Q_{PV}, as shown in the following explanation [60].

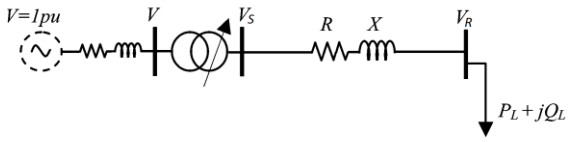

Figure 2-2 Single Load Infinite Bus (SLIB) without DER

Firstly, suppose a single load unit infinite bus (SLIB) as shown in Figure 2-2 that is transformed from a distribution system as according to Canova et al. [59] as previously explained (through impedance transformation), has the voltage at the sending end as written as follow,

$$\bar{V_S} = \bar{V}_R + \bar{I}(R + jX) \tag{2.2}$$

whereas $\bar{I}$ is the phasor representation of the current flowing through the line, $\bar{V_S}$ defines the voltage in phasor at the sending-end, $\bar{V}_R$ defines the voltage in phasor at the receiving-end, R stands for the line resistance, and X stands for the line reactance. The power supplied from the 'power source' is then can be referred into

$$P + jQ = \bar{V_S}\bar{I}^*. \tag{2.3}$$

From equation (2.2) and (2.3), the current flowing through the line can be written

$$\bar{I} = \frac{P - jQ}{\bar{V_S}} \tag{2.4}$$

As such, by placing equation (2.4) into (2.2), the voltage drop between the sending end and receiving end can be written as shown in equation (2.5).

$$\Delta V = \bar{V_S} - \bar{V_R} = \frac{RP + XQ}{\bar{V_S}} + j\frac{XP - RQ}{\bar{V_S}} \tag{2.5}$$

In this reference, [60], the angle difference between the sending end voltage and the receiving end voltage are relative to the $R + jX$. On a distribution grid that has low *X/R* ratio, this implies the voltage drop is approximately relative to the active component impedance, R [60]. With this assumption, the effect of the reactive component impedance, X relating to the voltage drop are relatively small. Hence if the voltage at the sending end $\bar{V_S}$ is set as the reference, then

the sending voltage phase angle can be set $\angle\theta_{V\_S} = 0$. Implying the above equation can be rewritten as follows.

$$\Delta V \approx \frac{RP + XQ}{\bar{V}_S} \tag{2.6}$$

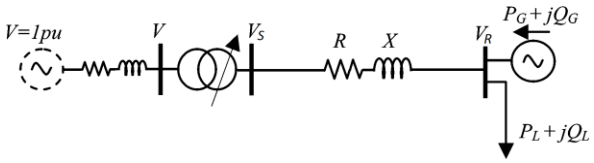

Figure 2-3 Single Load Infinite Bus (SLIB) with DER [60]

On a SLIB with DER, the system representation can be seen in Figure 2-3. In such condition, The DER as power source is likely to cause the voltage increase as compared to the condition without the supplied power [60]. On the condition when the PV provides more power than the load, the steady-state voltage rise can be formulated into equation (2.7).

$$\Delta V = V_R - V_S \tag{2.7}$$

Since in the distribution system the effect of the reactive component impedance relating to the voltage drop are relatively small, then with the help of (2.6), the steady-state voltage rise along the distribution network can be written as follows (2.8).

$$\Delta V = V_R - V_S \approx \frac{RP + XQ}{V_S} \tag{2.8}$$

with $P = (P_G - P_L)$ and $Q = (\pm Q_G - Q_L)$. It can be seen on the steady-state voltage increment on DER-connected distribution grid is directly proportional to the amount the active power supplied by the distributed generators, owing to the fact of the low *X/R* ratio of the network.

2.5.2 Steady-State Voltage Rises on Different Percentage Of DER Shares

A better understanding of the steady-state voltage rises effect on multiple penetration levels by considering different *X/R* ratio is given.

According to Eftekharnejad et al. in [2], there is a relationship between the steady-state load bus voltage and the penetration level of the DER units. This relationship and its impact to the steady-state voltage rise depend on the grid line impedance, load profiles, and the output (active) power of the DERs (in [2], DER is represented as rooftop-PV). The aforementioned functions that are influencing the steady-state voltage rise trends does not particularly for DER with unity power factor operation, but also DER with (for instance) under-excitation operating settings [2], (such operation that has been discussed, as solution to prevent unwanted steady-

state voltage rise [9]–[11]). Therefore, the analytical expression provided by Eftekharnejad et al. in [2] is also suitable for DER under such requirement (under-excitation operating settings).

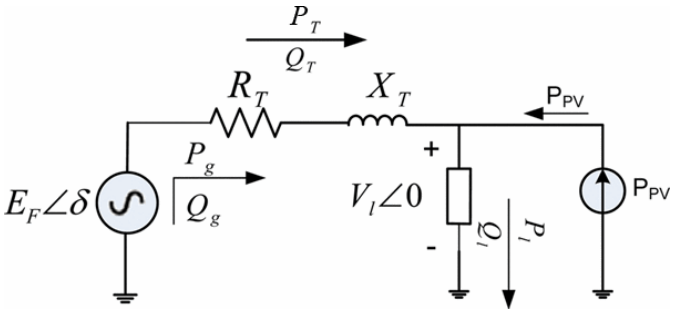

Figure 2-4 Thevenin equivalence for representing DER-connected Single Load Infinite Bus (DER-SLIB) from [2]

Suppose a Thevenin equivalence circuit is given in Figure 2-4. Similar to previously mentioned, the external grid acts as the external power source with its voltage, E_F. While the PV source, P_{pv}, connected at the equivalent load bus, with voltage value, V_l. The load bus voltage phase, $\angle\theta_{V_l} = 0$, while the voltage phase angle of the external grid, $\theta_{E_F} = \delta$. The Thevenin line impedance, $R_T + jX_T$, while the load profile, is obtained from

$$P_l + jQ_l = \frac{(V_l)^2}{(Z_{Thev\_load}\angle\delta_{Thev\_load})^*}, \tag{2.9}$$

with $Z_{Thev\_load}\angle\delta_{Thev\_load}$ is the impedance load obtained through impedance transformations. Consider a conventional power source as shown equation below [2],

$$S_g = (E_F\angle\delta)I^* \tag{2.10}$$

According to Eftekharnejad et al. in [2], along with equation (2.11)

$$E_F\angle\delta = |E_F|(cos\delta + jsin\delta) \tag{2.11}$$

and equation (2.12)

$$I^* = \left[\frac{|E_F|(cos\delta + jsin\delta) - |V_l|}{R_T + jX_T}\right]^* \tag{2.12}$$

which then can be modified into equation (2.13)

$$I = \frac{|E_F|(cos\delta - jsin\delta) - |V_l|}{R_T - jX_T}, \tag{2.13}$$

the equation (2.10) can be translated into equation (2.14)

$$S_g = \frac{|E_F|(cos\delta + jsin\delta)(|E_F|(cos\delta - jsin\delta) - |V_l|)}{R_T - jX_T}, \tag{2.14}$$

whereas from (2.14) the active and reactive power can be given as follows

$$P_g = \frac{|E_F|}{{R_T}^2 + {X_T}^2}\left(|E_F|R_T + |V_l|(X_T sin\delta - R_T cos\delta)\right) \tag{2.15}$$

$$Q_g = \frac{|E_F|}{{R_T}^2 + {X_T}^2}(|E_F|X_T - |V_l|R_T sin\delta - |V_l|X_T cos\delta). \tag{2.16}$$

Active and reactive losses along the external grid line are

$$S_T = V_T I^* \tag{2.17}$$

S_T can be translated into

$$S_T = \frac{|E_F|(cos\delta + jsin\delta) - |V_l||E_F|(cos\delta - jsin\delta) - |V_l|}{R_T - jX_T} \tag{2.18}$$

whereas its active and reactive power are

$$P_T = Re\{S_T\} = \frac{|E_F|^2 R_T - 2|E_F||V_l|R_T cos\delta - |V_l|^2 R_T}{{R_T}^2 + {X_T}^2} \tag{2.19}$$

$$Q_T = Im\{S_T\} = \frac{|E_F|^2 X_T - 2|E_F||V_l|X_T cos\delta - |V_l|^2 X_T}{{R_T}^2 + {X_T}^2} \tag{2.20}$$

Suppose the reactive power comes from the conventional power source is $Q_g = Q_T + Q_l$, then assuming Q_l is the reactive power load. P_l is the active power load. Suppose the reactive power load is defined as $Q_l = kP_l$, whereas k is an arbitrary ratio, then through equation (2.16), (2.20), and $Q_g = Q_T + Q_l$, the equation (2.21) is yielded

$$|V_l||E_F|(X_T cos\delta - R_T sin\delta) = kP_l\left({R_T}^2 + {X_T}^2\right) + |V_l|^2 X_T\,. \tag{2.21}$$

It should be noted that

$$P_l = P_{pv} + P_g - P_T \tag{2.22}$$

with P_{pv} is the active power being generated by the PVs, then combining (2.15), (2.19), and (2.22) gives

$$|V_l||E_F|(-X_T cos\delta - R_T sin\delta) = \left(P_{pv} - P_l\right)\left({R_T}^2 + {X_T}^2\right) - |V_l|^2 R_T \tag{2.23}$$

From the equation (2.23), substituting it with (2.21), yields

$$\begin{aligned} |V_l|^4 + \left(P_{pv} - P_l\right)^2\left({R_T}^2 + {X_T}^2\right)^2 - kP_l{}^2\left({R_T}^2 + {X_T}^2\right) - 2|V_l|^2 R_T\left(P_{pv} - P_l\right) \\ + 2kP_l{}^2 X_T|V_l|^2 - |V_l|^2|E_F|^2 = 0 \end{aligned} \tag{2.24}$$

Solving the polynomial equation (2.24) through algebraic equation solver provided by MATLAB yields four solutions from which it produces the voltage of the DER-connected load bus, V_l, for every active power given from the DER (P_{pv}) [2]. This voltage magnitude is plotted versus the PV generation and is shown in Figure 2-5 for two different values of R_T.

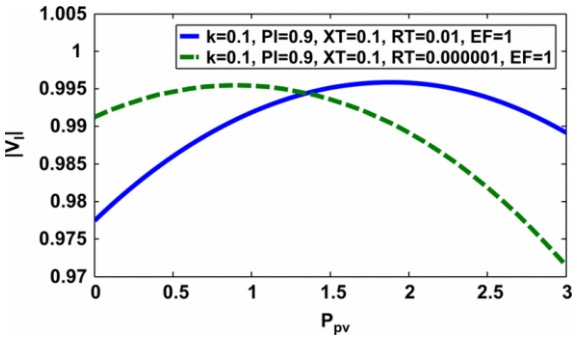

Figure 2-5 Variations of the load voltage versus the amount of solar generation for the DER-connected Single Load Infinite Bus (DER-SLIB) as illustrated in Figure 2-4 [2]

Figure 2-5 shows the load bus voltage variation with the change in the amount of PV generation for two different 'Rt' values ('Rt' - resistance of the transmission network). 'Blue' and 'green' colour present different level of resistance, 0.01 and 0.000001, respectively. Note the value of 0.01 and 0.000001 for the 'Rt' that are used in the study, [2], is meant to situate line with different *X/R* ratio. Normally *X/R* ratio for the distribution area is smaller than in the transmission area [61], [62]. Although the selection of the values is not based on actual lines, the numbers are still appropriate for the sake of the illustration of the study. Hence it can be assumed that 'green' line in Figure 2-5 represent voltage rise in 'transmission line', while 'blue' line represents 'distribution line' – indicating a stronger trend of voltage rise in distribution line [2]. Therefore, it should be noted that by evaluating steady-state load voltage rise by using equation (2.21), V_l increment is influenced by the increment of P_{pv} – considering invariability R_T, X_T, and P_l. the example illustrates the increasing DER active power will increase the steady-state DER's PCC voltage level.

Figure 2-5 also gives a clear indication of the impact of *X/R* ratio to the steady-state voltage rise, that the rising rate is observed stronger at a lower voltage.

2.5.3 Simulation of Steady-State Voltage Rise due to DER Connections

In order to prove the steady-state voltage rise theory as provided in section 2.5.1 and 2.5.2, steady-state voltage rise estimation due to the presence of the DER units through simple Newton-Raphson power flow analysis is demonstrated. The test system used in these case studies is the well-known IEEE-39 bus test system, which can be found in [63]. Through simple Newton-Raphson power flow analysis by using MATLAB as a tool, the steady-state voltage rise is observed.

The power flow analyses are made, and the estimated voltage profile is obtained for each gradual DERs penetration from 0% up to 50% by each 2.5% of the total load. The DER installations are placed on non-generator buses, and its placements are given on different

conditions/scenarios. The location of the DER installations is made to meet a condition; the DER that is closely located in the load (urban/residential area). In the simulation, the condition is made by placing the DER at the bus with the load, such as bus 15. The simulations are demonstrated on four scenario tests. The first scenario is set by applying the DER connection at bus 15, as can be seen in Figure 2-6. The remaining scenarios, the second, third, and fourth are set by applying the DER connection at several buses, which are described more clearly in Table 2-1. It can be seen from Table 2-1; the first column defines the scenarios. The second column defines the total number of the bus which connected by the DERs. The location of the DER-connected bus for each scenario are shown in the third column. The fourth column defines the number of the Figure which the result is shown.

The location for the DER connections is made meant to distribute the DER active power output in order to observe the impact of the DER on multiple locations to the steady-state voltage rise of the system. Even though the scenario settings are not based on actual condition, the scenario settings are still suitable for the simulation - to prove the aforementioned steady-state voltage rise theory.

Table 2-1 Scenario of the simulation tests

Scenario	number of DER-connected bus	Number of the bus of the DER connections	Figure
1	1	15	2 - 7
2	5	15, 16, 18, 26 and 27	2 - 8
3	10	15, 16, 18, 26, 27, 24, 25, 28, 4 and 21	2 - 9
4	15	15, 16, 18, 26, 27, 24, 25, 28, 4, 21, 3, 7, 8, 12, and 20	2 - 10

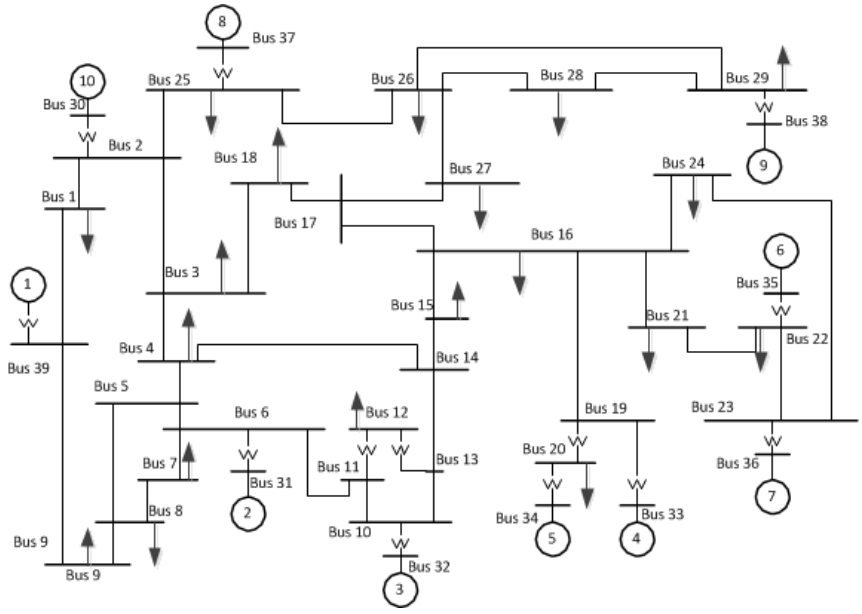

Figure 2-6 IEEE-39 bus test system

In doing the simulations, increasing DER's penetrations are made by adding the active power level of the DER in which the total amount of the DER's active power are in proportion to the percentage of the total loads. For instance, 30% DER penetration means the DER provides active power equal to 30% of the total amount of the grid loads. The DER's active power penetrations are made for replacing the active power generated by the large synchronous generators. As such, 30% DER penetration level means that there are 30% of the total active power that is generated by the synchronous generators are decreased. So, on 50% DER penetration, it means the DER provides active power equal to 50% of the total amount of the grid loads synchronous generators are operated at 50% of its capacity. The reduction of the active powers of the synchronous generators is distributed evenly. As such, on 50% DER penetration, it means the synchronous generators are operated at 50% of its capacity.

The result of the power flow analyses for each scenario can be seen in the Figure from 2-7 to 2-10. The voltage difference for each DER's increased power output from 2.5% to 50 of the total load can be seen. In the Figure (2-7, 2-8, 2-9, and 2-10), the first axis (vertical) represents the voltage difference/steady-state voltage rise rate in pu, the second axis (horizontal) represents the DER active power increment level in percent, and the third axis (diagonal) represents the bus numbers.

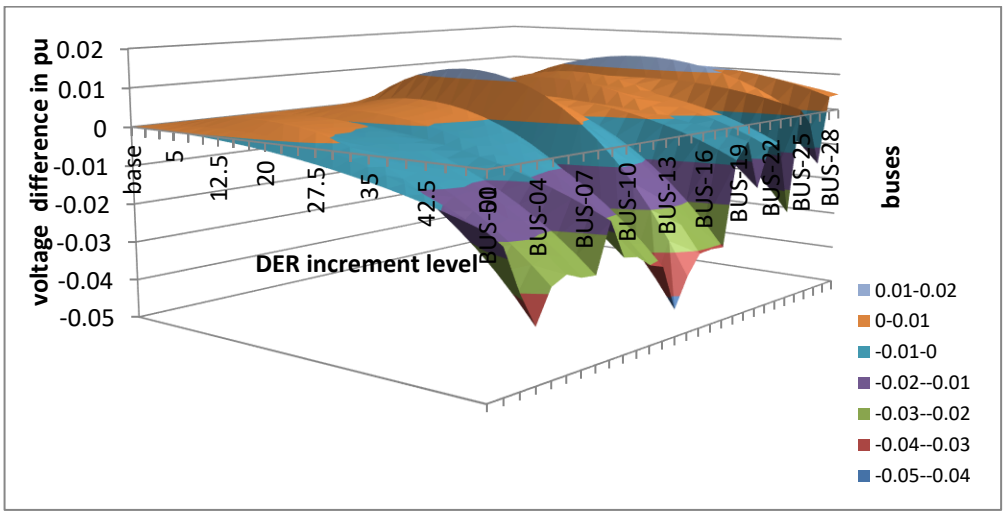

Figure 2-7 steady-state voltage rise rate from bus 1 to 29 (non-generator connected buses) with DER's different penetration level up to 50% at bus 15

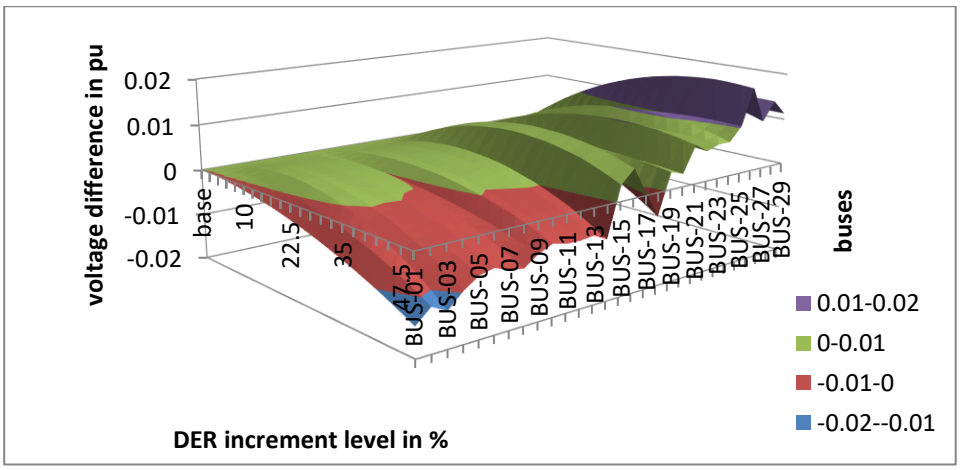

Figure 2-8 steady-state voltage rise rate from bus 1 to 29 (non-generator connected buses) with DER's different penetration level up to 50% on five buses

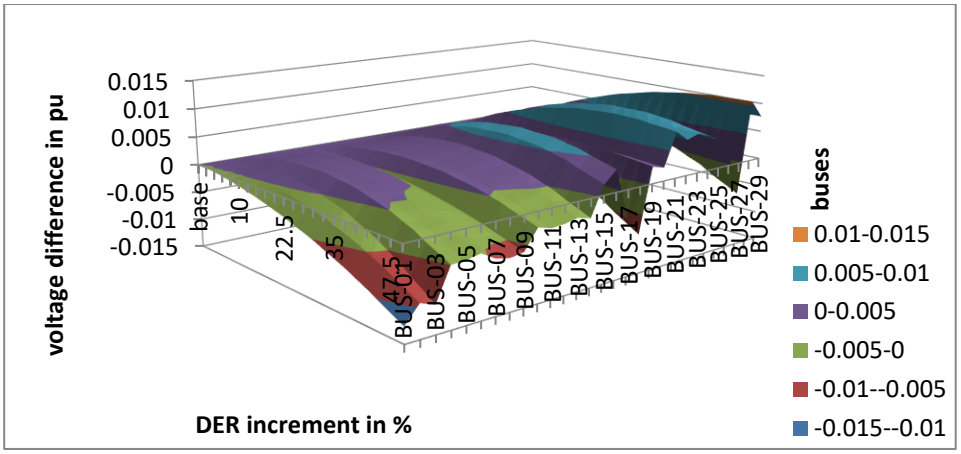

Figure 2-9 steady-state voltage rise rate from bus 1 to 29 (non-generator connected buses) with DER's different penetration level up to 50% on ten buses

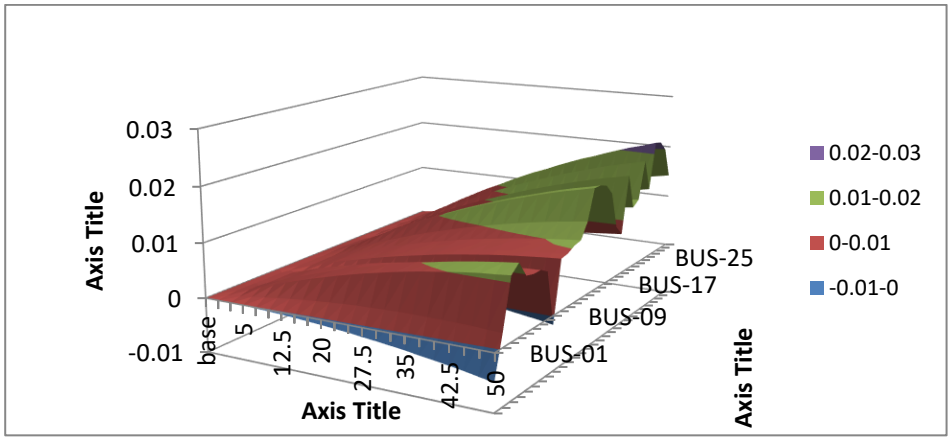

Figure 2-10 steady-state voltage rise rate from bus 1 to 29 (non-generator connected buses) with DER's different penetration level up to 50% on 15 buses

From the simulated results several points can be obtained. As the DER penetration increases,

the voltage of the buses is observed increase as well. In all Figure (from 2-7 to Figure 2-10), it is shown by the time the DER's penetration increases, as shown in the horizontal axis, the voltage levels at the buses, which the bus number is shown in the diagonal axis, are shown rising. The voltage increment levels are observed to vary for each bus. In Figure 2-7 the active power generated by the DER at the bus 15 causes steady-state voltage increases at the remaining buses as well. This is due to the buses surrounding the bus 15 are affected by the active power flown from the DER [2]. As a result, more buses with DER connection leads to a more apparent steady-state voltage rise, as shown in the remaining scenarios (Figure 2-8, 2-9, and 2-10). As such, it can be seen from the simulated results as shown in Figure 2-10 (scenario 4), the steady-state voltage are observed to keep increasing at even 50% DER penetrations, whereas on the results from scenario 3 (Figure 2-9), the steady-state voltage increments are somewhat declining at around 35% DER penetrations. In general, the voltage rise rate increases as the DER penetration level rise, and then slowly decline as the penetration level keeps rising. The rising trends seem aligned with Figure 2-5. Thus the simulation evidence supports the theoretical analysis based on Eftekharnejad et al. in [2] (chapter 2.5.2).

Commonly a larger number of buses with DER connection will lead to increase of steady-state voltage rise rate. Note that steady-state voltage at the DER connection defines the pre-fault voltage value for dynamic simulation studies. Therefore, the investigation of the steady-state voltage rise is necessary before LVRT dynamic simulation, as it defines the initial conditions for the LVRT transient study.

2.6 Review on Several Unwanted Steady-State Voltage Rise Mitigation Methods

The DER penetrations present a solution in the prevalence the need for a greener power source. It can also serve as a power source for a remote area, such as in small island whereas space can be very limited. Its presence in grid connections, however, has been causing several technical challenges. For instance, the presence of highly active power flown from housing estates single phase roof-top PVs has often been accused of being the source of unwanted single phase steady-state voltage rise which results in the unbalanced condition of the distribution system [64]. Voltage unbalance is considered to be one of the leading causes of power quality problems which can be detrimental to the performance of power equipment, since, under unbalanced voltage conditions, power networks incur more power losses and heating effects, rendering them less stable [65]. As such, steady-state overvoltage is one of the most apparent issues of highly penetrated DER grids since it not only leads to a power quality issue but also a problem that can degrade system reliability [66], [67], and the implementation level of DER applications. Steady-state overvoltage that is caused by the

unwanted steady-state voltage rise can be a critical issue since it causes DER systems to be tripped off or disconnected, which may affect both power delivery reliability and the DER owner's revenue. Initially, unwanted steady-state voltage rise exists because of the reverse power flow [68]; usually, this happens during light load and high DER generation conditions [4]. The reason for the implementation of under-excited DER operation is to prevent unwanted steady-state voltage rise. This implementation is in effect and is mandated by a grid code, such as the German Grid Code (GGC), [54]. The unwanted steady-state voltage rise issue, however, can be tackled through several different approaches. These various approaches are explored briefly along with the short review of the under-excited DER operation by considering the benefits and the challenges of different methods. Following this discussion, the reason as to why we have chosen to concentrate on reactive power control for the DER operation will become more evident.

2.6.1 Some Prevention Methods for The Unwanted Steady-State Voltage Rise

Several studies have mentioned the effectiveness of the under-excited operation of DER, a condition of which the DER absorbs reactive power in order to reduce the increased level of unwanted steady state voltage (non-transient condition) [11], [69]. As described in the studied literature, the solution for the unwanted steady-state voltage rise is achieved by allowing the PV to operate under-excited. So far such practice has been applied in some grid codes. In Australia, it is reported that any PVs which connect to a distribution grid are expected to be operated under-excited with 0.9 power factor when the PV's active power operating are at minimum 50% of its maximum active power capacity [70]. UK grid code requires *onshore non-synchronous generating unit*, which including onshore power park, such as, wind or PV park, has reactive capability corresponding to 0.95 lagging power factor at rated MW in the event of overvoltage up to 1.05 pu at their point-of-common-coupling (PCC) [36]. The Republic of Ireland Grid Code, EirGrid, requires their Power Park Module (PPM) has controllable reactive power capability equivalent to its ±0.95 power factor. So in the event of overvoltage PPM will absorb reactive power to prevent further overvoltage [33]. Similar to the EirGrid, the System Operator for Northern Ireland (SONI) Grid Code has the same steady-state voltage support requirements [32].

Another method of implementing reactive power regulation as a means to prevent unwanted steady-state voltage rise can be found in [11]. The under-excited operation is regulated based on the so-called 'active power dependent' (APD) method. The method is made to prevent unwanted steady-state voltage rise through two choices of approaches; active power capping and under-excited operation. It enables the DER to choose the most appropriate in terms of the

effectiveness of the method and for the better benefit of the DER user. Unwanted steady-state voltage rise prevention through excessive active capping results in unwanted active power loss. Meanwhile, minimising unwanted steady-state voltage rise through DER's under-excited operation will result in an additional line loading due to reactive power absorbed by the DER. As such, the method is intended to find a favourable trade-off solution from the two approaches concerning security (unwanted steady-state voltage rise) and economical factor (minimising line losses due to the under-excited operation and minimising the unnecessary active power capping which results to unwanted power losses). The study about APD is also presented in [71]. Unlike in [11], the study is more complicated since the aim of the method is not only for preventing unwanted voltage rise, but also to improve the operating performance of the unbalanced three-phase system. The active and reactive power curtailment is utilised for each phase. Further, the peak and low operating condition of the DER is also considered in the study. During peak operation, reactive power is limited in accordance with the *X/R* ratio of the networks, while during low operation the PV is expected to optimise its reactive support considering its minimum loss.

Several studies have exposed the usefulness of under-excited operation in minimising unwanted steady-state voltage rise. Under-excited PV operation with active curtailment is possibly selected when traditional voltage regulator such as transformer tap cannot mitigate the unwanted steady-state voltage rise [69].

2.6.2 Active Power Curtailment as a Means to Minimise Unwanted Steady-State Voltage Rise

Active power curtailment is often used for preventing unwanted steady-state voltage rise that is usually caused by reverse power flow [55]. However, the idea of active power curtailment is selected when it comes to prioritising the system security instead of the 'DER owner's revenue'. This approach is discussed in [72], whereas the strategy for the unwanted steady-state voltage rise prevention is done by utilising active power capping method (here, active power capping is the same with the power curtailment as in [71]). The active power is adaptively set in real time with the help of PV inverters. This method can maintain voltage profiles below a default upper limit while maximising the PV generation and fairly distributing the active power curtailments among all the PV systems in the local grid. The benefit of this method is that each of the PV systems in the network has an equal chance to supply electricity and shares the same fair amount of responsibility for regulating the voltage stability. Both steady-state and dynamic simulation studies have been carried out and show the effectiveness of the method. However, the dynamic stability study considered only the sudden irradiance

change with an account to the low and peak load condition. This [71] study did not cover the FRT/LVRT stability aspect when the system is subjected to a disturbance (such as three-phase fault).

2.6.3 Energy Storage for Unwanted Steady-State Voltage Rise Prevention Tool and FRT/LVRT Supports

As mentioned in section 2.6.2 earlier, a high penetration of DERs into low-voltage (LV) distribution networks creates reverse power-flow and voltage-rise problems. This phenomenon usually happens when the generation from DERs substantially exceeds the local load demand. Thus, the most straightforward approach to mitigate both unwanted steady-state voltage rise issue and FRT capability is to upgrade the existing distribution network by introducing storage facilities, such as battery systems. This approach has been discussed in several studies [73]–[75]. In all of these studies, the storage is utilised to absorb excessive solar PV power locally during PV peak insolation, and the stored energy is used during the evening for the peak-load support. Particularly in [75], a charging/discharging control strategy is developed by accounting the current state of charge (SoC) of the storage and the intended duration of charging/discharging period to exploit the available storage capacity effectively. The storage strategy can also mitigate the impact of sudden changes in PV output, due to intermittent irradiance, by employing the storage into a short-term discharge mode. The charging rate is tuned dynamically to recover the charge drained during the short-term discharge to ensure that the level of SoC is as close to the desired SoC as possible. This method is useful for mitigating the negative impacts of solar PV, and support the evening peak-time load demand management while utilising the available capacity of the storage device.

Further, it was reported that the utilisation of battery storage could be useful as well for assisting the DER in improving LVRT voltage sag, such as presented in [76]. In the study, through Wide Area Measurement System (WAMS) the battery is monitored and is used for coordinating the utilisation of the battery energy storage system (BESS) to improve voltage sag in the event of fault disturbance. The focus of this study is to evaluate the effectiveness of the active and reactive power injected by a BESS-assisted DER in improving the voltage sags. The studied systems are made by considering as well the presence of the dynamic type of load, such as motor load is also considered in this study. From the simulated result, it is demonstrated that both of the active and reactive power injection by the BESS-assisted DER could support the voltage of the connected bus following a three-phase fault disturbance. The simulation results are compared with the non-BESS-assisted DER scenario. It is shown that voltage sag improvement is observed to be better than when the DER is also equipped with the BESS.

The results and the work discussed above show the usefulness of energy storage as a tool to prevent unwanted steady-state voltage rise and helping the DER to improve FRT capability. Further, the help of batteries can also for reducing the effects of intermittent DER. However, for an economic perspective, the implementation of energy storage is an expensive solution. It is claimed that from [77] the 'Benefit/Cost' Ratio (B/C ratio) for the investment of coupling PV and Storage can be more expensive than PV only. Even it is also claimed that B/C ratio of coupling PV and Storage is often reported high, though not as high as PV only, it is mainly due to the investment tax credit (ITC) scheme [77]. The investment tax credit (ITC), such as the one in the US, which known as the federal solar tax credit, allow us to deduct 30 percent of the cost of installing a solar energy system from the federal taxes. When it comes to DER's voltage support, reactive power compensation that comes from DER support is still a preferred method for voltage support at transmission level [2], [78], [79] and in distribution level [62], [80]. As such, the idea for underlying the reasons for energy storage installation along with the DER implementation is needed.

2.6.4 Aspects Considering The Need for Energy Storage Installations

Initially, the use of energy storage in the DER integration studies is mostly for covering the nature of DER's intermittency [81]–[86], since their intermittent nature challenges the system's long-term and ability to meet the peak demand [82], [83]. For example, the implementation of PVs along with its battery in both grid-connected and micro-grid modes allows the PVs enabled to do peak supply-shaving and transferred the energy during peak load low supply [87]. Many energy storage discussions are mainly focussing on its implementation with DER as to cover DER's drawback during its low performance.

To emphasise the importance of energy storage, the intermittency of DERs is often significant in a rural/isolated area. Many researchers suggest the utilisation of energy storage in an isolated grid since in such condition (rural/isolated area) energy storage is usually served to provide ancillary service order to support the relatively low-voltage rural/isolated grid stability [88]. For instance, the study in [89] illustrates off-grid solutions based on PV-diesel hybrid systems with battery backup during the night that are operationally ready to provide communities with electricity services in rural areas. Since the lack of efficient energy management to balance supply and demand that results from frequent outages especially during night and increase the diesel fuel consumption, the study focuses on how energy from the batteries in the hybrid system can be managed during the night and efficiently distributed among the loads such that the critical loads like hospitals and telecom towers get maximum energy security. A more specific study about the rural LV-grid study is described in [90]. The topic of this paper is to

study the influence of battery energy storage systems (BESS) on a rural LV grid. Three scenarios are analysed. Load-flow analyses for the grid with and without PV and BESS, by considering different points of time in summer and winter are done in this paper. It is claimed that during sunny summer days at noon, the BESS could reduce the high steady-state voltages along several feeder lines, reduce the loading of the majority of cables and distribution transformer, and reduce the losses to be covered by utilities. From the observed studies, it can be claimed that energy storage presence in the rural/isolated area is essential. However, it will be shown in the following paragraph, under an extreme situation, such as when the DER's intermittencies is high, and the power source is scarce due to clouds in the winter, or no wind at all, utilising battery alone to cope the DER's intermittencies is not enough to secure the grid stability.

It is claimed from a reported study, that utilising BESS alone with PVs could be less effective in a rural island LV grid, unless a combinational power source, such as with diesel generators, are employed [91]. The study claimed that potential instability due to the PV intermittencies and the battery limits is often the inherent problem, especially when the island is very small and the cloud is frequently present. In the study, the problem could be overcome with the utilisation of the diesel. With the help from the diesel, when the battery discharge is at the limit, and the PVs are not in operation, the loads are still supplied, and hence the grid stability can be maintained. For further example, in [92], a power management strategy for water pump storage on a stand-alone PV based system is presented. The role of the water pump storage is similar to the diesel in the previous study. The aim of the power management strategy is feeding the induction motor and optimal charging/discharging of the battery with respective of power availability from PV. The maximum power of the PV panel was obtained by using perturb and observe (P&O) algorithm. Their study shows that with the water pump storage, the studied system has fast and effective response under variation irradiance levels. It can be observed that energy storage in the rural/isolated area can be useful for coping with the DER intermittency, under the condition that the steady power sources, such as diesel and water pump storages, are present and readily available whenever the battery capacity is at its limit.

The purpose of the battery storage for the grid-connected DER can be a little bit different. The battery storage for non-rural/isolated grid is often treated as storage, rather to be used to minimise the DER intermittency problem. Unlike in rural/isolated grid, since the DER and its storage are connected to a strong network, the problem of the DER's intermittency can be avoided. Since, when the DERs are at its low performance, the local loads can still be supplied by the grid. Moreover, the grid is still under the support of abundant power sources. As such, even though the battery storage on grid-connected DER can be relied on as storage, or as an additional power source to support ancillary services, such as steady-state and LVRT voltage

support, its presence is often treated as tertiary needs.

Section 2.6.5 will present the introduction of the *feed-in tariff* scheme which allows the DER's (EXIM) export-import metering system, enabling the DER's owner to export the DER's additional power source to the grid instead of storing it into the battery. As such, in the following section, the consideration of the of utilising the battery on grid-connected DER is discussed further. The discussion is made to confirm the necessity standpoint of the battery usage along with the emergence of the *feed-in tariff* scheme and its relevancy to employ a battery to assist DER's LVRT voltage support.

2.6.5 Appraising Energy Storage Usefulness with Some Other Methods for Unwanted Steady-State Voltage Rise Prevention and FRT/LVRT Capability

The importance of DER with energy storage implementation on a large grid planning that is still relying on conventional generator's ancillary services is discussed by considering the economic viability in [55]. By considering several options available for mitigating unwanted steady-state voltage rise problem and short/transient voltage instability, it is claimed that the idea of using energy storage for mitigating unwanted steady-state voltage rise problem and short voltage instability seems fit when, for instance, unwanted steady-state voltage rise problem could not be solved by power curtailment approach due to 'DER owner's revenue' issue, or, a condition that is the FRT capability inherently provided by the DER for solving voltage cannot maintain its function anymore.

Also, Carsten Heinrich et al. in [55] claim that, although a combination of power curtailment and reactive voltage support for unwanted steady-state voltage rise prevention and FRT capability is not economically favourable, the bargain as a 'trade-off' for system stability is still better than installing the battery as energy storages. Besides, relying on storages as the only investment strategy as a means both unwanted steady-state voltage rise prevention and helping to improve the DER FRT capability was not seems economically sensible. From their simulated result, in the grids with 30% DER penetration, although storages in combination with reactive power control (RPC) and/or curtailment can be cheaper than grid expansions strategy (ex. adding energy storage), there is only little energy to be stored and hence little potential could be used from the energy storage as for long-term solution. Even more in the cases of DER penetrations 50%, and 70% of the total load, energy storage will not represent an economical alternative. It is understood since the Benefit/Cost Ratio of DER with battery, as reported in [77], is much less than PV alone. Even more, it is reported that on the distribution level, share in total PV installed capacity in Germany and Australia, as examples, in the recent past has been estimated as 80% and 99% respectively. Thus under such penetration level,

relying voltage support through the use of storage on PV installations, for an economic perspective, would be less promising. Also, for the curtailment method itself, although it seems promising strategy, this method seems less profitable in the 70% PV penetration scenario, since it is more expensive than grid expansions strategy (ex. adding energy storage) [55]. The definition of the cost in the work of Carsten Heinrich et al. in [55] is the cost of the installations and also the operational cost of the planned grid. The detail of the costs can be studied in detail in their research [55]. Overall, under the circumstance of large DER penetration scenario, reactive power regulation provides the most reliable way to answer unwanted steady-state voltage rise, and possibly FRT issue, considering its availability in the DER's inverter. Further, the adaptation of export-import (EXIM) capability - a capability which allows exporting the DER's power source to the grid instead of storing it into the battery [55], [93], may become a more favourable solution than employing energy storage to solve the on-grid DER's intermittency source.

2.6.6 Summary on The Review about Unwanted Steady-State Voltage Rise Mitigation Methods

On the issue relating to the unwanted steady-state voltage rise, various different of approach as solution, whereas the ultimate goal is to minimise the unwanted steady-state voltage rise that is originated from the reverse power flow (RPF) due to the presence of DER, has been long discussions in many studies [2], [9]–[11], [54]. From the author findings, generally, there are three approaches to mitigate the unwanted steady-state voltage rise issue. First is the reactive power regulation by applying under-excited DER operation [10], [11], [54], the second is active power capping [69], and the third is by applying energy storage installation [94], [95]. Reactive power regulation is the most preferred while under certain circumstance; it is more suitable to cap DER's active power, through curtailing its active power [72]. Although on the other hand, active power capping is not proposed very often in literature since limiting active power as means for reducing the unwanted steady-state voltage rise is not beneficial for a longer term of DER usage [96]. The battery as for energy storage is often preferable for mitigating DER's issue, aside from the unwanted steady-state voltage rise, but also the intermittency nature of the DER itself [94], [97]. However, its implementation is expensive and not so economically favourable as compared to the implementation of DER with export-import (EXIM) capability [93], [98]–[100].

Thus, from the previous discussion, relating the methods for minimising unwanted steady-state voltage rise, it can be assumed that the method through reactive power regulation is the best bargain. Further DER's reactive power regulation has been demonstrated useful not only

for minimising the unwanted steady-state voltage rise in many studies [9]–[11], [54], [101], but also for improving LVRT voltage sag / transient voltage stability [3]–[5], [14], [23], [51], [51]. Therefore, DER's transient voltage support through reactive power regulation is the main feature of this study.

2.7 DER Regulation Strategies as Means for LVRT Voltage Support

Reactive power regulation/support is done by injecting additional reactive power via additional reactive current injection (aRCI). The necessities of LVRT voltage sag improvement through DER's transient voltage support is required by the grid code (GC), that any DER connected to a grid, should contribute to the grid disturbance mitigations in the future, including fault [3], [4], [19]. It is important to understand the typical response of the inverters, especially during LVRT, and further to understand what is the mechanism through which the DERs' inverter provides the LVRT ancillary service and what are its limitations.

Following chapter 2.7.1 and 2.7.2 strategies relating LVRT voltage support through active and reactive power regulations are reviewed.

2.7.1. DER's Reactive Power Regulation Strategies for LVRT Voltage support

In essence, The DER's Reactive power-based LVRT voltage support is done via additional reactive current injection (aRCI). The reactive current injection is a linear function of voltage difference - between pre-fault condition with the during fault condition - and the injection level of the aRCI - known as the K-factor [3]. This implies that for any DER which experienced a voltage bus value outside a pre-specified dead band (figure 2-11), are required to perform voltage support for voltage sag mitigation via aRCI (ΔI_q) [102]. In other words, once a transient voltage sag is detected, there will be a reactive current I_q injected into the grid. The value of this current depends on the various factor as shown in (2.22) and (2.23).

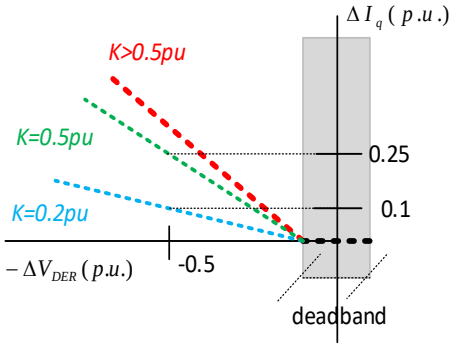

Fig. 2-11 Reactive current support during Low Voltage Ride Through

$$I_q = I_{q0} + \Delta I_q \quad [3] \tag{2.25}$$

$$\frac{\Delta I_q}{I_n} = \frac{K.((U-U_q)\pm U_{deadband})}{U_n}\ [3] \quad (2.26)$$

ΔI_q is the additional reactive current for the reactive power support during LVRT, I_{q0} is the pre-fault reactive current, I_n is the nominal current of the PV (reactive current during steady-state/normal condition), U_n is the nominal voltage of the PV, U is the voltage during FRT, and U_0 is the pre-fault voltage where its nominal value is within the range of the $\pm U_{deadband}$. $U_{deadband}$ represents voltage dead band to prevent the aRCI function being too sensitive with the transient voltage deviation and is usually pre-specified upon DER installation for 10% of the nominal voltage U_n [33]. This dead band (which is seen in Fig. 2-11), however, can also be pre-specified to be smaller than 10%, and sometimes can be completely removed (defined as 0%) [3]. This reactive power regulation is initiated during transient conditions and activated when the positive sequence voltage U deviates from the pre-fault voltage U_0 (exceeds the $\pm U_{deadband}$). An example of the real application of the voltage dead band setting was reported in [70]. It is reported that the voltage dead band of the household-level photovoltaics in Australia were at ±4% which allows voltage variation without reactive support for ±4% along the LV cable connecting to each house's switchboard.

DER's Reactive power-based LVRT voltage support via aRCI is encouraged to become a standard in some renewable grid codes [32]–[36]. There are some alternative of reactive power injection (RPI) strategies; these are 'RPI with constant average active power control (RPI-Const.-P)', 'RPI with constant active current control (RPI-Const.-I_d)', and 'RPI with peak current control (RPI-Const.-I_{g_max})' [8]. The objective of RPI-Const.-P is to maximise the output energy with MPPT control during LVRT operation, whereas, the average active power can be maintained constant in the short-term period of the fault. RPI-Const.-I_d offers flexibility to the injection given on lower current rating inverters. The drawback of RPI-Const.-P and RPI-Const.-I_d is, however, the possibility of overcurrent during LVRT [103]. Hence RPI-Const.-I_{g_max} on [103] is designed to prevent unintentional inverter shutdown due to overcurrent protection. The operative strategy is done by allowing the magnitude of the injected grid current to be kept constant but consistently lower than the inverter current limitation during LVRT. In doing so, the active power will be reduced proportionally in order to inject sufficient reactive power during LVRT. All three mentioned RPI strategies have to inject full reactive current in case of severe voltage sag. Generally, the implementation of these type of LVRT reactive supports, as adopted in many grid codes, is motivated by the idea that when a DER that is mostly grid-interfaced with an inverter injects reactive power to a **highly inductive** Point of Common Coupling (PCC), it will increase the phase of the voltages sag **proportionally** to their phase current amplitudes [103].

It can be understood why the use of reactive supports is preferred in many grid codes [32]–

[36], [58] since it was initially for power park module which generally located in a relatively remote area, far away from the urban/residential area [4]. As such, it is often connected to an express feeder, which relatively has a higher *X/R* ratio than the low voltage connection lines that are usually located in an urban area. With the emerging growth of inverter-based DER in the urban/residential area, such as roof-top PVs, there is the need to evaluate some other means of LVRT voltage support, which is presented in the following section.

2.7.2 Some DER's Power Regulation Strategies for LVRT Voltage Support

DER's LVRT voltage support through a combination of active and reactive power regulation via additional active and reactive current (aRACI) is found in [1], [14]. Particularly by Boemer et al. in [1], claimed that impedance angle adjusted aRACI lead to higher effectiveness than either a pure reactive (aRCI) or active (aACI) current injection. Higher effectiveness of aACI is observed because the active and reactive current in accordance with the angle of the impedance between the DER and the located fault could keep the active and reactive current within Active and Reactive Current Transfer Limits of the DER. The theory of Active and Reactive Current Transfer Limits of the DER can be found in [5].

However, also Boemer et al. in [1] have found that Impedance angle adjusted aRACI was found to less effectively to support the LVRT than a pure reactive current injection (aRCI) under reverse power flow situations. It should be noted that many low-voltage-connected DERs such as mainly photovoltaics are situated in the residential area. The PVs regularly reach their peak operation during the daytime, a condition when the load of the house is at its lowest point. Thus, this implies that peak low-voltage-connected DERs will mostly be under reverse power flow situations. Furthermore, LVRT through aACI and aRACI needs a continuous standby of 'additional active reserve power' from the DER, which means that DER must be operated under sub-optimum condition. This is a condition that is not economically favourable for long-term of DER usage [55].

With that in mind, aRACI, and even aACI should not be adapted as LVRT support preference in future DER connection requirements. The above argument emphasises the reason as to why the study is focused on reactive power regulation.

The employment of LVRT/transient voltage support, whether through active or reactive power regulation as proposed by many researchers, has the purpose of improving the voltage sag at the PCC of the DER. By doing so, the voltage stability could be improved. The voltage support is employed on a condition of a certain level threshold of voltage sag, with a particular duration of time. The criteria are documented on the grid code relating to LVRT requirements, which is described in the following section.

2.8 The Grid Code Requirement on DER Connection, DER Fault-Ride-Through, and Its Voltage Support Strategies

The implementation of DER units enforces the grid utility to regularly check and improve their regulations and standards through the grid codes. This sets of rules are not only restricted to popular DER such as photovoltaic (PV) and wind power farms but also any electric power sources that are directly connected to the distribution network or connected to the network on the customer site [6]. A grid code serves the mission of defining the physical connection point requirements to be followed by energy production equipment to be connected to the grid. In addition, a regulatory framework defines the requirements for permanent connection and the relevant network parameters to be supported, in a way to secure system operation. A grid code has a particular role in this integration paradigm. By complying with these rules, all DER owners may contribute to the system stability [104].

The grid codes set the full range of ancillary services, similar to conventional synchronous machines, to support the network during the disturbance [105]. In this code, both steady state and transient state requirements are covered in their technical aspect. Steady-state requirements are about the perfect balance between generation and demand, such that the grid stability is maintained irrespective of the operational activity of both the loads and the supplies [104]. With the continuous, intermittent generation from the DERs at larger-scale, the balancing requirement becomes more complex and less predictable. Therefore, the steady-state requirement covers operation under such condition that balance between generation and demand is achievable so that the power flow at PCC of the DER is steadily measurable [60], [106], [107], whereas the transient state requirement looks into the performance of the DER during the transient state following disturbances or faults [22], [78], [88], [108]–[111].

2.8.1 Grid Codes on DER Reactive Power Regulation for Steady-State Operations Requirements

To achieve steady-state stability of the grid under all condition of the operational activity of both the loads and the supplies, the voltage profile of the grid has to be maintained within an acceptable range [112]. Maintaining the steady-state voltage stability through DER reactive power regulation has been adopted in many grid regulations [32]–[35], [37], [40], [58], [113]. From the studied review, the reactive power capability that is set in the grid code on each country is defined differently. This is understandable since each country has different interpretation relating the typical steady-state voltage range at the DER's PCC and the typical reactive power capability of certain generating units that are made. For instance, on synchronous-based generating units, the specification relating to the reactive power capability

can be seen on the generator performance charts/generator nameplate which specifies their reactive power capability limits [114]. Minimum short circuit ratio is also usually specified, as for the case of United Kingdom (0.4 pu for units under 1600 MVA and 0.5 pu for larger units) [36] or Northern Ireland (0.5 pu) [32], [33]. For non-synchronous generators, such as inverter-based DERs, grid codes define the reactive power capability as in the form of 'PQ' and 'UQ' diagrams. 'P' stands for the active power, 'Q' stands for the reactive power, and 'U' stands for the voltage. Figure 2-12 [32], [33], [37], [40], [58], [113], [115] shows the comparisons of reactive power limits for non-synchronous power plants in terms of reactive and active power (PQ diagram). It can be seen that Australia and New Zealand have the most relaxed requirements. The requirement shows in Figure 2-12 define the reactive operating limits which allowed the DER to keep the steady state voltage stability.

From the Figure 2-12, the reactive power generation requirement is specified up to 80% of the active power output since the simultaneous generation of maximum active and reactive power will unnecessarily affect the reliability of the DERs. The need for steady-state voltage support is low at high levels of active power. Reactive power requirement is also reduced for low power output below 50% for the case of the Republic of Ireland, whereas below 20% seems to be observed for Spain Grid code. For Northern Ireland, the reactive power requirement is observed to be more relaxed on below 50%.

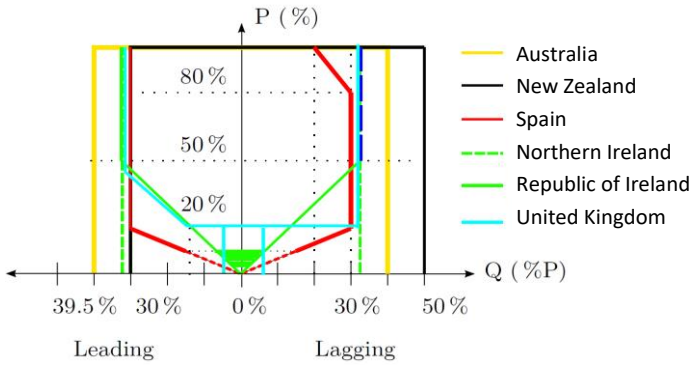

Figure 2-12 Comparison of PQ diagrams (reactive power capability region for distributed generator)

The steady-state voltage limitations at the PCC of the DER connection also affect reactive power capability. Many grid codes further indicate voltage limits for the compliance of the reactive power requirement through UQ chart, as shown as an example in the Figure 2-13 [32]–[35], [37], [40], [58], [113]. For inductive compliance, for instance, Spanish regulation sets a maximum voltage limit of 1.05 p.u. and for capacitive condition, a minimum limit of 0.95 pu. For New Zealand [115], voltage limits depend on the voltage level, with 1.1 and 0.95 pu for 220 kV. For 110 kV transmission level, it must be within 1.1 and 0.9 pu; a requirement that is relatively more relaxed than on Spain grid and Northern Ireland grid code [32], [33]. It

is observed that under-excited/lagging capacity may decrease as steady-state PCC voltage increases because of converter current constraints. Overexcited/leading capacity is observed wider with the increase of terminal voltage.

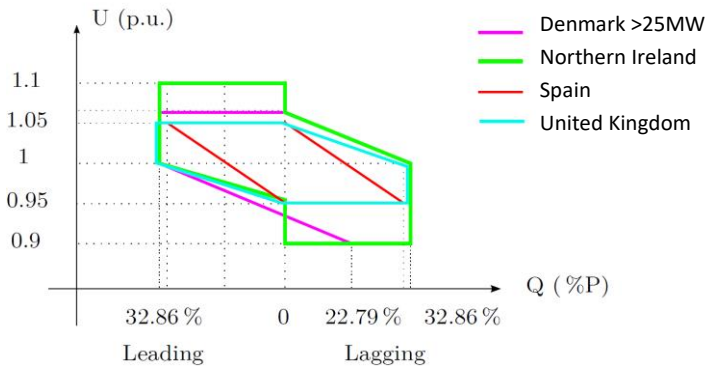

Figure 2-13 Comparison of UQ diagrams for distributed generator (wind farms)

2.8.2 Grid Codes on DER Transient Voltage Support and Its Minimum Standard Requirements

Transient Voltage recovery requirements should be met into different forms. Some grid code classified the voltage recovery based on the type on the generating unit, and some define the voltage recovery requirements generally. The Australian Energy Market Operator (AEMO) requires the voltage recovery on both *scheduled* and *non-scheduled* generating system for above 30MW voltage level at the connection point to within 2% of the setpoint for at least 7.5 s [58]. The AEMO defines that voltage recovery through DER voltage support must be made through reactive power regulation via reactive current. The Danish technical regulation [35] on PV power plants above 11kW suggests its voltage recovery must be able to reach to its voltage settling time condition for no later than 10 seconds. For wind power plant above 11kW, it must be designed to withstand voltage sags down to 20% of the voltage in the Point of Connection throughout a minimum of 0.5 seconds without disconnection. For other power plants that are above 11kW, it must be designed to withstand transitory condition for up to 100 ms. The voltage support for the PVs and Wind park power plant is made via reactive power regulations as well.

The UK National Grid [36] requires *onshore non-synchronous generating unit* which connected below 110kV capable of retaining 85% of the steady-state voltage lasting 2.2 seconds. For the *onshore synchronous generating unit*, it is required that the terminal connecting voltage should reach 90% in less than 1.5 seconds. Also, the rise time within 75% of the voltage change shall be met less than 0.6 seconds. Similar to the previously mentioned grid codes, the voltage support required by the UK grid code is made via reactive power

through reactive current regulation as well and should be within 140ms. For longer durations of voltage sags, they are required to provide an active power output at least in proportion to the retained voltage at the grid entry point and must generate maximum reactive current without exceeding their transient rating limits, while remaining transiently stable.

In the German Grid Codes [116], [117], the voltage recovery should reach 90% of the steady-state for at least within 1.5 s, while the voltage recovery rise should reach 90% from its nominal pre-fault value for at least within 1.35 s. During faults, the renewable power sources are required to support the network voltage during a voltage sag through additional reactive power. The voltage control according must be activated in the event of a voltage sag of more than 10 % of the effective value of the power source voltage. The power source must be capable of feeding the required reactive power within 20 ms into the network. When the reactive power injection is in working, the active power shall be reduced proportionally to the reactive power needed to improve the voltage sag. The duration of reactive power support is expected up to 150ms (unlike Great Britain which limits reactive support for up to 140 ms) [3].

In the EirGrid Grid Code (The Republic of Ireland) [33], *Controllable Power Park Module* (Controllable PPM), which could be interpreted as wind and PV park module, should attempt to control the voltage back towards the nominal voltage and should be at least proportional to the voltage sags. The reactive current response shall be supplied within the rating of the Controllable PPM, with a rise time no higher than 100ms and a settling time no greater than 300ms, while the active power must remain to withstand during the voltage sags. For System Operator for Northern Ireland (SONI) Grid Code [32], voltage recovery of the controllable PPM should able to achieve its settling time in no more than 300ms, to reach within +/-10% of its steady-state voltage value. The PPM should provide voltage support via reactive power injection at least from 90% of its steady state active power response, measured by output, at the point of connection to the distribution system within 1 second of the voltage recovery to the normal range.

In Spain [37], PPM must be able to resist voltage sags down to 20% of the nominal voltage over a time span of 500 ms. Spain also requires the voltage rise time should be at least 60% within 500ms. Spain requires maximum reactive power injection should be given during three-phase faults. However, for two and one phase faults, the maximum permitted injected reactive power is 40% of the rated power after the fault entrance by a 150 ms.

Voltage recovery requirements should be met in many grid codes in one of several ways. For the sake of study, the voltage recovery requirements are summarised in Table 2-2. Though the comparison is loosely defined, it can be seen based on ‘slope', ‘rise time' and ‘settling time'. Table 2-2 overviews the minimum transient voltage recovery should be met as required in

many grid codes. In order to ensure the grid stability, during transient voltage recovery, the DER's voltage support from the DER is required.

Table 2-2 Minimum Voltage Support requirements should be met in many grid codes

Region	Slope	Rise time	Settling time
Australia [58]	-	2 s for a 5% step until 2% of the voltage setpoint	±5% of the steady-state voltage for at least within 7.5 s
Denmark [35]	-	-	10 s with an accuracy of 0.5% of voltage setpoint
UK [36] onshore non-sync. gen.	2-7%	75% for <0.8 s	<2.2 s for at least 85% of its nominal voltage
UK [36] onshore sync. gen.		At lowest 20% for <1.05 s	<1.5 s for at least 90% of its nominal voltage
Germany [117]	-	90% for at least within 1.35 s	<1.5 s for at least 90% of its nominal voltage
Ireland (EirGrid) [33] & Northern Ireland (SONI) [32]	1-10%	90% of its nominal voltage for at least within 2.375 s	<3 s for at least 90% of its nominal voltage
Spain [37]	0-25%	60% s for <0.5 s	Settling Time within 1.5s, for +/-10% of its pre-fault voltage value

The means of the voltage support which is chosen, either through active or reactive power-based regulation, depends on which grid code is being referred to. The DER's voltage supports are aimed to improve the voltage sag magnitudes, and to allow the voltage recovery time as soon as possible. As such, the rise time and the settling time of the voltage are essential for determining the effectiveness of the voltage support. From table 2-2, it can be seen that the UK grid code has the most stringent rise time, whereas the Germany grid code has the most stringent settling time. Meanwhile, ideally, the rise time and the settling time of the transient voltage recovery should be met, at best, as short and quick as possible. However, the time rise and settling time requirements are commonly made based on the practical experiences achieved from monitoring the power system operation/behaviour. As such, there is no appropriate way of determining rise time and settling time of the transient voltage recovery for universal application.

2.8.3 Grid Codes on DER Fault-Ride-Through Requirements

In this section, several transient voltage recoveries in the form of Fault-Ride-Through (FRT) requirements from several grid codes are presented. It will be shown in general, the major difference between distinct FRT patterns is in the time duration, which the RESs are requested to withstand the fault and stay connected to the grid. The DERs are also required to remained

connected in the event of stability disturbance [32]–[35], [37], [40], [58], [113]. The ability of DER unit to stay connected with the main grid during short voltage instability events for a specified time frame without DER being disconnected is referred to as Fault-Ride-Through (FRT) capability [4]. FRT requirement is presented in the form of a transient voltage deviation limits vs time. DERs are also required to provide voltage support as well [23], which is described further in section 2.8.4.

Two requirements can be defined relating to the Fault Ride-Through (FRT) requirement: Low Voltage Ride Through (LVRT) for voltage sag and High Voltage Ride Through (HVRT) for transient over-voltage. HVRT is less common, however, but reportedly exist in some grid connection rules, which is described in the following.

2.8.3.1 Low Voltage Ride Through (LVRT)

For LVRT, its patterns are classified based on two characteristic patterns; depth and duration of the voltage sag [104], [118]. It can be seen in the Figure 2-14 [32], [33], [37], [58], [113], [118], the minimum level of voltage sag is less diverse than the duration for the DER's LVRT capability, which clearly indicated closeness agreement of the DER's LVT requirement among all of the grid codes in term of interpreting minimum allowable voltage sag. Meaning that even though different grid codes have different LVRT duration, their voltage sag standard is less diverse. This concludes the fact that little differences are to be made regarding the depth of voltage sag on several grid codes regarding LVRT from various countries [88], [119]. The LVRT is created in order to accommodate inverter-based DER's behaviour following severe faults such as three-phase short circuit at their PCC, and allowing them to keep their power supply passed through to the grid whenever possible during their timely acceptable transient period to the normal (steady-state) condition [3], [5] or to unavoidably disconnect the DER [120].

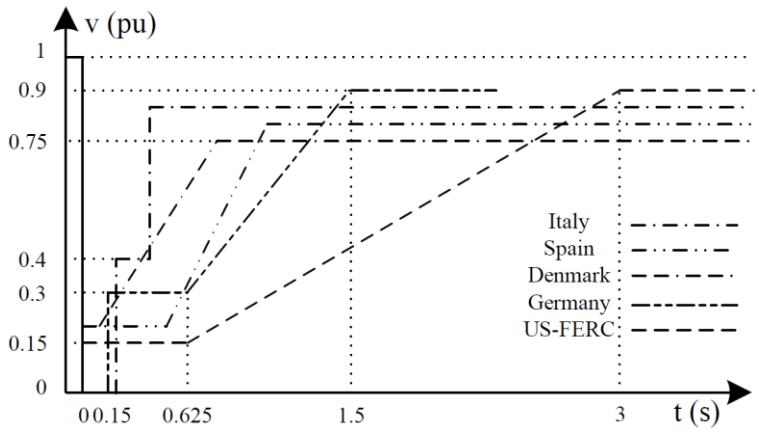

Figure 2-14 The LVRT from different countries

All described grid codes cover LVRT requirements. Reportedly the same rules for any type of

generation apply in Australia, French counterpart, and UK power systems. Meanwhile, for the New Zealand grid code, separate requirements are proposed to be met by generators connected to the North Island and the South Island [115]. In the case of Australia [58], [113], the standard proposed by the Australian Energy Market Operator (AEMO) which acts as the National Transmission Planner, require the LVRT duration to be at maximum 450 ms. On The Denmark grid code, however, any generation power plant with a rated active power more than 11 kW must ride through low voltage sags [34], [35], and no different LVRT standard is applied between synchronous, PVs, and wind power generations [34], [121].

In Great Britain [36], for faults shorter than 140 ms no specific profile is mentioned, and it is only stated that any generator connected to the transmission grid should be able to ride through voltage sags for a maximum duration of 140 ms. The UK Grid Code has a different standard of LVRT requirements for each of their type of power sources. Their power plant classification can be broad. However, particularly for their Small Power Station, it can be classified into: Type A, Type B, Type C, and Type D; which their sizes have to be; below 1MW, between 1MW and below 10MW, between 1MW and below 10MW, and above 50MW; respectively. For type A, they do not provide LVRT voltage support. Their voltage support is only for steady-state. For Type B, C and D, they have to provide LVRT voltage support. Figure 2-15 shows UK LVRT requirements for Type B, C and D Power Park Modules connected above 110kV. Note that in the UK grid code, there is LVRT classification for the synchronous generating unit as well. However, only the LVRT classification for power park module is presented since it is the focus area of this thesis.

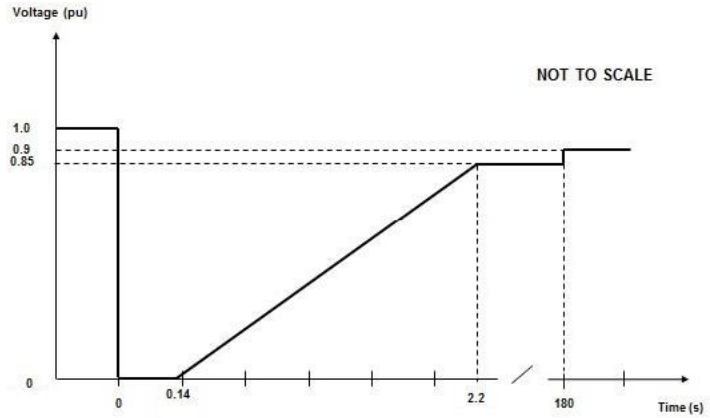

Figure 2-15 UK LVRT requirements for Type D Power Park Modules with a grid entry point above 110kV [36]

For connections below 110kV, the LVRT requirement is shown in Figure 2-16.

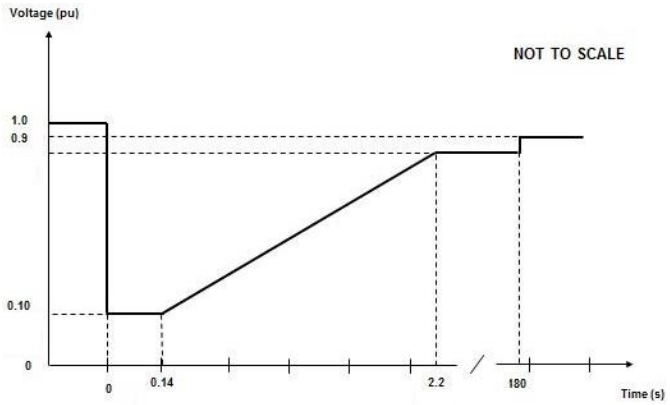

Figure 2-16 UK LVRT requirements for Type B, C, and D Power Park Modules connected below 110kV [36]

It can be seen for power park modules connected below 110kV, during voltage sag (below 140ms), the modules are allowed to be disconnected when the LVRT voltage reaches below 0.1 pu. For power park modules connected above 110kV, during a voltage sag, the modules have to 'zero' ride through, since it must remain connected even though the voltage reaches 0 pu [36].

Further during LVRT, power park module for type B, C, and D (except for type A, <1MW) are also required to provide fast fault reactive power regulation via reactive current injection as well. These aspects are discussed in more detail in the UK Engineering Recommendation (EREC) G99 [122], which covers the requirements for the connection of generation equipment in parallel with the public distribution network. The faults referred to are Transmission System faults which clear within 140 ms and which will be seen in the Distribution Network as a voltage depression/voltage sag. The injected current from each power park module must be in proportion and remain in phase with the change in system voltage at the PCC during the period of the voltage sag. The detail of the fast fault reactive current injection for power park module can be shown in Figure 2-17.

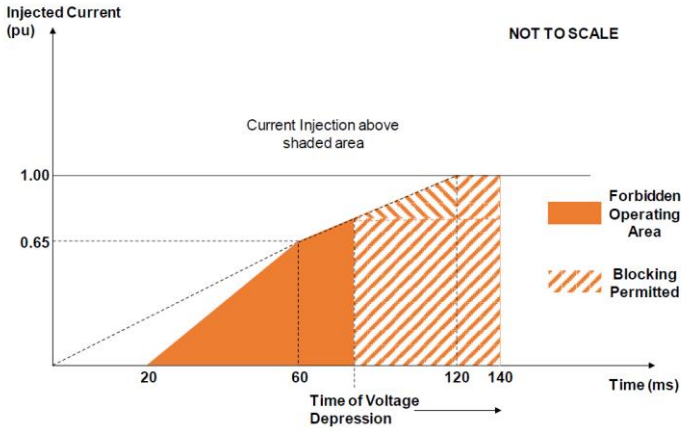

Figure 2-17 Chart showing area of reactive current injections for voltage depressions/sags [122]

Figure 2-17 shows the chart showing the permitted area (above the shaded area) of reactive current injections for voltage depressions. During the first 20 ms, the power park modules are allowed to inject reactive current at full level. During 20 ms to 60 ms, if the voltage is still depressed, then the injected reactive current can be given in proportion to the retained voltage at the PCC but shall still be required to remain above the Forbidden Operating Area as shown in the Figure 2-17. For over 60 ms, if the retained voltage reaches below the 'Blocking Permitted' area, then the power park modules/the DERs is permitted to block (i.e. reduce the current injection) in order to mitigate against the risk of transient overvoltage instability that would otherwise occur due to transient overvoltage excursions [122].

On the German Grid Code, the power generating units must not be disconnected during a voltage even drop-down to 0% of rated voltage (V_{rated}), within a duration of 150 ms. Assuming that the post-fault voltage magnitude is greater than borderline 1, zone A – as shown in figure 2-18 [123], the power plants may not lead to DER disconnection. If during post-fault the grid voltage magnitude is in zone B, the power plants should be ridden through. In zone C, a short-time disconnection can be carried out in any case. Sometimes, longer disconnection times are also possible. After a short-time disconnection in the zones B and C, active power must be online within a gradient of at least 10% of the normal capacity per second. Underneath the zone D, there are no requirements for maintaining the grid connection [123].

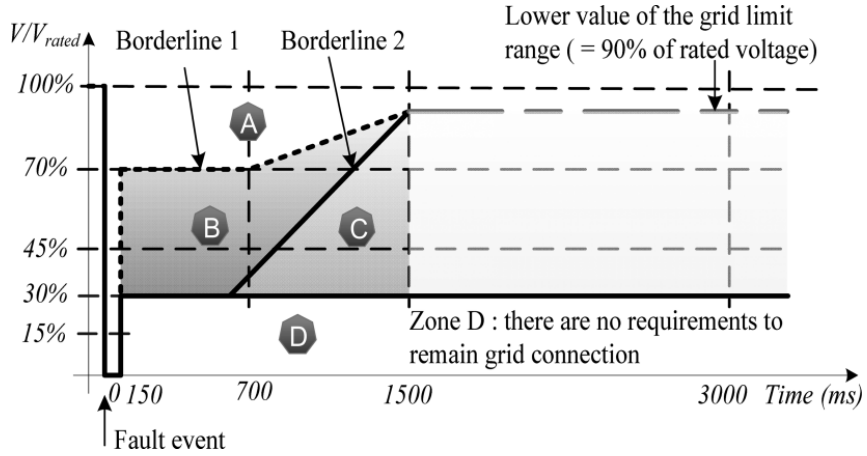

Figure 2-18 Technical Guidelines for Power Generating Units following FRT/LVRT

Overall from the explained above grid codes, although only three-phase faults have been represented, some grid codes require specific treatments depending on the short circuit type. For the Australia case, the three-phase fault has to be ridden through on shorter times (120 ms) compared to the other type of the fault (250 ms) on 250 kV networks. For grid code from Northern Ireland and the Republic of Ireland, Transmission System Operators (TSOs) employ a generalised LVRT profile for all types of faults. So, an LVRT standard applies to all conditions balanced or unbalanced fault. In Denmark, all DER has to ride through regardless

of unbalanced faults. Particularly on wind power plants, it has to ride through within the LVRT requirements when at least two unrelated faults appeared within 2 minutes. In the UK, for non-synchronous power park module which connected above 110kV, a ‘zero voltage sag' LVRT requirement has to be met.

Further, to ensure the grid stability, many grid codes also require minimum active power recovery that should be met for the DERs, following LVRT. The recovery of active power generation required in many regions is given in Table 2-3.

Table 2-3 Active power recovery after fault clearance

Region	Time in s	P (% of pre-fault P)
Australia [58]	0.1 s after clearance	95%
French [124]	10 s after clearance	95%
UK [36]	0.5 s after clearance	90%
Ireland (SONI [32] & EirGrid [33])	0.5 s after clearance	90%

Following a successful fault clearance, normally, the active power recovery is delayed to ensure the post-fault voltage stability is secured firstly. A sudden feeds-in of active power could cause voltage fluctuations, and hence it could result in system instability, especially in weak power grids [125]. As such, the time delay for the DER’s active power recovery should be fairly fast enough but shall not cause unwanted voltage fluctuations. The post-fault active power recovery time is commonly determined according to the practical experiences obtained from power system operation monitoring. The summarised active power recovery after fault clearance required from the grid codes as presented in Table 2-3 are made based on the practical experience from the respective grid operators. It can be observed the least stringent requirement; the French Grid Code requires a time delay of maximum 10 s, which is the most relaxed among other presented requirements.

The design of the active power recovery requirements is generally made by considering the compromise for a quick active power recovery (as in order to immediately supplying the load) and, while on the same time, ensuring the voltage stability through adjusting appropriately active power recovery speed. As such, the active power recovery speed, aside from being made to adjust with the renewable ratings, it should be made to account with the grid adaptability – meaning, the active power recovery would not impose the grid post-LVRT voltage stability. The need for appropriate DER's active power recovery settings is important since it would secure the post-LVRT voltage stability.

2.8.3.2 High Voltage Ride Through (HVRT)

On the grid codes, voltage-time profiles are also defined for overvoltage or voltage swell conditions. This voltage profile requirement is usually defined to prevent caused by sudden

large load switching, capacitor energising or faults in the network. This requirement is referred to as HVRT. On Spain and Australia [37], [58], [124] for instance, for both synchronous and non-synchronous generation (inverter-based DER), as in the following Figure 2-19 [37], [58], [124], the highest value of respectively 1.25 and 1.3 p.u. has to be withstood for up to 50 ms. After 50 ms, the overvoltage may remain observed, and thus the DER remain connected until the time of 1 s, with a maximum overvoltage 1.15 pu and 1.18 pu for Spain and Australia respectively.

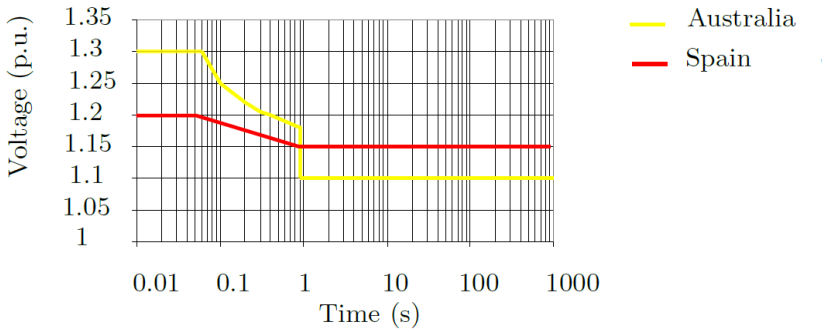

Figure 2-19 HVRT requirement in Australia and Spain

2.8.4 Summary of The DER Requirement on Strategies for DER's LVRT Voltage support

The presented summary is made to overview voltage support styles adopted in many countries. Most grid codes favour reactive power regulation as the means to allow their DER's to support voltage during LVRT. Even though many studies suggest that the growth trends of the DER will be most likely on low voltage connections, such as roof-top PVs [4], the current grid codes do not yet consider the need of requiring low voltage connected DER's to provide LVRT voltage support as well. For instance, in the UK [36], [122], for the non-synchronous generating unit with a capacity lower than 1MW, the reactive power regulation is provided only for steady-state voltage support. The Northern Ireland (SONI) [32] & The Republic of Ireland (EirGrid) [33] requires their Non-Centrally Dispatched Generating Units (ex. distributed roof-top PVs), to provide the reactive power regulation only for steady-state voltage support. Similar treatment is to be found in the German Grid Codes as well [126].

Table 2-4 and 2-5 summarise the voltage support strategies from various grid codes. The first column defines the Grid Codes of which the DER's LVRT voltage support strategies is adopted, while the second column defines the power source classifications which subject to the requirements. The third column, defines the power source sizes and the fourth column defines the means of voltage support. The fifth column descibes the minimum voltage support standard should be met, and lastly, the sixth column presents additional descriptions.

Table 2-4 Summary of the DER's LVRT Voltage Support Strategies (Part 1)

Grid Code	the power source classifications which subject to the requirements	power source size	Means of Voltage Support	minimum voltage support standard should be met	additional description
UK	onshore non-synchronous generating unit (including DC Connected Power Park) Modules	<1MW (type A)	not available (reactive power regulation only for steady-state voltage support)	-	-
	onshore non-synchronous generating unit	1MW≤ and <10MW (Type B)	reactive power regulation via reactive current injection	the rise time minimum: 75% for <0.8 s and the steady-state volt. settling time: <2.2 s for at least 85% of its nominal voltage	For voltage sags longer than 140 ms, the unit must provide active power at least in proportion to the retained voltage at the grid entry point and must provide maximum reactive power without exceeding their transient rating limits, while remaining transiently stable
	onshore synchronous generating unit		automatic excitation system	the rise time should be min.20% for <1.05 s and the steady-state settling time should be <1.5 s for at least 90% of its nominal voltage	
	onshore & offshore non-synchronous generating unit	10MW≤ and <50MW (Type C)	reactive power regulation via reactive current injection	the rise time minimum: 75% for <0.8 s and the steady-state volt. settling time: <2.2 s for at least 85% of its nominal voltage	
	onshore & offshore synchronous generating unit		automatic excitation system	the rise time should be min.20% for <1.05 s and the steady-state settling time should be <1.5 s for at least 90% of its nominal voltage	
	onshore & offshore non-synchronous generating unit	50MW≤ (Type D)	reactive power regulation via reactive current injection	the rise time minimum: 75% for <0.8 s and the steady-state volt. settling time: <2.2 s for at least 85% of its nominal voltage	
	onshore & offshore synchronous generating unit		automatic excitation system	the rise time should be min.40% for <1.05 s and the steady-state settling time should be <1.5 s for at least 90% of its nominal voltage	
Northen Ireland (SONI) & The Republic of Ireland (EirGrid)	Non-Centrally Dispatched Generating Units (ex. distributed roof-top PVs)	<5MW (for 2kW≤ and <5MW, the unit shall be monitored by the DSO)	not available (reactive power regulation only for steady-state voltage support)	-	-
	Controllable Solar & Wind Power Park Module	Capacity of 5 MW or more	reactive power regulation via reactive current injection	the voltage should be able to reach 90% of its nominal voltage for at least within 2.375 s. the voltage settling time should reaches at least <3 s for at least 90% of its nominal voltage	the active power must remain active during LVRT and must proportional to the voltage magnitude

Table 2-5 Summary of the DER's LVRT Voltage Support Strategies (Part 2)

Grid Code	the power source classifications which subject to the requirements	power source size	Means of Voltage Support	minimum voltage support standard should be met	additional description
Australia	non-synchronous generating system	-	reactive power regulation via reactive current injection	±5% of steady-state voltage setpoint within 2 s. should reach settling time of the voltage ±5% for at least 7.5 s	-
	synchronous generating system		excitation control systems	should able to rise the voltage to ±5% of steady-state voltage setpoint within <2.5 s. should reach settling time of the voltage ±5% for at least 7.5 s	
Deanmark	PV power plants Wind power plants synchronous power plant	above 11kW	reactive power regulation via reactive current injection	should able to rise the voltage to ±5% of steady-state voltage setpoint within <10 s	-
Germany	Non-Controllable Distributed Generating Unit	-	not available (reactive power regulation only for steady-state voltage support)	-	-
	Controllable Distributed Generating Unit		reactive power regulation via reactive current injection	the voltage recovery should reaches 90% of the steady-state for within 1.5 s, and the voltage rise should reaches 90% from its nominal pre-fault value within 1.35	When the reactive power injection is in working, the active power shall be reduced proportionally to the reactive power needed to improve the voltage sag
Spain	Controllable Solar & Wind Power Park Module	≥10MW	reactive power regulation via reactive current injection	the voltage recovery should reaches 90% of the steady-state for within 1.5 s, and the voltage rise should reaches 60% from its nominal pre-fault value within 0.5	During the whole transient regime, the facility must be able to inject into the grid at least the nominal apparent current

2.9 The Potential Research Gap as The Summary of The Literature Review

It has been observed that the current DER requirements on LVRT voltage support usually are coming in three types; the reactive power-, the active power-, and the combinational active and reactive power-based LVRT voltage support. Each country has its preference for providing the LVRT voltage support. To the date, it has been revealed that the attention on the DER LVRT requirements has been given to the renewable park type, a group of wind turbines and PVs that is typically placed in a dedicated location that which often connected with a long express feeder. Roof-top PVs in the other hand, are often located at the top of housing estates, hotels, and sometimes hospital buildings, which unlike PVs park, it is often located closely

with the load, and commonly located within the urban/residential area.

Meanwhile, it is revealed that the effect of the *X/R* ratio of the DER connection affects the performance of the LVRT voltage support [3], [4], [23], [28]–[30], [50]. This is an interesting observation since many rooftop PVs are located in low voltage distribution connection. As such, many of grid-connected DERs, such as roof-top PVs, are connected on a low *X/R* ratio system. Further it is shown, for instance, by Alizadeh et al. in [20] through their simulation, the inverter-interfaced doubly-fed induction generator (DFIG) LVRT voltage support with reactive power regulation has better performance when connected on a grid with high *X/R* ratio systems, whereas contradictory result can be found on low *X/R* ratio grid [20]. This argument seems aligned with Martinez et al. in [127], Weise in [3], and Boemer et al. in [1]. The same argument can be found in many studies as well [28]–[30], [50], [110].

Moreover, it is revealed that among all of the LVRT voltage support types; the reactive power- (via additional reactive current injection - aRCI), the active power- (via additional active current injection - aACI), and the combinational active and reactive power-based LVRT voltage support (via additional active and reactive current - aRACI); the reactive power-based control that via aRCI is found to be the best preference for LVRT voltage support.

Even though some of the studies favour the use of the combinational active and reactive power-based voltage support (via aRACI), such as claimed in some studies [5], [19], it has been revealed that aRACI less effective to support the LVRT than aRCI under reverse power flow condition. Many low-voltage-connected DERs are situated in the urban and housing complex. The PVs frequently reach their peak operation during the daytime, a condition when the load is at its relatively low point. As such, the peak low-voltage-connected DERs will mostly be under reverse power flow situations.

Furthermore, LVRT voltage support via aACI and aRACI needs a continuous standby of ‘additional active reserve power' from the DER. As such, DER must be operated under the sub-optimum condition which is not economically advantaging [55]. Although this can be solved with the use of power storage, the introduction of *feed-in tariff scheme*, the employment of the EXIM (Export-Import) net meters [98]–[100], the utilisation of battery as power storage would be seen less appealing solution due to economic factor [77]. Therefore, it is strongly suggested that reactive power-based LVRT voltage support will be the likeliest possible option for distribution grid connected-DER as well.

However, as according to the studied literature review, the current grid codes do not yet consider the need of requiring low voltage connected DER's to provide LVRT voltage support as well. In the UK [36], [122], for the non-synchronous generating unit with a capacity lower than 1MW, the reactive power regulation is provided only for steady-state voltage support.

The Northern Ireland (SONI) [32] & The Republic of Ireland (EirGrid) [33] requires their Non-Centrally Dispatched Generating Units (ex. distributed roof-top PVs), to provide the reactive power regulation only for steady-state voltage support. the German Grid Codes also do not require their Non-Controllable Distributed Generating Unit to provide LVRT voltage support as well [126].

It has been shown the current DER LVRT requirements in many grid codes does not consider the aforementioned aspects – the fact the need to consider the effectiveness of the distributed connected-DER's aRCI in improving LVRT voltage sag. This gives us the potential research gap that is hence presented in the author's research. Investigating the relationship of the effective rate of the reactive power-based LVRT voltage support and the *X/R* ratio of the network is the main feature of the presented research.

Currently, the most extensive study that considers the impact of the *X/R* ratio of the grid to the DER connection has been found on studies which investigate the impact of the *X/R* ratio to the steady-state voltage stability of the DER-integrated grid. This topic has been presented in section 2.5. It provides valuable insights on how is the grid characters, which many researchers indicated by the *X/R* ratio of the grid, gives impact to the increment steady-state voltage of the grid-connected DER. It further presents valuable information about the method of estimating the steady-state voltage increment of the DER-connected grid under different *X/R* ratios. Through their analytical methodologies, along with their assumptions, such as; DER representation in their analysis, the representation of DER location with respect to the observed grid, the representation of the power supply which comes from the transmissions, and so on; the impact of different *X/R* ratios to the steady-state voltage increment of the DER-connected grid could be estimated. The formulation on assumptions and the approximations they made upon presenting their analytical methodologies are useful for constructing the thesis author's perspective on how the *X/R* ratio is impacting the steady-state voltage increment of the DER-connected grid. This valuable information is useful for helping for the thesis author to develop the proposed methodology for estimating the effectiveness of reactive power-based Low Voltage Ride-Through support of the DER, which is then presented in chapter 3.

Chapter 3 A Simple Method for Estimating the Effectiveness of Reactive Power-based Low Voltage Ride-Through Support of the DER

3.1 Introduction

Ancillary services, such as Distributed Energy Resources' (DERs') low-voltage ride-through (LVRT) voltage support through reactive power regulation, are becoming common. The DERs' reactive power-based LVRT voltage support is made to improve the short-term voltage stability in power systems. The regulation of the reactive power by adding their additional reactive current injection (aRCI), is made in proportion to the voltage sag. However, the effectiveness of the LVRT voltage support is very much influenced by the characteristic of the DER's grid connections.

Chapter 3 presents a methodology for estimating the effectiveness of voltage support. Unlike through the commonly computer-assisted approach, such as through dynamic RMS simulation, the benefit of the proposed methodology is on the computing process needed, which is much simpler since the construction of the dynamic DER modelling is not needed, and the evaluation of the effectiveness can be gained even when the grid information is incomplete. Grid planners often face problems relating to the grid data unavailability and challenges relating to the construction of the DER modelling. A more straightforward approach to do the estimation may help the task at hand. Therefore, from a practical viewpoint, the proposed methodology can support distribution system operators (DSOs), or a DER grid planner in the event they need to justify effective grid support requirements for fault ride-through on a distribution network.

Its accuracy is validated against typical positive-sequence-RMS simulation results obtained using PowerFactory DIgsilent software for well-characterised networks. There are several suitable RMS simulation tool that are reported in many studies. Aside from DIgsilent [3], [4], [43], [128], there are; ETAP [129], [130], NEPLAN [131], [132], PowerWorld [133], [134], PSS/E [135], [136], etc. The reason that the DIgsilent is chosen as the comparative tool is explained in section 3.7, particularly subsection 3.7.1.

3.2 The Background The Need for DER's Reactive Power-based LVRT Voltage Support Modelling

The implementation of Distributed Energy Resources (DERs) has become a significant concern especially when their high penetration is considered. It is well known that conventional power plants using synchronous generators can handle faults without the need to

be disconnected, while at the same time injecting short-circuit currents during voltage sag. This feature of synchronous generators is crucial in a power system helping to raise the voltage around the location of the fault [5]. Initially, DER's implementation and its impact related to the grid faults was not considered critical. Hence, as a means of protecting the electronic components of the DERs, these inverter-based generating units were disconnected during grid faults. Such a disconnection mechanism can be achieved through under-voltage protection. However, with the increasing penetration of DERs, the disconnection may become counterproductive. Usually, when a grid fault occurs, the fault's impact can be sensed in a wide area surrounding the fault, as it propagates away from the fault site throughout the power system. Consequently, this can lead to several DER units automatically tripping. Such disconnection in series of DER groups will result in a considerable cascading loss of electricity generation. Therefore, to avoid the problems mentioned above, with the ongoing plans to increase the penetration of DER units, DER with reactive power support on low-voltage ride-through (LVRT) is required.

The voltage sag improvement during LVRT through the reactive power support needs to be evaluated. As such, it is necessary for the DER grid planner to estimate the effectiveness of the reactive power support through modelling of DER along with its reactive power support.

3.3 Challenge of the Modelling

Evaluating the effectiveness of the reactive power support can be done through RMS simulation. However, using a detailed dynamic DER modelling in the simulation tool will increase the complexity of the models, and hence it increases the computational effort needed and data required. Contrarily, modelling power systems elements through an oversimplification may lead to a solution that does not adequately solving the problem that needs to be addressed. Examples of the oversimplification can be seen in many grid codes, whereas their DER requirements were originally studied and specified in simple system configurations at which either the transmission or the distribution system level was highly simplified [32]–[37], [40], [58], [113]. The accuracy of the integrated power system model in these studies may be significantly reduced to an extent it neglected the interaction of transmission and distribution systems with large amounts of DG [4] with advanced control features, such as their dynamic voltage support [23].

Compromising model both accuracy and simplicity of modelling power systems elements can be a laborious task. Hence, designing LVRT voltage support that should meet the desired needs, such as the magnitude, permitted duration of the lowest voltage sag and the balance/unbalance distribution matter, is highly influenced by the accuracy of the DER modelling of the corresponding grid, and the required data availability [3], [4], [14], [23], [51].

On determining LVRT voltage support and deciding the requirements of the minimum voltage sag that should be met and the voltage support that should be given, it is necessary to build a simulation of the grid including the DER models. Evaluating the effectiveness of the DER's LVRT voltage support through typical positive-sequence-RMS simulation commonly can be done when the required knowledge and the data availability to establish the simulation blocks of the DER modelling such as; photovoltaic array, DC voltage controller, Pulse Width Modulation (PWM) modelling, current controller, and the diagram block of the LVRT voltage support; are available [53]. When all previously mentioned information is at hand, the estimation could be successfully made through the RMS simulation.

It can be inferred that a laborious task is needed for estimating the effectiveness of the DER's LVRT voltage support. Moreover often on many occasions, the information needed is to construct the modelling incomplete and hence is often done through approximations. Hence on such situation, extensive work and knowledge to construct the DER modelling are needed.

3.4 The Key Contribution of the Proposed Methodology

The proposed methodology is made based on a simple phasor analysis, to estimate the effectiveness of the DER's reactive power-based LVRT voltage support effectively without the need of the extensive work and the knowledge on DER modelling that is commonly necessary when using dynamic RMS simulation. The proposed methodology can estimate the effectiveness of the DER's LVRT voltage support when it is highly influenced by the character of the DER connections - the *X/R* ratio of the network. It can further also cover several other aspects that have not been considered before, such as the increasing resultant steady-state voltage of the load bus where the DERs are connected, the short circuit impedance (Z_{SC}), the steady-state active and reactive power of the DER (P_{DER} and Q_{DER}), and the reactive power/aRCI setting (the value of the K-factor of the DER, where K-factor= $\Delta I_{reactive}/\Delta V$).

The proposed methodology offers simplicity since it does not require the knowledge on constructing the DER modelling and thus could avoid problem relating the DER data unavailability. Therefore, the main contribution of this study is a methodology and an approach to estimate the effectiveness of the LVRT voltage support that will benefit grid planning.

3.5 Analysis of DER's LVRT Voltage Support via aRCI on Different *X/R* Ratio

The proposed method is made to allow the estimation of the effectiveness of DER's LVRT voltage support via aRCI and is also capable of considering the effect of the *X/R* ratio of the system, steady-state active and reactive power of the DER (P_{DER} and Q_{DER}), and the rising resultant of the steady-state voltage of the DERs connected bus. To understand how the

proposed methodology works, it is best to understand firstly the effect of *X/R* ratio of the DER connection and then the estimation of the effectiveness of the DER's LVRT voltage support via aRCI, which are presented in the following sections.

3.5.1 The Effect of *X/R* Ratio of The DER Connection

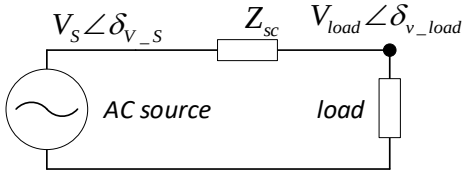

(a) Network diagram with Thévenin equivalent of grid without DER unit

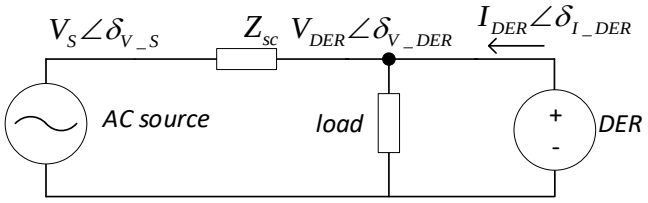

(b) Network diagram with Thévenin equivalent of grid with DER unit

Figure 3-1 Network diagram with the Thévenin equivalent of the grid, load, and DER unit

Let us consider the Thévenin equivalent network diagram as previously shown Figure 2-1 which is re-illustrated in Figure 3-1, whereas an AC voltage source $V_S \angle \delta_{V\_S}$ is defined as the external power source while a short-circuit impedance Z_{sc} (in this context, Z_{sc} can be referred as the transfer impedance Z_g as referred in Figure 2-1). Note that the definition of short-circuit impedance refers to the impedance between the location of the fault and the DER connection (the definition is detailed in chapter 3.3.2). A constant load representing the local load, along with its $V_{load} \angle \delta_{V\_load}$ is defined, as shown in Figure 3-1 (a). In Figure 3-1 (b), DER unit is connected to the distribution system, and thus a constant current $I_{DER} \angle \delta_{I\_DER}$ is present. In such a scenario, the steady-state voltage at the load bus ($V_{load} \angle \delta_{V\_load}$), is increased by ΔV. The risen steady-state voltage is defined as $V_{DER} \angle \delta_{V\_DER}$.

$$\Delta V = Z_{sc} I_{DER} \tag{3.1}$$

Suppose voltage ΔV has phase component 'x' as ΔV_x that in phase with the magnitude of $V_{load} \angle \delta_{V\_load}$ with δ_{V_load} as reference (as shown in Figure 3-2), then an orthogonal 'y' as the ΔV_y is defined perpendicular to the ΔV_x. As such, by neglecting the load, the two

components can be approximated as [137]

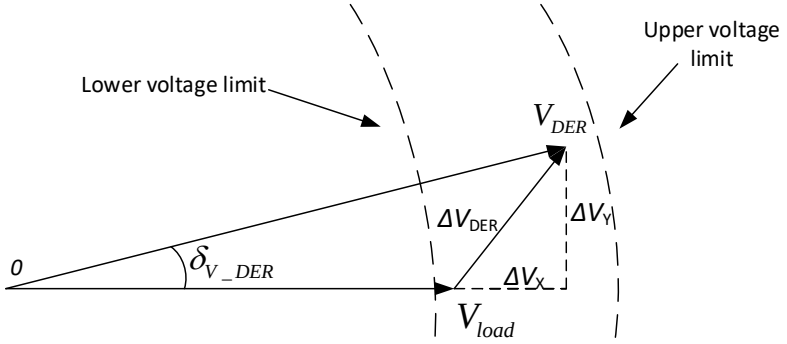

Figure 3-2 Phasor diagram of steady-state voltage change due to DER unit power [137]

$$\frac{\Delta V_x}{V_{LOAD}} \approx \frac{1}{S_{sc}}(P_{DER}\cos\varphi_{sc} + Q_{DER}\sin\varphi_{sc}) \tag{3.2}$$

$$\frac{\Delta V_y}{V_{LOAD}} \approx \frac{1}{S_{sc}}(P_{DER}\sin\varphi_{sc} - Q_{DER}\cos\varphi_{sc}) \tag{3.3}$$

with P_{DER} and Q_{DER}, and S_{sc} is the active and reactive power supplied by the DER unit, and short-circuit power of the corresponding system, respectively, whereas φ_{sc} is obtained from (3.4).

$$\tan\varphi_{sc} = \frac{X_{SC}}{R_{SC}} \tag{3.4}$$

X_{SC}/R_{SC} from the above equation is yielded from Z_{sc}. The definition of short circuit power S_{sc} is related to how does the external grid short-circuit power of the corresponding bus is formed (more detail in chapter 3.6). The value P_{DER} and Q_{DER} represent the value of the steady-state condition. -Q_{DER} represents DER's in the under-excitation setting. DER on unity power factor operation has zero Q_{DER}.

As illustrated in Figure 3-2, V_{DER} is obtained by adding (3.2) and (3.3) to V_{LOAD}, as follow

$$V_{DER}\angle\,\delta_{V\_DER} = (V_{LOAD} + \Delta V_X) + j\Delta V_Y \tag{3.5}$$

The phasor diagram of V_{DER} as shown in Figure 3-2, illustrates a situation where the steady-state voltage has risen due to DER connection and is within the voltage limit $V_{DER}\angle\,\delta_{V\_DER}$. It represents the voltage magnitude and phase at the load bus when the DER is connected. Therefore, ΔV_{DER} represents the voltage increment from $V_{load}\angle\,\delta_{V\_load}$ to $V_{DER}\angle\,\delta_{V\_DER}$. S_{DER} represent the apparent power of the DER. Also from (3.2), (3.3), and (3.5), it can be concluded that the steady-state voltage rise due to the DER connection, depends on the *X/R* ratio of the short-circuit impedance as well as the DER's normal operating settings.

Figure 3-3 [138] illustrate the effect of different *X/R* ratio (with the DER's normal operating settings) to the steady-state voltage rise at the DER connection. From this figure, it can be

concluded that the voltage rise due to the DER's presence is more apparent on lower voltage networks (assuming lower voltage connection has lower *X/R* ratio than high voltage connection), whereas in higher voltage level the effect of DER's presence is likely less observed. In Figure 3-3 V_{LOAD} (the voltage of the load bus without DER) is taken as the reference, whereas the V_{DER} is the voltage of the load bus with DER. Red, yellow, and green coloured line represent *X/R*>1, *X/R*=1, and *X/R*<1, respectively.

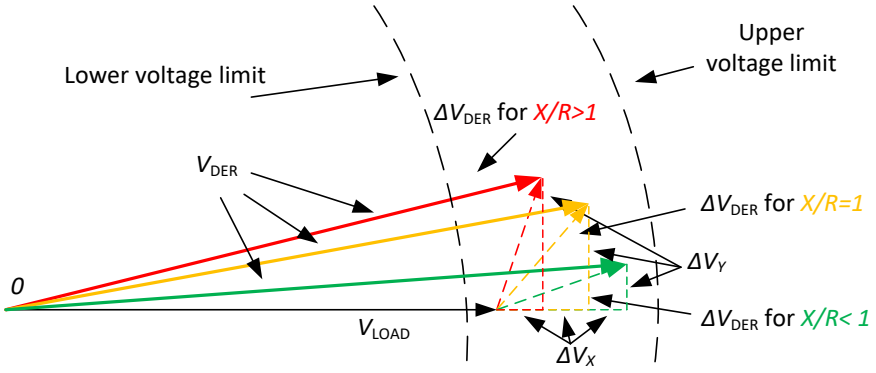

Figure 3-3 Phasor diagram of steady-state voltage rise due to the DER presence for different *X/R* ratios, by considering (3.2), (3.3), and (3.4) [138]

It can be seen when the DER penetrations increases, as presented from Figure 3-3, the magnitude of the steady-state voltage increment (V_{DER}) will reach voltage limit sooner when the DERs are connected on a low *X/R* ratio grid. Contrary results will happen when the DERs are connected on a high *X/R* ratio grid. It should be noted that the consideration of *X/R*>1, *X/R*=1, and *X/R*<1; as high 'high', 'medium', and 'low'; are presented for illustrations only, which intended to help better understand standpoint of the *X/R* ratio of the grid on affecting the steady-state voltage magnitude of the DER-connected grid.

It will be shown in the next section, the resulted phasor diagram as shown from Figure 3-3 helps us understand better how such the *X/R* ratio of the DER-connected grid affects the voltage sag improvement level during LVRT.

3.5.2 Estimating the Effectiveness of the DER's LVRT Voltage Support via aRCI

It is understood that DER's aRCI is perpendicular with their active current. Therefore according to [1], [5], if the DER is operated in unity-power factor, and assuming that the *X/R* ratio of the connection between the DER and the point-of-common-coupling (PCC) of the DER is negligible, the active current of the DER's normal operating setting is in phase with V_{DER} – implying that aRCI (I_{aRCI}) is perpendicular with 'V_{DER}'. Therefore, the effectiveness of I_{aRCI} during LVRT on different *X/R* ratio based on (3.4) by considering (3.2), and (3.3), can be observed in Figure 3-4. Further, in the Figure 3-4, it is observed DER's aRCI during LVRT

is more effective when the DER is connected at high voltage grid (high *X/R* ratio) rather than at low voltage grid (low *X/R* ratio). This can be observed in Figure 3-4, through 'a' (red, *X/R*>1), 'b' (yellow, *X/R*=1), and 'c' (green, *X/R*<1), whereas these 'a', 'b', and 'c' represent the voltage sag magnitude level of the grid with aRCI-enabled DER connections. The best voltage sag improvement is observed when the DER is connected to high *X/R* ratio grid ('a'). The least voltage sag improvement is observed when the DER is connected to low *X/R* ratio grid ('c'). The dashed line represents the voltage sag magnitude when the DER is not injecting aRCI ('No aRCI V_{DER}'), whereas the bold non-dashed line represents the voltage sag magnitude when the DER is injecting aRCI ('With aRCI V_{DER}').

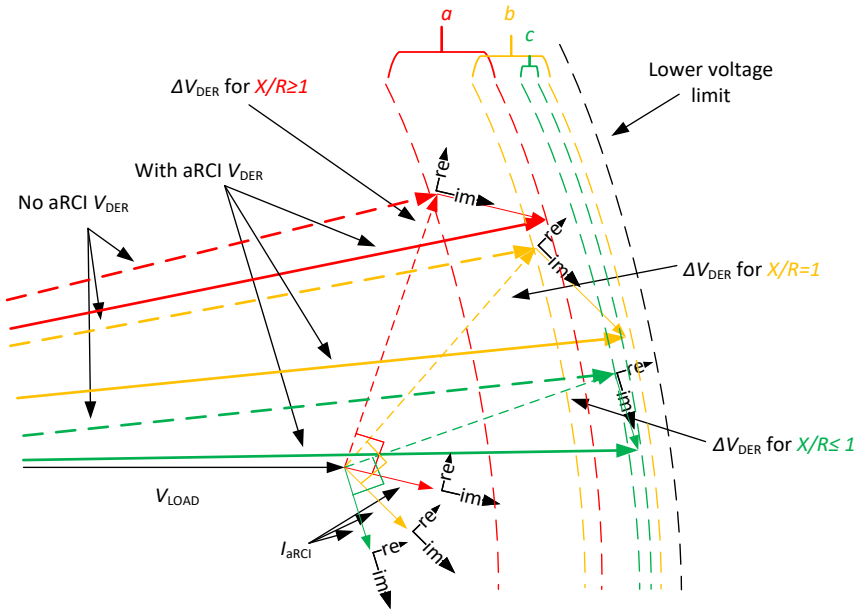

Figure 3-4 The effectiveness of aRCI during LVRT on different *X/R* ratio based on (3.4) by considering (3.2), and (3.3). a, b and c signs, at the top of the figure, represent voltage sag improvement level when the DER injects aRCI under different *X/R* ratio [138]

Figure 3-4 provides useful understanding for analysing the effectiveness of DER's LVRT voltage support via aRCI on different *X/R* ratio. Normally transient voltage control (for both enabling the system to do both LVRT and HVRT) via reactive power regulation (such as with static-VAR compensator (SVC), or STATCOM) is traditionally applied in the high-voltage transmission grid [3]. The impedance is dominated by the reactance element and therefore provides effective transient voltage control. At a lower voltage, however, such as in distribution system, whereas with low *X/R* ratio, in theory, could be less effective [11], although, from an economic point of view, it is preferable as discussed in chapter 2.6.6.

3.6 The Philosophical Understanding of The Reactive Current Injection

On transient voltage sag, the DER unit must inject an additional reactive power via reactive

current injection (aRCI) proportionally to the voltage deviation [3]. In principle, the operation of this support is based on pre-defined settings - a setting that is generally made/decided upon the DERs installation, or made based on the DSO's configuration standard. The support kicks in shortly following a detectable transient voltage sag to assist the local distribution load voltage. The support is done to keep devices that cannot ride through voltage sags on-line, such devices are loads and some 'passive' DER, remain connected to the grid [23]. As mentioned in chapter 2.7.1, the reactive power support depends on the voltage deviation during LVRT and is proportional to a gain, the K-factor [3].

As such, the philosophical understanding of the reactive current injection can be explained as follow. First, the magnitude of the aRCI is subject to a gain (K-factor setting). The higher the gain, the higher will be the magnitude of the aRCI. Further upon fault state, the voltage deviation that is used is input signal to the aRCI function, translates the magnitude level of the aRCI. Along with the K-factor setting, the aRCI is affected with the value of the voltage deviation. Note that the realisation of the aRCI injection is happened under transient condition, within order of milliseconds [139], whereas the 'state derivative' condition of the dynamic component of the aRCI function along with the DER modelling can be ignored [140]. In another word, upon estimating voltage sag at the fault location, it is possible to measure the improved voltage sag at the DER connection, without the need to measure the 'state derivative' of the dynamic properties of the DER. Assuming one knows the amount of the steady-state active power DER and the planned gain of the K-factor, without understanding the dynamic characteristic of the DER modelling fully, and even possibly without understanding fully the dynamic characteristic the local load, it is possible to measure the effectiveness of the aRCI on improving the voltage sag.

The proposed methodology in this study is made by underlying the philosophy as mentioned earlier and is made based on the understanding that is given from section 3.5. The idea about the 'state derivative' in dynamic RMS simulation will be understood better in the section 3.7.2 and will be later understood that the complexity of the 'state derivative' in dynamic RMS simulation can be omitted upon estimating the effectiveness of the aRCI through the proposed methodology.

3.7 Dynamic RMS Simulation on Power System Analysis (PSA) tool

Usually, the selection of the power system simulation tool is chosen to fit the purpose of the usage. The purpose often falls into four categories as follows [141]. *Power system analysis (PSA)*, *operation decision support*, *investment decision support*, and *scenario decision support*. RMS simulation is categorised as PSA as it usually dealing with power flows, fault level studies, and dynamic stability. Several PSA tools have been developed to study the

performance of power systems; nevertheless, the problem is how effective these tools can be applied in the design and simulation of electrical power systems.

3.7.1 Brief Review on PSA Tool

The effectiveness of the selected tools can be considered on; *deployability* - how easily a tool can be made available to the designer taking into consideration compatibility with the existing infrastructure, *simplicity* - the tool should offer design and analysis methodologies necessary to handle the complexity system at minimum effort, and *the modularity and expandability* – structured according to a clear hierarchy that enables future revision and expansion of the software [142].

Further, as mentioned in [142], traditional PSA tools, such as PSS/E and Eurostag, for instance, though they are capable of performing all fundamental types of power system analysis such as load flow, small signal stability, dynamic simulation, and voltage stability studies, it suffer from their closed architecture where it is very difficult to observe or even modify most of the component models. User-defined models can be added in these tools but in the form of low-level Fortran code - a complicated process which may be prone to user/human error. Moreover, on Fortran environment, built-in shelf libraries; such as predefined-generator and -motor modelling; do not exist. As such, it has to be entirely designed by the user. Also, traditional PSA tools suffer from their limited debugging capabilities; hence, it becomes very difficult for the software to detect the source of the programming errors especially from the user designs.

Modern PSA tools, such as ETAP, PowerWorld, NEPLAN and DigSilent PowerFactory, have flexible structure to allow more straightforward addition of new components, such as manufacturer-based models. It even allows the user to add their model much affordable - as affordable as building a model in the MATLAB Simulink. Plus, most of these modern PSA tools have been used for wind and photovoltaic integration studies [43], [130], [143].

Most of these tools have research or student license, which claimed to be cheaper than their regular license, though, it is not disclosed on their webpage. DigSilent PowerFactory, however, discloses the research license price for 50 euros per year [144]. Further, The University of Southampton facilitated the thesis author to get access for DigSilent PowerFactory training for renewable integration in Germany. Thus, with such access being given to the author by The University of Southampton, DigSilent PowerFactory is chosen as a comparative tool for the RMS simulation.

3.7.2 Common Procedure on Simulating Transient Stability in The Commercial Software Tools

The procedure of transient stability simulation using commercially available simulation tools such as Simulink and DIgsilent is discussed here.

LVRT study is usually considered as short transient stability that is originated from a short circuit fault. Similar to other transient studies, like load shedding, generator shedding, upon simulating in a simulation tool (such as in Simulink or Digsilent), LVRT is done through two processes. It is firstly initialised by a load flow computation. The load flow computation is done to profile **the steady-state bus voltage of the all corresponding buses**. After all steady-state bus voltages are profiled, then the next process, the transient computation through dynamic RMS simulation is done. During LVRT simulation, several elements, such as the dynamic models of generators, loads, and possibly the DERs, are included to perform the dynamic simulation. The dynamic elements characterise the system behaviour during transient simulation.

A faulty condition is defined as the system under short circuit conditions. Faulty condition due to short circuits such as three-phase fault, two-phase to a neutral fault, and so on, is indicated by sudden changes in the system's voltage profile (transient voltage deviation). The transient voltage deviations can be estimated through short-circuit analysis [140]. The elements in the system that have dynamic characteristics, such as the DERs, the generators, etc. which are connected to the corresponding buses, will react to the sudden **transient voltage changes on all** corresponding buses. The magnitudes of **transient voltage changes of the corresponding buses** depend on their **locations respective to the faulty bus**, and their **steady-state voltage value prior fault condition (pre-fault steady-state voltage)** [139].

On simulating dynamic DER's transient stability, DER's **pre-fault steady-state voltage** is obtained from steady-state power flow computation. These initial conditions represent the steady-state operating point at the beginning of the simulation, fulfilling the requirements that the derivatives of all state variables of loads, machines, controllers, etc., are zero [139]. Thus estimating steady-state voltage rise due to DER connection on DER grid planning is necessary before simulating DER's dynamic transient stability.

On typical procedure/sequence on simulating transient stability of a system, such as in DIgsilent for instance [139], a transient condition due to the system's short circuit in the dynamic RMS simulation is expressed by the **transient voltage changes**. Thus, during the fault, the resulted **transient voltage changes** are vital since they will define **the initial state on the dynamic transient simulation**. This 'initial state' that is expressed by the **transient**

voltage changes are used **to initiate transient conditions for all power system elements including all controller units and mechanical components** [139]. As such, in the simulation, through the transient voltage changes, dynamic RMS simulation could be processed, and hence the dynamic response of all dynamic element (as responding the voltage changes) could be observed. Figure 3-5 illustrate the typical procedure of transient stability simulation.

The computation starts with the estimation of **the steady-state voltage of all corresponding buses (**$V_i \angle \delta_{V\_i}$). Typically this is done through the Newton-Raphson method [139]. In the DIgsilent simulation tool, for example, the simulation uses an iterative procedure to solve AC power flows. Next, the short circuit current at the faulted location ($I_f \angle \delta_{I\_f}$) is estimated. Knowledge of **the impedance of network components** is necessary for the current calculation [145]. For a three-phase fault case, the three-phase components are balanced, and hence only positive sequence impedance is needed. For asymmetrical fault case, however, positive negative and zero sequence impedance are necessary. After the sequence impedance of the network components is estimated, the short-circuit current at the faulted location ($I_f \angle \delta_{I\_f}$) is computed. From $I_f \angle \delta_{I\_f}$, **short circuit current contribution from the corresponding buse**s ($I^i{}_{cont\prime\_f} \angle \delta^i{}_{I\_cont\prime\_f}$) could be estimated [140]. The calculation of **short circuit current contribution from the corresponding buses (**$I^i{}_{cont\prime\_f} \angle \delta^i{}_{I\_cont\prime\_f}$**)** is then obtained through a short-circuit fault computation [146]. Then, the **transient voltage changes (**$V^i{}_f \angle \delta^i{}_{V\_f}$**)** of all corresponding buses are estimated from **the positive sequence of the steady-state voltage** with **voltage sag (**$V_i \angle \delta_{V\_i} - \Delta V^i{}_f \angle \delta^i{}_{V\_f}$**)** [146].

In the DIgsilent tool [139], the transient voltage changes ($V^i{}_f \angle \delta^i{}_{V\_f}$) is converted into ($v^i{}_{f_d} + v^i{}_{f_q}$) to ease the computation of the derivative state of all corresponding element, that is often in '*dq* representation' form. The 'dq' representation will allow for processing the interactions with the state variables of the dynamic elements, such as the DER units, in order to produce the dynamic response of the system. The state variables of the DER units represented in DIgsilent, using the '*dq* form', have zero derivatives in pre-fault condition. On **transient voltage changes** ($v^i{}_{f_d} + v^i{}_{f_q}$), non- zero derivatives of the state variables of the DER exists. As such during **transient voltage changes**, the value of the state variables of the DER units, such as the state variables of the DER's phase-locked loop, *and the dq*-current loop controller, derivate iteratively with respect to **the transient voltage changes** as to produce the dynamic response of the DER.

Unlike the process described above which implemented in DIgsilent, the following the proposed method does not need to fulfil the requirements to compute the derivatives of all state variables. Thus the proposed methodology offers simplicity, but it is still able to retain

fairly acceptable accuracy.

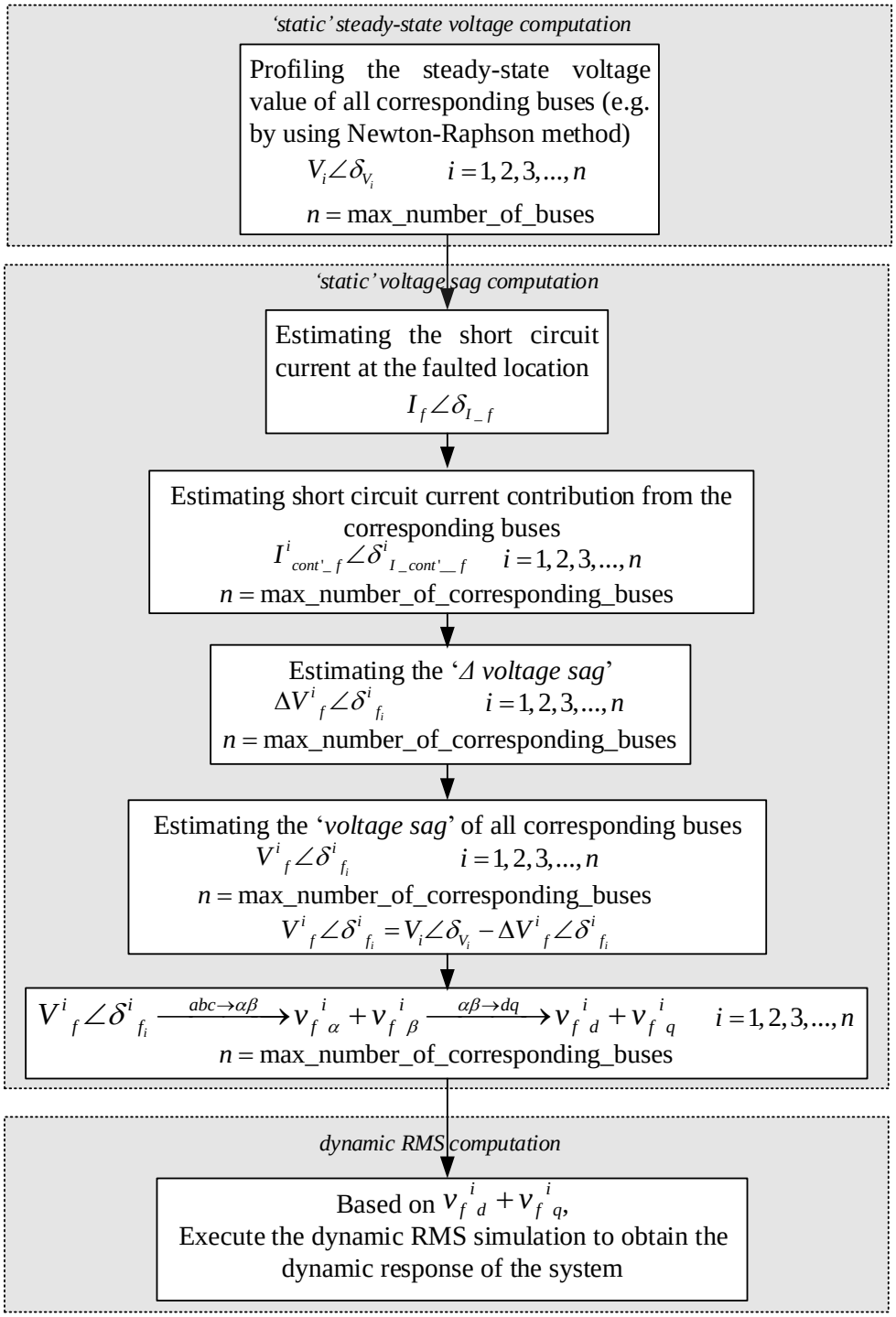

Figure 3-5 Typical procedure of transient stability investigation, as implemented in available commercial software tool such as DIgsilent.

3.8 Proposed Simple Method for Analysing The Effectiveness of the DER's Reactive Support

The methodology proposed here has **five** distinct steps. First, all loads in the network of interest are represented by equivalent impedances. Secondly, an equivalent Thevenin circuit of the

network is established. Thirdly, the steady-state voltage rises due to DERs connections, $\Delta V_{DER} \angle \Delta\varphi_{DER}$, is estimated using a modified superposition analysis. Fourthly, the potential voltage sag in the observed network with DER connections needs to be estimated. Finally, the effectiveness of the DER's reactive power support may be estimated.

The basic principle of the proposed method is that the observed part of the network needs to be transformed into a relatively simplified equivalent impedance description. On a condition which all no-DER-connected nodes have steady-state voltage closely to its normal operating setting, 1 per unit, according to Elrayyah et. al in [101], one could estimate the steady-state voltage rise of the DER connected node through an approach that is presented in the first to third step in the proposed methodology, as in the following explanation. The estimation of steady-state voltage rise on DER connected node proposed by Elrayyah et al. in [101] is claimed to have reasonable accuracy.

3.8.1 First Step

Consider a system with several nodes representing load points, e.g. housing estates, and its representation as shown in Figure 3-6. Each node denotes an aggregated loading point (at 220V consumer level voltage). The 'external network', outside the observed portion of the network, can be illustrated as an 'infinite node', which in this calculation serves as a 'voltage source'. Furthermore, suppose the planned location of the DER is at the most remote node (n+2). Then, assuming the steady-state voltage profiles of all nodes are available through local measurements, the average peak and low active and reactive power consumptions (P_{avg_load} and Q_{avg_load}) may be profiled. Hence the equivalent load impedance of each loading point (node), Z_{avg_load}, can be expressed as

$$Z_{avg\_load} \angle \delta_{avg\_load} = \frac{V_{load} \angle \delta_{load}{}^2}{(P_{avg\_load} + jQ_{avg\_load})^*} \tag{3.8}$$

where $V_{load} \angle \theta_{load}$ is obtained from the steady-state positive sequence (phase to phase) voltage of the node. Assuming this analysis is for grid planning, $V_{load} \angle \delta_{load}$ can be easily obtained and is the steady-state nominal voltage before the DERs are implemented. The rising steady-state nominal voltage due to the presence of the DER will be considered in the third step.

The aggregated DERs are represented as current sources. The circuit diagram using the impedance representation of the loads, along with the DERs as current sources, is shown in Figure 3-7.

After the impedance representation is completed, a single line diagram of the observed system

can be represented as shown in Figure 3-7. The circuit can now be used for the second step of establishing the equivalent Thevenin circuit of the network.

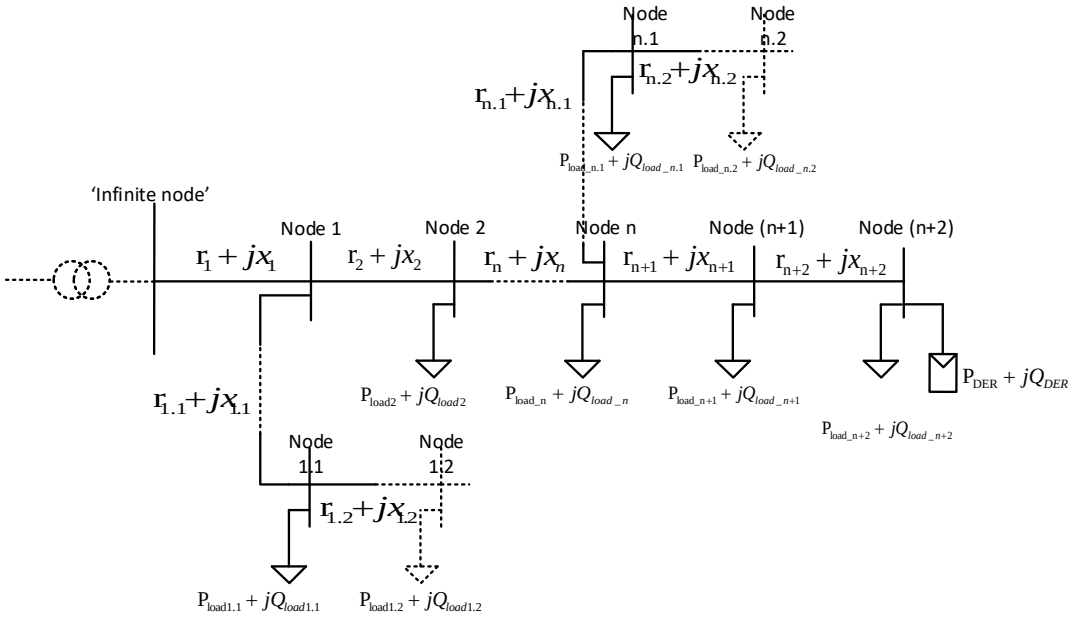

Figure 3-6 an example distribution part of a network

3.8.2 Second Step

To obtain the equivalent Thevenin circuit representation of the network, several stars to delta transformations (Y to Δ) may be necessary. These transformations are detailed as follows and are shown graphically in Figures 3-8 (a) to (d). Each external branch is first transformed into Z_{b1} and Z_{b2}. After the transformed star impedance is obtained, Z_{b1} and Z_{b2} are connected in parallel with respective nearby impedances (Figure 3-8 b).

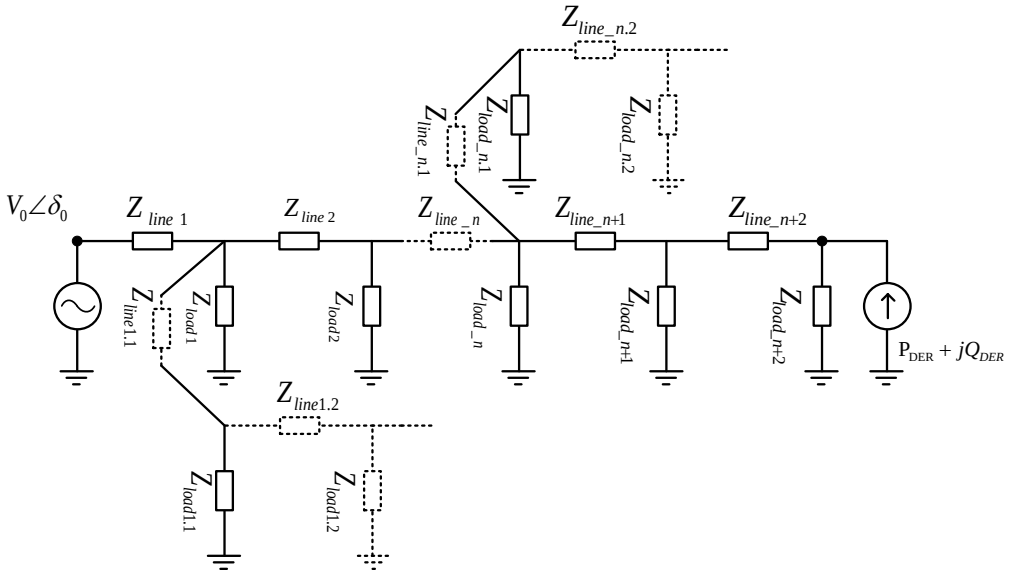

Fig. 3-7 transforming all active and reactive power load into impedance forms

Note that $Z_{ext\_grid} \gg Z_{v2}$, since Z_{ext_grid} is the overall impedance of the outer part of the observed network (external grid). Therefore, one can assume that the impedance of the infinite bus (the outer part of the observed network) can be represented by Z_{ext_grid}, as shown in Figure 3-8 (d) [101].

Essentially, the external grid represents an 'external element' that is outside of the system under consideration (this can be referred to as an element outside the HV side of the transformer which is connected to the 'infinite node' in Figure 3-6) [101]. However, for transient stability analysis, one should define it as an existing element, in the form of aggregated properties that affect the calculations [147], [148]. These properties include the short-circuit current of the 'external grid' I''_k, the positive sequence nominal voltage $V_0 \angle \delta_0$ and its positive sequence *X/R* ratio of the 'external grid' [148]. Technically I''_k is the value of the short-circuit current at the feeder connection point, which in this sense is the 'infinite node' in Figure 3-6. So if I''_k is known, then the equivalent impedance Z_{ext_grid} of the external grid at the 'infinite node' should be determined by

$$Z_{ext\_grid} = \frac{c_{factor} \cdot V_0}{\sqrt{3} . I''_k} \tag{3.9}$$

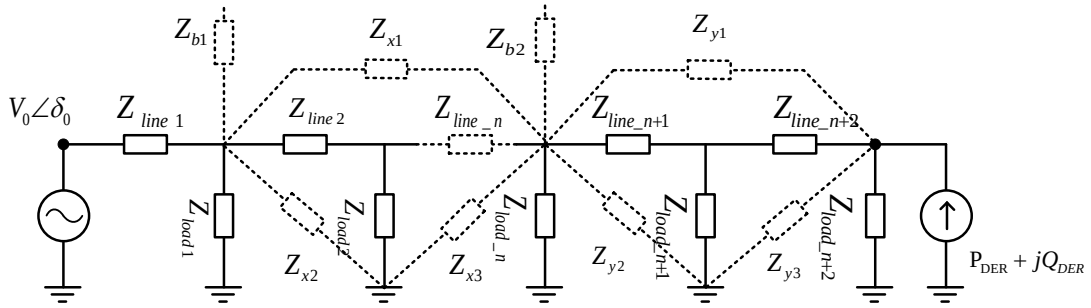

Fig. 3-8 (a)

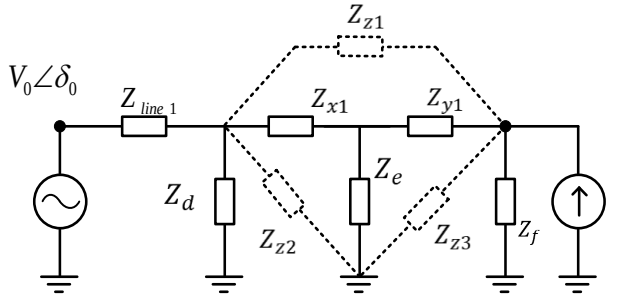

$Z_d = Z_{load1} // Z_{x2} // Z_{b1}$ $\quad P_{DER} + jQ_{DER}$

$Z_f = Z_{y3} // Z_{load\_(n+2)}$

$Z_f = Z_{b3} // Z_{x3} // Z_{load\_n} // Z_{y2}$

Fig. 3-8 (b)

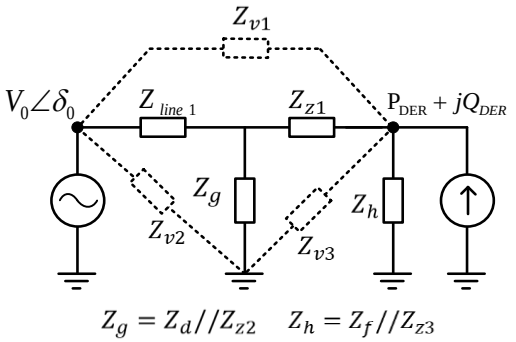

Fig. 3-8 (c)

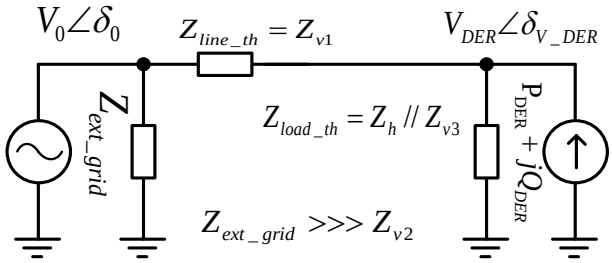

Fig. 3-8 (d)

Figure 3-8 an example of impedance transformation of the example diagram circuit into the equivalent Thevenin circuit

where c_{factor} represents a voltage correction factor for the measured positive sequence voltage at the external grid [147]. The calculation of the external grid impedance (Z_{ext_grid}) is made with the help of the equivalent voltage source (V_0) of the external grid. Meanwhile, the value of the V_0 should reflect the conditional status of the operational data of the load of the consumers, tap-changers position of transformers, excitation of generators, and so on. Requiring all conditional status of the operational data, for estimating Z_{ext_grid}, would impose a computational burden, and sometimes could be tedious especially some of the data are hard to obtain. As such, the present of c_{factor}, as explained in [147], is meant to help Z_{ext_grid} measurement in equation (3.9)

If the *X/R* ratio is known as well, then R_{ext_grid} and X_{ext_grid} could be estimated as

$$X_{ext\_grid} = \frac{Z_{ext\_grid}}{\sqrt{1+\left(\frac{X}{R}\right)^{-2}}} \tag{3.10}$$

with

$$R_{ext\_grid} = \left(\frac{X}{R}\right)^{-1}.X_{ext\_grid} \tag{3.11}$$

In the absence of national standards, it seems reasonable to choose a voltage correction factor between 0.95 and 1.10 [147]. However, for the simplicity of our study, the value of 1 has been

chosen. Z_{ext_grid} can be used to represent the 'characteristic' of the external grid. If the intention is to estimate I''_k, for example through the well-known short circuit numerical analysis [147], [148], this can be done by isolating the observed grid from the node were the HV transformer is feeding to, and then perform a short-circuit calculation. Then one can obtain I''_k, the short-circuit *R*, and the short-circuit *X* so that the *X/R* ratio can easily be found. Alternatively, these properties can be obtained through the blueprint of the grid data [148]. $V_0 \angle \delta_0$ is obtained from the LV side of the transformer in Figure 3.6. For simplicity, $V_0 \angle \delta_0$ is taken as a reference, and thus δ_0 is set 0.

3.8.3 Third Step

Once the Thevenin circuit is successfully obtained, the third step of the proposed methodology could be initiated. The purpose of the third step is to estimate the increased steady-state voltage due to the DER's presence ($V_{DER} \angle \delta_{V\_DER}$). $V_{DER} \angle \delta_{V\_DER}$ needs to be calculated since it represents the steady-state voltage value of a DER-connected node, on a condition prior voltage sag. As explained in section 3.4 the voltage sag improvement valuation is obtained by comparing the voltage sag with and without the reactive support, which means, it requires the increased steady-state voltage $V_{DER} \angle \delta_{V\_DER}$.

From this, the resultant of the additional reactive current injection aRCI (ΔI_{Q_DER}, later on) is determined, in step four. $V_{DER} \angle \delta_{DER}$ is obtained through calculation which is described in the following paragraph.

To estimate the increased steady-state load bus voltage due to the DER connection ($\Delta V_{DER} \angle \Delta\delta_{V\_DER}$), first, the simplified Thevenin Circuit Diagram as in Figure 3-8 (d), that was used for our superposition analysis, is transformed into two points of reference, as shown in Figure 3-9 (a and b). The first reference (Figure 3-9 a) considers the external grid voltage source as a short circuit, while the second reference (Figure 3.9 b) treats the DER as an open source. Note that to do the superposition analysis, the DER is commonly represented as a current source. The representation of the DER as a current source is shown in the first reference (Figure 3-9 a). Assuming that for grid planning the rated active and reactive power of the DERs of $P_{DER} + jQ_{DER}$ is obtained, it is very likely $I_{DER} \angle \delta_{I\_DER}$ is obtainable without knowing the nominal voltage at the load node that is already connected with the DERs ($V_{DER} \angle \delta_{V\_DER}$), which is the aim of the calculation. Therefore, to obtain $V_{DER} \angle \delta_{V\_DER}$, a modification of the calculation is necessary. The modification can be accomplished by assuming the DER element to be a negative load, or defining the DER's element as 'negative impedance'.

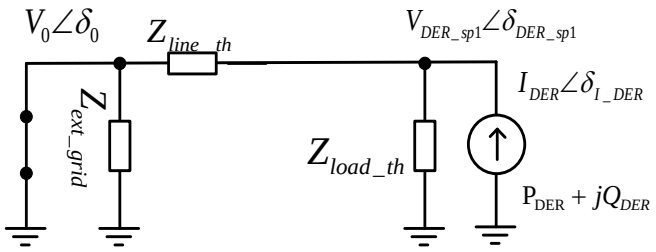

(a) Superposition analysis by using External grid as a source

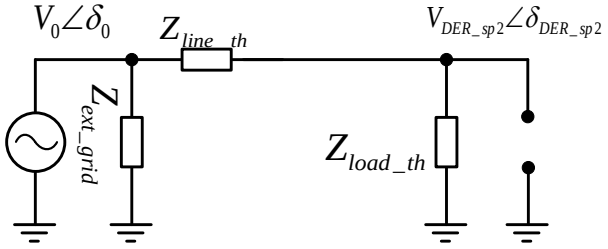

(b) Superposition analysis by using DER as a source

Figure 3-9 (a and b) Superposition analysis using the simplified Thevenin Circuit Diagram from the second step

Treating the DER element as a negative load is a common approach [2], [15], [149]. Defining the DER's element as 'negative impedance', for steady-state voltage rise calculations due to DER's presence, is not as accurate as when the DER is defined as a ZIP model [54]. However, defining the DER element as a negative load is still acceptable for a steady-state voltage rise estimation for non-complex systems. The network simplification made in the second step is used here again.

First, the condition when the DER is present while the grid reference node is assumed to have zero voltage (Figure 3-9 a) is considered. Under this condition, the steady-state voltage at the Thevenin load node $V_{DER\_sp1}\angle\,\delta_{DER\_sp1}$ may be found as

$$V_{DER\_sp1}\angle\,\delta_{DER\_sp1} = (I_{DER}\angle\,\delta_{I\_DER}).\frac{Z_{load\_th}.Z_{line\_th}}{Z_{load\_th}+Z_{line\_th}} \tag{3.12}$$

The second case represents a condition where the grid reference node is considered while the DER is assumed to have zero current (open circuit) (Figure 3-9 b). Therefore, the steady-state voltage at the Thevenin load node $\Delta V_{DER\_sp2}\angle\,\Delta\delta_{DER\_sp2}$ may be obtained from

$$V_{DER\_sp2}\angle\,\delta_{DER\_sp2} = (V_0\angle\,\delta_0).\frac{Z_{load\_th}}{Z_{load\_th}+Z_{line\_th}} \tag{3.13}$$

The actual increased steady-state voltage $V_{DER}\angle\,\delta_{DER}$ is then obtained by combining equations (3.12) and (3.13)

$$V_{DER}\angle\,\delta_{V\_DER} = \left(V_{DER_{sp1}}\angle\,\delta_{DER_{sp1}}\right) + (V_{DER\_sp2}\angle\,\delta_{DER\_sp2}) \tag{3.14}$$

Upon grid DER planning, if the DER's capacity plan is defined with active and reactive power ($P_{DER} + jQ_{DER}$), then $V_{DER\_sp1}\angle\,\delta_{DER\_sp1}$ in (3.12) cannot be obtained, as to find $I_{DER}\angle\,\delta_{I\_DER}$ the actual increased steady-state voltage $V_{DER}\angle\,\delta_{V\_DER}$ is needed. Therefore, as an alternative, from $P_{DER} + jQ_{DER}$, one could treat it as a negative load $-(P_{DER} + jQ_{DER})$. Then the $Z_{load\_th}\angle\theta_{load\_th}$ is modified into $Z_{loadDER\_th}\angle\theta_{loadDER\_th}$ as follows

$$Z_{loadDER\_th}\angle\theta_{loadDER\_th} = \frac{V_{load}\angle\delta_{V\_load}{}^{2}}{(P_{load\_th} - P_{DER} + jQ_{load\_th} - jQ_{DER})^{*}} \tag{3.15}$$

Here, $V_{load}\angle\delta_{V\_load}$ is the steady-state voltage of the load node without the DER connections. In a real situation, obtaining $V_{load}\angle\delta_{V\_load}$ can be done through voltage inspection at the local bus-station panel.

Note that in the second step the equivalent load is still represented by $Z_{load\_th}\angle\theta_{load\_th}$. Then in (3.15), $Z_{load\_th}\angle\theta_{load\_th}$ is transformed into a form of $P_{load\_th} + Q_{load\_th}$ by simply using (3.8). After $P_{load\_th} + Q_{load\_th}$ is obtained, (3.15) is substituted to (3.13). $\frac{Z_{load\_th}}{Z_{load\_th}+Z_{line\_th}}$ in (3.13) describes the overall impedance that represents both the load and the DER element. This modification yields the actual increased steady-state voltage $V_{DER}\angle\,\delta_{V\_DER}$ as shown below

$$V_{DER}\angle\,\delta_{V\_DER} = (V_0\angle\,\delta_0).\frac{Z_{loadDER\_th}\angle\theta_{loadDER\_th}}{Z_{loadDER\_th}\angle\theta_{loadDER\_th}+Z_{line\_th}} \tag{3.16}$$

The steady-state voltage rise due to the DER connection could then be estimated using the above equation. The results from this approach are validated by simulations using PowerFactory DIgsilent, as presented in chapter 3.7.

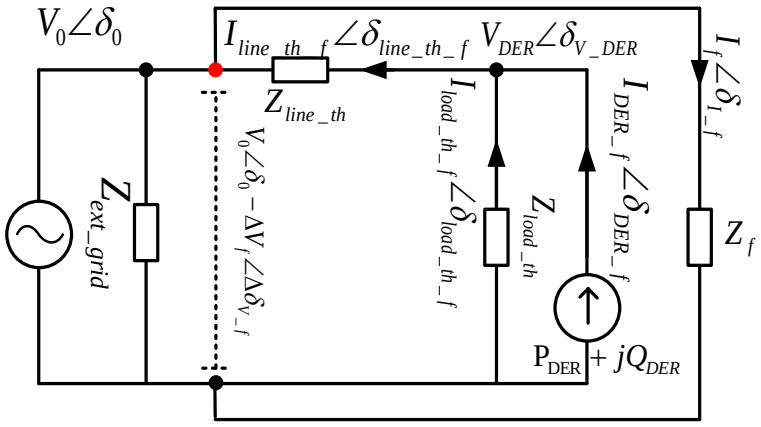

Figure 3-10 representation of the observed system under the faulty condition

3.8.4 Fourth Step

With $V_{DER}\angle\,\delta_{V\_DER}$ now calculated, the fourth step can be undertaken. This step estimates the potential voltage sag at the DER's connection node ($V_{DER\_f}\angle\,\delta_{V\_DER\_f}$). As mentioned in the introduction, a 3-phase transmission line fault is used as an illustration. Suppose a transmission fault occurs somewhere in the outside part of the observed network and causes a voltage sag at the 'infinite node' in Figure 3-6, as such that it cause the voltage at the 'infinite node' to drop. The fault estimation can be done using a conventional symmetrical component fault analysis. The impedance fault Z_f includes the effect of the transmission line on the voltage drop at the observation point (represented as $V_0\angle\,\delta_0 - \Delta V_f\angle\Delta\delta_{V\_f}$ in Figure 3-10). The fault is shown as a red dot in Figure 3-10. Note that since a 3-phase fault is used to illustrate the method, the observed-system representation is given for the positive sequence only. In Figure 3-10 $I_f\angle\,\delta_{I\_f}$ represents the short circuit current contribution from ($V_0\angle\,\delta_0 - \Delta V_f\angle\Delta\delta_{V\_f}$), $I_{line\_th\_f}\angle\,\delta_{I\_line\_th\_f}$ is the short circuit current contributed from the line, $I_{Ioad\_th\_f}\angle\,\delta_{I\_Ioad\_th\_f}$ is the short circuit current contributed from the load, while $I_{DER\_f}\angle\,\delta_{I\_DER\_f}$ is the short circuit current contributed from the DER.

Before estimating $V_{DER\_f}\angle\,\delta_{V\_DER\_f}$, the knowledge of $I_{line\_th\_f}\angle\,\delta_{I\_line\_th\_f}$ is required. However, the short circuit current $I_f\angle\,\delta_{I\_f}$ is needed in order to get $I_{line\_th\_f}\angle\,\delta_{I\_line\_th\_f}$. It can be seen from Fig. 6 that $I_f\angle\,\delta_{I\_f}$ could be obtained from

$$I_f\angle\,\delta_{I\_f} = \frac{V_0\angle\,\delta_0}{Z_{3ph\_th}+Z_f}.\frac{1}{\sqrt{3}} \tag{3.17}$$

with

$$Z_{3ph\_th} = \left(Z_{line\_th} + Z_{loadDER\_th}\right)//Z_{ext\_grid} \tag{3.18}$$

Note that $Z_{loadDER\_th}$ is obtained from (3.15) as previously explained. Then, by using the same Figure 3-10, $I_{line\_th\_f}\angle\,\delta_{I\_line\_th\_f}$ can be found as

$$I_{line\_th\_f}\angle\,\delta_{I\_line\_th\_f} = \frac{Z_{ext\_grid}}{Z_{ext\_grid}+Z_{line\_th}+Z_{loadDER\_th}} * I_f\angle\,\delta_{I\_f} \tag{3.19}$$

Once $I_{line\_th\_f}\angle\,\delta_{I\_line\_th\_f}$ is obtained, then $V_{DER\_f}\angle\,\delta_{V\_DER\_f}$ can be estimated by first calculating $\Delta V_{DER\_f}\angle\,\Delta\delta_{V\_DER\_f}$

$$\Delta V_{DER\_f}\angle\,\Delta\delta_{V\_DER\_f} = \sqrt{3}.Z_{loadDER\_th}.I_{line\_th\_f}\angle\,\delta_{I\_line\_th\_f} \tag{3.20}$$

and then finding $V_{DER\_f}\angle\,\delta_{V\_DER\_f}$ as

$$V_{DER\_f}\angle\,\delta_{V\_DER\_f} = V_{DER}\angle\,\delta_{V\_DER} - \Delta V_{DER\_f}\angle\,\Delta\delta_{V\_DER\_f} \tag{3.21}$$

Note that $V_{DER}\angle\,\delta_{V\_DER}$ was obtained in the third step, see (3.16).

3.8.5 Fifth Step

After $V_{DER\_f}\angle\,\delta_{V\_DER\_f}$ has been estimated, the fifth step of the proposed methodology can be triggered. The magnitude of the aRCI (ΔI_{Q_DER}) can be estimated. The aRCI during the LVRT, ΔI_{Q_DER}, is defined as

$$\Delta I_{Q\_DER} = K_{I_q}.\frac{|\Delta V_{DER\_f}|\mp V_{db}}{V_0} \tag{3.22}$$

where K_{I_q} is the *K*-factor as explained in Figure 2-11 (chapter 2.7.1). The DER's reactive current I_{Q_DER} during LVRT is described by

$$I_{Q_{DER}} = I_{q_{ref}} = \begin{cases} I_{Q\_DER\_prefault} + \Delta I_{Q\_DER}\,, -I_{max} \le I_{Q\_DER} \le I_{max} \\ I_{max},\ -I_{max} > I_{Q\_DER} > I_{max} \end{cases} \tag{3.23}$$

$I_{Q\_DER\_prefault}$ is the DER's pre-fault reactive current that is simply obtained from

$$I_{Q\_DER\_prefault} = I_{DER_{prefault}}.\cos(\varphi) \tag{3.24}$$

where φ is

$$\varphi = tan^{-1}\left(\frac{imaginary(S_{DER}{}^{*})}{real(S_{DER}{}^{*})}\right) + \delta_{V\_DER\_f} \tag{3.25}$$

while $I_{DER_{prefault}}$ is the DER's pre-fault current

$$I_{DER_{prefault}} = \frac{S_{DER}}{\sqrt{3}.(V_{DER}\angle\,\delta_{V\_DER})^{*}} \tag{3.26}$$

Here, $\mp V_{db}$ (equation (3.22)) represents the voltage dead-band in per unit, as illustrated in Figure 2-11 (chapter 2.7.1). However, since our investigation is concerned only with the effectiveness of the aRCI, for simplicity, the voltage dead-band is omitted. When the DER is injecting reactive current the active current I_{P_DER} during LVRT is given by

$$I_{P\_DER} = I_{d\_ref} = \sqrt{{I_{max}}^2 - {I_{Q\_DER}}^2} \tag{3.27}$$

The application of the dead-band is often made to prevent the DER's inverter to be at risk of overcurrent and, thus, overheating due to this reactive control strategy [3]. In (3.27) $I_{max} = 1$. Hence the DER current during LVRT $I_{DER\_f}\angle\,\delta_{I\_DER\_f}$ can be defined as

$$I_{DER}\angle\,\delta_{I\_DER} = I_{P\_DER} + jI_{Q\_DER} \tag{3.28}$$

However, it should be noted that $I_{P\_DER} + jI_{Q\_DER}$ in (3.22-3.27) is defined on the stationary reference frame. To represent this current in the grid synchronous reference frame, $I_{P\_DER} +$

jI_{Q_DER} has to be synchronised with the grid frequency. Normally this is done [150] by converting (3.28) into

$$I_{DER}\angle\,\delta_{I_{DER}} = \left(I_{d_{ref}}\cdot\cos\theta' - I_{q_{ref}}\cdot\sin\theta'\right) + j\left(I_{d\_ref}\cdot\sin\theta' + I_{q\_ref}\cdot\cos\theta'\right) \quad (3.29)$$

whereas $\cos\theta'$ and $\sin\theta'$ relate to the dq/stationary reference frame of the DER. In practice, this procedure can be done by the phase-locked loop (PLL) device of the DER's inverter. In our method, $\cos\theta'$ and $\sin\theta'$ are represented as follows

$$\cos\theta' = \frac{real(V_{DER\_f}\angle\,\delta_{V\_DER\_f})}{absolute(V_{DER\_f}\angle\,\delta_{V\_DER\_f})} \quad (3.30)$$

$$\sin\theta' = \frac{imaginary(V_{DER\_f}\angle\,\delta_{V\_DER\_f})}{absolute(V_{DER\_f}\angle\,\delta_{V\_DER\_f})} \quad (3.31)$$

Note that the real and the imaginary parts of $I_{DER}\angle\,\delta_{I\_DER}$ in (3.29) is the orthogonal axes of the synchronous reference frame. Thus I_{Q_DER} in (3.26) may be defined as the q-axis current reference of the DER (I_{q_ref}), whereas I_{P_DER} in (3.27) as the d-axis current reference (I_{d_ref}). In this method, $I_{DER}\angle\,\delta_{I\_DER}$ in (3.28-3.29) applies to a fault condition as well, hence

$$I_{DER\_f}\angle\,\delta_{I\_DER\_f} = I_{DER}\angle\,\delta_{I\_DER} \quad (3.32)$$

Equation (3.32) is important as with $I_{DER}\angle\,\delta_{I\_DER}$ it allows the effectiveness of the aRCI to be evaluated. The evaluation can be done by performing the procedures from (3.22-3.32) twice, first by applying the DER's K-factor $K_{I_q} = 0$, and then applying DER's K-factor K_{I_q} with the desired setup. After two different values of $I_{DER}\angle\,\delta_{I\_DER}$ have been obtained, say, $(I_{DER\_f}\angle\,\delta_{I\_DER\_f})_{K_{I_q}=0}$ and $(I_{DER\_f}\angle\,\delta_{I\_DER\_f})_{K_{I_q}=n}$, then $\Delta I_{DER\_f}\angle\,\Delta\delta_{I\_DER\_f}$ can be calculated as follows

$$\Delta I_{DER\_f}\angle\,\Delta\delta_{I\_DER\_f} = (I_{DER\_f}\angle\,\delta_{I\_DER\_f})_{K_{I_q}=n} - (I_{DER\_f}\angle\,\delta_{I\_DER\_f})_{K_{I_q}=0} \quad (3.33)$$

$\Delta I_{DER\_f}\angle\,\Delta\delta_{I\_DER\_f}$ represents the difference of DER's current contributions during a fault condition with and without the aRCI. Therefore, by adding $\Delta I_{DER\_f}\angle\,\Delta\delta_{I\_DER\_f}$ with $I_f\angle\,\delta_{I\_f}$ from (3.17), the short circuit current of the system with aRCI-enabled DER, $I_{f\_aRCI}\angle\,\delta_{I\_f\_aRCI}$ can be estimated as

$$I_{f\_aRCI}\angle\,\delta_{I\_f\_aRCI} = I_f\angle\,\delta_{I\_f} + \Delta I_{DER\_f}\angle\,\Delta\delta_{I\_DER\_f} \quad (3.34)$$

After $I_{f\_aRCI}\angle\,\delta_{I\_f\_aRCI}$ has been obtained, (3.19-3.21) are repeated with $I_f\angle\,\delta_{I\_f}$ from (3.19) replaced by $I_{f\_aRCI}\angle\,\delta_{I\_f\_aRCI}$. The improved voltage due to DER's aRCI is obtained as $V_{DER\_f}\angle\,\delta_{V\_DER\_f}$ from (3.21). $(V_{DER\_f}\angle\,\delta_{V\_DER\_f})_{K_{I_q}=n}$ is the improved voltage sag, while

$(V_{DER\_f} \angle \delta_{V\_DER\_f})_{K_{I_q}=0}$ is the non-improved voltage sag. Finally, the effectiveness of the DER's aRCI could be evaluated through comparing the different voltage sags between the cases with and without aRCI, $(V_{DER\_f} \angle \delta_{V\_DER\_f})_{K_{I_q}=n}$ and $(V_{DER\_f} \angle \delta_{V\_DER\_f})_{K_{I_q}=0}$, respectively

$$\Delta V_{DER_f} \angle \Delta\delta_{V_{DER_f}} = (V_{DER\_f} \angle \delta_{V\_DER\_f})_{K_{I_q}=n} - (V_{DER\_f} \angle \delta_{V\_DER\_f})_{K_{I_q}=0} \quad (3.35)$$

The flowchart of the proposed methodology is shown in Figure 3-11.

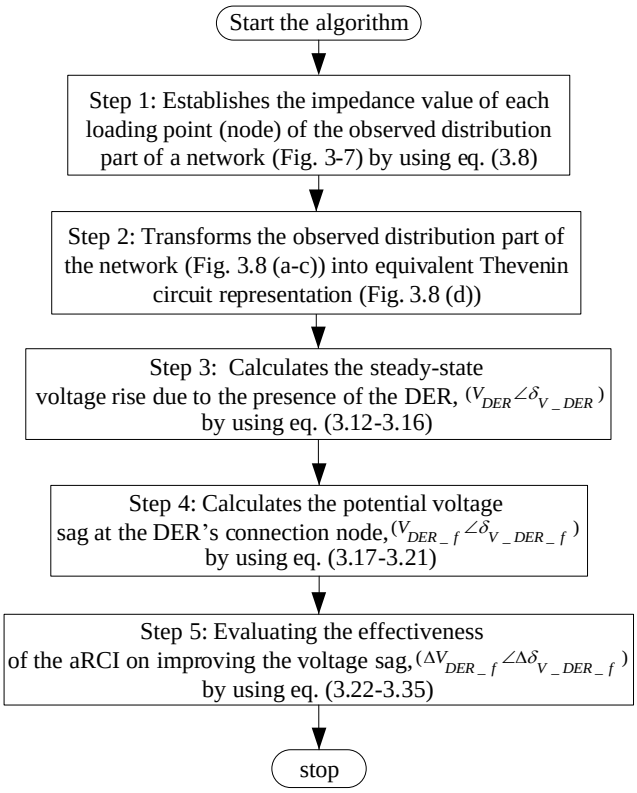

Figure 3-11 Overall flowchart of the proposed methodology.

3.9 The Evaluation of The Proposed Methodology Against the DIgsilent on Estimating The LVRT Voltage Sags

To validate the proposed methodology a typical distribution network is assumed and is used as the test case. In order to assess the validity of the proposed methodology, the evaluation of the LVRT voltage sag improvement through aRCI is made by using the proposed methodology and the DIgsilent dynamic RMS simulation methodology. The results of the voltage sag improvement from both methodologies are then checked to see whether the proposed methodology gives result close to the result obtained from DIgsilent dynamic RMS simulation. The simulation results in sections 3.9.1 to 3.9.5 show that without the need for building the dynamic DER modelling, the proposed methodology could give results similar to the one obtained from DIgsilent dynamic RMS simulation. This approach hence gives advantages for

a grid planner working on DER's LVRT voltage support evaluation, in the event of inadequacy of the grid data (due to the DER's manufacture confidentiality, limited grid data information, and so on).

Upon designing the distribution network, some aspects need to be considered to fit the situation of the case. First, regular distribution networks normally have a low *X/R* ratio (systems below 35kV usually have the *X/R* ratio of 10 or less, according to IEC-60909). Therefore the network used for this evaluation should have similar characteristics. As such, the simplified Thevenin Circuit Diagram of the test network that is shown in Figure 3-8 (d), should ha*ve the X/R* ratio of the external grid of 10 or less. In this study, *the X/R* ratio of 10 is chosen. Further, the MVA_{base} is chosen as 5MVA. Assuming the short circuit apparent power, S''_k, for all cases to be 20MVA, yields the per unit value of 4 pu. Distribution load power at the Thevenin bus, P_{load_th} *(pu),* is one pu. The validation case uses 80% DER penetration; hence MVA_{DER} is set to 0.8 pu. Ten samples of the case are chosen, whereas each case is set to situate different grid *X/R* ratios. The *X/R* ratios of the equivalent line impedances are set from 1 to 10 for the case from 1 to case 10, respectively. Each case for the system has different equivalent line impedance, $R_{line\_th} + jX_{line\_th}$, as shown in table 3-1. The impedance fault Z_f is set to 0.144+j.0.144 pu for all cases. In the simulation cases, the impedance fault is given in order to situate the fault is located on the transmission system. The design of the aRCI is made to improve transient voltage which sourced from transmission fault and does not relate directly to faults on the Distribution Network [122]. The load node voltage is assumed to be already known through regular checks. *X/R* ratio of the external grid, $R_{ext\_grid} + jX_{ext\_grid}$, are chosen uniformly 0.01436+j.0.1436 per unit.

Table 3-1 The Observed system parameters in Thevenin Circuit Diagram

Parameters	$R_{line\_th} + jX_{line\_th}$ (pu)	$V_{load}\angle\delta_{V\_load}$ (pu∠deg)
case 1	0.00721688+j. 0.00721688	0.987∠-0.75719
case 2	0.00721688+j. 0.01443376	0.987848∠-1.487
case 3	0.00721688+j. 0.02165064	0.987904∠-2.218
case 4	0.00721688+j. 0.02886752	0.9877975∠-2.9494
case 5	0.00721688+j. 0.0360844	0.9875115∠-3.68213
case 6	0.00721688+j. 0.04330128	0.9870645∠-4.4165
case 7	0.00721688+j. 0.05051816	0.9864475∠-5.15312
case 8	0.00721688+j. 0.05773504	0.9856575∠-5.89253
case 9	0.00721688+j. 0.06495192	0.984691∠-6.63525
case 10	0.00721688+j. 0.0721688	0.983545∠-7.38187

3.9.1 Steady-State Voltage Rise Estimation Results Analysis

The results estimated using the proposed methodology have been compared with the same results obtained using the DIgsilent as shown in Table 3-2. The error/different estimation of the proposed methodology as compared to the results obtained using the DIgsilent are shown in Table 3-3. It can be seen that the steady-state voltage rise V_{DER}, are estimated quite accurately by the proposed method. For V_{DER}, as shown in Table 3-2, fairly small error are observed for all case. The error/different estimation for V_{DER} and δ_{V_DER} are obtained through

$$error = \frac{(X)_{proposed\_method}}{(X)_{DigSilent\_method}} * 100\%, \tag{3.36}$$

where the $error$ represents the difference in estimation of the V_{DER} and δ_{V_DER} respectively, whereas the $(X)_{proposed\_method}$ represents V_{DER} and δ_{V_DER} obtained from the proposed method estimation and the $(X)_{DigSilent\_method}$ represents V_{DER} and δ_{V_DER} obtained from the DigSilent estimation.

For instance, the V_{DER} estimation obtained using the proposed method for case 1 has a different estimation/error for 0.037% (V_{DER}). The largest V_{DER} is to be found for case 10 which is 0.1987%, however, this is still acceptably small. Although different estimation/error for δ_{V_DER} for the case 1 is 14.544% (δ_{V_DER}), which is comparatively higher than the remaining case, the proposed method that has an estimation for -0.15, is still reasonably close enough with the DIgsilent method that has estimation δ_{V_DER} for -0.18.

Table 3-2 Comparison of Steady-State Voltage Rise Result ($V_{DER}\angle\ \delta_{V\_DER}$) Between The Proposed Method and The Powerfactory DIgsilent Method

Results	$V_{DER}\angle\ \delta_{V\_DER}$ (pu∠deg)	
Method used	DIgsilent	Proposed method
case 1	0.998∠-0.18	0.998∠-0.15
case 2	0.998∠-0.32	0.998∠-0.30
case 3	0.999∠-0.47	0.998∠-0.45
case 4	0.999∠-0.62	0.999∠-0.60
case 5	1.000∠-0.77	0.999∠-0.75
case 6	1.000∠-0.92	1.000∠-0.89
case 7	1.001∠-1.07	1.000∠-1.04
case 8	1.001∠-1.22	1.002∠-1.19
case 9	1.001∠-1.36	1.003∠-1.33
case 10	1.002∠-1.51	1.004∠-1.48

Table 3-3 Different Estimation/Error of The Steady-State Voltage Rise Result Between The Proposed Method and The Powerfactory DIgsilent Method in %

Cases	$error$	
	V_{DER}	δ_{V_DER}
case 1	0.037	14.544
case 2	0.0631	7.376
case 3	0.078	5.0697
case 4	0.05	3.7948
case 5	0.067	3.107
case 6	0.041	2.698
case 7	0.003	2.468
case 8	0.054	2.352
case 9	0.123	2.327
case 10	0.199	2.374

* $error$ (Different Estimation of the proposed method from the DIgsilent method) for each; V_{DER}, and δ_{V_DER}; are obtained from equation (3.36)

3.9.2 'LVRT with No aRCI' Case – Results Comparison

The comparison of **non**-aRCI enabled LVRT result between the proposed method and the PowerFactory DIgsilent method are shown in Table 3-4 and 3-5. For V_{DER_f} the highest error is observed for case 10 (2.868%), whereas the smallest error is observed for case 1 (1.675%). The remaining different estimation/error between the two methods are shown in Table 3-6. $I_{dq\_absolute\_f}$ represents the current magnitude in per unit, $I_{d\_ref\_f}$ represents the current magnitude in per unit in *d* axial of the *dq* axis in per unit, $I_{q\_ref\_f}$ represents the current magnitude in per unit in *q* axial of the *dq* axis in per unit, $I_{P\_DER\_f}$ represents the active current magnitude in per unit, $I_{Q\_DER\_f}$ represents the reactive current magnitude in per unit.

Table 3-4 Comparison of non-aRCI Enabled LVRT Result Between The Proposed Method and The Powerfactory DIgsilent Method for case 1-5

Results	Method used	Case 1	Case 2	Case 3	Case 4	Case 5
$V_{DER\_f}\angle\,\delta_{V\_DER\_f}$ (pu∠deg)	DIgsilent	0.610∠-9.87	0.609∠-9.67	0.609∠-9.47	0.608∠-9.28	0.608∠-9.07
	Proposed method	0.620∠-7.34	0.620∠-6.99	0.620∠-6.64	0.620∠-6.30	0.620∠-5.95
$I_{dq\_absolute\_f}$ (pu)	DIgsilent	1.000	1.000	1.000	1.000	1.000
	Proposed method	0.997	0.995	0.992	0.990	0.987
$I_{d\_ref\_f}$ (pu)	DIgsilent	1.000	1.000	1.000	1.000	1.000
	Proposed method	0.997	0.995	0.992	0.990	0.987
$I_{q\_ref\_f}$ (pu)	DIgsilent	0.004	0.006	0.009	0.011	0.014
	Proposed method	0.003	0.005	0.008	0.011	0.013
$I_{P\_DER\_f}$ (pu)	DIgsilent	0.986	0.986	0.988	0.989	0.990
	Proposed method	0.990	0.988	0.986	0.985	0.983
$I_{Q\_DER\_f}$ (pu)	DIgsilent	-0.168	-0.162	-0.156	-0.150	-0.144
	Proposed method	-0.125	-0.116	-0.107	-0.098	-0.089

Table 3-5 Comparison of non-aRCI Enabled LVRT Result Between The Proposed Method and The Powerfactory DIgsilent Method for case 6-10

Results	Method used	Case 6	Case 7	Case 8	Case 9	Case 10
$V_{DER\_f}\angle\,\delta_{V\_DER\_f}$ (pu∠deg)	DIgsilent	0.609∠-8.87	0.609∠-8.67	0.608∠-8.47	0.609∠-8.28	0.609∠-8.08
	Proposed method	0.621∠-5.62	0.622∠-5.29	0.623∠-4.96	0.625∠-4.65	0.626∠-4.34
$I_{dq\_absolute\_f}$ (pu)	DIgsilent	1.000	1.000	1.000	1.000	1.000
	Proposed method	0.985	0.982	0.980	0.977	0.975
$I_{d\_ref\_f}$ (pu)	DIgsilent	1.000	1.000	1.000	1.000	1.000
	Proposed method	0.984	0.982	0.979	0.977	0.974
$I_{q\_ref\_f}$ (pu)	DIgsilent	0.016	0.019	0.021	0.024	0.026
	Proposed method	0.015	0.018	0.021	0.023	0.026
$I_{P\_DER\_f}$ (pu)	DIgsilent	0.990	0.991	0.992	0.993	0.993
	Proposed method	0.981	0.979	0.977	0.976	0.973
$I_{Q\_DER\_f}$ (pu)	DIgsilent	-0.138	-0.132	-0.126	-0.12	-0.114
	Proposed method	-0.081	-0.072	-0.064	-0.056	-0.048

In the following Table 3-6, the error/different of non-aRCI enabled LVRT result between the proposed method and the Powerfactory DIgsilent method are presented. It can be seen the estimation difference between the proposed method and the Powerfactory DIgsilent method, particularly on voltage sag magnitude V_{DER_f}, are acceptably small.

Fairly large different estimation between the proposed method and the Powerfactory DIgsilent method are observed on the voltage sag phase $\delta_{V\_DER\_f}$ and the reactive current injection $I_{Q\_DER\_f}$. This finding can be seen on the significant different/error rate on $I_{Q\_DER\_f}$ and $\delta_{V\_DER\_f}$ as shown in table 3-6. These differences will be discussed further in section 3.10 (in the section of fifth important aspects from the simulated results).

Table 3-6 Different Estimation/Error of The non-aRCI Enabled LVRT Result in %

Cases	$error$						
	V_{DER_f}	$\delta_{V\_DER\_f}$	$I_{dq\_absolute\_f}$	$I_{d\_ref\_f}$	$I_{q\_ref\_f}$	$I_{P\_DER\_f}$	$I_{Q\_DER\_f}$
Case 1	1.675	25.584	0.260	0.260	25.714	0.375	25.610
Case 2	1.789	27.707	0.520	0.520	13.330	0.203	28.501
Case 3	1.773	29.882	0.780	0.790	7.059	0.132	31.498
Case 4	1.957	32.115	1.040	1.040	4.545	0.394	34.600
Case 5	2.023	34.386	1.300	1.290	3.704	0.657	38.046
Case 6	2.022	36.709	1.550	1.550	6.250	0.929	41.619
Case 7	2.167	39.063	1.800	1.800	2.151	1.201	45.317
Case 8	2.500	41.440	2.050	2.050	2.358	1.472	49.288
Case 9	2.578	43.836	2.290	2.291	2.521	1.733	53.333
Case 10	2.868	46.249	2.531	2.536	2.845	2.004	66.530

*$error$ (Different Estimation of the proposed method from the DIgsilent method) for each; V_{DER_f}, $\delta_{V\_DER\_f}$, $I_{dq\_absolute\_f}$, $I_{d\_ref\_f}$, $I_{q\_ref\_f}$, $I_{P\_DER\_f}$, and $I_{Q\_DER\_f}$; are obtained by replacing each parameter with '*X*' from equation (3.36)

3.9.3 'LVRT with aRCI on K-factor=0.5' Case – Results Comparison

In this section, the scenario on LVRT voltage support via aRCI with K-factor 0.5 is presented. The comparison of aRCI enabled LVRT result between the proposed method and the Powerfactory DIgsilent method are shown in Table 3-7 and 3-8 for case 1-5 and 6-10 respectively. It can be seen from table 3-7 and 3-8, voltage sag V_{DER_f} improvement is observed as compared with the 'non-aRCI' case as shown in table 3-4 and 3-5. For instance, on case 1, the voltage sag for 'non-aRCI' case as shown in the table 3-4 are estimated 0.610 pu and 0.620 pu through DIgsilent and the proposed method respectively. The voltage sag for 'aRCI with K-factor=0.5' case are estimated 0.623 pu (DIgsilent method) and 0.634 pu (proposed method). Therefore with aRCI, one could conclude that LVRT voltage support may improve voltage sag during the transient fault. The voltage sag improvement is observed 1.280% and 1.345%, according to the DIgsilent and the proposed method, respectively, whereas on case with highest *X/R* ratio of the system, case 10, the voltage sag improvement are observed 2.200% (DIgsilent method) and 2.129% (proposed method). The overall voltage sag improvement of the aRCI-enabled system between the proposed method and the DIgsilent method in % (with K-factor=0.5) are presented in Table 3-13.

Table 3-7 Comparison of aRCI Enabled LVRT Result Between The Proposed Method and The Powerfactory DIgsilent Method K=0.5 for case 1-5

Results	Method used	Case 1	Case 2	Case 3	Case 4	Case 5
$V_{DER\_f}\angle\,\delta_{V\_DER\_f}$ (pu∠deg)	DIgsilent	0.623∠-12.76	0.624∠-12.73	0.625∠-12.71	0.625∠-12.68	0.627∠-12.65
	Proposed method	0.634∠-5.99	0.634∠-5.71	0.642∠-5.42	0.642∠-5.14	0.642∠-4.86
$I_{dq\_absolute\_f}$ (pu)	DIgsilent	0.834	0.834	0.834	0.834	0.835
	Proposed method	0.831	0.829	0.827	0.825	0.823
$I_{d\_ref\_f}$ (pu)	DIgsilent	0.812	0.811	0.812	0.811	0.811
	Proposed method	0.809	0.806	0.803	0.800	0.798
$I_{q\_ref\_f}$ (pu)	DIgsilent	0.190	0.192	0.194	0.196	0.198
	Proposed method	0.191	0.194	0.197	0.200	0.202
$I_{P\_DER\_f}$ (pu)	DIgsilent	0.834	0.834	0.834	0.834	0.835
	Proposed method	0.827	0.824	0.820	0.817	0.814
$I_{Q\_DER\_f}$ (pu)	DIgsilent	0.006	0.008	0.011	0.013	0.015
	Proposed method	0.086	0.095	0.103	0.111	0.119

Table 3-8 Comparison of aRCI Enabled LVRT Result Between The Proposed Method and The Powerfactory DIgsilent Method K=0.5 for case 6-10

Results	Method used	Case 6	Case 7	Case 8	Case 9	Case 10
$V_{DER\_f}\angle\,\delta_{V\_DER\_f}$ (pu∠deg)	DIgsilent	0.627∠-12.63	0.629∠-12.61	0.629∠-12.59	0.631∠-12.57	0.631∠-12.55
	Proposed method	0.643∠-4.59	0.644∠-4.32	0.645∠-4.06	0.646∠-3.81	0.649∠-3.56
$I_{dq\_absolute\_f}$ (pu)	DIgsilent	0.835	0.835	0.835	0.835	0.835
	Proposed method	0.821	0.819	0.818	0.816	0.814
$I_{d\_ref\_f}$ (pu)	DIgsilent	0.811	0.810	0.810	0.810	0.810
	Proposed method	0.795	0.792	0.790	0.788	0.786
$I_{q\_ref\_f}$ (pu)	DIgsilent	0.186	0.201	0.203	0.205	0.206
	Proposed method	0.205	0.207	0.210	0.212	0.214
$I_{P\_DER\_f}$ (pu)	DIgsilent	0.835	0.834	0.835	0.835	0.835
	Proposed method	0.811	0.808	0.805	0.802	0.800
$I_{Q\_DER\_f}$ (pu)	DIgsilent	0.017	0.019	0.021	0.024	0.026
	Proposed method	0.086	0.134	0.141	0.148	0.154

In the following Table 3-9, the error/difference of aRCI enabled LVRT result with K-factor=0.5 between the proposed method, and the Powerfactory DIgsilent method is presented. It can be seen that the estimation difference between the proposed method and the Powerfactory DIgsilent method, particularly on voltage sag magnitude V_{DER_f}, are relatively acceptable.

Again, reasonably large different estimation between the proposed method and the Powerfactory DIgsilent method are observed on and the reactive current injection $I_{Q\_DER\_f}$ and the voltage sag phase $\delta_{V\_DER\_f}$. Similar to table 3-6, it is observed that there are relatively significant differences for $I_{Q\_DER\_f}$ and $\delta_{V\_DER\_f}$. These differences will be discussed further in section 3.10 (in the fifth important aspects from the simulated results).

Table 3-9 Different Estimation/Error of The aRCI Enabled LVRT Result K=0.5 in %

Cases	$error$						
	V_{DER_f}	$\delta_{V\_DER\_f}$	$I_{dq\_absolute\_f}$	$I_{d\_ref\_f}$	$I_{q\_ref\_f}$	$I_{P\_DER\_f}$	$I_{Q\_DER\_f}$
Case 1	1.823	53.029	0.348	0.419	0.632	0.899	93.039
Case 2	1.587	55.183	0.612	0.629	1.146	1.283	91.226
Case 3	2.704	57.335	0.863	1.047	1.651	1.631	89.689
Case 4	2.720	59.476	1.103	1.332	2.095	2.049	88.448
Case 5	2.505	61.594	1.402	1.640	2.481	2.421	87.352
Case 6	2.488	63.685	1.630	1.937	9.268	2.792	86.371
Case 7	2.398	65.742	1.892	2.209	3.182	3.082	85.479
Case 8	2.512	67.757	2.107	2.469	3.350	3.533	84.719
Case 9	2.488	69.722	2.334	2.716	3.564	3.904	84.011
Case 10	2.827	71.632	2.467	2.964	3.777	4.266	83.398

*$error$ (Different Estimation of the proposed method from the DIgsilent method) for each; V_{DER_f}, $\delta_{V\_DER\_f}$, $I_{dq\_absolute\_f}$, $I_{d\_ref\_f}$, $I_{q\_ref\_f}$, $I_{P\_DER\_f}$, and $I_{Q\_DER\_f}$; are obtained by replacing each parameter with '*X*' from equation (3.36)

3.9.4 'LVRT with Maximum aRCI' Case – Results Comparison

In this section, the scenario on LVRT voltage support via maximum aRCI is presented. To create maximum aRCI, K-factor is set arbitrarily to 6. The comparison for aRCI enabled LVRT results are shown in Table 3-10 and 3-11 for case 1-5 and 6-10 respectively. It can be seen from table 3-10 and 3-11, voltage sag V_{DER_f} improvements are observed as compared with the 'aRCI' case with K-factor set to 0.5 as discussed in section 3.9.3. These voltage sag reductions can be seen as improvements due to the higher k factor, which hence showing the aRCI is useful to improve the voltage sag.

Both methodologies, DIgsilent and the proposed approach show improvements in terms of voltage sag for aRCI cases when compared with the "non-aRCI" cases. The improvements are better for the test cases that have higher *X/R* ratios. The overall voltage sag improvement of the maximum aRCI-enabled system calculated with the proposed method and the DIgsilent method in % are presented in Table 3-14.

Table 3-10 Comparison of maximum aRCI Enabled LVRT Result Between The Proposed Method and The Powerfactory DIgsilent Method for case 1-5

Results	Method used	Case 1	Case 2	Case 3	Case 4	Case 5
$V_{DER\_f}\angle\,\delta_{V\_DER\_f}$ (pu∠deg)	DIgsilent	0.697∠-23.80	0.706∠-24.29	0.713∠-24.79	0.721∠-25.29	0.729∠-25.80
	Proposed method	0.719∠-1.82	0.718∠-1.75	0.739∠-1.68	0.739∠-1.60	0.739∠-1.53
$I_{dq\_absolute\_f}$ (pu)	DIgsilent	1.000	1.000	1.000	1.000	1.000
	Proposed method	1.000	1.000	1.000	1.000	1.000
$I_{d\_ref\_f}$ (pu)	DIgsilent	0.000	0.000	0.000	0.000	0.000
	Proposed method	0.000	0.000	0.000	0.000	0.000
$I_{q\_ref\_f}$ (pu)	DIgsilent	1.000	1.000	1.000	1.000	1.000
	Proposed method	1.000	1.000	1.000	1.000	1.000
$I_{P\_DER\_f}$ (pu)	DIgsilent	0.400	0.406	0.411	0.417	0.423
	Proposed method	0.128	0.122	0.116	0.110	0.104
$I_{Q\_DER\_f}$ (pu)	DIgsilent	0.916	0.914	0.911	0.908	0.906
	Proposed method	0.992	0.993	0.993	0.994	0.995

Table 3-11 Comparison of maximum aRCI Enabled LVRT Result Between The Proposed Method and The Powerfactory DIgsilent Method for case 6-10

Results	Method used	Case 6	Case 7	Case 8	Case 9	Case 10
$V_{DER\_f}\angle\,\delta_{V\_DER\_f}$ (pu∠deg)	DIgsilent	0.737∠-26.31	0.744∠-26.82	0.751∠-27.34	0.759∠-27.86	0.766∠-28.39
	Proposed method	0.739∠-1.46	0.761∠-1.39	0.761∠-1.32	0.769∠-1.25	0.770∠-1.18
$I_{dq\_absolute\_f}$ (pu)	DIgsilent	1.000	1.000	1.000	1.000	1.000
	Proposed method	1.000	1.000	1.000	1.000	1.000
$I_{d\_ref\_f}$ (pu)	DIgsilent	0.000	0.000	0.000	0.000	0.000
	Proposed method	0.000	0.000	0.000	0.000	0.000
$I_{q\_ref\_f}$ (pu)	DIgsilent	1.000	0.999	1.000	0.999	1.000
	Proposed method	1.000	1.000	1.000	1.000	1.000
$I_{P\_DER\_f}$ (pu)	DIgsilent	0.429	0.435	0.440	0.446	0.452
	Proposed method	0.098	0.092	0.086	0.081	0.076
$I_{Q\_DER\_f}$ (pu)	DIgsilent	0.903	0.901	0.898	0.895	0.892
	Proposed method	0.995	0.996	0.996	0.997	0.997

In the following Table 3-12, the error of maximum aRCI enabled LVRT result between the proposed method and the Powerfactory DIgsilent method are presented. It can be seen that the resulting error of voltage sag magnitude V_{DER_f} on the proposed method, are at maximum

3.64%. According to N Jenkins et al. in [151], on a voltage magnitude estimation method, error estimation for around 3% is acceptable.

Large differences in estimation between the proposed method and the Powerfactory DIgsilent method are observed on the active current injection $I_{P\_DER\_f}$ and the voltage sag phase $\delta_{V\_DER\_f}$. These differences will be discussed further in section 3.10 (in the fifth important aspects from the simulated results).

Table 3-12 Different Estimation/Error of The Maximum aRCI Enabled LVRT Result in %

Cases	$error$						
	V_{DER_f}	$\delta_{V\_DER\_f}$	$I_{dq\_absolute\_f}$	$I_{d\_ref\_f}$	$I_{q\_ref\_f}$	$I_{P\_DER\_f}$	$I_{Q\_DER\_f}$
Case 1	3.099	92.361	0.000	0.000	0.000	68.074	8.228
Case 2	1.758	92.804	0.000	0.000	0.000	70.010	8.611
Case 3	3.647	93.239	0.000	0.000	0.000	71.883	8.986
Case 4	2.455	93.662	0.000	0.000	0.010	73.693	9.471
Case 5	1.331	94.071	0.000	0.000	0.010	75.485	9.767
Case 6	0.281	94.462	0.000	0.000	0.010	77.169	10.162
Case 7	2.231	94.835	0.000	0.000	0.100	78.808	9.551
Case 8	1.358	95.188	0.000	0.000	0.020	80.359	10.971
Case 9	1.308	95.519	0.000	0.000	0.100	81.847	10.214
Case 10	0.496	95.828	0.000	0.000	0.030	83.253	11.786

*$error$ (Different Estimation of the proposed method from the DIgsilent method) for each; V_{DER_f} , $\delta_{V\_DER\_f}$, $I_{dq\_absolute\_f}$, $I_{d\_ref\_f}$, $I_{q\_ref\_f}$, $I_{P\_DER\_f}$, and $I_{Q\_DER\_f}$; are obtained by replacing each parameter with '*X*' from equation (3.36)

3.9.5 The Effectiveness of The aRCI on Improving The Voltage Sag – Results Comparison

The effectiveness of the aRCI on improving the voltage sag for all cases on both maxed aRCI and aRCI with K-factor 0.5 are shown in Table 3-13 and 3-14. It is observed that for higher *X/R* ratio cases the DER's LVRT voltage support via aRCI to minimise the voltage sag is more efficient.

Table 3-13 Voltage Sag Improvement of aRCI-enabled system Between The Proposed Method and The DIgsilent Method (K=0.5)

Cases	Voltage Sag Improvement in %		The Percentage Difference Between The Results
	Proposed Method	DIgsilent Method	
Case 1	1.34	1.28	4.69
Case 2	1.35	1.5	10.00
Case 3	2.14	1.6	33.75
Case 4	2.15	1.7	26.47
Case 5	2.15	1.87	14.97
Case 6	2.11	1.83	15.30
Case 7	2.11	1.98	6.57
Case 8	2.12	2.1	0.95
Case 9	2.12	2.15	4.69
Case 10	2.13	2.2	10.00

Table 3-14 Voltage Sag Improvement of maximum aRCI-enabled system Between The Proposed Method and The DIgsilent Method

Cases	Voltage Sag Improvement in %		The Percentage Difference Between The Results
	Proposed Method	DIgsilent Method	
Case 1	9.57	8.68	10.25
Case 2	9.56	9.65	0.93
Case 3	11.71	10.4	12.60
Case 4	11.7	11.3	3.54
Case 5	11.69	11.7	0.09
Case 6	11.79	12.81	7.96
Case 7	13.84	13.53	2.29
Case 8	13.83	13.8	0.22
Case 9	14.44	15.02	10.25
Case 10	14.89	15.34	0.93

It can be seen from the voltage sag improvement of the aRCI-enabled system with K-factor 0.5 (K=0.5) as shown in Table 3-13, the smallest percentage difference between the results simulated from the proposed methodology is observed in the case 8 (0.95%). The highest percentage difference between the results simulated from the proposed methodology is, however, observed in case 3 (33.75%). For the scenario of maximum aRCI injection (as in Table 3-14), the smallest percentage difference between the results simulated from the proposed methodology is observed in the case 2 and 10 (0.93%), whereas the highest percentage difference between the results simulated from the proposed methodology is observed in case 3, for 12.60%. The difference estimation of the voltage sag improvement obtained from the proposed methodology to the DIgsilent can be understood since, in the DIgsilent methodology, the estimation of the voltage sag improvement is made through dynamic RMS simulation. In the proposed methodology, the estimation of the voltage sag improvement does not account the state derivative of the dynamic component of the DER – this matter is better explained in fifth important aspects from the simulated results (section 3.10).

3.10 Discussion

The methodology proposed in this chapter is made for evaluating the effectiveness of the DER's reactive power-based LVRT voltage support. Without the extensive work on constructing the DER modelling which is a common requirement on dynamic RMS simulation methodology, the proposed methodology can estimate the effectiveness of the DER's LVRT voltage support on improving the voltage sag. It has been proven that the proposed methodology offers a more straightforward strategy and can compromise the accuracy and simplicity of the simulation modelling by tackling problem relating to the data restrictions.

With a simpler computation process, the evaluation result of the investigated voltage support has been proven fairly close to the results obtained through the dynamic RMS simulation that is done via DIgsilent simulation tool. This outcome is supported by some indications which are shown in the following points.

1. The voltage sag improvements predicted by the proposed method are fairly close to the DIgsilent results, with the differences of the voltage sags estimation V_{DER_f} in all cases as indicated by the '% |Error|' are acceptably small. With the most considerable % |Error| of the voltage sags estimation V_{DER_f} to be found at 3.64% on the case 3 on scenario maximum aRCI Enabled LVRT, as shown in the table 3-12, the proposed method can estimate the effectiveness of aRCI at mitigating voltage sags effectively. The smallest % |Error| of the voltage sags estimation V_{DER_f} to be found at 1.3% on the case 9 on scenario maximum aRCI Enabled LVRT, as shown in the table 3-12 as well.

2. Further, the steady-state voltage rise estimated by the proposed method is relatively close to the DIgsilent results as well. The error of the steady-state voltage rise estimation V_{DER} in all cases as shown in table 3-3 are observed largest at only 0.2%, as shown on the case 10, whereas the smallest error steady-state voltage rise estimation V_{DER} to be found at 0.003%, as shown on the case 7.

3. Table 3-13 and 3-14 show that, on the same level of reactive current injection, a lower voltage sag improvement can be observed on a lower *X/R* ratio system. This trend seems aligned with the argument that the DER connection to higher *X/R* ratio leads to more effective aRCI (better voltage sag improvement), which was claimed in previous studies, [27], [45]–[49]. It implies that the performance of the DER's LVRT voltage support via aRCI is highly dependent on the characteristic for the distribution grid (*X/R* ratio of the observed grid). Though in this study, *X/R* ratio variations are only set at the equivalent line impedance, $R_{line\_th} + jX_{line\_th}$, as shown in the table 3-1, as explained in the first step and the second step of the proposed method (chapter 3.6), equivalent line impedance represents the 'collective impedance' of the observed grid in a form of a line between the external grid and the DER connection that obtained from impedance transformation process. Hence one could imply equivalent line impedance $R_{line\_th} + jX_{line\_th}$ represent *the X/R* ratio of the observed grid.

4. The level of the reactive current being injected is affected by the transient voltage sag ΔV_{DER_f} (as implied in the equation 3.22 and thereby 3.23). To estimate ΔV_{DER_f}, steady-state voltage rise magnitude $|V_{DER}|$ is needed. Thus estimating $|V_{DER}|$ is essential since it is observed from equation 3.21 $|V_{DER}|$ determining the transient voltage sag V_{DER_f}.

5. It has been shown that differences in estimation between the proposed methodology and the Powerfactory DIgsilent method are observed on the voltage sag phase $\angle\delta_{V\_DER\_f}$, which results to the different estimation on the reactive current injection $I_{Q\_DER\_f}$ (as in Table 3-9), and the active current injection $I_{P\_DER\_f}$ (as in Table 3-12). These findings can be understood due to the fact that in the DIgsilent method, the voltage sag improvement is made through dynamic RMS simulation, and θ' is obtained from PLL. The DIgsilent method considers the dynamic aspect of the simulation. In the proposed methodology, θ' is obtained from equation (3.30) and (3.31). (3.30) and (3.31) as suggested in [150], to serve a similar function to the PLL**.** In the case of DIgsilent software, this is done via the time-domain RMS dynamic simulation; this transformation is available within the DER's inverter model, phase-locked-loop (PLL), which is part of the DIgsilent model. The proposed methodology does not handle the dynamic aspects of the PLL's performance; however, it does not need to as its purpose is completely different. Further note that the estimation of $\cos\theta'$ and $\sin\theta'$ that are obtained from (3.30) and (3.31) rely on $V_{DER\_f}\angle\,\delta_{V\_DER\_f}$. In the DIgsilent, $V_{DER\_f}\angle\,\delta_{V\_DER\_f}$ is obtained based on each step of the derivation of all state variable during time-domain RMS dynamic simulation. This different way of interpreting $V_{DER\_f}\angle\,\delta_{V\_DER\_f}$ and the way of obtaining θ', results in the different estimation of $I_{P\_DER\_f}$ and $I_{Q\_DER\_f}$. However, different results of θ' that are attributed by the different way of interpreting PLL function between the proposed methodology and the DIgsilent method only causes the different interpretation of $\angle\delta_{V\_DER\_f}$. On estimating the effectiveness of aRCI, V_{DER_f} is the value to determines the voltage sag improvement. As such, these different results ($\angle\delta_{V\_DER\_f}$, $I_{Q\_DER\_f}$ as in Table 3-9), and $I_{P\_DER\_f}$ as in Table 3-12) can be ignored since the difference does not adversely affect the voltage sag estimation from the proposed methodology.
6. Aside from the fifth aspect mentioned above, in most cases, the differences are small and acceptable as the proposed method does not account fully for the dynamic nature of the phenomenon simulated, unlike the DIgsilent simulation. Further, the proposed method can still be used reliably to estimate the voltage sag improvements.

The main feature of the proposed methodology is that it could estimate the effectiveness of aRCI on improving voltage sags without the need the knowledge relating the dynamic characteristic of the DER and way to construct the DER dynamic modelling. Therefore with such feature, with the proposed methodology one could understand clearer 'the flow' the whole process of estimating the effectiveness of aRCI on improving voltage sags, from the process of the voltage sags to the evaluation of the voltage sags improvement on the aRCI-enabled DER-connected bus. Furthermore, from a practical viewpoint, the proposed methodology can

support distribution system operators (DSOs), or a DER grid planner in the event of grid data and the modelling inadequacies upon DER's LVRT voltage support evaluation.

3.11 Summary

Methodology for estimating the effectiveness of DER's voltage control via additional reactive current injection (aRCI) as for LVRT support is given. As explained in the introduction, without needing to perform a computation process that inherently has iterative nature (computing derivatives of all state variables of the DER to estimate the dynamic response of the DER), the proposed methodology still could successfully estimate the effectiveness of aRCI in improving voltage sags. Further one could take benefit from the proposed methodology on a grid planning to estimate the effectiveness of the DER's LVRT voltage support via aRCI without the need to concern if the grid information is incomplete – in the event of grid data and the modelling inadequacies upon DER's LVRT voltage support evaluation.

Chapter 4 The Dynamic Modelling of The DER's aRCI-based LVRT Voltage Support

4.1 Introduction

It has been explained from chapter 3 that LVRT voltage support is highly influenced by the *X/R* nature of the DER connection. This matter can be understood as short-circuit current is determined by the impedance characteristic which neighbouring the located fault. The DER's current regulation during the voltage sag determines the active and the reactive part of the contributed short-circuit current injected by the DER. Meaning, when the additional reactive current is injected, some amount of the reactive part of the short-circuit fault current is compensated by the 'additional' reactive part of the contributed short-circuit current from the DER. It will be presented in this chapter; this understanding can be proven in the perspective of the dynamic RMS simulation. To do so, a proposed dynamic modelling of the DER's aRCI-based LVRT voltage support that is based on the reactive power regulation standard as previously shown in section 2.7.1, is presented. The presented modelling of the DER, along with the proposed modelling of the aRCI-based voltage support is made to understand better the dynamic response of the system - the voltage response following LVRT, the voltage improvement sag with respect to the amount of the additional reactive current being given, and so on.

The realisation of the voltage support modelling needs the construction of DER modelling as a whole system. Meaning, the design of the DER system along with its connection in the grid may be required. It should be understood; however, that the DER system modelling is very situational, subject to the purpose of the study, as some generalisations and the assumptions of the modelling are normally made. The DER modelling for studying LVRT voltage support is different to, for instance, DER modelling for studying DER's MPPT optimisations. In the following, some aspects: the common DER modelling and its control structure, along with some considerations needed upon designing the DER model; are presented. These aspects are given to help understand better the required knowledge to construct studied DER modelling.

As has been explained from section 3.7, MATLAB Simulink offers a very reliable *modularity and expandability* for power system transient stability analysis. It also gives us a complete database for the DER modelling, spanning from the modelling of the PV arrays, its *dq* reference frame-based current controller, to the PWM modelling. Even it provides us a complete freedom in the event we need a modification of the components. Thus, the dynamic modelling is made with the help of MATLAB Simulink.

Section 4.2 to 4.5.7 reviews the DER modelling, along with some consideration needed (presented in section 4.3 and 4.4) before designing the DER model for LVRT study. DER modelling in this research is presented in section 4.5.1 to 4.5.7. Further simulation result relating DER response on various level of aRCI following a fault is presented in section 4.7. Section 4.8 presents discussion relating the mechanism of the DER's Reactive power-based LVRT voltage support and correlate it with the simulation results which showed in section 4.7. The summary is given in section 4.9.

4.2 DER Modelling and Its Control Structure

There are plenty of varieties of PV inverter topologies; often the control structures can also be very different as well [150]. As such, the modulation algorithm has to be specific for each topology. In this study, an overview of a typical DER PV structure is presented in Figure 4-1. Transformer-less PV inverter with the boost stage is used as an illustration. Figure 4-1 depicts common PV representation, along with its typical functions that are shown in the coloured boxes.

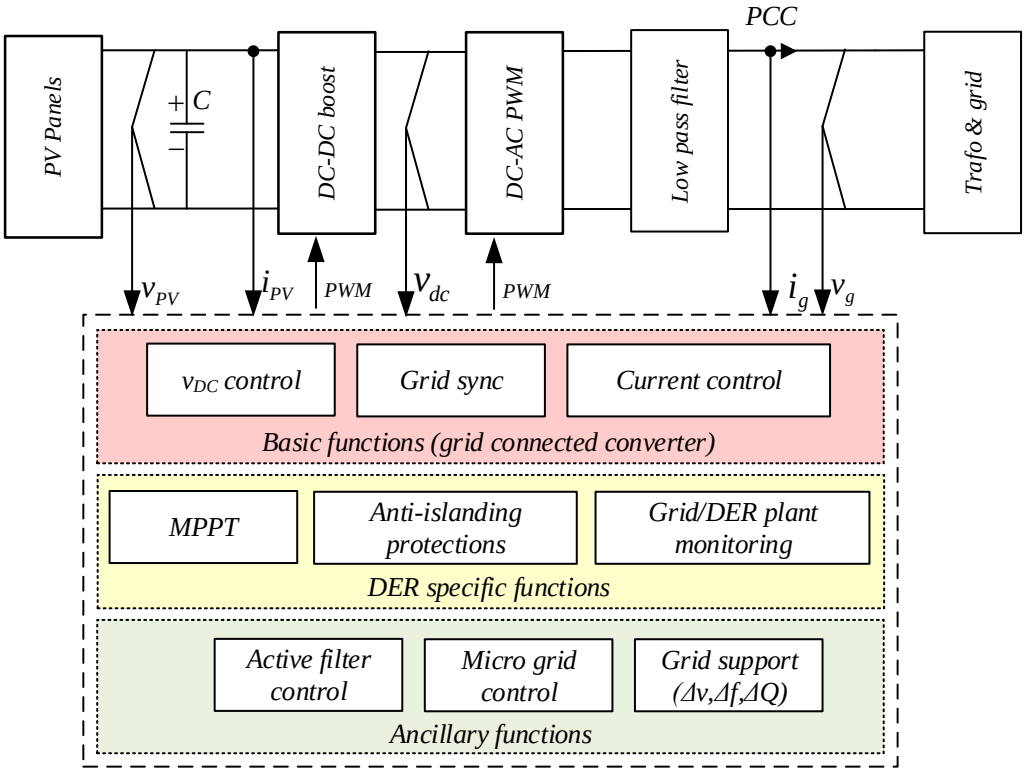

Figure 4-1 Generic control structure for a PV inverter with boost stage [152]

The representation is common for all grid-connected inverters. The AC power output of the PV is generated through DC to AC conversion with a PWM converter. The DC current that is fed into DC-AC PWM converter is generated from DC to DC boost at the DC link. The DC current that is fed into DC to DC boost is smoothed by the capacitive element at the DC link

since the DC current from the PV panels is usually fluctuating with changes in irradiance. In the AC grid part, a low pass filter is provided at the inverter to provide a smoother sinusoidal AC output, minimising the harmonic effect being generated by the inverter.

From Figure 4-1, the functions that commonly available on the DER, such as v_{DC} control, grid sync, current control, and so on, are shown and clustered in the coloured boxes. The operation of these functions requires inputs and feedback signals; such as v_{PV} (measured voltage at the PV array), i_{PV} (measured current at the PV array), v_{DC} (measured boosted the voltage of the DC link), i_g (measured AC current), and v_g (measured AC current). Depending on the desired control strategy; these functions are employed to regulate either DC-AC PWM converter, or DC-DC boost, or both to achieve the desired control strategy. For instance, grid support function commonly employed for minimising unwanted voltage sags. Such a function is provided by applying DER with transient voltage control. The transient voltage control is done through regulating the DER's active and/or reactive power output reference. As such, during DER's active and/or reactive power regulation, the signal v_g is used as feedback to evaluate the effectiveness of the regulation in improving the voltage sag.

Grid-connected DER has typically basic functions. DER specific functions, such as MPPT (that is used for extracting maximum available power from PV module), are commonly available on medium voltage level grid-connected DER [1]. DER ancillary functions are still regarded as tertiary need, and only a few medium voltage level grid-connected DER have these functions [4]. However, many studies show that DER should be provided with these ancillary functions. One of these ancillary functions is generally in the form of LVRT voltage support. In recent studies, it is suggested that DER with ancillary functions should be provided not only by the medium voltage level grid-connected DER but also low voltage level grid-connected DER as well [3]. To better understand the need for DER's LVRT voltage support as its ancillary services, it is best to overview some basic functions of the grid-connected DER that are commonly available. The function as shown in the following paragraph is generalised as based on Figure 4-1.

From Figure 4-1, the basic functions of the grid-connected DER, along with its every function can be generalised as follows.

1. The v_{DC} control, a function that is made to ensure the unwanted DC voltage fluctuation level , arising from the radiance intermittency, could be kept within acceptable limits [53]. This function is typically meant to ensure the DER's reliability in the grid. All DER normally have this function.
2. Grid synchronisation, a control function that is made to ensure the DER connection to the AC grid, and is made for enabling the DER on the operation at the unity power factor [3],

[4]. Grid synchronisation is also required to ensure the DER's power which comes in the forms of DC source, can be delivered to the AC grid.

3. Current control, a function that is made to ensure the DER operation stable, in the case of significant grid impedance variations [3], [4], [14]. The current control usually is available to ensure the DER could ride through fault, without being disconnected from the grid.

In addition, some specific functions of the grid-connected DER are also available. These specific functions are described in the following numbered points.

1. MPPT control, which is a control function that allows DER to track rapid irradiation changes [153]. The MPPT control is generally equipped in some PV park to allow the moving of the PV direction relative to the sun radiance in order to ensure optimum energy harvest.

2. Anti-islanding protections, which is a control function that allows DER to protect itself from the unwanted effect of localised/islanded grid condition [18], [154].

3. Grid/DER plant monitoring [68], which is a function that allows DER to detect voltage/frequency for the anti-islanding protections and for the ancillary function [18].

Further, the ancillary functions of the grid-connected DER are typically given as follows.

4. Active filter control, a control function that is made for enabling the DER able to provide 'reactive compensation' in order to minimise the rate of the unwanted unbalanced three-phase voltage on an unbalanced three-phase distribution load [155].

5. Microgrid control, a control function that is made for enabling the DER capable of doing active or reactive power sharing without having the need for communications/centralised coordination between the DERs [156]. Microgrid control allows DER to work not only in grid-connected operations but also on the stand-alone operating mode. DER on stand-alone operating mode allows them to regulate the island voltage while the output power is dictated by the load.

6. DER grid support, a control function that is made for allowing the DER to provide transient voltage support through active and reactive power regulations during LVRT [3], [4], [14]. The DER transient voltage support that is made via either active-, reactive-, or both active and reactive-power regulation, are categorised into this function.

The modelling of the DER along with its control structure depends on the purpose of the study since some simplifications (such as the assumption of some certain part of the DER model) are commonly considered. This is often made to suit a certain objective of the study. For instance, the design of DER modelling for investigating LVRT support usually does not

consider the design of the MPPT control. Such consideration is often made since the time interest for simulating LVRT support usually is less than 10 or 20 seconds. MPPT control is made to handle the PV array direction in order to ensure optimum energy yields following sun irradiance changing level, whereas the irradiance changing level is within an order of minutes or more. As such, within such time frame, the simulation of LVRT support assumes that the DER receives constant irradiance level. In the following section, more detail considerations regarding the DER modelling are presented, to understand better the requirements needed before constructing DER modelling for simulating LVRT support, which is the main focus of this study.

4.3 Consideration of the DER Modelling

Aspects needing to be considered relating to DER dynamic modelling usually are on, how the functions (as shown in figure 4-1) of the DER are modelled. In order to understand better the consideration needed for the DER modelling, some cases relating to DER modelling considerations are given.

On DER LVRT study, the DER dynamic modelling is focused more on the grid-interface aspect such that the function relating to the grid synchronisation, current control and grid support is considered. This typical DER modelling can be found in some LVRT transient stability studies [3], [4], [14], whereas some of its dynamic aspects, such as the DC voltage regulator, or the MPPT controller, are not considered. In such study, the DC side output (as in *dq* reference frame) of the DER is often simplified as a constant current.

There are studies on modelling the DER where the MPPT controller and the DC voltage regulator are considered. Such study is usually about the impact of the radiance changing to the stability of the DER's AC output, whereas the DER modelling is made to account the effect of the irradiance intermittency to the DER's energy yields [62]. The objective of such a study is to observe and (in most of the cases), to minimise the unwanted effect of the radiance intermittency [157]. Further, there are studies, whereas the DER's functions, such as the MPPT controller, DC voltage regulator, and even the function that is relating to the grid synchronisation, are considered, such that the DER modelling is more complex [53], [158]. In such studies, the objective is usually made to investigate the impact of the irradiance intermittency to the DER's power output to the grid. Overall many DER modelling for such studies commonly focus on the investigation of either for; tuning, improving, or sometimes proposing a modification on these functions [53], [158].

Study relating DER modelling that focused on the effect of the unbalanced three-phase distribution grid to the DER performance can be found in [159], [160]. Such a study usually focuses DERs on medium voltage level connections, whereas the DERs are directly connected

to the three phase lines. In such study, the DER modelling commonly consider the design of the DC voltage regulator and the function relating to the grid synchronisation. The DC voltage response on the DC link is utilised to observe and determine the three-phase voltage unbalance rate of the distribution grid. Under the condition of the unbalanced voltage, DC voltage response tend to fluctuate more than on balanced condition.

There is the study that is mainly focusing on the design and optimising the MPPT control function. These studies are usually about MPPT control improvement by taking into account the effect of radiance changing to the DER operability. The study is usually involving in the design of the v_{DC} control as well. The quality of the proposed MPPT design can be seen at the DC voltage response. It is known the DC current intermittency is due to the quality of the MPPT control in handling the radiance changes [153], [157]. Thus, in order to test the effectiveness of the MPPT control, the DC current output is needed as it is used as a means for evaluation [153], [157]. As such, DER modelling that is purposed for the design and optimising the MPPT control function usually considers the v_{DC} response on the radiance changings [153], [157].

On the study about transient LVRT support, the DER control structure modelling has to consider the modelling of the grid support ancillary function (*Δv,Δf,ΔQ*). The DER's grid support ancillary function is usually in the form of transient voltage support, frequency support, or reactive compensator. Particularly on transient voltage support, it is made through some ways, either through additional active current injection (aACI), additional reactive current injection (aRCI), or combinational additional active and reactive current injection (aRACI) [1]. DER studies on transient LVRT issue do not consider the MPPT function and DC voltage regulator. This can be understood since the time frame of interest of the LVRT study is relating to the duration of the voltage sag that is often in milliseconds; hence the DER's DC output (v_{DC}) is often considered constant, such that the design of the PV panel and the MPPT function can be neglected. This approach can be found on [14], [22], [78].

In this study, the design of the DER is made on MATLAB Simulink. It will be shown later each component needed to build the model in the following sections 4.3.

4.4 Some Principles of The DER Modelling and Its Grid Synchronization Mechanism

The aim of the design of the AC power inverter control is to establish its feeding mechanism to the main grid. Particularly on grid-connected DER, the purpose of the DER's AC power inverter control is to regulate the DER's AC output frequency so that can be synchronised with the grid frequency. It can be seen previously in Figure 4-1, i_g and v_g which represent the signals of the grid current and grid voltage that are used for DER AC output synchronisation.

Through these signals, the DC-AC power conversion is regulated such that the DER's AC current output could then have the same frequency as the grid.

Simulating dynamic response of DER on the transient condition, that requires signals i_g and v_g as control input which later then to be used to synchronise DER's AC output, requires complex computation. Since on synchronising DER's output, the operation mode of the grid inverter (for example, unity power factored operation) and the reference power strategy (the way establishing DER's voltage control through reactive power, for instance) should be considered such that the controlled AC current and/or voltage output, should be set by underlying the principle of instantaneous power theory [161]. For better understanding, Figure 4-2 shows the implementation of instantaneous power theory on the mechanism of current and/or voltage control of grid-interfaced DER. Instantaneous power theory is useful for building DER modelling in the MATLAB Simulink.

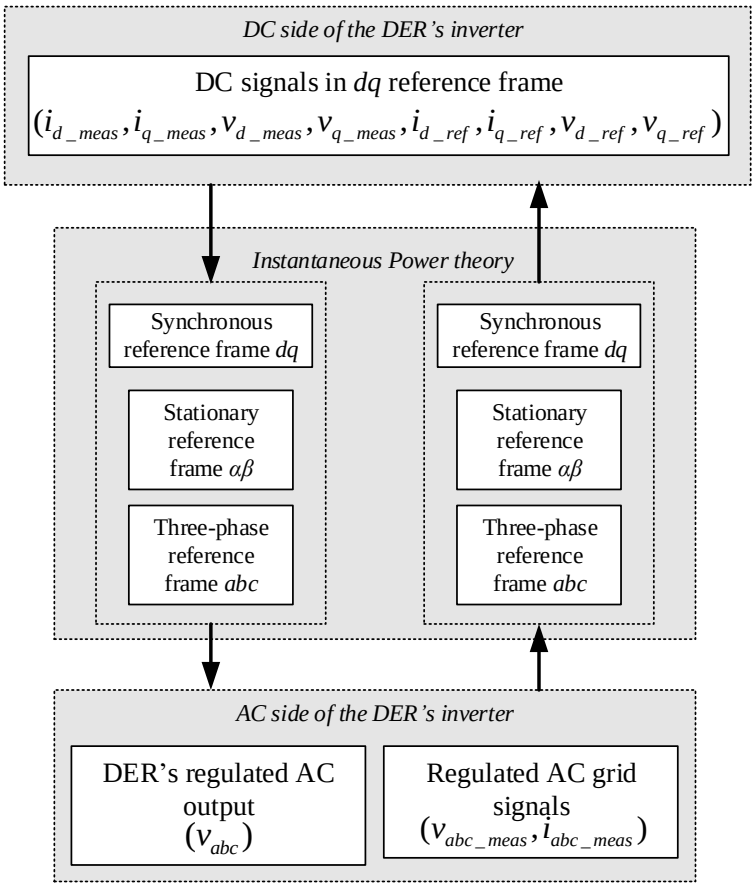

Figure 4-2 the implementation of instantaneous power theory on synchronising DER's DC current signals to the grid frequency on dynamic simulating computation [150]

In order to understand figure 4-2, further implementation of instantaneous power theory on synchronising DER's DC current signals to the grid frequency is given in the following paragraph with the help of illustration that is given in figure 4-3.

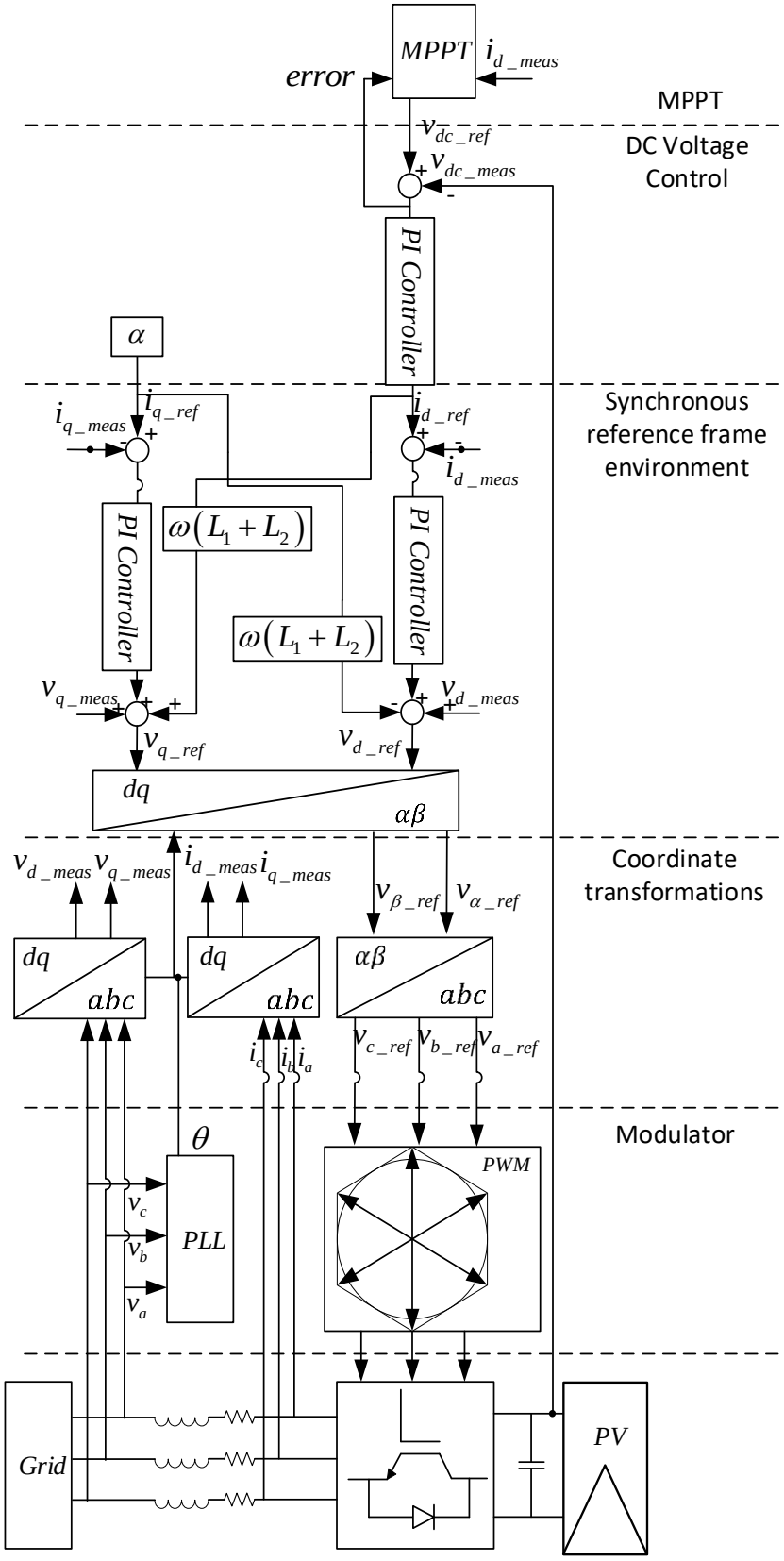

Figure 4-3 The full diagram of the control methodology and the modulation of Grid-connected DER. The design is illustrated by considering all control structure, as detailed from Figure 4-1 [158]

Assuming the DC current on *dq* reference frame (i_{d_ref}, i_{q_ref}) of the DER's inverter which is already regulated by the DC-DC boost is generated, then the value difference between (i_{d_ref}, i_{q_ref}) and the *dq* measured current (i_{d_meas}, i_{q_meas}) generate signals to regulate voltage reference. The regulated reference voltage that is being added by the *dq* measured voltage (v_{d_meas}, v_{q_meas}) represent *dq* reference regulated voltage v_{d_ref}, v_{q_ref}. A better illustration depicting this process is shown in figure 4-3. to generate (i_{d_ref}, i_{q_ref}), (i_{d_meas}, i_{q_meas}), and (v_{d_meas}, v_{q_meas}) that is in *dq* reference frame, a medium of synchronisation between *abc* to *dq* reference frame is needed. In order to do so, a device called the phase-locked loop (PLL) is required. The work of PLL uses the principle of the instantaneous power theory as shown in Figure 4-2. It can be seen to obtain (v_{d_ref}, v_{q_ref}), (i_{d_ref}, i_{q_ref}), (i_{d_meas}, i_{q_meas}), and (v_{d_meas}, v_{q_meas}), it needs v_{abc_meas} and i_{abc_meas} to be converted into their stationary ($\alpha\beta$) reference frame and then finally into their *dq* reference frame. A similar procedure is needed to obtain v_{abc}. As seen from Figure 4-2, to get v_{abc}, v_{d_ref}, v_{q_ref} that is in *dq* reference frame need to be converted through two steps. The first is to convert it into their stationary ($\alpha\beta$) reference frame. After their ($\alpha\beta$) reference form are obtained, the respective value is then can be converted into their three-phase *abc* sinusoidal AC form. Again, all these conversions require a value, θ, which is obtained by the PLL.

To represent such processes of the conversion as shown in Figure 4-2, it needs a regulated θ. Understanding further on how's the signals conversions that require θ is processed, along with the use of the converted signals by all the DER's corresponding dynamic elements, is explained in the following paragraph.

Again, from Figure 4-3, it illustrates all the necessary elements to construct dynamic modelling of the DER. The representation of the DER modelling which consider all dynamic aspect, from PV array, Inverter Control (which comprise DC Voltage regulator, current regulator, Phase-Locked-Loop (PLL) measurements, and the MPPT regulator), Pulse Width Modulator (PWM), and the L filter of the DER's inverter, is visualised. The DER modelling is clustered into each function, the MPPT, the DC voltage control, the synchronous reference frame environment, the coordinate transformation functions, the modulator, the PV panel, and the DER connection to the grid circuit. It can be seen DER's power generation that is generated from the DC current output through PWM and then is inverted into AC outputs takes several steps.

To generate an AC regulated power, DC power source from PV array, which is represented in a DC form by the signal v_{dc_ref}, take several steps before it can finally successfully reaches into its AC form. To begin with, first, the AC outputs are synchronised with the help of the 'modulator', which modulates the DC current into *abc*-AC outputs. The 'modulator' signals the switching sequence to the PWM with the of '$\alpha\beta \rightarrow abc$ module' block. It is shown

$v_{a\_ref}, v_{b\_ref}, v_{c\_ref}$ by using $\alpha\beta \rightarrow abc$, are converted from v_{α_ref} and v_{β_ref}. The signals v_{α_ref} and v_{β_ref} are obtained from v_{d_ref} and v_{q_ref} , with the help of signal θ. θ is regulated by the phase-locked-loop (PLL) device. From the figure, it can be seen its output signal, θ, is necessary for $\alpha\beta \rightarrow dq$ and $dq \rightarrow \alpha\beta$ conversions.

On 'synchronous reference frame environment', v_{d_meas} and v_{q_meas} are converted from v_a, v_b, v_c through $abc \rightarrow dq$ module. Between 'synchronous reference frame environment' and 'modulator', there is 'coordinate transformations', which serves as coordinate signal conversions, between abc, dq, and $\alpha\beta$. v_{d_ref} and v_{q_ref} are obtained from the addition of the *PI controller* output signals, the v_{d_meas} and v_{q_meas} and the i_{d_ref} and i_{q_ref} [150]. $\omega(L_1 + L_2)$ represent the cross-coupling effect due to line inductance L_1 and L_2 [150], [162]. The 'cross-coupling effect' is attributed by the fact that the d part of the PI controller outputs is affected by the q part of the output filter $-i_{q\_ref}\omega(L_1 + L_2)$, whereas the q part of the PI controller outputs is affected by the d part of the output filter $i_{d\_ref}\omega(L_1 + L_2)$ [150], [162]. Note ω on $-i_{q\_ref}\omega(L_1 + L_2)$ and $i_{d\_ref}\omega(L_1 + L_2)$ defines $2\pi f$. f is the nominal steady-state frequency of the system. Finally the generated v_{d_ref} and v_{q_ref}, through dq to abc conversion, becoming $v_{a\_ref}, v_{b\_ref}, v_{c\_ref}$ to act to modulate the PWM outputs.

Above paragraphs in this section provide a useful understanding of designing DER in the simulation tool. Next section describes the DER on MATLAB Simulink. The design of the DER is made based on the principles described in this section.

4.5 DER Modelling on MATLAB Simulink

In this study, DER modelling on MATLAB Simulink based DER is presented in this section. the DER modelling on Simulink is designed using underlying principles of the dynamic aspect of the DER as shown in Figure 4-3. Several elements are needed to build DER's dynamic modelling on Simulink. These are PV array (in this study, PV is chosen), Inverter Control (which comprise DC Voltage regulator, current regulator, Phase-Locked-Loop (PLL) measurements, and the MPPT regulator), Pulse Width Modulator (PWM), and the filter of the DER's inverter.

4.5.1 PV Array [163]

In the Simulink library, some of the elements are predefined, such as the PV array, PWM, inverter control, and the PLL. The PV array blocks, as shown in Figure below (which shows PV array with 7 modules of string and 88x24 parallel), implements an array of photovoltaic (PV) modules.

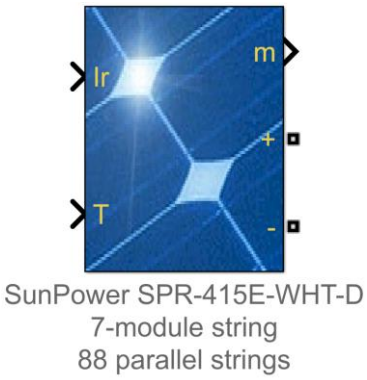

Figure 4-4 PV array model from MATLAB Simulink Library [163]

The PV array is built of strings of modules connected in parallel, each string consisting of modules connected in series. This block allows the predefined PV modules to be customised according to the corresponding study. The PV array block uses two input, irradiance level and the temperature of the environment. The two inputs can be seen in Figure 4-4, with symbol 'Ir' and 'T', respectively. In this study, on LVRT study both irradiance level and the temperature of the environment are considered constant, with 1000 W/m^2 and 45 Deg. Celsius, respectively. For the outputs, it has three, the two polar output (+ and -) that represent the positive and the negative side of the PV array output circuit, and the 'm', which represents the measured DC current and the DC voltage output of the array. The three outputs can be seen in Figure 4-4.

There is a selection of pre-defined PV array modules can be used, which each define the array characteristics differently. For example, as shown in Figure 4-5, SunPower SPR-415E-WHT-D), which the default module data that is used in the study has array characteristics, are shown below. SunPower SPR-415E-WHT-D is selected arbitrarily in this study.

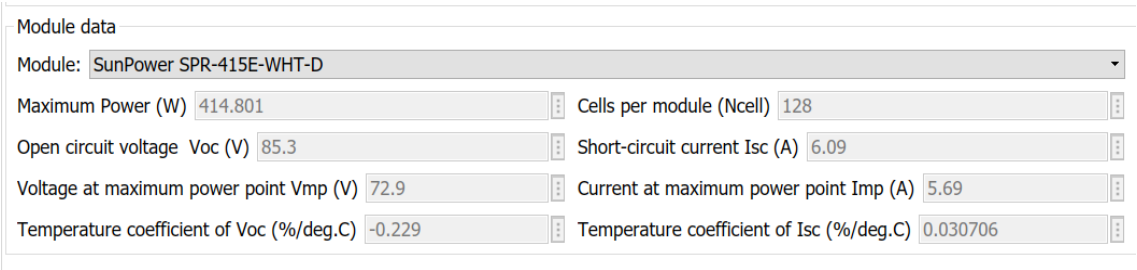

Figure 4-5 the block parameters of the pre-defined PV array module on MATLAB Simulink used in the study [163].

The model is built based on the design from the Sandia National Laboratories [164]. Principally, the PV Array block is a five parameter model using a current source I_L (light-generated current), a diode (I_0 and nI parameters), series resistance R_S, and shunt resistance R_{sh} to represent the irradiance- and temperature-dependent I-V characteristics of the modules. The five parameters, along with the other parameters to characterise the PV array is shown in the following Table 4-1.

Table 4-1 PV array block parameters [163]

Parameters	value
Light-generated current I_L (A)	7.8649
Diode saturation current I_0 (A)	2.9259e-10
Diode ideality factor (nl)	0.98117
Shunt resistance R_{sh} (ohms)	313.3991
Series resistance R_S (ohms)	0.39383
Boltzmann constant k (J.K-1)	1.3806e-23
electron charge q (C)	1.6022e-19
cell temperature T (K)	25
number of cells connected in series in a module *Ncell*	60
Diode voltage V_d (V)	0.7

Where diode current I_d is obtained from

$$I_d = I_0\left(\exp(\frac{V_d}{V_T}) - 1\right) \tag{4.1}$$

Whereas terminal voltage V_T is obtained from

$$V_T = \frac{kT}{q}.nl.Ncell \tag{4.2}$$

The circuit diagram of the PV array is shown below.

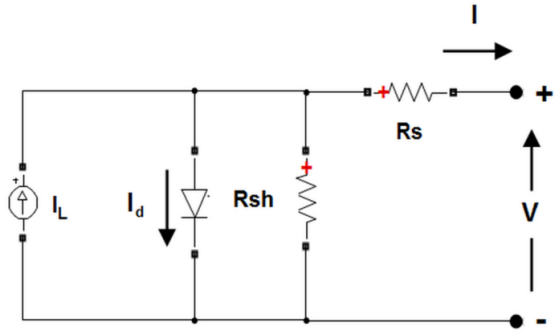

Figure 4-6 circuit diagram of the PV [163]

In this study, the PV has a 250kW power rating, which means it has 88 parallel strings with 7 series-connected modules per string (this can be seen in figure 4-4). The 250kW capacity is selected for the study. The below table shows the PV array's characteristic, along with the five parameters are predefined from the MATLAB Simulink library [163].

Through maximum power point tracking, with irradiance level for 1000W/m^2 and temperature for 25 degrees C, the output power, the voltage and the current at maximum power point of the PV array that is used in the studied modelling can be found as shown in the Figure 4-7.

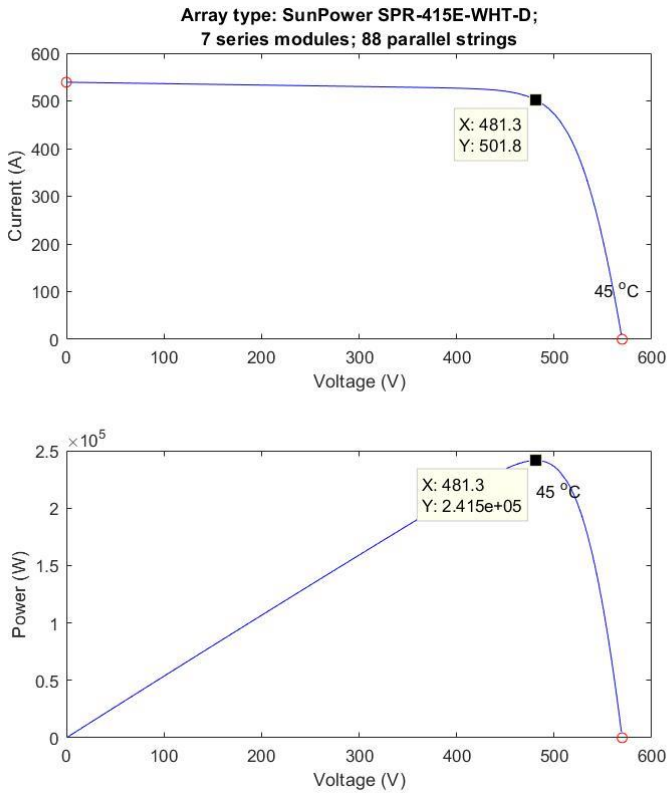

Figure 4-7 I-V characteristics of the PV (above) and The output power of the PV (below)

From figure 4-7, the three outputs are summarised in Table 4-2. The modelled PV array represents model 'PV array' at the right-bottom corner as shown in figure 4-3. Next, the modelling of the pulse width modulation system is explained in the next section.

Table 4-2 PV outputs with maximum power point tracking

Output power at maximum power point (kW)	241.5
Voltage at maximum power point Vmp (V)	481.3
Current at maximum power point Imp (A)	501.8

4.5.2 Pulse Width Modulator (PWM) [165]

PWM from Figure 4-3 can be represented by using '3-Level IGBTs Bridge' from the Simulink library that is shown in Figure 4-8.

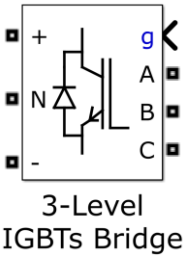

Figure 4-8 3-Level IGBTs model from MATLAB Simulink Library [165]

The Three-Level Bridge block implements a three-level power converter that consists of three

arms of power switching devices. Each arm consists of four switching devices along with their antiparallel diodes and two neutral clamping diodes as shown in the figure below.

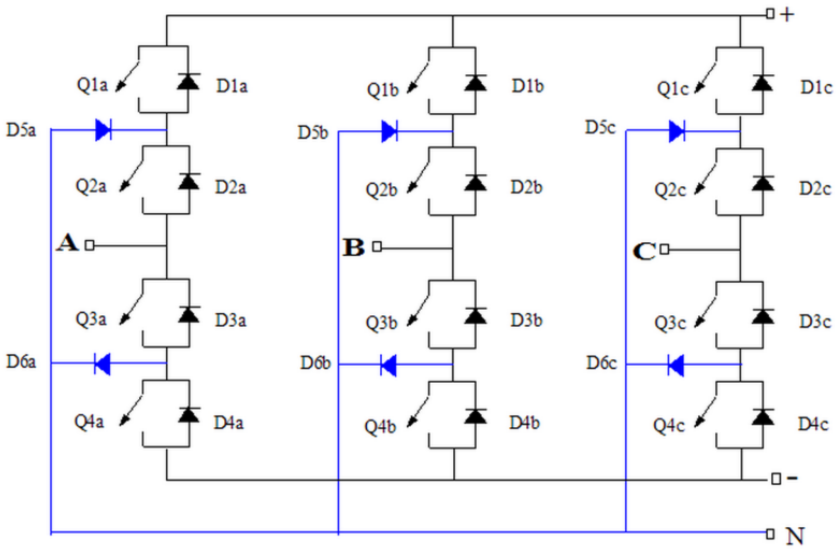

Figure 4-9 three-level power converter with three arms of power switching devices from MATLAB Simulink Library [165]

In the predefined MATLAB Simulink toolbox, the type of power switching device (IGBT, GTO, MOSFET, or ideal switch) and the number of arms (one, two, or three) are selectable from the dialogue box. When the ideal switch is used as the switching device, the Three-Level Bridge block implements an ideal switch bridge having a three-level topology as shown in Figure 4-10. The detail explanation of how the Three-Level Bridge block is operated can be found in [165].

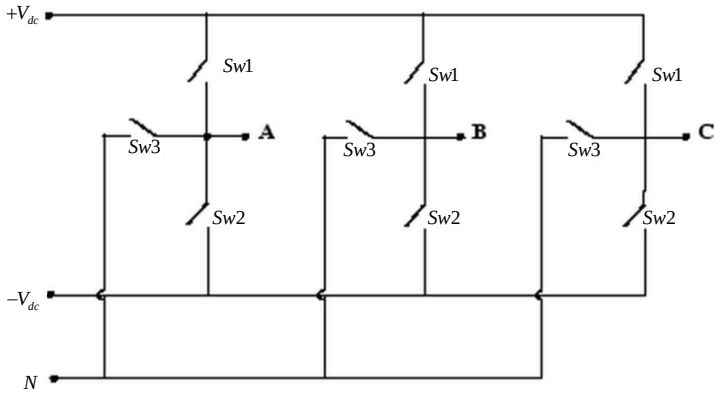

Figure 4-10 three-level topology switch bridge from MATLAB Simulink Library [165]

In this study, the number of bridge arms is selected 3, while the snubber resistance and the snubber capacitance, in ohms (Ω) and in Farad (F), are 10^{-6} and infinite, respectively. The IGBT internal resistance, R_{on} in ohms (Ω), the Forward voltage, V_f in voltage (V), and the Diode Forward voltage, V_{fd} in voltage (V), are 10^{-3}, 0, and 0, respectively.

4.5.3 Inverter Control modelling [166]

Inside the Inverter Control model, there is a DC Voltage regulator, current regulator, Phase-Locked-Loop (PLL) measurements, and the MPPT regulator. Note that though Inverter Control is a predefined element that is available in the Simulink, to fit with the modelling purpose (as for transient LVRT study), these elements are modified since, in the predefined Inverter Control, there is no Reactive power-based LVRT voltage support function. Figure 4-11 illustrates the predefined inverter control provided by the Simulink.

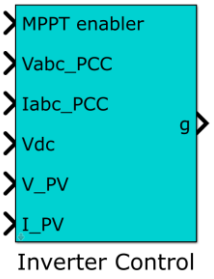

Figure 4-11 Inverter control from MATLAB Simulink Library [166]

It can be seen from the Figure; the Inverter Control has six inputs. ‘MPPT enabler' enables the MPPT functions provided by the MPPT regulator. This function will be enabled when the input of the ‘MPPT enabler' is set ‘1'. When the input of the ‘MPPT enabler' is set ‘0', it means the inverter control will disable the MPPT functionality. On a transient LVRT study that considers constant irradiance and constant temperature, the MPPT control can be excluded from the inverter control structure. This can be done by assuming the voltage, the current and the power of the PV array are known. ‘Vabc_PCC’ and ‘Iabc_PCC' are the three-phase ‘abc' voltage and the three-phase ‘abc’ current measured at the PCC of the DER. ‘Vabc_PCC’ and ‘Iabc_PCC’, as in *abc* reference frame, are used to construct ωt, v_d and v_q through PLL device. This is explained later in the ‘PLL section'. ‘Vdc' is obtained through DC voltage output measured at the PV array. In the Simulink modelling, this can be done by measuring the voltage between the output ‘+' and the ‘-' of the PV array, as shown in Figure 4-4. ‘V_PV' (voltage output) and ‘I_PV' (current output) are obtained from the PV array. Both can be referred to as the ‘V' and the ‘I' from Figure 4-12, whereas representing the ‘V' and the ‘I' in Figure 4-6. ‘g' as the output of the Inverter Control represents the modulating signal as input for the IGBT, which can be seen in Figure 4-11. The overall element that constructs the Inverter control module is shown in the Figure below. It shown in Figure 4-12 ‘PWM signal generator’ output signal is processed to modulate the IGBT.

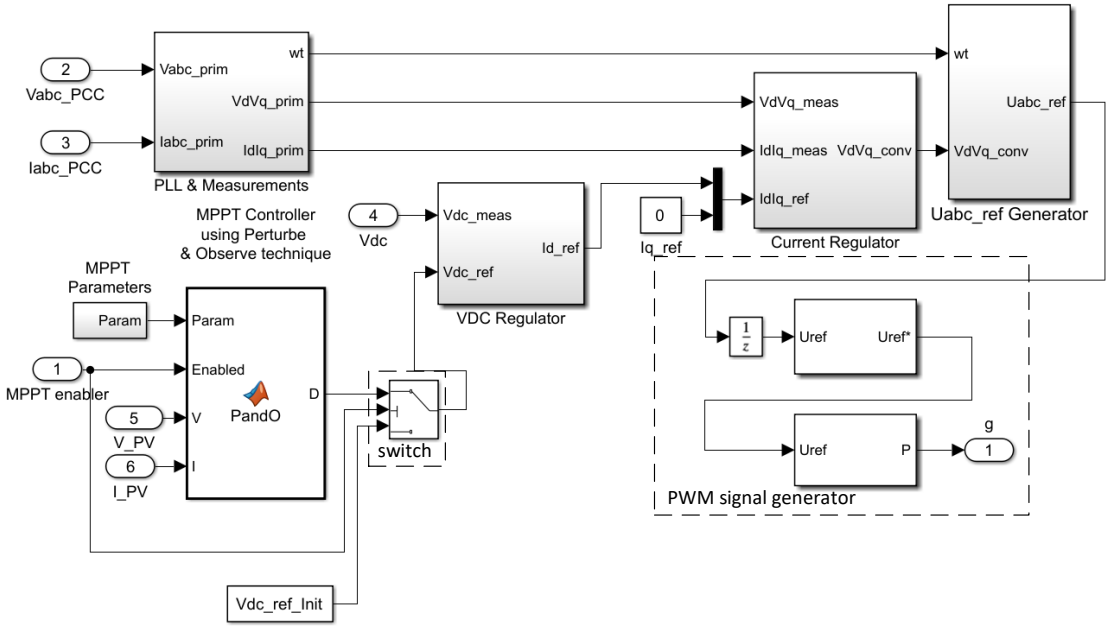

Figure 4-12 Inside the Inverter control from MATLAB Simulink Library [166]

It can be seen from Figure 4-12, six inputs represent the feed-in signal as seen in Figure 4-11. On the inverter control, when the MPPT enabler is set 1, then the 'V_PV' and 'I_PV' are processed through an MPPT controller, as seen in the Figure above. Note the 'V_PV', and 'I_PV' represent the $\mathcal{E}$ from Figure 4-3. Therefore, 'V_PV' and 'I_PV' act as feedback for the MPPT function. Through 'V_PV' and 'I_PV', and some MPPT parameters, the perturbed and observed technique (P&O) module defines the DC voltage reference, v_{dc_ref}, which then together with the measured DC voltage, v_{dc_meas}, are used to regulate the d-axis reference current, i_{d_ref}. The 'switch' as seen in Figure 4-12, represents the MPPT enabler function. On the transient LVRT study, the radiance is often considered constant. Thus a constant v_{dc_ref} for 480 volts, through 'Vdc_ref_Init' (as seen in Figure 4-12) is utilised. In this situation, the MPPT enabler is set 0, and the v_{dc_ref} on Vdc regulator receives 'Vdc_ref_Init' instead. The MPPT controller in the predefined inverter control uses the perturbed and observed technique (P&O) to optimise DC current output to handle radiance changing, which can be studied more in detail in [157].

4.5.4 DC Voltage Controller [150]

The design of the DC voltage controller is usually made for minimising the intermittency effect of the DC output of the PV array. On a unity power factor PV operation, such that on $i_{q\_ref} = 0$, the α is set as 0 (the α can be seen in Figure 4-3). In the Simulink modelling, the Vdc regulator, which received v_{dc_meas} and v_{dc_ref} as input, regulates i_{d_ref} through PI controller, can be seen in Figure 4-13.

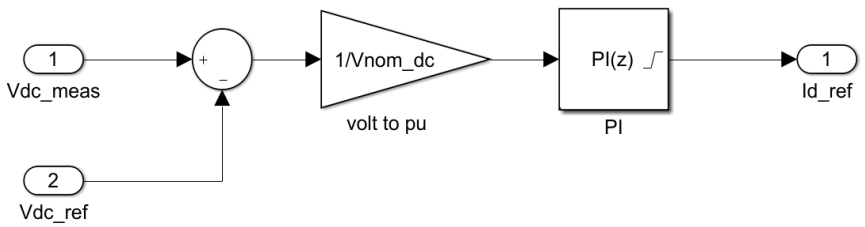

Figure 4-13 Diagram block of the Vdc regulator [150]

From Figure 4-12, it can be seen v_{dc_meas} is the measured v_{dc}, whereas v_{dc_ref} represents the reference v_{dc}. Note that the inputs and the outputs of the Vdc controller as shown in Figure 4-12 is similar to Figure 4-3. In the *Vdc* controller (Figure 4-13), the sum of v_{dc_meas} and v_{dc_ref} is transformed into i_{d_ref} through the PI controller. The PI controller uses Δv_{dc} in pu as the input signal. Its output is i_{d_ref}. In the predefined Simulink modelling (defaulted version in the MATLAB) [166], the predefined PI controller has a default value for 2 and 400 on the proportional and the integral gain, respectively.

Later, it will be shown on transient LVRT study, the output of the Vdc controller i_{d_ref} will also be regulated by the aRCI function.

4.5.5 PLL & Measurements [150], [167]

Grid synchronization is necessary on grid-connected power converters since it allows the power converter to work on the system frequency uniformly. The synchronisation is done through employing Phase Lock Loop (PLL) control. In principle, the Phase Lock Loop (PLL) control system works by tracking the frequency and phase of a sinusoidal three-phase signal by using an internal frequency oscillator, so that the PLL control system adjusts the internal oscillator frequency to keep the phases difference between the one measured with the one as a reference, zero. The PLL diagram block is shown in Figure 4-14 [150]. In this study, v_{abc} need to be transformed into v_{dq}. However, several steps need to be taken. v_{abc} is firstly needed to be transformed into $v_{\alpha\beta}$ through equation

$$\begin{bmatrix} v_\alpha \\ v_\beta \end{bmatrix} = \frac{2}{3}\begin{bmatrix} 1 & -\frac{1}{2} & -\frac{1}{2} \\ 0 & \frac{\sqrt{3}}{2} & -\frac{\sqrt{3}}{2} \end{bmatrix}\begin{bmatrix} v_a \\ v_b \\ v_c \end{bmatrix}. \tag{4.3}$$

The $v_{\alpha\beta}$ can be transformed into v_{dq} with

$$v_{dq} = \begin{bmatrix} v_d \\ v_q \end{bmatrix} = \begin{bmatrix} \cos(\theta) & \sin(\theta) \\ -\sin(\theta) & \cos(\theta) \end{bmatrix}\begin{bmatrix} v_\alpha \\ v_\beta \end{bmatrix}. \tag{4.4}$$

In the PLL function (Figure 4-14), v_q signal is used to generate ω through PID controller. By adding ω with ω_c, ω' is then generated. With integral function (1/s), θ is then obtained.

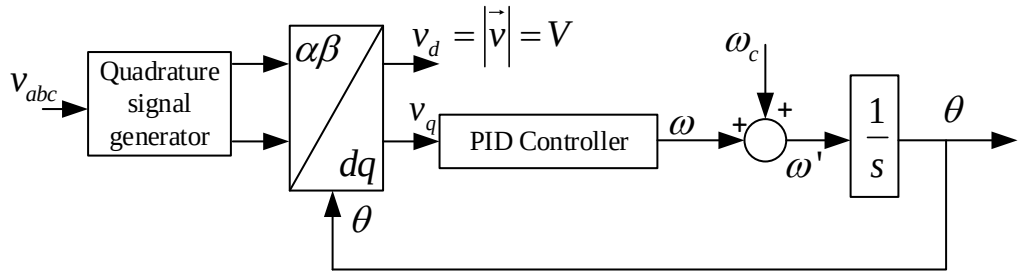

Figure 4-14 Diagram block of the PLL [150]

Note from Figure 4-14 one could conclude that the different angle between the axis of $\alpha\beta$ and the axis of dq is defined by θ. Since the PID controller is connected to the v_q output, as shown in Figure, 4-14 the virtual input vector *'v'* will rotate, coincide in time with the q axis of the dq reference frame in the steady state. Thus, it can be implied on the steady-state condition, when the $\alpha\beta$ axis aligned with *the* dq axis, then $d\theta/dt=0$. In the PLL representation, the v_d signal will serve as the amplitude of the input voltage vector and the phase-angle detected by the PLL will be in-phase with the virtual input vector v. This means that the detected phase-angle will be lagging for 90° with respect to the one of the sinusoidal input voltage. The representation of the above PLL in MATLAB Simulink, and the measurements, which comprise per unit conversions, from v_{abc} to v_{dq}, can be seen in Figure 4-15 [167].

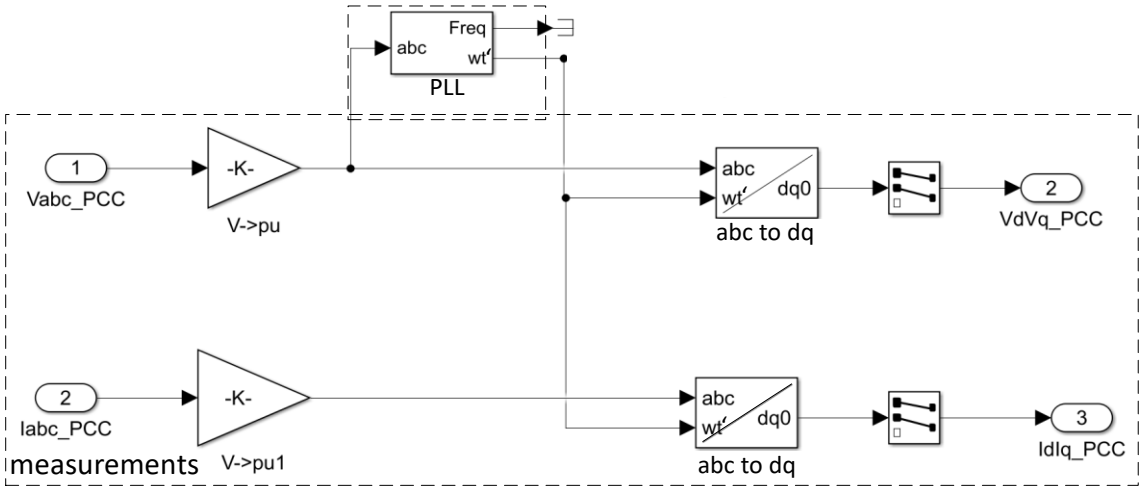

Figure 4-15 Model of the PLL along with the measurement blocks from MATLAB Simulink Library [167]

The *abc* to *dq* conversion box can be seen in the below figure 4-16. It can be seen from the figure the input v_{abc} signals are converted into $v_{\alpha\beta}$. The conversion is done by applying equation (4.3). The signals $v_{\alpha\beta}$ is then converted into v_{dq}. The conversion is done by applying

equation (4.4) with the help signal θ as illustrated in figure 4-14 (in figure 4-15 and 4-16, it is represented by wt').

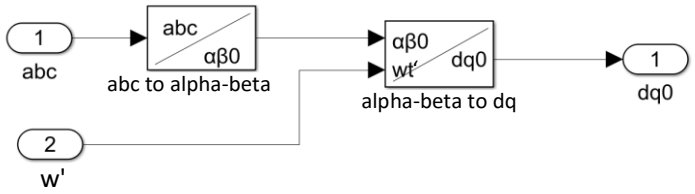

Figure 4-16 Inside the PLL block [167]

The predefined PLL (phase) is used in the model building on the top part of Figure 4-15. According to the MATLAB technical reference [167], for general purpose, k_p, k_i, and k_d of the PID controller are set 180, 3200, and 1, respectively. It can be seen '*wt*', as (θ) referred in the model, is used to define 'VdVq_PCC' (v_{dq}), and 'IdIq_PCC' (i_{dq}). The principle of the instantaneous power theory as shown in Figure 4-2 helps to understand the function of θ on the transformation of v_{abc} to v_{dq}.

The transformation of v_{abc} to $v_{\alpha\beta}$, and then from $v_{\alpha\beta}$ to v_{dq} that is done in the PLL diagram block requires Clarke and Park transformation [150]. The Clarke transformation converts balanced three-phase quantities, which in this case is the v_{abc}, into balanced two-phase quadrature quantities ($v_{\alpha\beta}$). The conversion of v_{abc} to $v_{\alpha\beta}$ is made for easier mathematical modelling in the MATLAB Simulink design. Further, in order to synchronise the voltage ($v_{\alpha\beta}$) as in $\alpha\beta$ reference frame to the synchronous (dq) reference frame that is relative to the grid frequency, $v_{\alpha\beta}$ is converted into v_{dq} as in dq reference frame, through Park transformation. Park transformation converts vectors in a balanced two-phase $\alpha\beta$ stationary system into dq rotating/synchronous reference frame. In the dq rotating reference frame, the d axis is at an angle θ. For better understanding, the transformations, vector representation of the signals v_{abc}, $v_{\alpha\beta}$, and v_{dq} on PLL and the measurements block is presented in Figure 4-17. It can be seen the signal v_{abc} is represented with the A, B, and C axis; the signal $v_{\alpha\beta}$ is presented with the α and β axis; and the v_{dq} is represented with d and q axis.

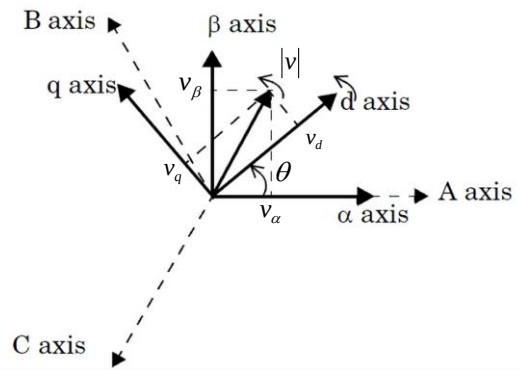

Figure 4-17 The vector representation of the signals v_{abc}, $v_{\alpha\beta}$, and v_{dq} on PLL and the measurements block [150].

From Figure 4-12, it can be seen the signals 'VdVq_PCC' (v_{dq}), and 'IdIq_PCC' (i_{dq}) are then transferred to the Current Regulator block. Observing the d axis of i_{dq} on 'IdIq_PCC' is referred to be the i_d, then the q axis of i_{dq} as 'IdIq_PCC' represents i_q as shown in Figure 4-3. Both i_d and i_q from Figure 4-3 can be seen on the Simulink model (as shown in Figure 4-16), referred to the 'IdIq_PCC' (i_{dq}). The definition 'PCC' stands the Point of Common Coupling (PCC) of the DER.

4.5.6 The Modelling of The DER Current Controller [150], [166]

Current control has the responsibilities of the power quality issues and current protection of the inverter, whereas its form is in DC quantities [150]. In a DC quantity, every deviation of the grid voltage and/or the grid current will be reflected in the response of the corresponding (d- and q-axis) components. The transient response that is transformed into d- and q-axis components would result in a more straightforward solution to filter and to control all corresponding signals that in DC quantities by means of Proportional-Integral (PI) based controllers [152]. The predefined current control modelling has a default value for 0.3 and 20 on the proportional and the integral gain, respectively [166]. From figure 4-3, it can be seen the i_{d_ref} signal is in accordance with the DC voltage regulator. i_{d_ref} is utilized as the reference for the active part current controller, whereas the reactive part current reference is usually set to be zero in normal operation – in figure 4-3, such condition is set by applying $\alpha=0$. When the reactive power has to be controlled in some cases, such as when the DER has to provide voltage support through reactive current injection during LVRT, a reactive power reference must be set such that the DER current controller could regulate reactive current injection in the event of LVRT voltage deviation. Such control, namely reactive-based current regulation, is presented in the next section.

As shown in figure 4-3, the current control is located in synchronous (dq) reference frame. By applying the Park transformation to the three-phase variable and i_{abc_meas}, it allows the

possibility of the current control in the *dq*-control form. The term '*meas*' refers to the measured value. Current control is generally with the help of PLL. It can be seen the current control from Figure 4-3, are redrawn into Figure 4-18. The PLL and the DC voltage (v_{dc}) controller are also given for better illustrating the functionality of each component. It can be seen the PLL output, θ, is used to transform i_{α_meas} and i_{β_meas} into i_{d_meas} and i_{q_meas}. Similarly, when the current controller generates signals v_{d_ref} and v_{q_ref}, to transform the two signals into v_{α_meas} and v_{β_meas}, it needs PLL output, θ. θ is also used to generate v_{d_meas} and v_{q_meas}.

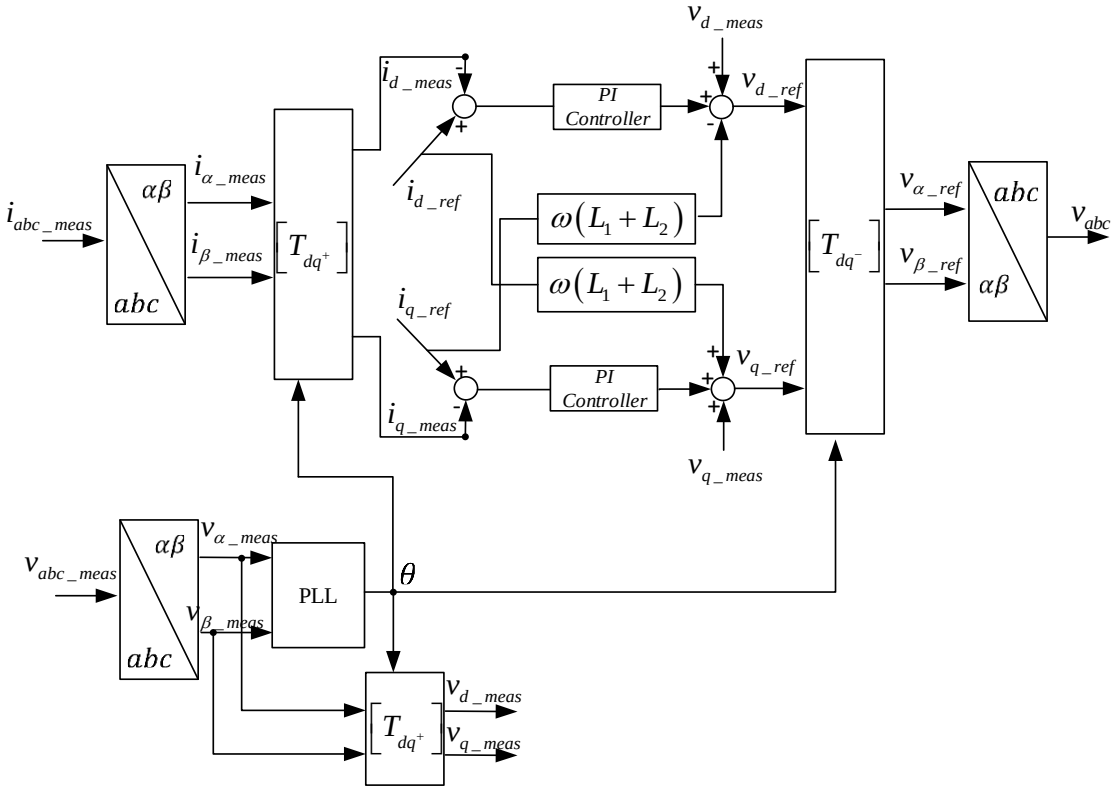

Figure 4-18 Diagram block of current control along with related supporting signals from the PLL and the DC voltage (v_{dc}) controller [150]

with

$$\left[T_{dq^+}\right]=\begin{bmatrix}\cos(\theta) & \sin(\theta)\\ -\sin(\theta) & \cos(\theta)\end{bmatrix}\ [150] \tag{4.5}$$

$$\left[T_{dq^-}\right]=\left[T_{dq^+}\right]^T=\begin{bmatrix}\cos(\theta) & -\sin(\theta)\\ \sin(\theta) & \cos(\theta)\end{bmatrix}\ [150]. \tag{4.6}$$

It can be seen on DER unity power factor operating setting, the i_{q_ref} is set 0, as seen in the figure 4-18.

4.5.7 The Proposed Modelling for The DER Current Control with aRCI Functions

The proposed modelling for the DER's current controller with the aRCI functions is presented. The proposed modelling is made based on equation 2.22 and 2.23 as explained in section 2.71. The main principle of aRCI function is to enable the DER to have the capability to regulate the idref and iref during LVRT. For enabling the aRCI function, the i_{d_ref} and i_{q_ref} input for the above modelling block (Figure 4-18) is needed to be added with the aRCI function modelling block (Figure 4-19). From Figure 4-19, it can be seen the aRCI function modelling is made by adding some diagram block at the output of the DC voltage (v_{dc}) controller and adding some function for the signals i_{q_ref}. The modelling is shown in Figure 4-19. The modification can be observed on the red-dotted squared functions.

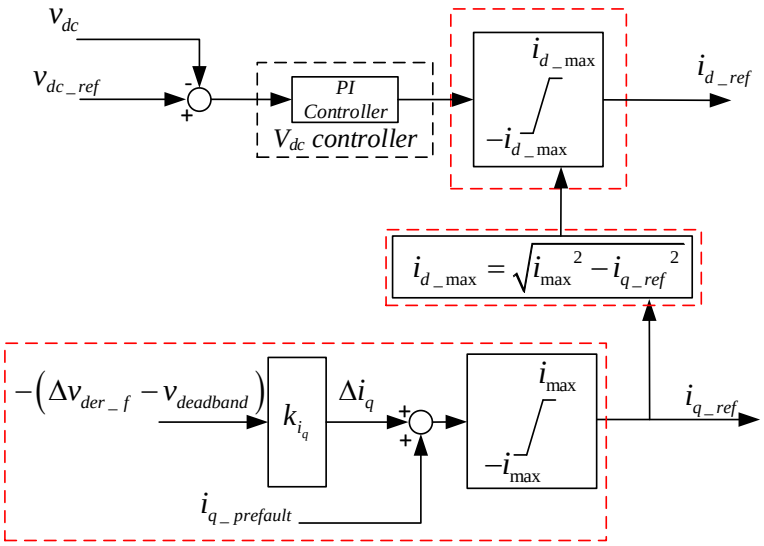

Figure 4-19 The Proposed Modelling for the DER current control with aRCI functions

As it can be seen from Figure 4-19, when there is a voltage sag that is detected at the DER connection, the different of the pre-fault voltage magnitude and the fault voltage magnitude Δv_{der_f}, is used as the input signals to determine the amount the additional reactive current being injected to the grid Δi_q. The voltage dead band $v_{deadband}$ sometimes is used to prevent the aRCI function from being too sensitive with the small voltage fluctuation. When the dead band is enabled, the signal Δv_{der_f} is deducted by $v_{deadband}$, and then multiplied by the K-factor, k_{i_q}, that is already set up upon DER installation. v_0 is the steady-state voltage at the DER connection. Commonly the $v_{deadband}$ is set at 10% of the v_0 [3], [33]. Signal Δi_q is added by the pre-fault reactive current, $i_{q\_prefault}$, to represent the regulated reactive current reference i_{q_ref}. The signal i_{q_ref} is limited by maximum current magnitude, i_{max} and $-i_{max}$, that is set to prevent overcurrent. Some studies set the value to be 1.5 and -1.5 for i_{max} and

$-i_{max}$ respectively [5], [168]. However, some studies set i_{max} and $-i_{max}$ for 1 and -1 [3]. In this study, i_{max} and $-i_{max}$ are set 1 and -1. The definition of i_{max} and $-i_{max}$ are related to the physical limitation of the inverter. Further, since the objective is to investigate the impact of the grid characteristic and the fault on the effectiveness of the LVRT voltage control via aRCI. As such, the determination of i_{max} and $-i_{max}$ may possible to not to be included in consideration of simulation testing. For simplicity, the voltage dead band $v_{deadband}$ is set 0% since it would not affect the objective of the study. Next section is about defining the simulation test system.

4.6 Defining Simulation Test System

In this section, simulation test system for the purpose of evaluating the aRCI-enabled DER response during LVRT is presented. The simulation test is done by using MATLAB Simulink. The three-phase DER model is connected to a distribution grid. The distribution system test example is shown in Figure 4-20. It presents typical single line diagram which commonly representing low voltage distribution grid. A three-phase single line diagram with five buses is shown. The distribution grid is connected to a main supply/infinite bus. The infinite bus has the line to ground voltage 120 kV, connected to a lower voltage level bus, Bus 2, that has the line to ground voltage 25 kV via Trafo 1. The photovoltaic/DER is connected to a line to ground voltage 0.25 kV bus 4. Trafo 2 connects bus 4 with the line to ground voltage 25 kV bus 3. Three distribution loads which representing community area are observed in the simulation testing.

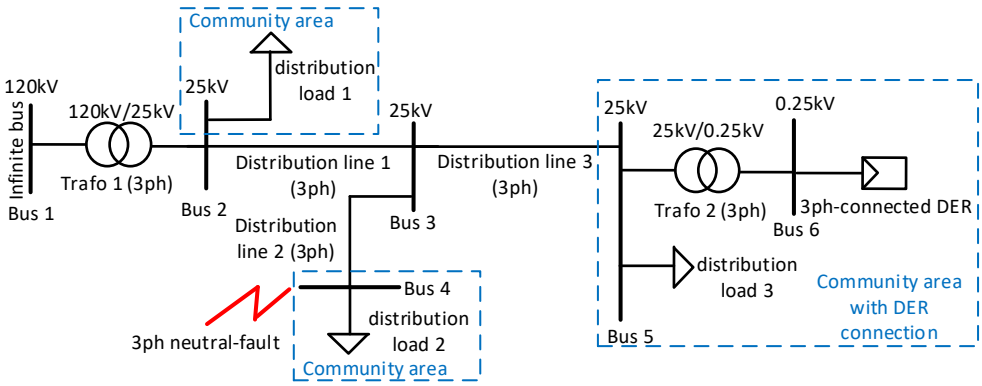

Figure 4-20 Single line diagram of the distribution grid used in the simulation testing

The consideration of the used test system on how the modelled DER connected to the bus, along with the aggregated load connections, and the representation of the infinite bus, is similar to the studies in [4], [14], [120], [169]. In their studies the load modelling is made based on a simple power load, whereas the infinite bus is made to situate the distribution system is connected to a strong grid. The design of the test system, the modelled distribution grid, is intended to illustrate typical distribution network and is to be made having typical distribution

network characteristic which used in many studies that relate to the distribution level DER issue.

Infinite bus, as shown in Figure 4-20, represent the external grid – the grid of the external part of the observed network. In the simulation, MATLAB Simulink Dynamic Three-Phase Source block is used. Dynamic Three-Phase Source block implements a balanced three-phase voltage source with an internal R-L impedance. Its source is the three-phase voltage sources that are connected in Y to an internally grounded neutral. It has internal resistance and inductance that are specified by the three-phase inductive short-circuit power and *X/R* ratio. On a defined three-phase inductive short-circuit power, S_{sc}, the internal inductance, $L_{internal}$, is defined through

$$L_{internal} = \frac{{v_{base}}^2}{S_{sc}} . \frac{1}{2\pi f} \tag{4.7}$$

with

$$R_{internal} = \frac{2\pi f . L_{internal}}{(X/R)_{ratio}} \tag{4.8}$$

and

$$X_{internal} = R_{internal}(X/R)_{ratio}. \tag{4.9}$$

Through three above equations, the parameters of the external grid ($L_{internal}$, $R_{internal}$, and $X_{internal}$) could be defined, and are shown in the table below.

Table 4-3 Parameters of External Grid

Parameters	value
Phase-to-phase voltage v_{rms} (kV)	120
Frequency (Hz)	60
3-phase short-circuit level at base voltage S_{sc} (MVA)	2500
Phase-to-phase base voltage v_{base} (kV)	120
$(X/R)_{ratio}$	7
$L_{internal}$ (H)	0.015
$R_{internal}$ (Ω)	0.82
$X_{internal}$ (Ω)	5.76

The table below shows the parameter of the two transformers (Transformer 1 and Transformer 2) in the system.

Table 4-4 Parameters of Transformer 1

Nominal power S_N (MVA)	47
Frequency (Hz)	60
Winding 1 parameters [$v_{rms\_ph\_ph}$ (kV) R_1 (pu) L_1 (pu)]	[120 2.67x10^{-3} 0.08]
Winding 1 connection	Yg (Wye grounded)
Winding 2 parameters [$v_{rms\_ph\_ph}$ (kV) R_2 (pu) L_2 (pu)]	[25 2.67x10^{-3} 0.08]
Winding 2 connection	Delta (with lagging to high-voltage winding (Y) by 30 degrees)
Magnetisation resistance R_m (pu)	500
Magnetisation inductance L_m (pu)	500

Table 4-5 Parameters of Transformer 2

Nominal power S_N (MVA)	250
Frequency (Hz)	60
Winding 1 parameters [v_{rms_ph-ph} (kV) R_1 (pu) L_1 (pu)]	[25 1.2x10^{-3} 0.03]
Winding 1 connection	Yg (Wye grounded)
Winding 2 parameters [$v_{rms\_ph\_ph}$ (kV) R_2 (pu) L_2 (pu)]	[0.25 1.2x10^{-3} 0.03]
Winding 2 connection	Delta (with lagging to high-voltage winding (Y) by 30 degrees)
Magnetisation resistance R_m (pu)	500
Magnetisation inductance L_m (pu)	500

The parameters of remaining of the element of the system test, the distribution line and the loads, are shown in the below table.

Table 4-6 Distribution line 1, 2 and 3

positive-sequence resistances [r1] (Ohms/Km)	0.1153
positive-sequence inductance [l1] (H/Km)	1.05x10^{-3}
positive-sequence capacitance [c1] (H/Km)	11.33x10^{-9}
Line length for distribution line 1 (Km)	8
Line length for distribution line 2 (Km)	8
Line length for distribution line 3 (Km)	14

Table 4-7 Distribution load 1, 2, and 3

Distribution load 1 [MW MVar]	[30 2]
Distribution load 2 [MW]	[2]
Distribution load 3 [MW]	[0.5]

The DER penetration is set 50% of the distribution load 3. Thus 250kW of aggregated three-phase PV used.

Later in the simulation testing, to test the effectiveness of the DER's LVRT voltage support via aRCI, three-phase short-circuit is set at bus 4, as shown in Figure 4-20.

In the MATLAB Simulink, to represent short-circuit fault, a Fault block that similarly acts as breaker blocks which can be individually switched on and off to program the faults is used. The Fault block in the MATLAB Simulink modelling is shown in Figure 4-21. To simulate fault, in the system test (4-20), the *A, B, C* connector is connected to the bus 4. R_{on_A}, R_{on_B}, and R_{on_C} represent fault resistance. R_g represents ground resistance.

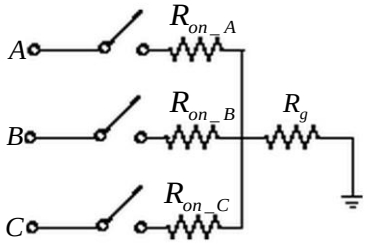

Figure 4-21 Fault block modelling on MATLAB Simulink

Below table represents the setting up the **three-phase short-circuit** for the simulation testing used in the study.

Table 4-8 Fault block parameters

Short circuit duration (ms)	150
$R_{on\_A}, R_{on\_B}, R_{on\_C}$ (Ω)	0.01
R_g (Ω)	0.01

Next section presents some simulated results.

4.7 Simulation Results

In this section, the simulated results of the aRCI-enabled DER response during LVRT are presented in order to evaluate the effectiveness of LVRT voltage control via aRCI. Several system's component response; voltage terminal at the DER connection in per unit (V_{DER}), *dq* reference current in per unit (i_{d_ref}, i_{q_ref}), *dq* measured current in per unit (i_{d_meas}, i_{q_meas}), *dq* measured current in per unit (v_{d_meas}, v_{q_meas}), DER's active power in kW (p), and DER's reactive power in kVAr (q); are shown.

The simulation runs for 3 seconds. The three-phase fault is set at 1.5 s. Since the fault duration is set for 150 ms, the fault is cleared at 1.65 s. The fault location is at bus four as shown in Figure 4-20. There are five scenario tests; DER with K-Factor (K_{I_q})=0, 0.5, 1, 1.5, & 2; which each are presented in the following section. The K-Factor number adjusts the aRCI magnitude of the DER following LVRT. As such, as according to equation (2.22) and (2.23), Higher K-factor results in higher aRCI magnitude. Following the simulation results, discussion relating to the simulation results is presented in section 4.8.

4.7.1 DER's Voltage response

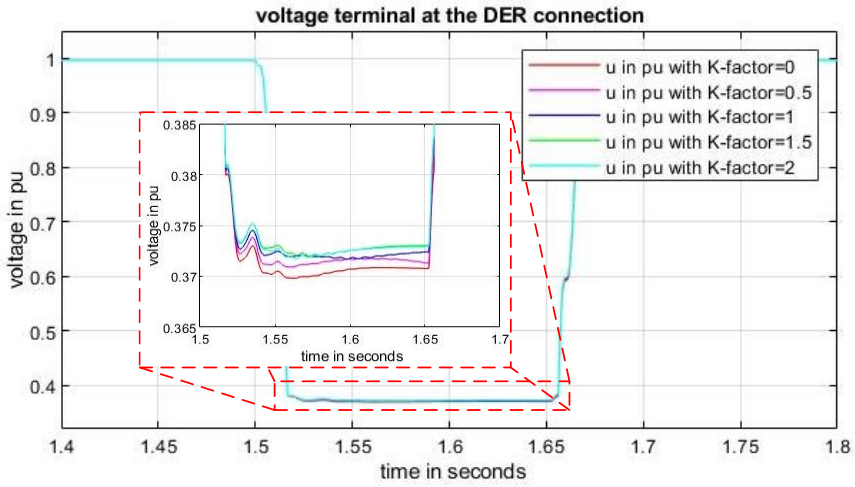

Figure 4-22 Response of the voltage terminal at the DER connection in per unit (V_{DER}) during LVRT

Table 4-9 the voltage sags at the DER connection in per unit (V_{DER}) during fault

Parameters	Symbol	Value				
K-factor	K_{I_q}	0	0.5	1	1.5	2
voltage sag	V_{DER}	0.370	0.371	0.372	0.3729	0.373

From Figure 4-22, it can be seen that voltage sags are observed at the DER connection during fault. On DER with no aRCI, when the voltage sags, it reached 0.371 pu. The simulation result of the DER with no aRCI can be observed at the scenario K-factor=0. Since no aRCI is given during LVRT, the voltage sags (red line) the lowest. On DER with aRCI, for instance, with K-factor 0.5, the voltage sags are improved to 0.371 pu. More voltage sag improvement can be observed on DER with aRCI on K-factor=1, for 0.372 pu. Voltage sag improvement on DER with aRCI on K-factor 1.5 and 2, are observed to reach 0.3729 pu, and 0.373 pu, respectively. On the table the value of the voltage sags are estimated at the condition in which the value during fault is relatively steady – voltage sags at which prior post-fault response (in this case, the value is taken at around 1.6-1.65 s). Overall improvement of the voltage sags on all scenarios can be seen in table 4-9. It can be seen that when the maximum aRCI is enabled, voltage sag improvement is observed from 0.37 pu to 0.373 pu. From the simulation result, it can be observed voltage sag improvement through reactive power based voltage support still can be achieved on the distribution level. The line for the DER park is normally has *X/R* ratio impedance for above 1.2. In the simulation study, the *X/R* ratio of the connection line are set $9x10^{-3}$, which is below 1.2 [170]–[172]. According to the simulation results, the use of LVRT voltage support via aRCI has a value even for a distribution system to improve the voltage grid stability. As such, it indicates the aRCI-based LVRT voltage support can be used on distribution-connected DER as well.

4.7.2 DER's *dq* Reference Current Response

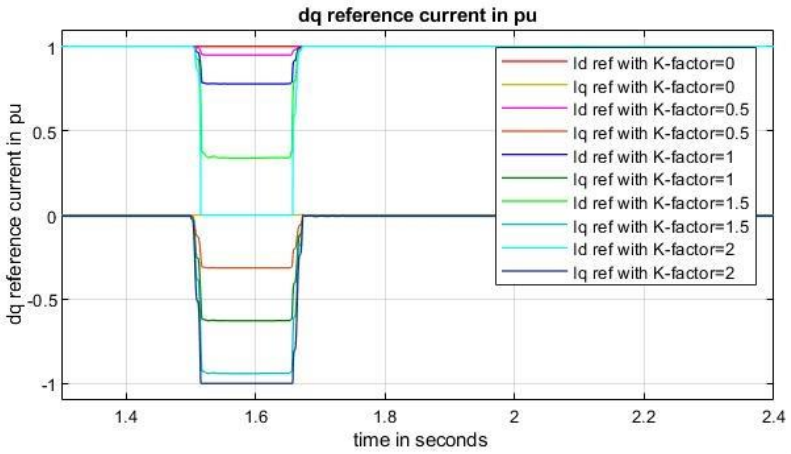

Figure 4-23 Response of the *dq* reference current in per unit (i_{d_ref}, i_{q_ref}) during LVRT

Figure 4-23 shows the *dq* reference current responses. On DER without aRCI, the K-factor is set to 0. On such condition, the *dq* reference current stays constant even during the fault. These responses can be seen in the figure, red line (i_{d_ref}) and dark-yellow line (i_{q_ref}). When the DER is with aRCI function, the *dq* reference current responding the fault by injecting *q* reference current (i_{q_ref}). Note the **sign convention** of the *q* reference frame in the simulation dictates *q* reference current injection is applied when i_{q_ref} is negative. In the figure, for instance on DER with aRCI on K-factor=0.5, *q* reference current injection means the i_{q_ref} goes down to -0.314 pu. However, on the *d* reference frame, dictates *d* reference current injection is applied when i_{d_ref} is positive. In the figure, for instance on DER with aRCI on K-factor=0.5, *d* reference current reduction means the i_{d_ref} goes down to 0.949 pu. On more K-factor, more i_{q_ref} is injected. As such, more i_{d_ref} is reduced in order to compensate for the magnitude of the i_{q_ref} injection. Overall the value of the *dq* reference current responses can be seen in the table 4-10.

Table 4-10 the *dq* reference current responses (i_{d_ref}, i_{q_ref}) during fault

Parameters	Symbol	Value				
K-factor	K_{I_q}	0	0.5	1	1.5	2
dq reference current in pu	i_{d_ref}	1.000	0.949	0.778	0.338	0.000
	i_{q_ref}	0.000	-0.314	-0.628	-0.940	-1.000

4.7.3 DER's Measured *dq* Current Response

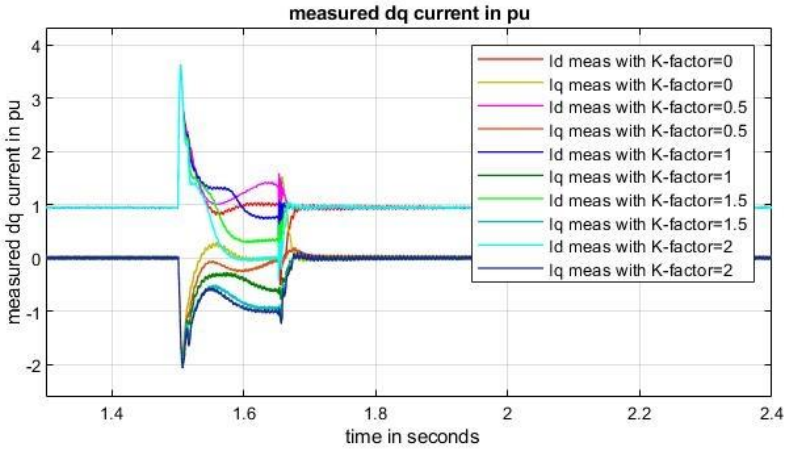

Figure 4-24 Response of the *dq* measured current in per unit (i_{d_meas}, i_{q_meas}) during LVRT

The *dq* measured current responses (i_{d_meas}, i_{q_meas}) during fault are observed in Figure 4-24. In general, it can be seen at the point when the fault is happening, *dq* measured current responds transiently. It can be seen the i_{d_meas} rises suddenly, up to around 3 pu, whereas the i_{q_meas} also behave transiently, goes down to almost -2 pu. The response of the both during the initialisation of the fault represents the value of short circuit current which contributed by the DER in the *dq* reference frame. The short circuit current contributed by the DER exists due to the immediate need of short-circuit current that is needed to be flown to the faulted bus [140]. Following transient fault, it can be seen that *dq* measured current reacts accordingly to reach back its settling condition.

Depend on the K-factor setting, when the zero K-factor is given, no aRCI is given; it can be seen that the *dq* measured current responses (i_{d_meas}, i_{q_meas}) oscillates towards its initial state (for i_{d_meas}=1, while i_{q_meas}=0). On DER with aRCI, for instance with K-factor 0.5, the *dq* measured current responses during fault are oscillated, and on its prior post-fault state (at around 1.6-1.65 s), both reach 1.069 pu and -0.156 pu for i_{d_meas} and i_{q_meas} respectively. On DER with aRCI on K-factor=1, the *dq* measured current responses reach 0.759 pu and -0.588 pu for i_{d_meas} and i_{q_meas} respectively, on its prior post-fault state. It can be observed the *dq* measured current responses are dictated by the *dq* reference current since it can be seen at prior post-fault state, *dq* measured current value are similar to the *dq* reference current. Overall the responses of all *dq* measured current responses on all scenarios can be seen in the table 4-11.

Table 4-11 the *dq* measured current responses (i_{d_meas}, i_{q_meas}) during fault

Parameters	Symbol	Value				
K-factor	K_{I_q}	0	0.5	1	1.5	2
dq measured current in pu	i_{d_meas}	0.000	1.069	0.759	0.337	0.004
	i_{q_meas}	1.000	-0.156	-0.588	-0.937	-1.005

4.7.4 DER's Measured *dq* Voltage Response

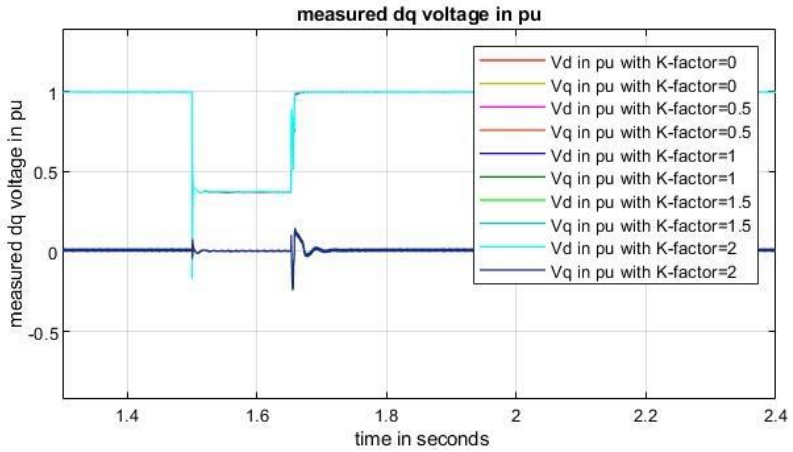

Figure 4-25 Response of the *dq* measured voltage in per unit (v_{d_meas}, v_{q_meas}) during LVRT

The responses of the *dq* measured voltage in per unit during fault are shown in Figure 4-25. The *dq* measured voltages that are represented in Figure 4-25 are measured at the PCC of the DER. As such, the *dq* measured voltages are the voltage as shown in Figure 4-22 that is in the *dq* reference frame. On DER with no aRCI, the *dq* measured voltage responses v_{d_meas} sags at 0.384 pu, whereas v_{q_meas} are relatively steady at 0 pu. On DER with aRCI, v_{d_meas} sags at relatively the same level. For instance with K-factor 0.5, the v_{d_meas} sags at 0.371 pu whereas on DER with aRCI on K-factor=1, 1.5, and 2, the v_{d_meas} sags at 0.37 pu. Overall *dq* measured voltage response on all scenarios can be seen in the table 4-12.

Table 4-12 the *dq* measured voltage in per unit (v_{d_meas}, v_{q_meas}) during fault

Parameters	Symbol	Value				
K-factor	K_{I_q}	0	0.5	1	1.5	2
dq measured voltage in pu	v_{d_meas}	0.384	0.371	0.370	0.370	0.370
	v_{q_meas}	0.000	0.000	0.000	0.000	0.000

4.7.5 DER's Active Power Response

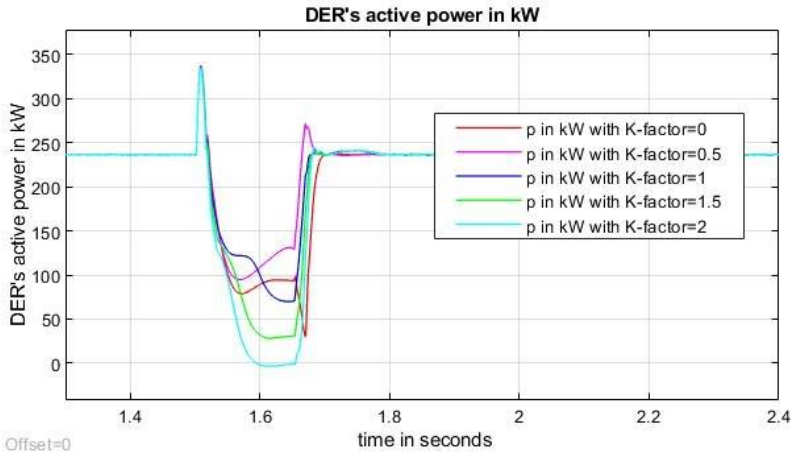

Figure 4-26 Response of the DER's active power in kW (p) during LVRT

On Figure 4-26, DER's active power responses in kW (p) during fault are observed. It can be seen in general, during the initialisation of the fault, that the DER's active power jumps almost 350kW. Note the DER's operational capacity in the simulation is 250 kW. The sudden increase of the DER's active power for all K-factor cases that are shown in Figure 4-26 are attributed by the short circuit power contributed by the DER, which appear due to sudden need of short-circuit power that is needed to be flown to the faulted bus [140] (the DER's active power responses, and the DER's reactive power responses, as discussed in section 4.7.6 as well, will be discussed in detail in section 4.8.1). On DER with no aRCI, it can be seen that the DER's active power during fault is shown on the red line. On DER with aRCI on K-factor 0.5, DER's active power during fault is shown on the pink line. The remaining DER's active power responses during fault are illustrated. Overall DER's active power responses on its prior post-fault state on all scenarios can be seen in the table 4-13. The DER's active power oscillations during fault are attributed by the dq measured current (i_{d_meas}, i_{q_meas}) and the dq measured voltage (v_{d_meas}, v_{q_meas}). The oscillations of the DER's active power will be explained in more detail in the discussions in section 4.8.

Table 4-13 the DER's active power in kW (p) during fault

Parameters	Symbol	Value				
K-factor	K_{I_q}	0	0.5	1	1.5	2
DER's active power in kW	(p)	93.928	130.890	69.990	29.810	0

4.7.6 DER's Reactive Power Response

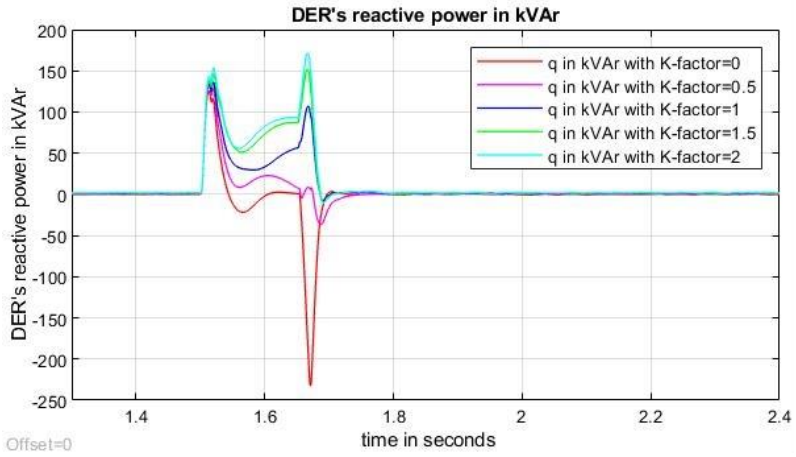

Figure 4-27 Response of the DER's reactive power in kVAr (q) during LVRT

On Figure 4-27, DER's reactive power responses in kVAr (q) during fault are illustrated. Similarly, with the DER's active power responses as explained in section 4.7.5, the sudden jumps of the DER's reactive powers are attributed by the short-circuit power that is needed to be flown to the faulted bus [140]. On DER with no aRCI, it can be seen that the DER's reactive power during fault is shown on the red line. On DER with aRCI on K-factor 0.5, more DER's reactive power during fault is observed. Most DER's reactive power is given during fault is observed DER with aRCI on K-factor 2. Overall DER's reactive power responses on its prior post-fault state on all scenarios can be seen in the table 4-14. Again the DER's reactive power responses are attributed by the dq measured current (i_{d_meas}, i_{q_meas}) and the dq measured voltage (v_{d_meas}, v_{q_meas}). The oscillations of he DER's reactive power will also be further explained in more detail in the discussions in section 4.8.

Table 4-14 the DER's reactive power in kW (q) during fault

Parameters	Symbol	Value				
K-factor	K_{I_q}	0	0.5	1	1.5	2
DER's reactive power in kW	(q)	0.830	16.276	50.110	86.270	92.136

4.8 Discussion

The discussion is presented to understand better the simulation results as illustrated in section 4.7. This section **is presented into two parts**. The **first** presents the discussion relating to the DER's dynamic response following LVRT and how's its response by injecting aRCI as to improve voltage sags. The first discussion is presented in order to understand dynamically better 'the flow' the mechanism of aRCI in improving voltage sag. The **second** part presents the discussion that is more focused on the voltage sags improvement through different K-factors settings.

4.8.1 DER's Dynamic Response and The aRCI Function Following LVRT

The purpose of this section is to illustrate the process of the DER in responding to the LVRT and how's the aRCI function react upon the voltage sag.

Initiated by the three-phase short-circuit at bus 4, the system voltage sags. The fault duration is set for 150 ms. The short-circuit that is set at bus 4, also cause voltage sags at the DER connection (Figure 4-22). Following voltage sags, the DER's inverter reacts accordingly. Depending on the DER's settings; if the K-factor was set at zero, it means the DER would not inject additional reactive current. When the K-factor was set at, for instance, 1, or 2, then additional reactive current is given following LVRT. When the additional reactive current is given, the voltage sag at the DER connection is improved. The process on how the DER's reaction following faults, and correlate it with the voltage support via reactive current injection, can be understood through the following process as explained in the following paragraph.

During LVRT, the transient behaviour of the *dq* measured voltage (v_{d_meas}, v_{q_meas}) and the *dq* measured current (i_{d_meas}, i_{q_meas}), constitute the DER response following the grid disturbance. In the RMS simulation, the dynamic response of the DER upon responding to the disturbance is attributed by the measured voltage and the measured current. Meaning, the two product, the measured voltage and the measured current, affect the derivative of the state variable of the DER's inverter dynamically. This process can be understood since (i_{d_meas}, i_{q_meas}) and (v_{d_meas}, v_{q_meas}) serve as input signals at the current controller and the PLL (as illustrated in Figure 4-18). As such, in the simulation modelling, every non-zero state derivate (the transient dynamic response [139]) of the DER modelling, is initiated by the transient response of the (i_{d_meas}, i_{q_meas}) and (v_{d_meas}, v_{q_meas}).

The product of the DER's LVRT voltage support is done through reactive regulation. The DER's active and reactive power regulation as means of their voltage support is attributed by the value of the *dq* measured voltage, and the *dq* measured current. In other words, these signals response (i_{d_meas}, i_{q_meas} and v_{d_meas}, v_{q_meas}), constitute the DER's active and reactive power response. This meaning can be translated into the following paragraph.

The DER's response as in the form of DER's active (*p*) (Figure 4-26) and reactive (*q*) (Figure 4-27) power response, are the product of the *dq* measured current (i_{d_meas}, i_{q_meas}) and the *dq* measured voltage (v_{d_meas}, v_{q_meas}). This process can be understood since the DER's active (*p*) and reactive (*q*) power are yielded from [173]

$$\begin{bmatrix} p \\ q \end{bmatrix} = \begin{bmatrix} v_\alpha & v_\beta \\ v_\beta & -v_\alpha \end{bmatrix} \begin{bmatrix} i_\alpha \\ i_\beta \end{bmatrix}, \tag{4.10}$$

whereas (i_α, i_β) and (v_α, v_β) which act as the measured current and the measured voltage on the stationary reference frame, are obtained from

$$i_\alpha = i_{d\_meas} cos\theta - i_{q\_meas} sin\theta, \tag{4.11}$$

$$i_\beta = i_{d\_meas} sin\theta - i_{q\_meas} cos\theta, \tag{4.12}$$

and

$$\begin{bmatrix} v_\alpha \\ v_\beta \end{bmatrix} = \frac{1}{\cos^2(\theta) + \sin^2(\theta)} \begin{bmatrix} \cos(\theta) & \sin(\theta) \\ -\sin(\theta) & \cos(\theta) \end{bmatrix} \begin{bmatrix} v_{d\_meas} \\ v_{q\_meas} \end{bmatrix}. \tag{4.13}$$

Thus, one could imply that the DER's active (p) and reactive (q) power response during fault are characterised by the response of the *dq* measured current, and the *dq* measured voltage.

However, it should be understood that when the DER has the aRCI function (as presented in the Figure 4-18 and 4-19), the *dq* measured current, is in principle dictated by the *dq* reference current. To better understand this concept, the understanding of the aRCI function that constitutes the *dq* reference current response is given in the following paragraph.

In principle, aRCI is achieved by regulating *dq* reference current. When aRCI function is enabled, additional i_{q_ref} is given. As according to the diagram block as shown in Figure 4-19, one could observe on a detectable voltage sags Δv_{DER_f}, the additional reactive current is then injected to the grid Δi_q, proportionally to the K-factor setting K_{I_q}. In order to prevent overcurrent, on i_{q_ref} injection, some i_{d_ref} is reduced proportionally. As such, one could see on *dq* reference current (i_{d_ref}, i_{q_ref}) as shown in Figure 4-23, more K-factor, which lead to the more i_{q_ref} injection, resulting in the lesser i_{d_ref}. Further the *dq* reference current (i_{d_ref}, i_{q_ref}) dictates *dq* measured current. Hence it can be seen on the prior post-fault state, *dq* measured current resembles *dq* reference current.

Through knowing that the *dq* measured current are dictated by *dq* reference current, one could observe the *dq* measured current response can be 'regulated' by manipulating the level of the aRCI injection. Noting the fact that DER's active (p) and reactive (q) power response during fault are characterised by the response of the *dq* measured current, and the *dq* measured voltage, it finally can be understood then how's the regulation of *dq* reference current through aRCI function can influence the voltage sags improvement.

4.8.2 The Impact of Different K-Factors to The Voltage Sags Improvement

Now on **the second** part the following discussion is given more about the impact of different K-factors on the voltage sags improvement. From the simulated results, it can be observed more reactive current injections could lead to more voltage sag magnitude improvement.

However, it should be noted that from the simulated results, the voltage sag improvement is limited by the *q* reference current increment. The voltage sag maximum improvement can be indicated when the *q* reference current increment reach -1 pu. This can be understood since when the *q* reference current reaches -1 pu, no more additional reactive current could be injected. The limitation is often made to prevent inverter's internal damage [150].

The study uses a regular distribution grid as the test system. As such, the system is with a highly resistive element – a condition that might impede the effectiveness of the reactive power injection support. However, it is found that based on the simulation results, reactive power based-LVRT voltage support still can be used to improve voltage sag. For instance, on K-Factor (K_{I_q})=0.5, the voltage sags at the DER connection improved from 0.370 pu to 0.371 pu. The aRCI injection causes q reference current (i_{q_ref}) change, from 0 to -0.314 pu. The *d* reference current (i_{d_ref}) is reduced to 0.949 pu during fault as to compensate the magnitude of the aRCI injection. It can be seen during fault the oscillated *dq* measured current are again, transiently oscillate, and during its prior post-fault state, converge towards to the value of the *dq* reference current. Unlike the previous scenario, there is DER's reactive (q) power injection as a result of enabling aRCI function. Further on K-Factor (K_{I_q})=1, the voltage that sags at the DER connection improved better at 0.372 pu. The aRCI injection causes q reference current (i_{q_ref}) shifting during the fault, from 0 to -0.628 pu, which indicates the level of the reactive current injection is larger than the previous scenario. Again, the *d* reference current (i_{d_ref}) is reduced to 0.778 pu during fault as to compensate further increment of the q reference current. The *dq* measured current has similar behaviour to the previous scenario - transiently oscillates, and during its prior post-fault state, converges toward the value of the *dq* reference current. The DER's reactive power injection on K-factor (K_{I_q})=1 reaches 50.11 MVAr, whereas on the previous scenario, on K-factor (K_{I_q})=0.5, DER's reactive power injection is only 16.276 MVAr. As such, compared to the previous scenario (on K-Factor (K_{I_q})=0.5), there is more DER's reactive power injection as a result of more aRCI injection.

It is shown from the simulation results in general, even though maximum reactive current injection is already given, it does not improve the voltage sag to a level at which it is worthwhile to implement the aRCI function. This finding can be found in the simulation study with the K-Factor (K_{I_q})=2. Even though it can be seen during LVRT, the *q* reference current (i_{q_ref}) reaches at -1 pu, indicating the reactive current that is injected is already at the maximum level that could be given by the DER, the voltage sags improvement is observed at best only at 0.373 pu, from 0.37 pu. Further, it can be seen as well from the simulation study, high amount of reactive power injection (for the case of K-Factor (K_{I_q})=2, the reactive power

injection reaches up to 92.136 MVAr) does not correlate with significant voltage sag improvement. Although this finding is already well-known and many researchers aware this observation [3], [4], [23], [28], [50], from our simulated studies, it is observed that the quality of the voltage sag improvement through reactive power-based voltage support, instead by K-Factor, is actually very much depends on the impedance characteristic of the system at which the DER is connected to (This finding will be better observed in the simulation test with system under different condition, which is presented in the chapter 5). In theory voltage sag is the product of the shorted-circuit current that is flown to the faulted location. The shorted-circuit current has its magnitude and the phase angle value that is relative to the grid impedance phase. As such, to summed it up with the simulation result evidenced in this study, the magnitude of the voltage sag improvement which through reactive power-based voltage support is determined by the grid impedance phase. In other words, it depends on the conditions, if the grid impedance has a high reactance part, then it will help the reactive power injection more effectively on improving the voltage sags. In our simulations, since the DER is connected in the distribution system, the grid impedance has a low reactance part. As such, it affects the reactive power injection adversely on improving the voltage sags.

Simulation results given in this chapter has shown the need to investigate the impact of grid characteristic on the effectiveness of DER's aRCI-based LVRT voltage support. The next chapter presents, through our dynamic RMS simulation cases, the evaluation of the effectiveness of the DER's aRCI-based LVRT voltage support on improving voltage sag under various typical *X/R* ratio of the distribution grid.

4.9 Summary

The realisation of the voltage support modelling requires the DER modelling as a whole system along with the grid connection. The dynamic modelling of the DER, along with the proposed modelling of the DER's aRCI-based LVRT voltage support in MATLAB Simulink is successfully made. The work of the DER modelling also helps better in understanding the process of DER's response dynamically, along with the aRCI mechanism on regulating the *dq* reference current (i_{d_ref}, i_{q_ref}), following a fault, as means to provide reactive power regulation in order to support the voltage sag improvement. Overall the modelling of the DER along with the proposed aRCI design has been made and could be dedicated for the investigation of the aRCI-based voltage support evaluation.

Further, understanding dynamically 'the flow' the mechanism of aRCI in improving voltage sag, as presented in this chapter, will help better on understanding DER's response dynamically to help to investigate the impact of the grid characteristic to the effectiveness of the DER's aRCI-based LVRT voltage support, in the next chapter 5.

Chapter 5 The Impact of Distribution Grid Characteristic to The Effectiveness of DER's aRCI Based LVRT Voltage Support

5.1 Introduction

Initially, the impact of the DER's connections to the grid stability was not considered critical. Thus to protect the electronic components of the DERs from unwanted disruptions, such as transient voltage faults, these units could be disconnected from the remaining grid during grid faults. The disconnections could be achieved by employing under-voltage protection. However, with the increasing penetration of DERs, the disconnections might cause unwanted transient grid instability. When a grid fault occurs, the fault impact that can be sensed in a wide surrounding area propagates away from the fault site throughout the power system. Consequently, this can cause several DER units to be automatically disconnected. Such disconnection of a group of DERs will result in a considerable cascading loss of electricity generation. To alleviate the problem, especially with the ongoing plans to increase the penetration of DER units, the voltage support capability will not only be required for the DERs at the medium voltage level, but also for the DERs on the distribution grid level. As such, investigating the impact of distribution grid characteristic to the effectiveness of DER's aRCI-based LVRT voltage support is necessary.

5.2 The Need for Investigating Impact of The Grid Characteristic to The aRCI-based Voltage Support Performance

The idea of LVRT voltage support through reactive power regulation at first was made since many wind and PV parks were connected to a long feeder – a condition that which most of the power source park was mainly connected to a medium voltage line [4]. As such, implementing LVRT voltage support through reactive power-based regulation was considered ideal, as most of these DER connections are made through long feeder which has relatively higher *X/R* ratio than connection lines on lower voltage level [1]. Because of the nature of the DER connections voltage level, as has been discussed in chapter 2, many grid codes require the LVRT voltage support only for MV-connected DER, but do not yet consider the need of LVRT voltage support for LV-connected DER. As such, there is a need to investigate the readiness of implementing aRCI-based LVRT voltage support for the DER on low voltage connections.

The grid's *X/R* ratio and the 'grid strength' define the grid characteristic [174]. It is well-known that the lines on the distribution level tend to have a lower *X/R* ratio than the line on transmission level [2], [4]. Furthermore, distribution lines tend to be weaker as compared to

the lines on a higher voltage level, as normally lines on distribution level have impedance level higher relative to the line on transmission level [175].

The studies about the impact of the *X/R* ratio on the voltage stability of the DER connected grid has been the scope of the research in many studies [48], [168], [170], [175], [176]. However, in most of the studies reviewed, only the steady-state voltage stability was considered in detail. The investigation of the transient LVRT stability of the DER-connected grid still can be found in many topics of interest. However, studies on LVRT stability of the DER-connected grid that consider distribution grid's *X/R* ratio and the 'grid strength' has not yet been made. In [3] the impact of various levels of the injected reactive power on different DER locations was analysed and provided useful information regarding the relationship between the injected reactive power level and the DER location relative to the fault location. It was found that DERs located close to the fault result in less LVRT voltage sag improvement. DERs that are relatively far from the fault location give a better LVRT voltage sag improvement. However, the study only considered DER on medium voltage level connections. Other studies relying on considering a group of rotating-based loads originated by air conditioning systems have been presented in [14], [78], [109], [110], but the effect of the *X/R* ratio of the system on the effectiveness of the DER's LVRT voltage support was not considered. DER's flexible LVRT voltage support via a reactive power based regulation as a means to solve asymmetrical faults are discussed in [177], [178]. However, none of them considered the effect of the *X/R* ratio of the system on the effectiveness of the voltage support. In [4] an investigation of LVRT of DER-connected grid at distribution and transmission levels is presented. It is found that generally, the voltage recovery time during LVRT of DER on low voltage level connection is longer than on higher levels. However, the investigation of voltage support was not carried out in this study.

From many previous studies so far, it is found that 'weak' distribution grid, which has typically high line impedance level [177], may introduce grid and DER instability during the post-LVRT state [175], [179]. The increased number of DERs on the distribution grid has been associated with the weakening of the grid strength [175], [176], [180]. Further, it has been observed that the strength of AC grids has significant implication to the stability of the DER connection into the AC grids [181], [182]. As such, transient stability analysis is required to evaluate whether the weak AC grid and the DER could withstand large disturbances. Particularly in the event of fault disturbance, there are potential voltage instability problems and system collapse happening, when the DER and the weak AC grid could not meet the reactive power demand to compensate the voltage deviations. Therefore, for such reason, when the DERs are connected to a weak AC grid, appropriate voltage support is required to ensure the DER-connected grid is stable during and after the fault clearance. Thus, there is a need to investigate

the effect of a weak distribution grid and its *X/R* ratio to the effectiveness of the DER's reactive power based LVRT voltage support and the voltage stability of the distribution system. In the following section, the association of the increasing number of the DER connections to the weakening of the grid strength will be explained.

5.3 The Implications of Growing Numbers of DER on Grid Strength

On a distribution system, such as medium voltage levels with long radial feeders, which far away from synchronous generators, the strength of the system can be characterised by the Short Circuit Capacity (SCC) value of the system [183]. The Short Circuit Capacity (SCC) is taken as

$$SCC = \frac{v_{grid}}{z_{grid}}, \tag{5.1}$$

whereas v_{grid} and z_{grid} represent the overall grid voltage and impedances. As such, it can be seen from equation (5.1), for illustration, the higher of the impedance level in pu of the grid, and assuming the voltage of the system under normal condition is in one pu, the lower is the value of the SCC. The SCC is a grid strength indicator of at the specified point or a bus. Thus, in theory, a system, which comprises of numerous generators and transmission lines will have multiple SCC from each bus [183].

It has been reported that the increasing number of DERs on the distribution grid has always been linked with the weakening of the grid strength [175], [176], [180]. This can be understood since, by definition from IEEE 1204 [183], a weak power grid has high impedance value relative to the point of connection of the DER. In other words, with the presence of the DER at the distribution level, the grid becomes weaker as more active power is being generated by the DER. The classification of the strength of the DER-connected grid, as in the form of the Short Circuit Ratio (SCR), can be understood as according to

$$SCR = \frac{SCC}{P_{DER}}, \tag{5.2}$$

whereas P_{DER} indicates the level of the DER's active power of the respective bus. The SCR is an indicator of the ability of the bus to maintain its voltage in response to the power variations. Thus, a grid with high SCR will be less sensitive to the bus voltage deviation than a grid with low SCR [183]. The increments of the DER's active power results in smaller Short Circuit Ratio (SCR). As such, smaller SCR will result to the weakening of the grid.

It should be understood that the strength of AC grids has a significant impact on the stability of the integration of DER into the AC grids [184]. By definition, the 'strength' of the grid, in general, is determined by its impedance and mechanical inertia, i.e., kinetic energy, stored in

the rotating parts of all connected generators [185]. Therefore, 'weak grid' differs to the 'grid with low SCR' since the value of the SCR, is simply a comparison of the AC grid short circuit capacity (SCC) and DC power injection at the specified bus – an indicator of the grid strength at the specified point or a bus [185]. Even so, although the SCR is not the precise strength indicator of the entire grid, still, it can be a useful evaluation tool for measuring the grid strength at a specified point, such as the Point of Common Coupling of the DER connections.

5.3.1 Some Classifications of The Strength of The AC Grid

The classification of the grid strength can be made based on the SCR level of the grid. Illustratively, the following is a definition of the strength of an AC grid, as according to IEEE 1204 [183]:

1. strong grid, when the SCR of the grid is greater than 3 pu
2. weak grid, when the SCR of AC grid is between 2 pu and 3 pu
3. very weak grid, when the SCR of AC grid is lower than 2 pu

It should be noted that the classifications of the strength of the AC grid are normally made based on the grid regulator's practical experiences gained from the monitoring of the power grid operations [184]. As such, the classifications can be different in each region. For example, in the German grid code [117], it is mentioned that the SCR at the grid connection point of the DER should be at a minimum of 6 pu, and should be guaranteed by the related Transmission System Operators (TSO) for the connection of the DER. In the Danish grid code [34], [35], the SCR is made to be at a minimum of 10 pu at the grid connection point of the DER. In the CIRED-CIGRE Joint Working group [186], the grid connection point of the DER is considered weak if the SCR is less than 5 pu, or if SCR at the MV collection grid is less than 4 pu. The grid connection point of the DER is considered to be very weak if SCR is less than 3 pu, or if the SCR at the MV collection grid is less than 2 pu. All the previously described standards agree that the lower the value of the SCR, the weaker the grid will be.

5.3.2 Weak Grid Indications

Further, although all of the above-mentioned SCR standards have different interpretation on what level of the grid SCR should be considered weak, in general, it is agreed that a grid becomes weak if one or more of the indications as shown in the below is exposed to the grid [34], [35], [117], [183], [184], [186].

1. if the DER-connected grid has high impedance lines, and/or not connected to a strong

neighbouring grid.

2. if the grid's synchronous power sources are replaced with a high number of DER connections.
3. if the grid has lines and/or buses at which the DER is connected, is located far away from the main network connections.
4. if rich wind/radiance resources are located far away from the load centres at which DER's PCC has to be connected via the long feeder.
5. if the DER is indicated has a high internal impedance (due to their transformers at their PCC).

5.4 Defining Typical *X/R* ratio of The Distribution Grid Lines

Many studies agreed that normally, the line in the distribution level has lower *X/R* ratio than the line in the transmission level [29], [187], [188]. The *X/R* ratio of the transmission line is very much attributed by the construction of the transmission line: the cross section of its conductors, the material of its conductors, the distance between its conductors and the insulator between its conductors [185]. Further, transmission lines are made to transmit electric power at a higher voltage than the distribution line. As such, the distance between the wires of the transmission lines is normally made much larger than the distribution line. Thus, such situation leads the transmission line has much higher magnetic energy storage, and consequently its inductance per unit length will be higher – meaning that the *X/R* ratio of the transmission line will be higher than that of the distribution line for the same current ratings [185].

The classification level of 'low' and 'high' *X/R* ratio for the low voltage (LV) and high voltage (HV) lines is not always consistent between studies. In [170], for instance, the range of the of typical 'low' and 'high' *X/R* ratio for the LV and HV line impedance for their DER integration study are between 0.62 and 2.1, while in [171], the range of the 'low' and 'high' *X/R* ratio are between 0.16 and 3.14. Further, better classification levels are given; 'low', 'medium', and 'high' *X/R* ratio for the low-, medium- (MV), and high-voltage lines, which can be found in [172]. Their definitions for the 'low', 'medium', and 'high' for the *X/R* ratio are 0.12, 1.2, and 3.22, respectively. In this thesis, since distribution level is the focus of the study, the variation of the *X/R* ratio for the investigation is to be made between from 0.12 and 1.2, based on the study in [172]. It will be shown in section 5.6 the *X/R* ratio used in the simulation study is presented in Table 5-2.

After the description of the low *X/R* ratio is given, section 5.5 is made to understand better the standpoint of the weak network relating to the stability of the DER-connected grid and its voltage support.

5.5 The Standpoint of The Weak Network Relating to The Stability of the DER-Connected Grid and Its Voltage Support

Most of the rich wind sources and places with high radiance level are far away from the infinite bus. The infinite bus is often referred to as the bus with a strong grid connection. In most situations, a strong grid connection is closely located to the large synchronous power sources [185]. Thus, by nature, the infinite bus has higher SCC than the buses that far away from the large synchronous power sources [147]. Since the wind and PV parks are often connected relatively far away from the infinite bus, the wind and PV parks are most likely connected via medium voltage long feeder to a weak AC grid.

Thus, as for the case for the DER (wind and PV) park type, since most of the DER park are connected via medium voltage connections and are connected to electrically weak AC grids, they are frequently prone to the voltage disturbance [188]. As such, to ensure the voltage stability of these DER park-connected grids, often the DER park is equipped with the reactive power-based voltage support [168]. The reactive power-based voltage support is provided through static compensation for the steady state voltage support, and/or dynamic compensation for the transient LVRT voltage support [186]. The voltage support is made to enhance the integration of DER park into the weak AC grids.

Meanwhile, the introduction of the rooftop PVs allows the DER connection to be made within the urban/residential area, such that long feeder which normally required for the DER connection, is no longer needed. Therefore, with no medium voltage connection present between the DER and the load point, it is likely the DER-connected grid will have lower *X/R* ratio since the DER is connected directly to the weak AC grid. Further, it can be seen according to equation (5.2) the SCR of the AC grid will be lower when the number of the DER connection to the grid is increased. Meaning, increasing the number of the DER connection can increase the potential voltage instability of the AC grid following disturbance. With that in mind, it is clear that there is a need to investigate further implementation of the reactive power-based LVRT voltage support on the DER which directly connected to the weak AC grid.

It will be shown from in the study, on a weak grid, the post-LVRT instability could be prevented through correctly-adjusted reactive power-based voltage regulation. Following the appropriate simulation, suitable reactive current injection levels could be estimated and then employed to prevent system instability.

5.6 Setting Up the Simulation Test for The Investigation

The simulation test uses the system similarly used from chapter 4. However, some modifications are made in order to fit the objective of the study in this chapter. Since the

objective of the study is to investigate the impact of the distribution grid characteristic to the effectiveness of DER's aRCI-based LVRT voltage support, several simulation test cases are carried out through different *X/R* ratio level and the 'strength' of the grid.

The realisation of the test cases is done by setting up differently the parameters of one of the distribution line of the test system. Different line parameters are made by varying the inductance level of the grid in every simulation test. By doing so, the variation of the *X/R* ratio and the AC grid strength could be made. To create such cases, the impedance of the Distribution Line 3 that connects bus 3 and bus 5, as shown in Figure 4-20 from section 4.6, is set differently as per scenario. Table 5-1 shows the impedance parameters of Distribution Line 3 for each scenario used in this study. The parameters of the Distribution Line 3 are reshown in Table 5-1, along with the different inductance setting to express different *X/R* ratio of the line that is shown in Table 5-2.

Table 5-1 The resistance and the capacitance of the 'Distribution Line 3' per unit length, in Ohms/km (Ω/km) and Farads/km (F/km)

positive-sequence resistances [r1] (Ohms/Km)	0.1153
positive-sequence capacitance [c1] (F/Km)	11.33×10^{-9}
Line length (Km)	14

Table 5-2 The inductance of the 'Distribution Line 3' per unit length, in Henries/km (H/km)

Scenario	positive-sequence inductance [l1] (H/Km)	*X/R* ratio of the distribution line (*)
1	1.4×10^{-2}	0.12
2	4.00×10^{-2}	0.35
3	7.90×10^{-2}	0.80
4	1.44×10^{-1}	1.2

(*) the selected *X/R* ratio is made based on the *X/R* ratio of the typical distribution line as has been used in the study in [172]

5.7 Simulation Results

Throughout the simulation study, the scenarios of the simulation, that was carried out by applying different grid *X/R* ratio and its strength, were made to evaluate the impact of the grid characteristic to the stability of the grid and the aRCI-enabled DER connections. However, in order to save space and avoiding the repetitive presentation of the simulation results, in the following subsections, only four scenario tests are presented and highlighted.

The realisation of the four selected scenarios which are aligned to the scenarios as in Table 5-2 is made to express some aspects. The design of the simulation test system in scenario 1 and 2 are made to assess the stability grid with the DER connection following LVRT under different *X/R* ratios. The design of the simulation test system in the scenario 3 and 4 are made to assess the stability of the weak grid with the DER connection following LVRT, and also to

assess the possibility of benefiting aRCI-based LVRT voltage control to not only improving the voltage sag but also for preventing post-fault instability.

5.7.1 Scenario 1

In this scenario, the simulation test is done in five different cases, with each simulation having different K-factor. The K-factor, K_{I_q}, is chosen 0, 0.5, 1, 1.5, and 2, to represent the different level injection of aRCI. In the section (section 5.7.1.1), the DER's dynamic response; voltage terminal at the DER connection in per unit (V_{DER}), dq reference current in per unit (i_{d_ref}, i_{q_ref}), dq measured current in per unit (i_{d_meas}, i_{q_meas}), dq measured current in per unit (v_{d_meas}, v_{q_meas}), DER's active power in kW (p), and DER's reactive power in kVAr (q); are shown. The simulation results are then discussed in the second sub-section (section 5.7.1.2).

5.7.1.1 Simulation Results on Scenario 1

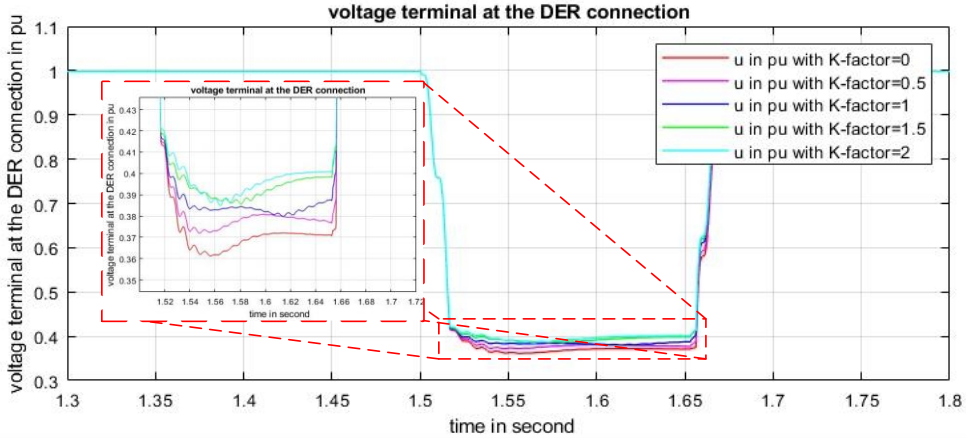

Figure 5-1 Response of the voltage terminal at the DER connection in per unit (V_{DER}) during LVRT with all corresponding K-factor settings (scenario 1)

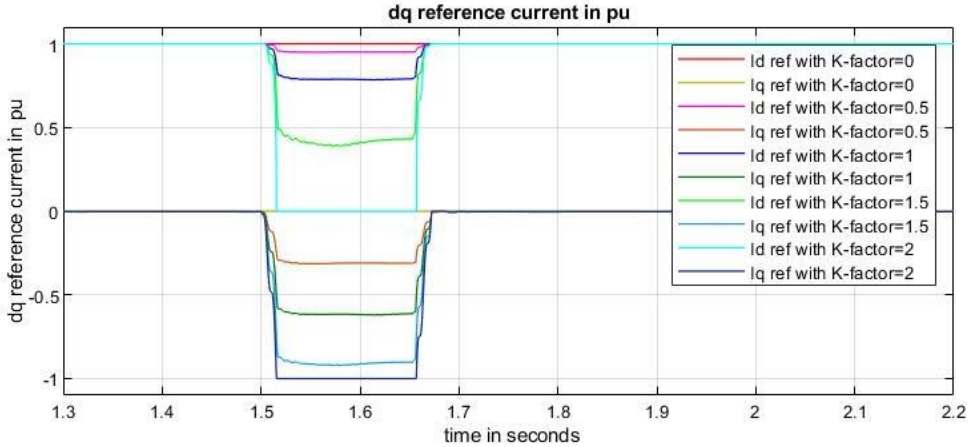

Figure 5-2 Response of the dq reference current in per unit (i_{d_ref}, i_{q_ref}) during LVRT with all corresponding K-factor settings (scenario 1)

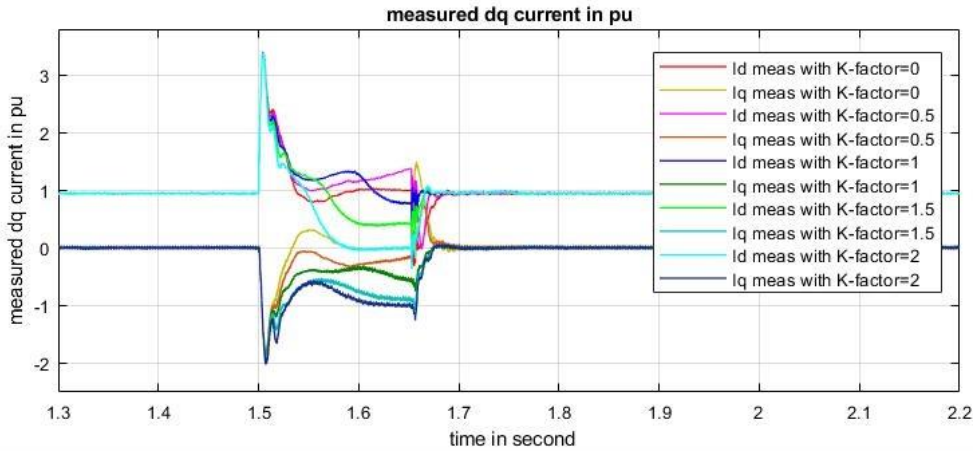

Figure 5-3 Response of the *dq* measured current in per unit (i_{d_meas}, i_{q_meas}) during LVRT with all corresponding K-factor settings (scenario 1)

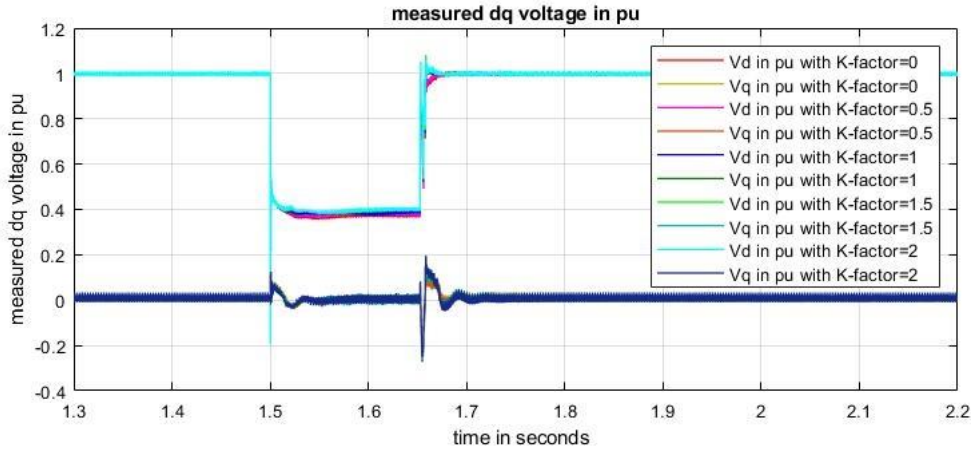

Figure 5-4 Response of the *dq* measured voltage in per unit (v_{d_meas}, v_{q_meas}) during LVRT with all corresponding K-factor settings (scenario 1)

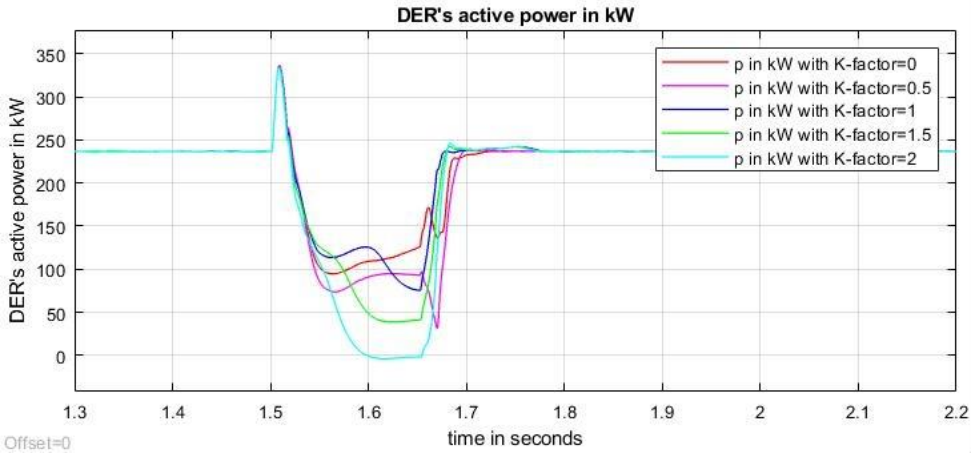

Figure 5-5 Response of the DER's active power in kW (p) during LVRT with all corresponding K-factor settings (scenario 1)

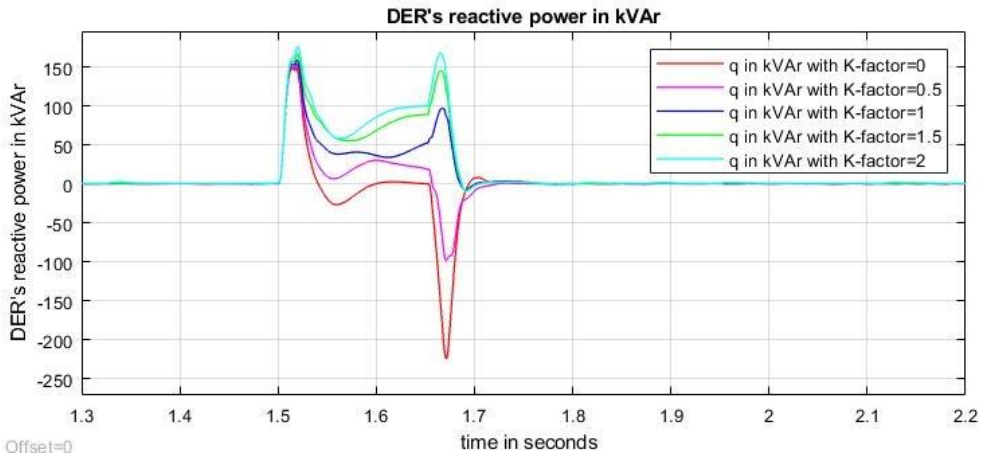

Figure 5-6 Response of the DER's reactive power in kVAr (q) during LVRT with all corresponding K-factor settings (scenario 1)

5.7.1.2 Observation on the Simulation Results from Scenario 1

As shown in the simulation results in section 5.7.1.1**,** the voltage sags at the DER connection can be improved when the aRCI are given. Higher aRCI level can be observed when higher K-factor is set. As shown in Table 5-3, when the DER is without aRCI function (K-factor=0), the voltage sags at 0.371 pu. Further, the *dq* reference current, as observed in Figure 5-2, stay constant during the fault. As a result, no additional DER's reactive power (q) is given (red line), as shown in Figure 5-6. The sudden jump of the active (Figure 5-5) and reactive (Figure 5-6) power at the initial state of the LVRT can be seen, which is attributed by the short circuit current contributed by the DER. The short circuit current in the *dq* reference frame can be seen in Figure 5-3. In the Figure, during the initial state of the LVRT, the magnitude of the d measured current (i_{d_meas}) increase suddenly almost three times before finally it steadily converges to its initial state. Similar to the q measured current (i_{q_meas}), its magnitudes decrease suddenly down to almost -2 pu, before finally it steadily converges to its initial state (1 pu). Note that the negative q reference is taken from the grid's perspective. Thus, when its direction is negative, it means the DER is injecting reactive current to the grid. This principle is applied to the i_{q_ref} and v_{q_meas} as well. It will be shown in the remaining scenarios that a similar sudden burst of the short-circuit current will be observed as well. This phenomenon will be better explained in the discussion, section 5.8.2.

On the case with K-factor=0.5, aRCI injection is observed to cause the i_{q_ref} move from 0 to -0.311 pu, resulting the i_{q_meas} shifted from 0 to -0.297 pu. As according to (4.10)-(4.13), this will cause DER to inject 21.33 kVAr to the grid during a fault. Hence, voltage sags reduction is observed, from 0.371 to 0.378 pu. Voltage sag improvement on K-factor=0.5 is observed for 1.887%. On the case with K-factor=2, it is observed as shown in Figure 5-2, maximum aRCI could be injected is given.

It can be observed that the K-factor variation leads to the variation of the voltage sag improvement magnitude (Figure 5-1). From the observed simulation results, the implication of the K-factor variation to the voltage sag at the DER connection can be explained, which is given as follows. Suppose when the voltage sag is happening, the DER's inverter will detect the difference of the pre-fault voltage magnitude and the fault voltage magnitude (Δv_{der_f}). This difference is then used to adjust the additional reactive current magnitude injection, Δi_q. The Δv_{der_f} is then multiplied by the adjusted K-factor, k_{i_q}. As such, one can imply that higher k_{i_q} leads to higher Δi_q. Note that i_{q_ref} is the product of pre-fault reactive current and Δi_q. Thus, from this point, one could see how is the k_{i_q} adjustment can regulate the level of the i_{q_ref}. Note that from Figure 5-2 and 5-3, the response of the measured q reference current, i_{q_meas}, is governed by the i_{q_ref}. The higher the negative magnitude of the i_{q_ref}, the higher will be the negative magnitude of the i_{q_meas}. Further, from Figure 5-3 and Figure 5-6, it can be implied that the higher negative magnitude of the i_{q_meas} results in higher reactive power magnitude being injected by the DER. As such, on higher k_{i_q}, the voltage sag restoration after LVRT is observed better; as shown in Figure 5-1 the grid could meet the reactive power demand to compensate the voltage deviations.

This can be indicated by the i_{d_ref} and i_{q_ref} are equal to 0 and -1, respectively. In this situation, DER injects 99.38 kVAr to the grid during fault. Hence, voltage sags reduction is observed at best, for 0.401 pu for voltage sag improvement for 8.086%. The overall observations of the LVRT simulation responses are presented in Table 5-3. It can be observed in general, higher aRCI leads to better voltage sag improvement.

Table 5-3 Overall observations of the LVRT simulation responses during fault for Scenario 1

Parameters	Symbol	Value				
K-factor	K_{I_q}	0.0	0.5	1.0	1.5	2.0
voltage sag	V_{DER}	0.371	0.378	0.385	0.398	0.401
	i_{d_ref}	1.000	0.950	0.786	0.422	0.000
dq reference current in pu	i_{q_ref}	0.000	-0.311	-0.617	-0.905	-1.000
	i_{d_meas}	1.007	1.192	0.797	0.385	0.000
dq measured current in pu	i_{q_meas}	0.006	-0.297	-0.676	-0.870	-0.933
	v_{d_meas}	0.374	0.378	0.390	0.403	0.409
dq measured volt in pu	v_{q_meas}	0.000	0.000	0.000	0.000	0.000
DER's active power in kW	(p)	121.600	93.660	76.790	40.390	0.736
DER's reactive power in kVAr	(q)	0.000	21.330	49.610	88.330	99.380
Voltage sag improvement rate in %	ΔV_{rate}	n/a	1.887	3.774	7.278	8.086

The voltage sag improvement that is shown in this study is made to demonstrate the usefulness of the reactive power-based voltage support from the DER in the distribution level grid. Should be understood that although in this scenario the voltage improvement under K-factor=2 case

is observed at 8.1% (as compared to the K-factor=0, or no reactive power injection is given), the simulation test uses a relatively small system (the total load of the grid is around 32MW, Table 4-7). Even more, the DER penetration level of the overall system is only 250kW, meaning the DER penetration level is less than 1%. As such, one could imply that there is a significant potential for the voltage sag improvement in the distribution level system for more than 8.1% when the DER penetrations are higher than the demonstrated simulation test.

5.7.2 Scenario 2

In this scenario, the simulation test cases are done five times. Similar to the previous scenario, maximum K-factor, K_{I_q}, is set up to 2. It will be shown in the simulation results since in this scenario the distribution line 3 has *X/R* ratio for 0.35, which is higher than previous scenario (0.12), the overall voltage sag improvements are observed better than in the previous scenario.

5.7.2.1 Simulation Results on Scenario 2

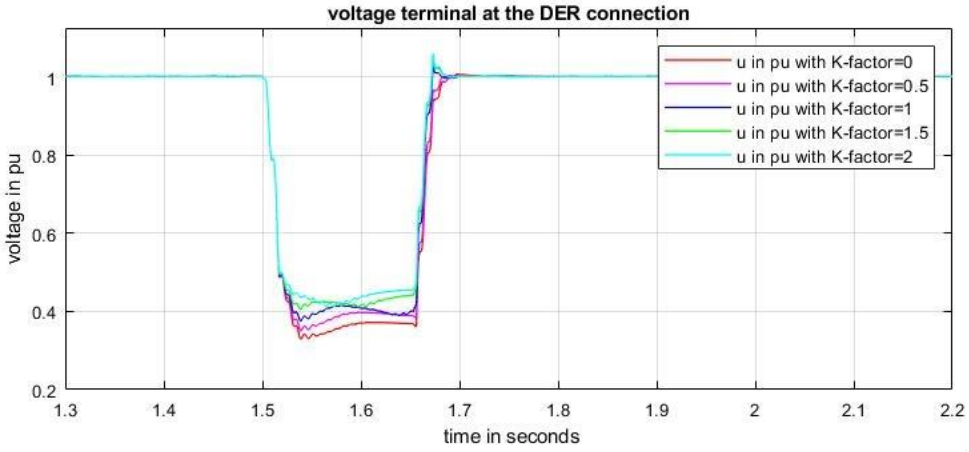

Figure 5-7 Response of the voltage terminal at the DER connection in per unit (V_{DER}) during LVRT with all corresponding K-factor settings (scenario 2)

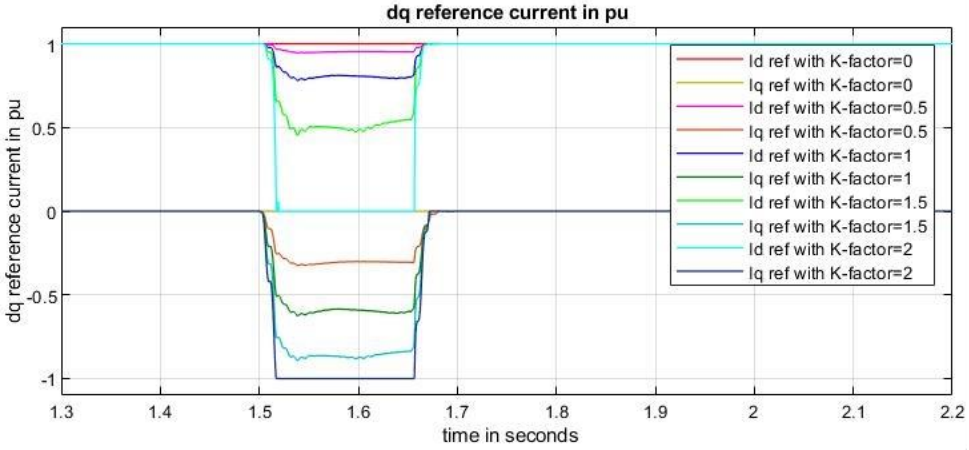

Figure 5-8 Response of the dq reference current in per unit (i_{d_ref}, i_{q_ref}) during LVRT with all corresponding K-factor settings (scenario 2)

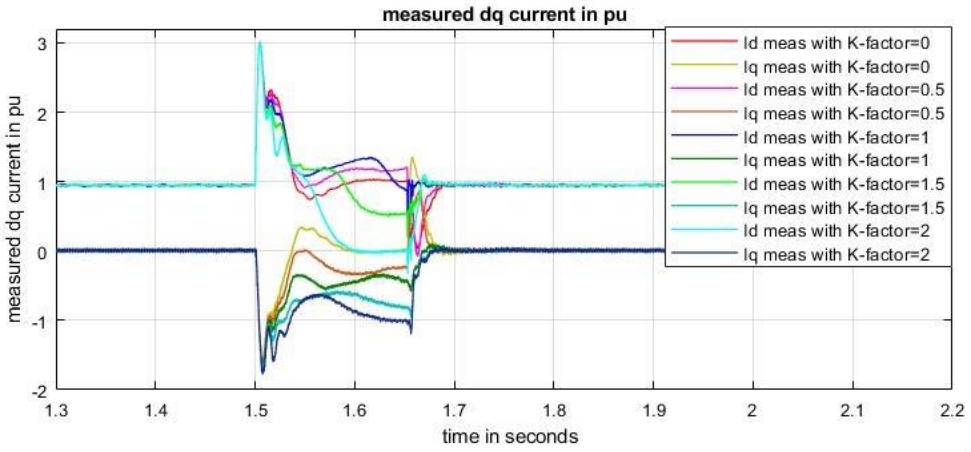

Figure 5-9 Response of the *dq* measured current in per unit (i_{d_meas}, i_{q_meas}) during LVRT with all corresponding K-factor settings (scenario 2)

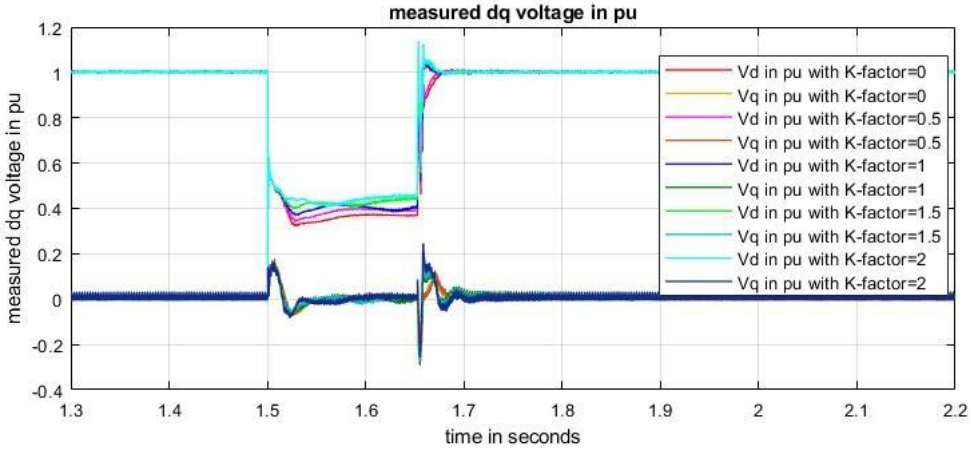

Figure 5-10 Response of the *dq* measured voltage in per unit (v_{d_meas}, v_{q_meas}) during LVRT with all corresponding K-factor settings (scenario 2)

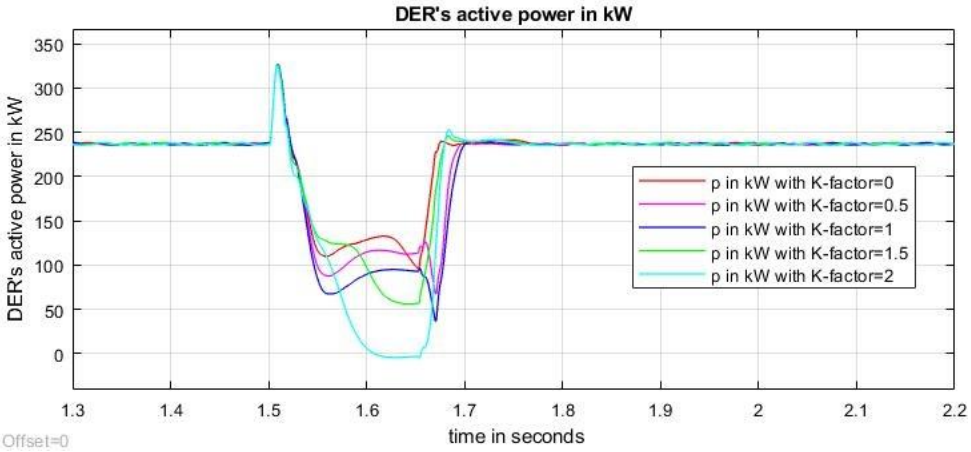

Figure 5-11 Response of the DER's active power in kW (p) during LVRT with all corresponding K-factor settings (scenario 2)

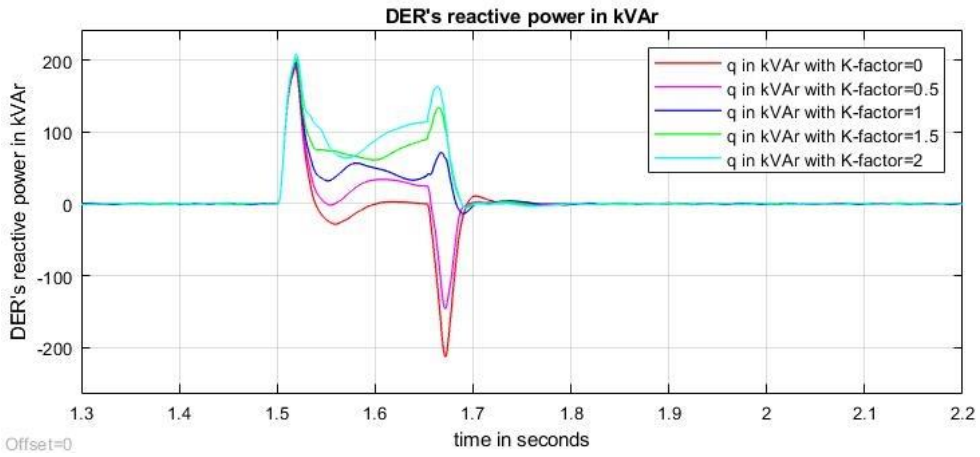

Figure 5-12 Response of the DER's reactive power in kVAr (q) during LVRT with all corresponding K-factor settings (scenario 2)

5.7.2.2 Observation on the Simulation Results from Scenario 2

From the simulation result, the voltage sags for the case K-factor=0 is observed at 0.369 pu, lower than the voltage sags on the same K-factor on the previous scenario (0.371 pu) – indicating in the Scenario 2 the grid is weaker than the one on scenario 1. However, it is observed that the overall voltage sag improvement rate is better than the one from the previous scenario. The observed result can be understood since the grid in the Scenario 2 has higher *X/R* ratio than in the previous scenarios. For instance, from Figure 5-7, on K-factor=1, the voltage sag improvement reaches 0.392 pu. In the previous scenario, with the same K-factor, the voltage sag reaches 0.385 pu. As such, from Scenario 2 the voltage sag improvement rate is observed at 6.233%, whereas on the same K-factor setting, the voltage sags improvement rate on Scenario 1 is observed at only 3.774%.

Further when the maximum aRCI is given (as seen on K-factor=2), in the Scenario 2 the voltage sag improvement rate is observed at 23.203% (at 0.455 pu), whereas in the Scenario 1 the voltage sag improvement rate is observed at only 6.086% (0.401 pu). Moreover, when a maximum reactive current is injected, under higher grid's *X/R* ratio, more reactive power could be injected by the DER. As such, these results indicate a strong influence of the *X/R* ratio of the grid to the performance of the aRCI on improving voltage sags during LVRT. The overall observations of the LVRT simulation responses are presented in Table 5-4.

Table 5-4 Overall observations of the LVRT simulation responses during fault for Scenario 2

Parameters	Symbol	Value				
K-factor	K_{I_q}	0.0	0.5	1.0	1.5	2.0
voltage sag	V_{DER}	0.369	0.390	0.392	0.438	0.455
dq reference current in pu	i_{d_ref}	1.000	0.953	0.797	0.528	0.000
	i_{q_ref}	0.000	-0.302	-0.603	-0.850	-1.000
dq measured current in pu	$i_{d\ meas}$	1.006	1.135	0.903	0.547	0.000
	i_{q_meas}	0.000	-0.234	-0.587	-0.828	-1.000
dq measured volt in pu	v_{d_meas}	0.367	0.386	0.401	0.441	0.466
	v_{q_meas}	0.000	0.000	0.000	0.000	0.000
DER's active power in kW	(p)	132.600	112.600	94.280	56.200	0.000
DER's reactive power in kVAr	(q)	0.000	25.540	33.370	85.960	112.400
Voltage sag improvement rate in %	ΔV_{rate}	n/a	5.691	6.233	18.699	23.306

5.7.3 Scenario 3

In this scenario, the positive-sequence inductance for the 'Distribution Line 3' is made almost six times of the positive-sequence inductance for the 'Distribution Line 3' in Scenario 1. The simulation setup is created to introduce the instability of the system due to the weak condition of the grid. Since the maximum reactive current injection is reached when the K-factor, K_{I_q} is 2.5, The K-factors for the cases is given from 0 to 2.5. As such, there are six simulation test case in this scenario (K-factors=0, 0.5, 1, 1.5, 2, & 2.5). Further, it will be shown in the simulation results, since in this scenario the grid impedances are higher than in the previous scenario, the DER connections are exposed to the potential instability of the weak grid condition. It will be shown as well that with the voltage support from the DER the potential instability could be avoided.

5.7.3.1 Simulation Results on Scenario 3

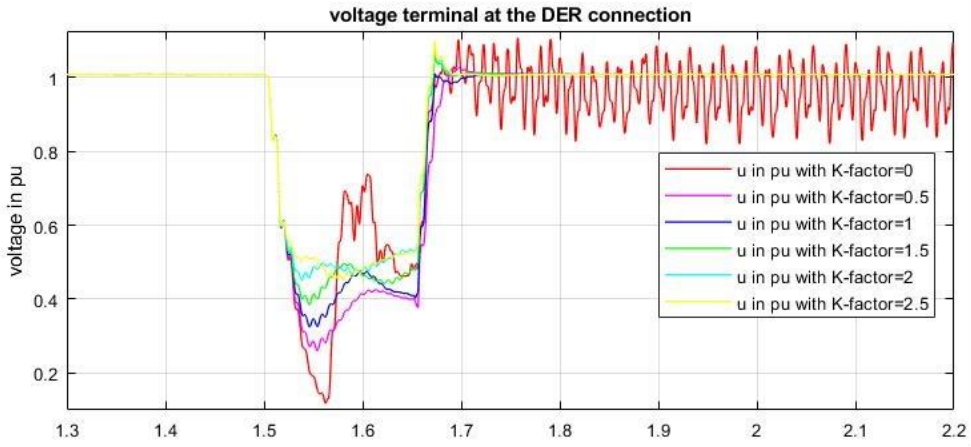

Figure 5-13 Response of the voltage terminal at the DER connection in per unit (V_{DER}) during LVRT with all corresponding K-factor settings (scenario 3)

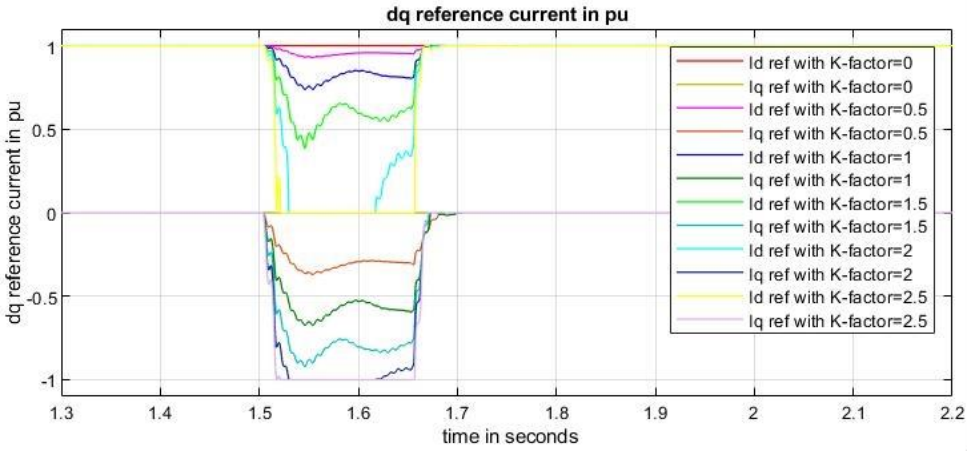

Figure 5-14 Response of the dq reference current in per unit (i_{d_ref}, i_{q_ref}) during LVRT with all corresponding K-factor settings (scenario 3)

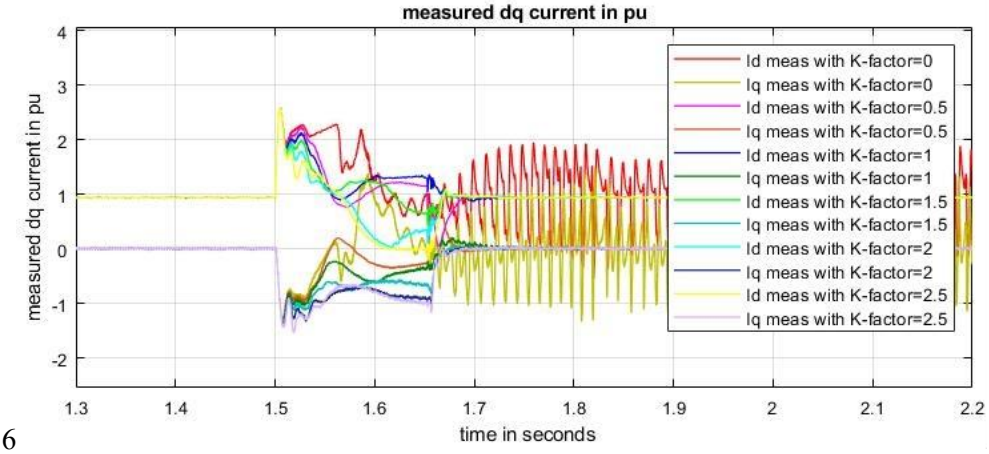

6

Figure 5-15 Response of the dq measured current in per unit ((i_{d_meas}, i_{q_meas}) during LVRT with all corresponding K-factor settings (scenario 3)

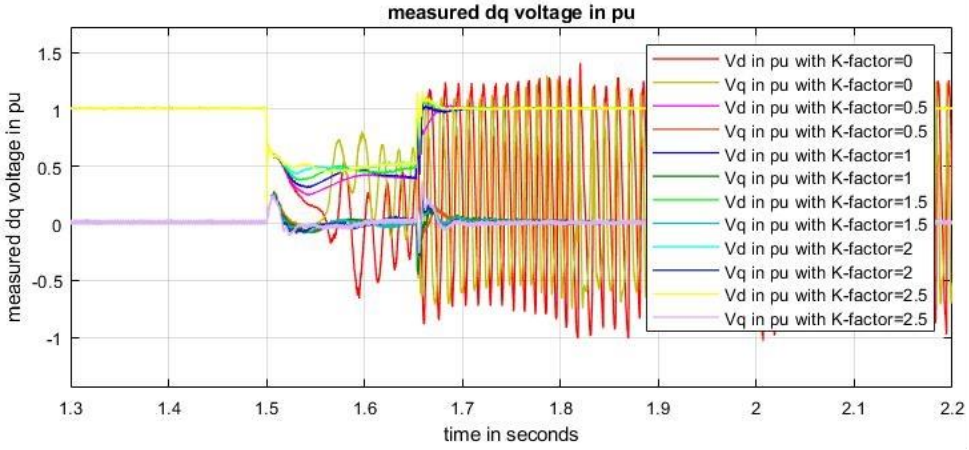

Figure 5-16 Response of the dq measured voltage in per unit (v_{d_meas}, v_{q_meas}) during LVRT with all corresponding K-factor settings (scenario 3)

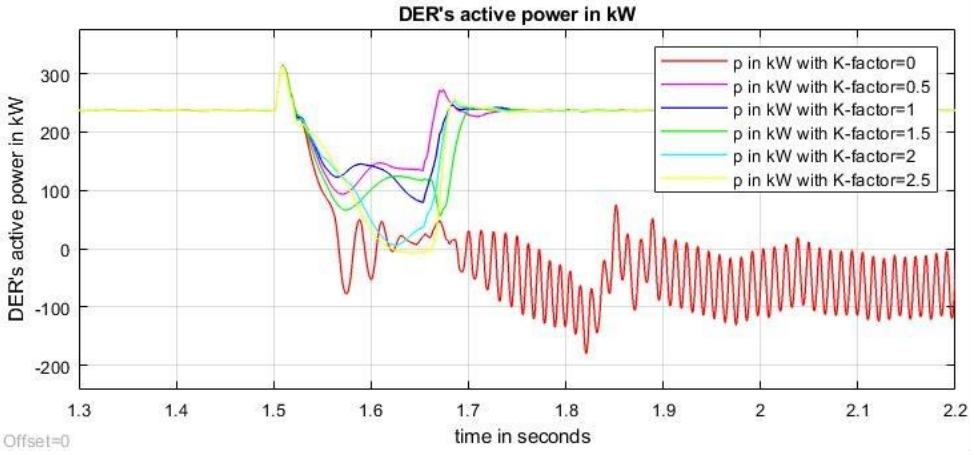

Figure 5-17 Response of the DER's active power in kW (p) during LVRT with all corresponding K-factor settings (scenario 3)

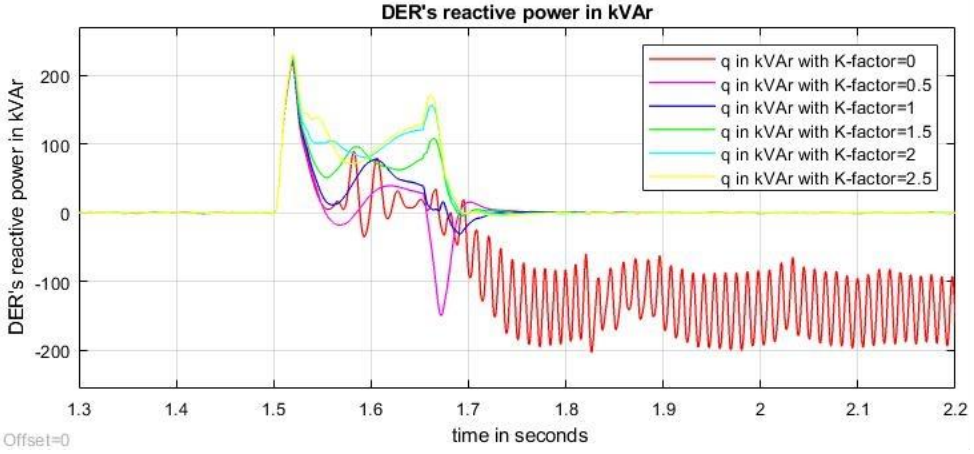

Figure 5-18 Response of the DER's reactive power in kVAr (q) during LVRT with all corresponding K-factor settings (scenario 3)

5.7.3.2 Observation on the Simulation Results from Scenario 3

On the case with K-factor=0 when the fault is happening at 1.5 s, the voltage begins to deviate, and then the voltage response goes unstable, even the fault is cleared at 1.65 s. The voltage response on K-factor=0 is shown the red line, as in Figure 5-13. As a result, the voltage response in dq reference, v_{d_meas} (red line), and v_{q_meas} (yellow line) are also observed unstable, as shown in Figure 5-16. It can be seen that the v_{d_meas} and v_{q_meas} oscillate during fault and these oscillations become more apparent even during post-fault. The response of the dq measured current in per unit, i_{d_meas} and i_{q_meas}, during fault also show signs of instability. The i_{q_meas} is shown do not return to its initial point on post-fault, and so is the i_{d_meas}. As a consequence, the DER's active and reactive power responses also deviate wildly and go unstable. These can be seen the red lines in Figure 5-17 and 5-18 for the active and reactive power responses, respectively.

From the simulation results, the instability of the system under the case when the K-factor=0, is indicated by the lost voltage restoration after the cleared fault as shown in the red line (Figure 5-13). The voltage instability as shown is observed since the short-circuit current compensation could not adequately compensate the short-circuit current needed to be flown to the located fault [140]. In reality, the system instability response during post-LVRT would not happen as much as has been illustrated in the simulated result. So once the system suffers the short circuit fault and then the voltage sags, let's suppose, down to 0.8pu, if the voltage sags duration is longer than 150ms, then normally the system protection, such as the undervoltage protection is activated and the distribution system is disconnected from the transmission grid to prevent further disturbance. In this study, the simulation analysis does not account system protection, such as under voltage protection that is normally available in the DER's point-of-common-coupling, which normally meant to prevent further system stability deterioration. The presented simulation in this study is meant to investigate the effect of the grid characteristic to the DER's voltage support performance. As such, the point of interest of the simulation test is during the LVRT state/during the voltage sag. Hence, although it can be inferred the post-LVRT state in the simulation outcome does not reflect the real situation, still, the purpose of the study is met.

Further on, it can be seen starting from K-factor=0.5 the system's response is showing its signs of stability. The voltage magnitude response in pu, in this case, is shown on the pink line as illustrated the Figure 5-13. Further as seen in Figure 5-16 the *dq* measured voltage responses, v_{d_meas} (pink line), and v_{q_meas} (brown line), are also seemed stable after fault. The response of the *dq* measured response, i_{d_meas} and i_{q_meas}, during fault are also shown remained stable as well. As a result, the DER's active and reactive power responses are observed stable.

On the case with K-factor=1.5, the voltage sags at 0.468 pu. The voltage sag improvement rate on K-factor=1.5 is observed better by 16.129% than the voltage sag improvement rate on K-factor=1 (2.978%). This result can be understood since higher K-factor, which results in the higher magnitude of the DER's reactive current, leads to higher reactive power injected to the grid. With the higher amount of the DER's reactive power being contributed to the shorted-circuit power at the faulted location, better voltage sag improvement at the DER connection could be made. Highest K-factor on the simulation test is given at 2.5. It is shown in this case, the i_{q_ref} is at -1 pu, indicating the reactive current injection reaches its maximum level. Thus, the voltage sags improvement reaches at its best, at 0.533 pu. 0.533 pu is the best voltage sag improvement in this scenario. Overall it can be observed higher K-factor may result in a better voltage sags improvement.

Table 5-5 Overall observations of the LVRT simulation responses during fault for Scenario 3

Parameters	Symbol	Value					
K-factor	K_{I_q}	0.0	0.5	1.0	1.5	2.0	2.5
voltage sag	V_{DER}	unstable	0.403	0.415	0.468	0.523	0.533
dq reference current in pu	i_{d_ref}	unstable	0.955	0.814	0.547	0.000	0.000
	i_{q_ref}	unstable	-0.293	-0.580	-0.820	-0.955	-1.000
dq measured current in pu	i_{d_meas}	unstable	1.141	1.180	0.648	0.358	0.000
	i_{q_meas}	unstable	-0.267	-0.397	-0.646	-0.928	-1.064
dq measured volt in pu	v_{d_meas}	unstable	0.407	0.417	0.476	0.518	0.520
	v_{q_meas}	unstable	0.000	0.000	0.000	0.000	0.000
DER's active power in kW	(p)	unstable	135.700	127.300	119.900	34.090	0.000
DER's reactive power in kVAr	(q)	unstable	31.090	45.450	66.420	118.800	124.200
Voltage sag improvement rate in % (*)	ΔV_{rate}	unstable	n/a	2.978	16.129	29.777	32.258

(*) as compared to the V_{DER} on the case with K factor=0.5

5.7.4 Scenario 4

In this scenario, the positive-sequence inductance for the 'Distribution Line 3' is ten times of the positive-sequence inductance for the 'Distribution Line 3' in Scenario 1. Similar to scenario 3, the simulation setup is made to introduce the instability of the system due to the weak grid. However, since the grid is much weaker than in the scenario 3, it will be shown even the DER's aRCI-based LVRT voltage support is given, by setting the K-factor at 1.5, the grid is still exposed by the system instability. It will be shown that the system instability can be avoided by setting the aRCI at a higher level. The simulation test is done four times, and the K-factor, K_{I_q}, is given from 1.5 to 3. Again, the no-aRCI case (K-factor=0), the case on K-factor=0.5, and 1 are not shown. In this scenario, the maximum aRCI case is given at the K_{I_q}=3.

5.7.4.1 Simulation Results on Scenario 4

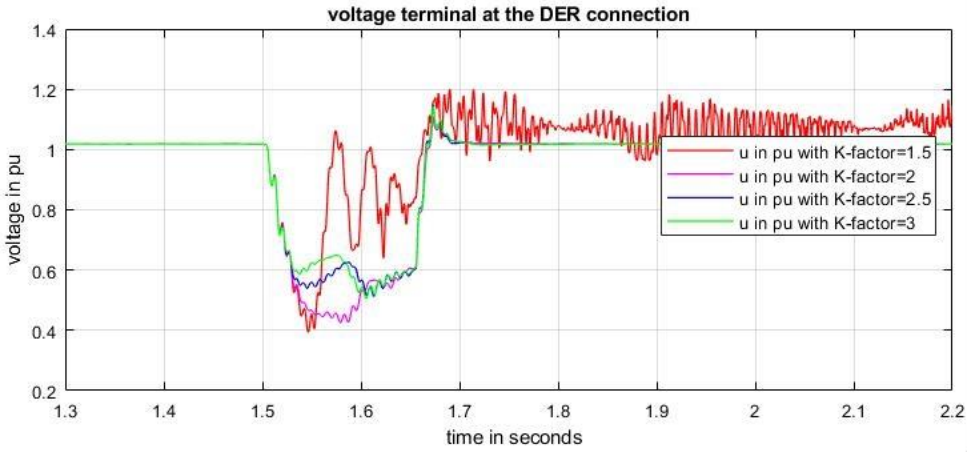

Figure 5-19 Response of the voltage terminal at the DER connection in per unit (V_{DER}) during LVRT with all corresponding K-factor settings (scenario 4)

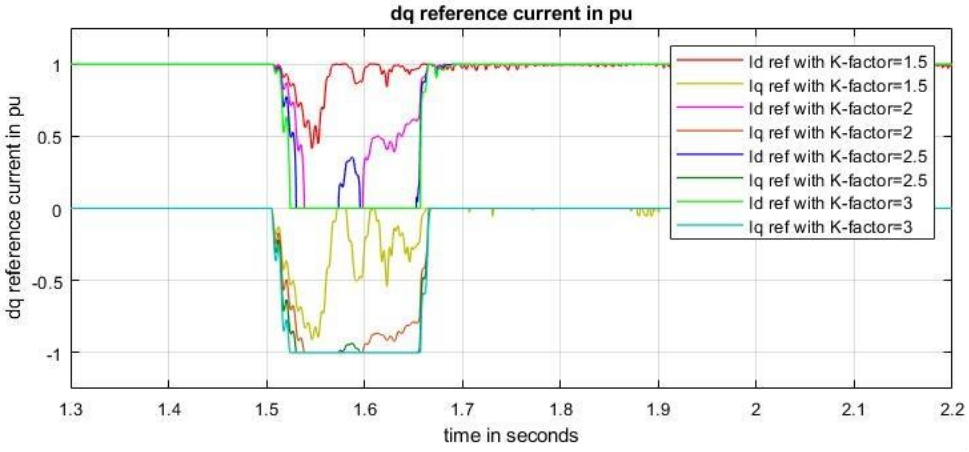

Figure 5-20 Response of the *dq* reference current in per unit (i_{d_ref}, i_{q_ref}) during LVRT with all corresponding K-factor settings (scenario 4)

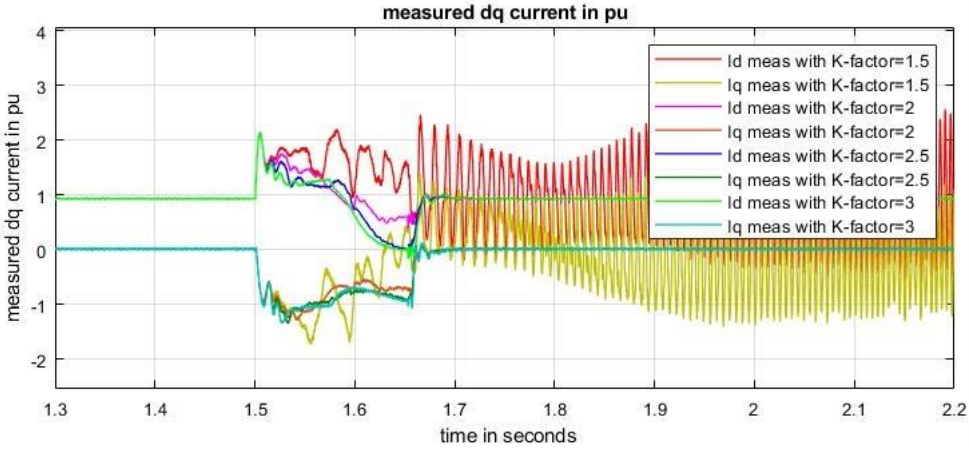

Figure 5-21 Response of the *dq* measured current in per unit (i_{d_meas}, i_{q_meas}) during LVRT with all corresponding K-factor settings (scenario 4)

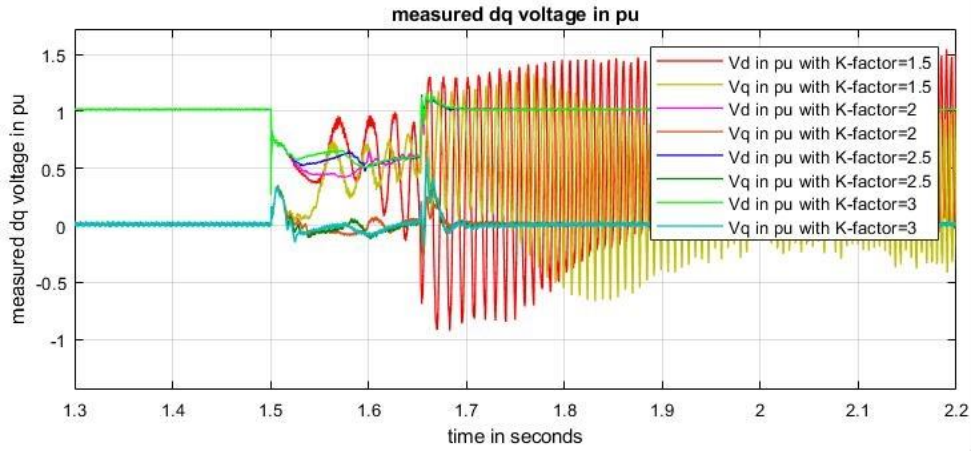

Figure 5-22 Response of the dq measured voltage in per unit (v_{d_meas}, v_{q_meas}) during LVRT with all corresponding K-factor settings (scenario 4)

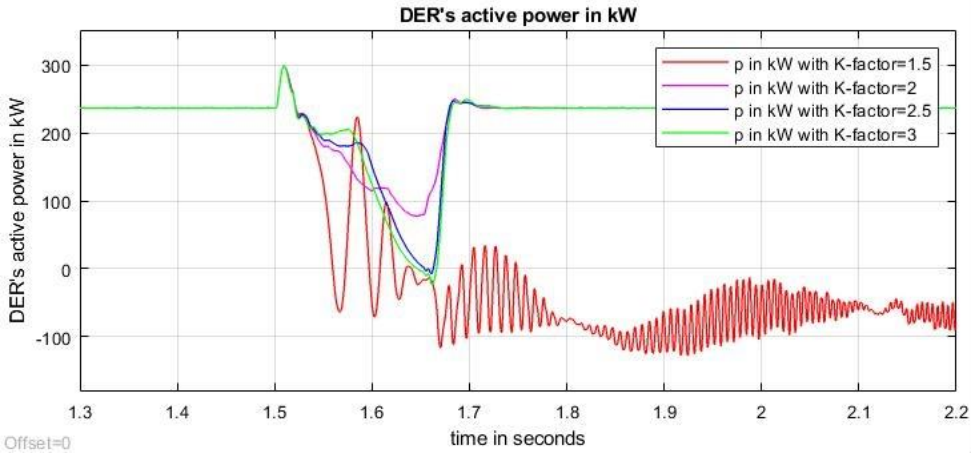

Figure 5-23 Response of the DER's active power in kW (p) during LVRT with all corresponding K-factor settings (scenario 4)

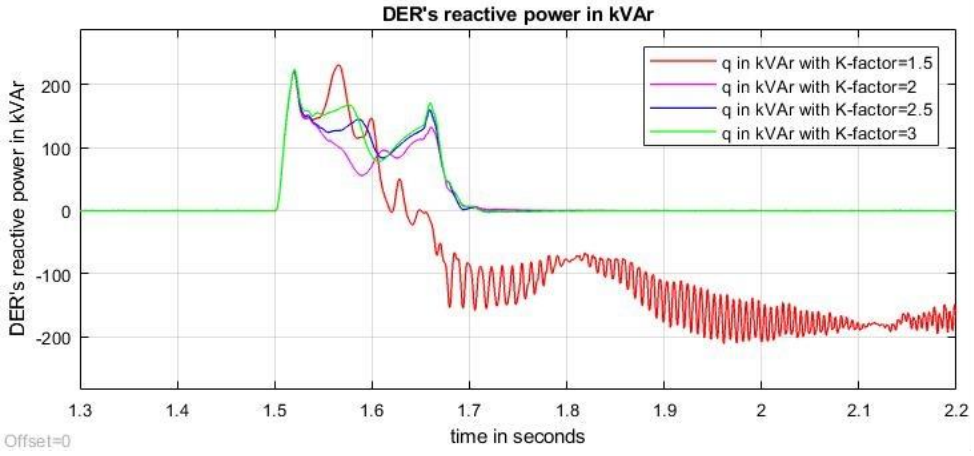

Figure 5-24 Response of the DER's reactive power in kVAr (q) during LVRT with all corresponding K-factor settings (scenario 4)

5.7.4.2 Observation on the Simulation Results from Scenario 4

On the case with K-factor=1.5, it can be seen in general as the short-circuit fault starts at 1.5

s, the voltage sag is happening, and then the voltage response goes unstable, even after the fault is cleared at 1.65 s. The voltage response on K-factor=1.5 is illustrated by the red line, as shown in Figure 5-19. Further, it can be seen due to the system's instability, the v_{d_meas} and v_{q_meas} oscillate during fault and its oscillations becoming more apparent even during post-fault. The instability response during fault is also observed at the response of the *dq* measured current (i_{d_meas} and i_{q_meas}), as shown in Figure 5-21. As a result, the DER's active and reactive power responses are also going unstable. These can be seen the red lines in Figure 5-23 and 5-24 for the active and reactive power responses, respectively.

On the case with K-factor=2, it can be seen that the system's response are stable. The voltage magnitude response (pink line, as shown in Figure 5--19) is shown. On the post-fault state, the voltage response goes stable and back to its initial state shortly after the fault is cleared. Same goes with the *dq* measured voltage responses. As shown in Figure 5-22, the v_{d_meas} (pink line), and v_{q_meas} (brown line) also seem stable after LVRT state. The response of the *dq* measured current response i_{d_meas} and i_{q_meas} are also shown remained stable (Figure 5-21). Again, as a result, the DER's active and reactive power responses are observed stable as well.

On the case with K-factor=2.5, the voltage sags at 0.599 pu. Again, the voltage sag improvement rate on K-factor=2.5 is observed better for 28.54% than the voltage sag improvement rate on the case with K-factor=2. Further on the case with K-factor=3, the voltage sag improvement is observed at 0.648 pu, better than the one on K-factor=2.5. The voltage sags improvement for this case is observed at best among other cases. The voltage sag improvement rate is observed 39.056%, better than the voltage sag improvement rate on the case with K-factor=2. Again, the overall observations of the LVRT simulation responses are presented in Table 5-6.

Table 5-6 Overall observations of the LVRT simulation responses during fault for Scenario 4

Parameters	Symbol	Value			
K-factor	K_{I_q}	1.5	2.0	2.5	3.0
voltage sag	V_{DER}	unstable	0.466	0.599	0.648
dq reference current in pu	i_{d_ref}	unstable	0.463	0.000	0.000
	i_{q_ref}	unstable	-0.920	-1.000	-1.000
dq measured current in pu	i_{d_meas}	unstable	0.528	0.034	0.000
	i_{q_meas}	unstable	-0.699	-0.864	-0.926
dq measured volt in pu	v_{d_meas}	unstable	0.583	0.580	0.572
	v_{q_meas}	unstable	0.008	0.002	0.000
DER's active power in kW	(p)	unstable	77.310	11.290	0.941
DER's reactive power in kVAr	(q)	unstable	92.550	122.400	129.500
Voltage sag improvement rate in % (*)	ΔV_{rate}	unstable	n/a	28.541	39.056

(*) as compared to the V_{DER} on the case with K factor=2.0

5.8 Discussion of the Simulation Results

From the simulation results, in the discussions, two important aspects are highlighted into two subsections. The first aspect is about the effect of the *X/R* ratio of the grid to the effectiveness of the aRCI on improving the voltage sag. The discussion of the first aspect is made to corroborate the proposed theoretical analysis of DER's LVRT voltage support via aRCI on different *X/R* ratio from the section 3.5 in the perspective of the dynamic RMS simulation results. The argument is the contribution of the study on the usefulness of the aRCI-based LVRT voltage support for DER on the distribution level is also presented as well. The second aspect is about the potential system instability during LVRT due to the 'weak' grid and its potential occurrence due to the continuous growth of the DER, which is connected directly to the distribution system. The discussion on the second aspect is then extended to present the potential solution of the aRCI-based LVRT voltage support to prevent the potential system instability. The discussion of the second aspect is made as the contribution of the study to support argumentatively the possibility for the realisation of the reactive power-based LVRT voltage support not only for DER park, which normally connected via MV long feeder, but also for the DER that is directly connected to the residential/urban area network.

5.8.1 The Influence of The Distribution Grid *X/R* Ratio to The DER Voltage Support on Voltage Sag Improvement

It can be seen the aRCI can be claimed to improve voltage sag, however, it is highly influenced by the *X/R* ratio of the grid. Larger *X/R* ratio results in better voltage sag improvement. By applying higher inductance level at the Distribution Line 3 (as shown in Table 5-1 and 5-2), it can be seen that the voltage sags improvement rate is better than on simulation test on smaller inductance level. This observation can be understood since higher K-factor results in higher q reference current (i_{q_ref}). the voltage support through the regulation of the i_{q_ref}, as has been explained before, according to the equation from (3.17) to (3.21), will be more effective in a situation in which the impedance of the grid has more reactance element than the resistive element. Note from (3.17) it can be referred short-circuit current magnitude, and its phase is highly depended to the short-circuit impedance - a condition in which short-circuit current phase is highly influenced by the short-circuit resistance and reactance level. Since the short-circuit current, in theory, if it is situated in a grid with grid impedance with medium level *X/R* ratio (such as exhibited in the scenario 4), will have the dominant effect to the reactance element of the system. Thus if such condition is happening, the injection of higher i_{q_ref} will better 'compensate' the contribution needed to the reactance part of the shorted-circuit current.

This is proven on the voltage sag improvement rate in % as described from Table 5-3 to Table 5-6. It is shown in general DER's aRCI-based voltage support in a grid with more inductance level could contribute better voltage sag improvement. For instance, in Scenario 2 with the case on the DER with K-factor=1, the voltage sag could be improved up to 6.233%, whereas in Scenario 1 with the case on the DER with K-factor=1, the voltage sag could be improved for only 3.774%. Another example is shown; in Scenario 2 with the case on the DER with K-factor=2, the voltage sag could be improved up to 23.306%, whereas in Scenario 1 with the case on the DER with K-factor=2, voltage sag could be improved for only 8.086%. Overall, it can be implied that the voltage support through aRCI performance on improving the voltage sag is highly influenced by the *X/R* ratio of the grid. As such, the aRCI-based LVRT voltage support performances presented in the dynamic simulation results are aligned with the proposed theoretical analysis of DER's LVRT voltage support via aRCI on different *X/R* ratio from the section 3.5.

The presented simulation results revealed a suggestion on the potential realisation of the reactive power-based voltage support for the DER on LV distribution connection. Although there is impeding effect of the low *X/R* ratio to the effectiveness of the discussed voltage support, voltage sag improvement through reactive power-based voltage support from distribution level DER is still encouraging. This outcome will provide useful insight for the future standard adaptations, such as for the grid codes around the world relating to the DER's LVRT voltage support. Note that from Table 2-4 and Table 2-5 as in section 2.8.4, it can be inferred that to the date most grid codes for the DER requirements consider reactive power regulation for the LV-connected DER only meant for steady-state voltage support, and are not meant for the LVRT voltage support. In addition, the use of LVRT voltage support through reactive power regulation was made for DER park which connected to a medium voltage line with *X/R* ratio impedance higher than the impedance of the connection lines on lower voltage level. As it has been described from section 5.4, such line for the DER park normally has *X/R* ratio impedance for above 1.2. In the simulation study, the *X/R* ratio of the connection line are set between 0.12 and 1.2, which is the typical *X/R* ratio of the connection line of the distribution system. As such, according to the simulation results, the use of LVRT voltage support through reactive power regulation via aRCI to improve the voltage grid stability can be made as well for the DER in the distribution level system.

It will be presented further in the following, the application of reactive power regulation for LVRT voltage support could be utilised to prevent weak grid system collapse

5.8.2 The Potential Use of The DER Voltage Support for Securing The Integration of DER on The Weak Distribution Grid

As it has been presented in section 5.3, the increasing number of DERs on the distribution grid has always been associated with the weakening of the grid strength [175], [176], [180]. This unavoidable phenomenon will be likely more visible in the future, and thus limit the DER growth. From the simulation results, as particularly exhibited in the Scenario 3 and 4, it has been revealed that weak DER-connected grid will be potentially exposed to the system collapse when the grid must undergo LVRT state. Nevertheless, the use of LVRT voltage support through reactive power regulation via aRCI could be implemented to prevent the potential instability when the grid must through LVRT state. The following paragraphs present the analysis of how the DER's aRCI-based LVRT voltage support could be made to prevent the system instability of the weak DER-connected grid.

To begin with, the system inability to withstand its stability during LVRT due to the 'weak' grid is most likely attributed by the Short-Circuit Capacity (SSC) insufficiency. The SSC insufficiency defines the condition in which the system/grid fails to provide an adequate amount of short-circuit current needed to be flown to the shorted-circuit location [140]. Though the consideration of 'weak' grid in this study is not quantified (as based on quantification method as suggested in [183]), the condition of the grid being 'weak' still can be situated in the simulation experiment by configuring the level of the impedance of the grid to a degree at which when the grid must undergo LVRT state, the system could not restore its stability [125]. Thus, as it has been demonstrated in the simulation study, the source of the system instability following LVRT is highly attributed by the insufficient amount of short-circuit current which flown to the shorted-circuit bus. This understanding can be inferred into the realisation of two possible conditions. If the DER and the external grid could compensate the short-circuit current flown to the faulty bus during the fault, which in this context is during the period of the voltage sag, then the system could withstand until the fault is cleared. However, if the DER and the external grid could not compensate the short-circuit current flown to the faulty bus during the period of the voltage sag, then the system could not withstand and hence the voltage oscillate uncontrollably.

In the simulation, adding impedance level through configuring inductance level of the simulated system as according to the Table 5-2, results in the higher amount of short-circuit current needed to be flown due to potential current dissipation during the current transmission to the located fault [140]. Therefore under the simulation cases with higher grid impedance, when the DER and the external grid do not have enough short-circuit capacity required to provide the short-circuit current needed to be flown to the faulted location, the system could

not keep up the minimum required short-circuit reactive power to ensure the voltage stability [2], [125], and thus during LVRT, the system can go unstable.

Meanwhile, as has been presented in the simulation results (as in Table 5-5 and 5-6), a higher level of the K-factor can result in a higher LVRT reactive power being contributed by the DER. Simulation tests in scenario 3 and 4 are made to show the case of the grid having a high impedance at which the system is becoming weak and prone to the voltage instability. By applying a higher level of the K-factor, the DER can regulate the higher magnitude of i_{q_ref}. As such, under such situation, the DER could inject a high amount of reactive power during LVRT, which is needed to compensate the minimum required short-circuit reactive power to ensure the voltage stability. Scenario 4 on the case with K-factor=1.5 illustrate the condition of the system being unable to compensate the minimum required short-circuit reactive power to ensure the voltage stability. In such situation, setting up the DER with higher K-factor level which results to a higher reactive power injection can secure the voltage stability and thus, preventing the post-LVRT instability of the system. With that requirement could be met, system instability following LVRT could be avoided. Further as has been claimed in [174], the growth of the DER number may be weakening the grid strength. Therefore, on such weak grid condition, DER's aRCI may be utilised to avoid system instability when the DER has to ride-through voltage sag. Overall, from the investigation on the use of the DER voltage support to secure the weak grid stability, potential suggestion in the following paragraph as the contribution of the study is presented.

It should be understood that as the DER at the distribution grid increases, the distribution system becoming weaker. Currently in many practices, many DERs, such as rooftop-PVs in the residential area, can be temporarily disconnected from the grid, and hence they are not required to do LVRT. From the studied literature, it has been revealed that even the LV-connected DER has to do LVRT as well in order to prevent cascading loss of the distribution system. The implementation of the LVRT for the LV-connected DER has been proven promising to prevent the cascading loss, and thus avoiding the system collapse [4]. As such, it can be seen that many grid codes require the DER on low voltage connection has to ride-through voltage sag as well. However, from the investigated simulation studies, there is a need further for the grid code to not only require the LV-connected DER to ride-through the voltage sag, but also to consider them to provide LVRT voltage support. From the simulated studies the aRCI-based LVRT voltage support could be utilised to prevent the weak grid collapse in the event it needs to ride-through the voltage sag. The weak grid is sensitive to the voltage deviations, and it is very likely the voltage deviations becoming more apparent by the time the number of the DERs are increased. The condition of the grid being more sensitive to the voltage deviations is becoming an impeding factor to the DER penetrations, and thus, it must

be solved. As such, the aRCI-based LVRT voltage support could offer the solution to keep the DER penetration planning in the distribution grid can be ensured.

5.9 Summary

In this chapter, the impact the the grid characteristic to the effectiveness of DER's aRCI-based DER's LVRT voltage support is explored and discussed. Four scenarios of the simulation tests, which are clustered in order to satisfy two aspects of the two previously mentioned grid characteristic, are presented. The first two scenarios and the last two scenarios as presented from section 5.7.1 to section 5.7.4 are made and presented to investigate the effect of grid's *X/R* ratio and to investigate the 'grid strength' to the effectiveness of DER's aRCI-based LVRT voltage support, respectively.

aRCI's mechanism and its performance in mitigating the voltage sag are successfully evaluated by observing the dynamic transient response of the DER following LVRT under first previously aspect as considerations. It is found that DER's aRCI-based LVRT voltage support can be claimed to improve voltage sag, however, very much depended with the *X/R* ratio of where the DER is connected. On the growing number of low-voltage connected DER, there is an impeding effect of the low *X/R* ratio of the distribution grid to the performance of the discussed voltage support. However, from the simulated study, the voltage sag improvement through reactive power-based voltage support from distribution level DER is still promising.

Further, on the aspect relating to the grid 'strength', the weak grid may take benefit from the aRCI feature provided by the DER to prevent system instability in the event of LVRT. According to [174], the growth of the DER number may be weakening the grid strength. As such, through appropriate grid planning DER's aRCI feature could be expected to prevent unwanted system instability following transient voltage sag, and thus preventing the system collapse.

Chapter 6 Summary, Suggestions and Future Work

In this chapter, the summary of the research carried out and reported in this thesis is given. Suggestions and strategies for grid planning upon implementing aRCI-based LVRT voltage support are presented; also, recommendations for future work is given.

6.1 Summary

The research undertaken and reported here has evaluated the effectiveness of aRCI-based transient voltage control as means of LVRT support for inverter-based DER. There is a wealth of evidence showing the growth of DER in the distribution grids. As many studies favour the use of aRCI based transient voltage control on the DER, there is a need to evaluate the usefulness and effectiveness of employing aRCI based transient voltage control in the distribution systems. The work undertaken in this project has been split into three main areas. The research contribution made in these three main areas are summarized below.

6.1.1 Effectiveness of DER's aRCI-based LVRT support on improving voltage sags

It has been revealed that transient LVRT voltage support through reactive power regulation is highly influenced by the *X/R* nature of the distribution grid. As it has been presented in chapter 3, the short-circuit fault current magnitude and its phase are determined by the resistive and the reactive components of the all corresponding impedances around the fault location. The active and reactive part of the current injected by the DER reflects the magnitude and the phase of the contributed short-circuit current given by the DER. As such, upon injecting additional reactive current, some amount of the reactive part of the short-circuit fault current is 'covered' by the extra amount given by the DER. One could observe from the simulated study that in a grid with higher *X/R* ratio impedance, aRCI results in better voltage sags improvement as compared with a grid with lower *X/R* ratio impedance. Through the proposed methodology developed in this work, the impact of the grid's *X/R* ratio on the effectiveness of aRCI on improving voltage sags is demonstrated [138].

The results discussed in chapter 3 reveal a prospective possibility on how to utilise reactive power-based LVRT voltage support for the DER on LV connection. Although it was discovered that there is an impeding effect of the low *X/R* ratio to the performance of the LVRT voltage support, the voltage sag improvement via aRCI from distribution level DER is still beneficial. The implementation of the aRCI-based LVRT voltage support was originally meant for DER park, which are connected to a medium voltage line for which the *X/R* ratio impedance is relatively higher than the *X/R* ratio of the distribution lines. The line feeder for the DER park

typically has *X/R* ratio impedance for above 1.2 [172]. Meanwhile, currently, most grid codes for the LV-connected DER requirements take into account the use of the reactive power regulation only for steady-state voltage support. The results presented here show that the use of aRCI-based LVRT voltage support for the DER on the distributed connections with the *X/R* ratio below 1.2 prove to be useful as well. This new insight provides valuable information for the grid regulator or grid planner that need to consider the LVRT voltage support requirements for the DER on LV connections.

6.1.2 Effective evaluation of DER's LVRT voltage support

An effective methodology that can be utilised for decision making strategy and used by distribution system operators or the DER grid planner in the event they need to produce an achievable, but effective grid support evaluation for DER's LVRT voltage support designs, is introduced in this thesis. Usually, the evaluation of the LVRT voltage support can be done with the help of the usual positive-sequence-RMS simulation tool. The construction of a suitable model can be made when the 'know-how' and the data describing the network and DER is available. However a too detailed representation of the DER connection will increase the computational complexity and data needed for the realisation of the task. Contrarily, using an oversimplified approach may end up to an outcome that does not effectively solve the realistic problem. Compromising model both accuracy and simplicity of modelling power systems elements can be challenging. The evaluation of the LVRT voltage sag is highly influenced by the accuracy of the model of the and data availability. However, often in many situations, the information needed to construct the model is incomplete, and thus, the construction is often done through assumptions. Hence on such condition, extensive work and knowledge to construct the DER modelling are necessary.

The methodology introduced in this work deals with these challenges, the compromise of the accuracy and simplicity of the simulation model, as a means to tackle the grid data restrictions and introduces a clear, logical and effective strategy on constructing the DER connection model. The proposed methodology also simplifies the computation process and helps the estimation of the effectiveness of aRCI on improving the LVRT voltage sag without the need to perform an iterative computation process which is often required in the dynamic RMS simulation. With a simpler computation process, the effectiveness estimation of investigated voltage support can be effectively obtained even when the grid information is incomplete. The methodology has been successfully demonstrated in chapter 3. Despite the estimation of the proposed methodology is made without an extensive work on the DER connection modelling, it can be seen that the results of the proposed methodology are fairly close to the RMS results obtained from a commercially available simulation tool (PowerFactory –DIgSILENT).

Hence through the proposed and implemented methodology a simplified and accurate DER model is achieved while the computation effort is minimised, for accurate DER's LVRT voltage support evaluation.

6.1.3 The Impact of Distribution Grid Characteristic on the Performance of the DER's Reactive Power Based LVRT Voltage Support

A thorough investigation on the impact of distribution grid characteristics on the performance of the DER's reactive power-based LVRT voltage support has been discussed and presented in this thesis. The increasing number of DERs on the distribution grid has always been linked with the weakening of the grid strength. The weakening level of the grid will be likely to get worse as the DER penetration keeps increasing. As such, this problem can effectively slow or stop the DER penetrations. From the simulated studies, it has been demonstrated that a weak grid with DER connections will be potentially susceptible to the system collapse when the grid must ride-through voltage sag. Even so, the use of LVRT voltage support through reactive power regulation could be applied to avoid the risk of the potential instability when the grid must ride through a LVRT state.

The contribution made in this thesis is to support the realisation of the reactive power-based LVRT voltage support not only for DER park but also for the DER which is closely located in the distribution area. Previously done studies show that there are still plenty of rooftop-PVs using automatic disconnection from the grid whenever the DER detects voltage sag. As such, most of them are not required to ride-through voltage sag. However, many grid codes enforce the LV-connected DER (rooftop-PVs) to ride-through voltage sag as well in order to avoid cascading power loss of the distribution grid. The practice of the LVRT for the LV-connected DER has been proven useful to prevent the system breakdown [4]. However, from our simulation studies, it is found that there is a need to consider the LV-connected DER not only to ride-through the voltage sag, but also to enforce the DER to provide LVRT voltage support as well. Our studies showed that the aRCI-based LVRT voltage support could be employed to avoid the weak grid failure when the system must ride-through the voltage sag. The weak grids are prone to transient voltage disturbance. It is highly possible that the transient voltage disturbance will be more obvious when DERs penetrations is high, which is a possibility as the penetration is increasing. When the grid is becoming more sensitive to the voltage disturbance, it will potentially restrain DER penetration planning. Thus, in order to keep the DER penetrations possible as well as keeping the grid secure, the problem has to be solved. As shown in the studies undertaken in this work the implementation of the aRCI-based LVRT voltage support could be the solution to ensure a safe and economical DER penetration planning in the distribution grid.

6.2 Suggestions and Strategies for The Grid Planning upon Implementing aRCI-based LVRT Voltage Support

Upon implementing aRCI-based LVRT voltage support, it is best to understand the topology of the distribution grid, the information required to construct the implementation, and as well the information available to support the planning. The investigation of the LVRT voltage sag improvement through RMS simulation methodology has been presented well in many pieces of research [3], [4], [27], [28]. The application of the RMS simulation has been proven effective in demonstrating effective simulation analysis tool. However, it should be considered that in many practices, the simulation analysis through RMS simulation tools requires extensive data to construct the simulation model, which are often made through approximations [1]. The task of the RMS simulation modelling requires careful assumptions, not to mention the relevant knowledge required to build the simulation task, which has been demonstrated in the simulation study presented in chapter 4. Further, the adjustment for the assumption itself requires comprehensive knowledge which often can be made through practical experiences from the relevant modelling works. Even more, when all the aforementioned prerequisites are met, the simulation design will be need to be tested to see whether the accuracy of the simulation results is sufficient. In general, this require extensive skills and broad knowledge for the construction of the model.

To deal with the data restrictions, approximations are often made for the best solutions. For a practical purpose, such as in industry sector whereas data availability and the time-schedule for the task can be very challenging, the work on designing dynamic RMS simulation models can be very exhausting. As such, in the event that some information is unobtainable or too cumbersome/difficult to estimate; such as the right 'size' on model aggregated dynamic characteristic of the DER, the right amount of the mixture of the adjacent loads, and the precise approximations for the active an reactive power profile of both from the DER and the distribution loads; then evaluation of the investigated voltage support through the proposed methodology that is presented in chapter 3 can be an effective and practical option. Through simplifications and reasonable assumptions; such as averaging the active and reactive power of the distribution loads, then aggregating the known impedance of the distribution line, and assuming the likeliest located voltage sag; the effectiveness of the support in minimising voltage sag could be estimated. The obtained result could be then used to judge the necessity of the implementation of the support..

6.3 Recommendations for The Future Work

With the research work presented in the thesis, the achievements have been summarised in the previous sub-sections. There are, still, potential unsolved issues adjacent to the investigation that has been carried out in this thesis, which can be expanded in future work. In the following, some of these possible topics are presented.

Further improvement of the proposed methodology which can include composite loads in the analysis

The work in this study was focused on evaluating the effectiveness of the DER's reactive power-based LVRT voltage support, which required simulation models that were relatively simplified as active and reactive power load models. Since the main aim of the work was to propose an evaluation methodology for DER's LVRT voltage support a compromise between the complexity of the model, data restriction computation time and accuracy was made. It has been shown that from the perspective of the LVRT voltage sag results the proposed compromise can deliver good and accurate results. However attempts to study the impact of the DER integration to the stability of the grid network by considering a more realistic load models has been presented in many studies [23], [169]. Therefore, for future research, it would be beneficial for the methodology developed here to be extended such that it can consider the composite load models in the evaluation.

Possible improvement of the proposed methodology for evaluating the effectiveness of the additional active and reactive current injection (aRACI)-based LVRT voltage support

Some research suggests using aRACI-based LVRT voltage support to improve the LVRT voltage sag [14], [189]. However, it has been explained in chapter 2 that the use of aRCI is preferred to the use of aRACI when the DER penetration is very high. Nevertheless, there are particular cases, where the DER penetration can be relatively low so that the use of aRACI would be preferred [1]. Such cases are possible when the DER penetration is limited by, for instance, the feeder hosting capacity [190]–[192]. Extending the proposed methodology not only for evaluating the effectiveness of the aRCI but, also aRACI would expand the applicability of the methodology and hence making it more practical.

Consideration of unbalanced three-phase voltage problem

Currently, many grid codes related to the DER connection requirements requires only positive-sequence DER's LVRT voltage support. Single-phase roof-top PVs, which are often connected to a low voltage distribution line, will have no issue since their voltage support is made to solve the respective phase line. The three-phase distribution line, unlike the three-phase transmission line, however, is likely to suffer of unbalanced three-phase voltage due to the

uneven shares of the distribution loads. The study of the DER's voltage support to minimise the unwanted unbalanced three-phase voltage has been featured in many research studies [29], [49]. It would be interesting for the future research to enhance the methodology developed here such that the effectiveness of the voltage support can be estimated for unbalanced voltage sag situations too.

Fault-induced delayed voltage recovery (FIDVR) in the distribution system with high shares of DERs

There is rising attention to the potential impact of fault-induced delayed voltage recovery (FIDVR) event to the distribution system with high shares of DERs [193]. FIDVR is the type of fault that is usually identified by a depressed voltage for 5 to 30 seconds following a fault and has been reported as important issue since it shows a temporary loss of regulated voltage in an area [194]. Numbers of FIDVR could lead a cascading risk to a greater area, mainly if another unexpected FIDVR occurs while the voltage is depressed. It is believed to be sourced by the stall of low inertia induction motors during the fault [195]. Motors at risk of stalling include compressor-driving loads such as residential air conditioners (RAC) [196]. The need for investigating further FIDVR event due to the presence of large numbers of RAC has raised a long discussion about how to model correctly such situations [197]. Decades of effort have improved the modelling of induction motors to accurately represent RAC loads. However, the characteristics of time variation, dispersed location, operational discontinuity, parameter uncertainty, and the diversity of the motor type make load modelling a difficult task [194].

Since the DERs will be most likely connected to the distribution grid and hence located very close to the loads, there is a real possibility that DERs will be exposed to FIDVR events. With the ongoing DER's penetration rising plan, there is a need to investigate the effect of FIDVR event to the DER's along with its voltage support function. The future work could be aimed to improve or modify the proposed methodology to estimate the effectiveness of the DER's LVRT voltage support that also considers the recent-emerging FIDVR issue. A residential or urban area with high radiance level is a promising place to grow DER penetrations. However, it has been discovered that such area are often with a high level of RAC [197]. Therefore, improving the proposed methodology to consider its applicability to the FIDVR issue will be likely to be relevant, as the FIDVR problem will potentially affect the DER penetration planning as well.

aRCI modeled in the Hardware-In-the-Loop (HIL) Simulation Study

Recently HIL has become an attractive simulation methodology in the research of power systems [198]. HIL simulations have become an increasingly used tool for the studies of renewable resources integration as these inverter-based power sources have become more popular [199]–[201]. With the HIL simulation tool, the control designs of the inverter for these

devices are tested and validated under realistic situation but in a secure and controlled environment. HIL simulations enable the study of practical tasks by examining some parts of the simulation components, such the grid system, while allowing the inverter as the Hardware-Under-Test (HUT) [202] to respond and to test the impact of changes in the control strategy. In the HIL-based simulations, the investigated power hardware is interfaced with a power system simulation, which is commonly running on a digital real-time simulator (DRTS) [203]. The running simulation reflects the real situation and provide realistic simulated input data to the controller hardware on a desirable timescale, from microseconds (which is normally for electromagnetic transient simulations) to sometimes in milliseconds (for RMS dynamic simulations).

Researchers need to understand their modelling limitations in a simulation study. There are also needs to understand the implications of the overall system behaviour to the investigated model and its associated control. In many situations, the simulated models are often employed inappropriately such that critical dynamic aspect of the model may not be well presented [204]. If this is happening, it will lead to an oversimplification of the system architecture and its constraints, therefore failing to obtain valid results [202]. Contrarily, it is often the problem that physics-based models become too detailed and thus create the undesired problem of requiring extensive simulation time, which in turn, for example, creating unwanted delays in the controller development [202]. The use of HIL could help as compromises in both accuracy and simplicity for the investigated modelling can be made. The design of the proposed aRCI modelling for LVRT voltage support as presented from chapter 4 has been demonstrated its usefulness for transient voltage recovery. It would be interesting for the future research if the proposed aRCI can be tested under the HIL simulation methodology. With the HIL methodology, the simulation case can be scale-up into an actual experimental level which can fully verify the efficacy of the modelling, while on the same time, keeping down the experimentation cost and time.

List of References

[1] J. Boemer, "On Stability of Sustainable Power Systems: Network Fault Response of Transmission Systems with Very High Penetration of Distributed Generation," 2016.

[2] S. Eftekharnejad, V. Vittal, Heydt, B. Keel, and J. Loehr, "Impact of increased penetration of photovoltaic generation on power systems," *IEEE Transactions on Power Systems*, vol. 28, no. 2, pp. 893–901, May 2013.

[3] B. Weise, "Impact of K-factor and active current reduction during fault-ride-through of generating units connected via voltage-sourced converters on power system stability," *IET Renewable Power Generation*, vol. 9, no. 1, pp. 25–36, 2015.

[4] W. L. Kling, M. Gibescu, B. G. Rawn, J. C. Boemer, and M. A. M. M. van der Meijden, "Response of wind power park modules in distribution systems to transmission network faults during reverse power flows," *IET Renewable Power Generation*, vol. 9, no. 8, pp. 1033–1042, Nov. 2015.

[5] O. Goksu, R. Teodorescu, C. L. Bak, F. Iov, and P. C. Kjaer, "Instability of Wind Turbine Converters During Current Injection to Low Voltage Grid Faults and PLL Frequency Based Stability Solution," *IEEE Transactions on Power Systems*, vol. 29, no. 4, pp. 1683–1691, Jul. 2014.

[6] T. Ackermann, G. Andersson, and L. Söder, "Distributed generation: a definition," *Electric Power Systems Research*, vol. 57, no. 3, pp. 195–204, Apr. 2001.

[7] H. Pulgar-Painemal, Y. Wang, and H. Silva-Saravia, "On Inertia Distribution, Inter-Area Oscillations and Location of Electronically-Interfaced Resources," *IEEE Transactions on Power Systems*, vol. 33, no. 1, pp. 995–1003, Jan. 2018.

[8] A. Hosseinipour and H. Hojabri, "Virtual inertia control of PV systems for dynamic performance and damping enhancement of DC microgrids with constant power loads," *IET Renewable Power Generation*, vol. 12, no. 4, pp. 430–438, 2018.

[9] S. Weckx, C. Gonzalez, and J. Driesen, "Combined Central and Local Active and Reactive Power Control of PV Inverters," *IEEE Transactions on Sustainable Energy*, vol. 5, no. 3, pp. 776–784, Jul. 2014.

[10] S. Weckx and J. Driesen, "Optimal Local Reactive Power Control by PV Inverters," *IEEE Transactions on Sustainable Energy*, vol. 7, no. 4, pp. 1624–1633, Oktober 2016.

[11] A. Samadi, R. Eriksson, L. Soder, B. G. Rawn, and J. C. Boemer, "Coordinated Active Power-Dependent Voltage Regulation in Distribution Grids with PV Systems," *IEEE Transactions on Power Delivery*, vol. 29, no. 3, pp. 1454–1464, Jun. 2014.

[12] A. Al-Riyami, K. Burt, G. Manhangwe, P. Pretlove, and S. Georgiopoulos, "An investigation into alternatives to directional overcurrent protection on grid transformers to improve the network capacity to accommodate reverse power flow," in *12th IET International Conference on Developments in Power System Protection (DPSP 2014)*, 2014.

[13] G. D. Carne, G. Buticchi, Z. X. Zou, and M. Liserre, "Reverse power flow control in a ST-fed distribution grid," *IEEE Transactions on Smart Grid*, no. 99, 2017.

[14] K. Kawabe, Y. Ota, A. Yokoyama, and K. Tanaka, "Novel Dynamic Voltage Support Capability of Photovoltaic Systems for Improvement of Short-Term Voltage Stability in Power Systems," *IEEE Transactions on Power Systems*, 2016.

[15] S. Eftekharnejad, V. Vittal, G. T. Heydt, B. Keel, and J. Loehr, "Small Signal Stability Assessment of Power Systems with Increased Penetration of Photovoltaic Generation: A Case Study," *IEEE Transactions on Sustainable Energy*, vol. 4, no. 4, pp. 960–967, Oct. 2013.

[16] D. Palmer, I. Cole, T. Betts, and R. Gottschalg, "Assessment of potential for photovoltaic roof installations by extraction of roof tilt from light detection and ranging data and aggregation to census geography," *IET Renewable Power Generation*, vol. 10, no. 4, pp. 467–473, 2016.

[17] E. Yao, P. Samadi, V. W. S. Wong, and R. Schober, "Residential Demand Side

Management Under High Penetration of Rooftop Photovoltaic Units," *IEEE Transactions on Smart Grid*, vol. 7, no. 3, pp. 1597–1608, May 2016.
[18] T. Ghanbari, H. Samet, and F. Hashemi, "Islanding detection method for inverter-based distributed generation with negligible non-detection zone using energy of rate of change of voltage phase angle," *IET Generation, Transmission & Distribution*, vol. 9, no. 15, pp. 2337–2350, Nov. 2015.
[20] S. M. Alizadeh, C. Ozansoy, and A. Kalam, "Investigation into the impact of PCC parameters on voltage stability in a DFIG wind farm," in *2017 Australasian Universities Power Engineering Conference (AUPEC)*, 2017.
[21] P. N. K. Sreelatha, J. Praveen, and V. Kamaraju, "Effect of unsymmetrical faults on distribution lines with different line X/R ratios and voltage restoration using DVR with Space vector control," in *2012 International Conference on Computing, Electronics and Electrical Technologies (ICCEET)*, 2012, pp. 92–97.
[22] K. Kawabe, Y. Ota, A. Yokoyama, and K. Tanaka, "Short-term voltage stability improvement by active and reactive power control using advanced fault ride-through capability of photovoltaic systems," in *2016 Power Systems Computation Conference (PSCC)*, 2016.
[23] G. Lammert *et al.*, "Impact of fault ride-through and dynamic reactive power support of photovoltaic systems on short-term voltage stability," in *PowerTech, 2017 IEEE Manchester*, 2017.
[24] Y. Wang and Y. Yuan, "A dynamic reactive power compensation method for high-power and high-voltage electronic motors based on self-adaptive fuzzy PID control," in *2016 IEEE Chinese Guidance, Navigation and Control Conference (CGNCC)*, 2016, pp. 10–15.
[25] S. Liu, Q. Yang, K. Jia, and T. Bi, "Coordinated fault-ride-through strategy for doubly-fed induction generators with enhanced reactive and active power support," *IET Renewable Power Generation*, vol. 10, no. 2, pp. 203–211, Feb. 2016.
[26] P. Mohammadi, A. Eskandari, J. Milimonfared, and J. S. Moghani, "LVRT capability enhancement of single-phase grid connected PV array with coupled supercapacitor," in *2018 9th Annual Power Electronics, Drives Systems and Technologies Conference (PEDSTC)*, 2018, pp. 193–198.
[27] L. Li, H. Zhou, F. Luo, X. Lin, and Y. Han, "Control Strategy for Low Voltage Ride Through (LVRT) Operation of Two-Stage Photovoltaic Power Generation System," in *2018 IEEE 4th Southern Power Electronics Conference (SPEC)*, 2018.
[28] H. Khan, S. J. Chacko, B. G. Fernandes, and A. Kulkarni, "An integrated controller to perform LVRT operation in PV systems connected to a LV grid during balanced and unbalanced faults," presented at the 2017 IEEE 3rd International Future Energy Electronics Conference and ECCE Asia (IFEEC 2017 - ECCE Asia), 2017, pp. 2002–2007.
[29] M. A. Shuvra and B. Chowdhury, "Distributed dynamic grid support using smart PV inverters during unbalanced grid faults," *IET Renewable Power Generation*, vol. 13, no. 4, pp. 598–608, 2019.
[30] M. Coumont and J. Hanson, "Analysis of Voltage Support during Fault Ride Through of Converter-Interfaced Distributed Generation Considering the Grid Impedance," in *NEIS 2018; Conference on Sustainable Energy Supply and Energy Storage Systems*, 2018.
[31] "Low voltage ride through," *Wikipedia*. 21-Feb-2019.
[32] "System Operator for Northern Ireland (SONI) Grid Code." EirGrid Group, 2018.
[33] "EirGrid grid code." EirGrid Group, 13-Dec-2018.
[34] "Technical regulation 3.2.5 for wind power plants above 11 kW." Energinet, 0-2016.
[35] "Technical regulation 3.2.2 for PV power plants above 11 kW." Energinet, 14-Jul-2016.
[36] "Complete Grid Code." National Grid Electricity Transmission plc, al, 22-Dec-2018.
[37] K. Loudiyi, A. Berrada, H. G. Svendsen, and K. Mentesidi, "Grid code status for wind farms interconnection in Northern Africa and Spain: Descriptions and

recommendations for Northern Africa," *Renewable and Sustainable Energy Reviews*, vol. 81, pp. 2584–2598, 2018.
[38] R. Alves, F. Reis, and C. Liang, "TSOs and DSOs collaboration: The need for data exchange," *Engineering and Industry Series, Deregulated Electricity Market Issues in South Eastern Europe*, 2015.
[39] E. Lambert *et al.*, "Practices and Architectures for TSO-DSO Data Exchange: European Landscape," in *2018 IEEE PES Innovative Smart Grid Technologies Conference Europe (ISGT-Europe)*, 2018.
[40] V. C. Nikolaidis, N. Papanikolaou, A. S. Safigianni, A. G. Paspatis, and G. C. Konstantopoulos, "Influence of fault-ride-through requirements for distributed generators on the protection coordination of an actual distribution system with reclosers," in *2017 IEEE Manchester PowerTech*, 2017.
[41] H. Sun *et al.*, "Review of Challenges and Research Opportunities for Voltage Control in Smart Grids," *IEEE Transactions on Power Systems*, 2019.
[42] Y. Tohidi, M. Farrokhseresht, and M. Gibescu, "A Review on Coordination Schemes Between Local and Central Electricity Markets," in *2018 15th International Conference on the European Energy Market (EEM)*, 2018.
[43] K. Wang, Y. Wang, Z. Cheng, L. Liu, L. Jia, and Y. Liang, "Research on Reactive Power Control of the Grid-Side Converter of DFIG Based Wind Farm," presented at the 2018 2nd IEEE Conference on Energy Internet and Energy System Integration (EI2), 2018.
[44] V. Astapov, P. H. Divshali, and L. Söder, "The potential of distribution grid as an alternative source for reactive power control in transmission grid," in *2018 19th International Scientific Conference on Electric Power Engineering (EPE)*, 2018.
[45] T. L. Van, T. H. Truong, M. T. Cao, P. C. Nguyen, and H. Nguyen, "Improved Control Scheme for Low Voltage Ride-Through of PMSG-based Wind Energy Conversion Systems," in *2018 4th International Conference on Green Technology and Sustainable Development (GTSD)*, 2018, pp. 169–164.
[46] L. Niu, X. Wang, L. Wu, F. Yan, M. Xu, and X. Hu, "Low Voltage Ride-through Strategy for Wind Farm and VSC-HVDC," in *2018 International Conference on Power System Technology (POWERCON)*, 2018, pp. 2183–2188.
[47] S. Lu, M. Wang, C. Tai, M. Tsou, and F. Gu, "Formulation of Low Voltage Ride-Through Curve Considering Offshore Wind Farms Integrated into an Islanding Power System - A Case Study in Taiwan," in *2018 International Symposium on Computer, Consumer and Control (IS3C)*, 2018, pp. 117–120.
[48] R. Liu, J. Yao, J. Pei, X. Wang, P. Sun, and X. Guo, "Dynamic Stability Analysis of the Weak Grid-Connected DFIG-based Wind Turbines under Severe Symmetrical Faults," in *2018 International Conference on Power System Technology (POWERCON)*, 2018, pp. 1512–1517.
[49] X. Lin, Y. Han, P. Yang, C. Wang, and J. Xiong, "Low-Voltage Ride-Through Techniques for Two-Stage Photovoltaic System under Unbalanced Grid Voltage Sag Conditions," in *2018 IEEE 4th Southern Power Electronics Conference (SPEC)*, 2018.
[50] P. Gotseff, N. Wunder, A. Hoke, E. Ifuku, and R. Ueda, "Residential Advanced Photovoltaic Inverter Pilot Study Results for Select Distribution Secondaries in Hawai'i," in *2018 IEEE 7th World Conference on Photovoltaic Energy Conversion (WCPEC) (A Joint Conference of 45th IEEE PVSC, 28th PVSEC 34th EU PVSEC)*, 2018, pp. 1418–1423.
[51] Y. Yang, A. Sangwongwanich, H. Liu, and F. Blaabjerg, "Low voltage ride-through of two-stage grid-connected photovoltaic systems through the inherent linear power-voltage characteristic," in *2017 IEEE Applied Power Electronics Conference and Exposition (APEC)*, 2017, pp. 3582–3588.
[52] A. Mishra, N. K. C. Nair, and N. D. Patel, "Fault current characterisation of single phase inverter systems," in *2017 IEEE Power Energy Society General Meeting*, 2017.
[53] S. Roediger, R. Yan, and T. K. Saha, "Investigation of the impacts of three-phase photovoltaic systems on three-phase unbalanced networks," in *2012 IEEE Power and*

Energy Society General Meeting, 2012.
[54] A. Samadi, L. Soder, E. Shayesteh, and R. Eriksson, "Static Equivalent of Distribution Grids With High Penetration of PV Systems," *IEEE Transactions on Smart Grid*, vol. 6, no. 4, pp. 1763–1774, Jul. 2015.
[55] C. Heinrich, P. Fortenbacher, A. Fuchs, and G. Andersson, "PV-integration strategies for low voltage networks," presented at the 2016 IEEE International Energy Conference (ENERGYCON), 2016.
[56] C. Fu, C. Wang, and S. Alyami, "An LMI Based Stability Margin Analysis for Active PV Power Control of Distribution Networks with Time-Invariant Delays," in *2018 IEEE Power Energy Society General Meeting (PESGM)*, 2018.
[57] S. Ghosh, S. Rahman, and M. Pipattanasomporn, "Distribution Voltage Regulation through Active Power Curtailment with PV Inverters and Solar Generation Forecasts," *IEEE Transactions on Sustainable Energy*, vol. PP, no. 99, 2016.
[58] "National Electricity Rules." Australian Energy Market Operator (AEMO), 2018.
[59] A. Canova, L. Giaccone, F. Spertino, and M. Tartaglia, "Electrical Impact of Photovoltaic Plant in Distributed Network," *IEEE Transactions on Industry Applications*, vol. 45, no. 1, pp. 341–347, 2009.
[60] M. A. Mahmud, M. J. Hossain, H. R. Pota, and others, "Analysis of voltage rise effect on distribution network with distributed generation," in *18th IFAC World Congress*, Milano, Italy, 2011.
[61] S. Elsaiah, M. Benidris, and J. Mitra, "Analytical approach for placement and sizing of distributed generation on distribution systems," *IET Generation, Transmission & Distribution*, vol. 8, no. 6, pp. 1039–1049, Jun. 2014.
[62] R. Yan and T. K. Saha, "Investigation of Voltage Stability for Residential Customers Due to High Photovoltaic Penetrations," *IEEE Transactions on Power Systems*, vol. 27, no. 2, pp. 651–662, May 2012.
[63] Y. T. Tan, "Impact on the Power System with a Large Penetration of Photovoltaic Generation," 2004.
[64] Z. Ali, N. Christofides, L. Hadjidemetriou, and E. Kyriakides, "Diversifying the Role of Distributed Generation Grid Side Converters for Improving the Power Quality of Distribution Networks using Advanced Control Techniques," *IEEE Transactions on Industry Applications*, 2019.
[65] Y. J. Kim, "Development and Analysis of a Sensitivity Matrix of a Three-Phase Voltage Unbalance Factor," *IEEE Transactions on Power Systems*, vol. 33, no. 3, pp. 3192–3195, May 2018.
[66] D. F. Teshome, P. Bagheri, and A. Nassif, "Impact of Feeder Characteristics on Voltage Rise in Secondary Distribution Systems," in *2018 IEEE Power Energy Society General Meeting (PESGM)*, 2018.
[67] J. Schoene, M. Humayun, B. Poudel, V. Zheglov, and A. Gebeyehu, "Evaluation of the Effectiveness and Robustness of Residential-Scale Smart Photovoltaics," in *2018 IEEE/PES Transmission and Distribution Conference and Exposition (T D)*, 2018.
[68] H. Mortazavi, H. Mehrjerdi, M. Saad, S. Lefebvre, D. Asber, and L. Lenoir, "A Monitoring Technique for Reversed Power Flow Detection With High PV Penetration Level," *IEEE Transactions on Smart Grid*, vol. 6, no. 5, pp. 2221–2232, Sep. 2015.
[69] X. Su, M. A. S. Masoum, and P. J. Wolfs, "Optimal PV Inverter Reactive Power Control and Real Power Curtailment to Improve Performance of Unbalanced Four-Wire LV Distribution Networks," *IEEE Transactions on Sustainable Energy*, vol. 5, no. 3, pp. 967–977, Jul. 2014.
[70] C. E. Carter, M. Calais, P. Lu, and J. A. Crocker, "An evaluation of options to mitigate voltage rise due to increasing PV penetration in distribution networks," *Renewable Energy and Environmental Sustainability*, vol. 2, p. 39, 2017.
[71] X. Su, M. A. S. Masoum, and P. Wolfs, "Comprehensive optimal photovoltaic inverter control strategy in unbalanced three-phase four-wire low voltage distribution networks," *IET Generation, Transmission Distribution*, vol. 8, no. 11, pp. 1848–1859, 2014.

[72] S. Alyami, Y. Wang, C. Wang, J. Zhao, and B. Zhao, "Adaptive Real Power Capping Method for Fair Overvoltage Regulation of Distribution Networks With High Penetration of PV Systems," *IEEE Transactions on Smart Grid*, vol. 5, no. 6, pp. 2729–2738, Nov. 2014.

[73] K. N. Bangash, M. E. A. Farrag, and A. H. Osman, "Manage Reverse Power Flow and Fault Current Level in LV Network with High Penetration of Small Scale Solar and Wind Power Generation," in *2018 53rd International Universities Power Engineering Conference (UPEC)*, 2018.

[74] M. C. Kocer *et al.*, "Cloud Induced PV Impact on Voltage Profiles for Real Microgrids," in *2018 5th International Symposium on Environment-Friendly Energies and Applications (EFEA)*, 2018.

[75] A. T. Procopiou, K. Petrou, L. F. Ochoa, T. Langstaff, and J. Theunissen, "Adaptive Decentralized Control of Residential Storage in PV-Rich MV-LV Networks," *IEEE Transactions on Power Systems*, 2018.

[76] K. Kawabe and A. Yokoyama, "Study on short-term voltage stability improvement using batteries on extra-high voltage network," in *PowerTech (POWERTECH), IEEE Grenoble*, 2013.

[77] P. L. Denholm, R. M. Margolis, and J. D. Eichman, "Evaluating the technical and economic performance of pv plus storage power plants," National Renewable Energy Lab.(NREL), Golden, CO (United States), 2017.

[78] K. Kawabe and K. Tanaka, "Impact of Dynamic Behavior of Photovoltaic Power Generation Systems on Short-Term Voltage Stability," *IEEE Transactions on Power Systems*, vol. 30, no. 6, pp. 3416–3424, Nov. 2015.

[79] J. Krata, T. K. Saha, and R. Yan, "Large scale photovoltaic system and its impact on distribution network in transient cloud conditions," in *2015 IEEE Power Energy Society General Meeting*, 2015.

[80] S. P. Ghanegaonkar and V. N. Pande, "Coordinated optimal placement of distributed generation and voltage regulator by multi-objective efficient PSO algorithm," in *2015 IEEE Workshop on Computational Intelligence: Theories, Applications and Future Directions (WCI)*, 2015.

[81] V. Vega-Garita, A. P. Harsarapama, L. Ramirez-Elizondo, and P. Bauer, "Physical integration of PV-battery system: Advantages, challenges, and thermal model," in *2016 IEEE International Energy Conference (ENERGYCON)*, 2016.

[82] A. van Stiphout, S. Vaeck, and G. Deconinck, "The role of long-term energy storage in investment planning of renewable power systems," in *2016 IEEE International Energy Conference (ENERGYCON)*, 2016.

[83] A. van Stiphout and G. Deconinck, "The impact of long-term demand response on investment planning of renewable power systems," in *2016 13th International Conference on the European Energy Market (EEM)*, 2016.

[84] E. B. Ssekulima and A. A. Hinai, "Coordinated voltage control of solar PV with MPPT and battery storage in grid-connected and microgrid modes," in *2016 18th Mediterranean Electrotechnical Conference (MELECON)*, 2016.

[85] H. A. B. Siddique, M. J. R. Ahmad, and R. W. D. Doncker, "Optimal control and filter sizing of a multi-megawatt medium-voltage voltage-source converter for future grids," in *2016 IEEE 7th International Symposium on Power Electronics for Distributed Generation Systems (PEDG)*, 2016.

[86] M. S. Islam, N. Mithulananthan, and K. Bhumkittipich, "Feasibility of PV and battery energy storage based EV charging in different charging stations," in *2016 13th International Conference on Electrical Engineering/Electronics, Computer, Telecommunications and Information Technology (ECTI-CON)*, 2016.

[87] Y. Yang, H. Li, A. Aichhorn, J. Zheng, and M. Greenleaf, "Sizing Strategy of Distributed Battery Storage System With High Penetration of Photovoltaic for Voltage Regulation and Peak Load Shaving," *IEEE Transactions on Smart Grid*, vol. 5, no. 2, pp. 982–991, Mar. 2014.

[88] M. Dietmannsberger and D. Schulz, “Ancillary services and dynamic behavior of inverters connected to the low voltage grid,” in *Compatibility and Power Electronics (CPE), 2015 9th International Conference on*, 2015, pp. 49–56.
[89] J. Sridhar, G. R. C. Mouli, P. Bauer, and E. Raaijen, “Analysis of load shedding strategies for battery management in PV-based rural off-grids,” in *PowerTech, 2015 IEEE Eindhoven*, 2015.
[90] K. Veerashekar, P. L. Seta, and M. Luther, “Impact of Distributed Battery Energy Storage Systems on Low Voltage Grids with High Amount of Photovoltaics,” in *International ETG Congress 2015; Die Energiewende - Blueprints for the new energy age; Proceedings of*, 2015.
[91] J. Sachs and O. Sawodny, “A Two-Stage Model Predictive Control Strategy for Economic Diesel-PV-Battery Island Microgrid Operation in Rural Areas,” *IEEE Transactions on Sustainable Energy*, vol. 7, no. 3, pp. 903–913, Jul. 2016.
[92] B. Mirshekarpour and S. A. Davari, “Efficiency optimization and power management in a stand-alone photovoltaic (PV) water pumping system,” in *2016 7th Power Electronics and Drive Systems Technologies Conference (PEDSTC)*, 2016, pp. 427–433.
[93] K. Maharaja, P. P. Balaji, S. Sangeetha, and M. Elakkiya, “Development of bidirectional net meter in grid connected solar PV system for domestic consumers,” in *2016 International Conference on Energy Efficient Technologies for Sustainability (ICEETS)*, 2016, pp. 46–49.
[94] A. Merabet, K. Ahmed, H. Ibrahim, R. Beguenane, and A. Ghias, “Energy Management and Control System for Laboratory Scale Microgrid based Wind-PV-Battery,” *IEEE Transactions on Sustainable Energy*, no. 99, 2016.
[95] A. Luna *et al.*, “Optimal power scheduling for a grid-connected hybrid PV-wind-battery microgrid system,” in *2016 IEEE Applied Power Electronics Conference and Exposition (APEC)*, 2016, pp. 1227–1234.
[96] T. Kolacia and J. Drapela, “Voltage sensitivity to power flows related to distributed generation,” in *2016 17th International Scientific Conference on Electric Power Engineering (EPE)*, 2016.
[97] E. Ozdemir, S. Ozdemir, K. Erhan, and A. Aktas, “Energy storage technologies opportunities and challenges in smart grids,” in *2016 International Smart Grid Workshop and Certificate Program (ISGWCP)*, 2016.
[98] C. Fuyi, “The basic structure of the feed-in Tariff system in Japan,” in *2017 IEEE International Conference on Smart Grid and Smart Cities (ICSGSC)*, 2017.
[99] S. Huang and Q. Wu, “Dynamic Tariff-Subsidy Method for PV and V2G Congestion Management in Distribution Networks,” *IEEE Transactions on Smart Grid*, 2019.
[100] S. Zhou, Z. Hu, W. Gu, M. Jiang, and X. Zhang, “Artificial intelligence based smart energy community management: A reinforcement learning approach,” *CSEE Journal of Power and Energy Systems*, no. 99, Mar. 2019.
[101] A. Y. Elrayyah, M. Z. C. Wanik, and A. Bousselham, “Simplified Approach to Analyze Voltage Rise in LV Systems with PV Installations Using Equivalent Power Systems Diagrams,” *IEEE Transactions on Power Delivery*, no. 99, 2016.
[102] I. Erlich, F. Shewarega, S. Engelhardt, J. Kretschmann, J. Fortmann, and F. Koch, “Effect of wind turbine output current during faults on grid voltage and the transient stability of wind parks,” presented at the 2009 IEEE Power Energy Society General Meeting, 2009.
[103] Y. Yang, H. Wang, and F. Blaabjerg, “Reactive power injection strategies for single-phase photovoltaic systems considering grid requirements,” in *IEEE Applied Power Electronics Conference and Exposition - APEC*, 2014, pp. 371–378.
[104] E. M. G. Rodrigues, G. J. Osório, R. Godina, A. W. Bizuayehu, J. M. Lujano-Rojas, and J. P. S. Catalão, “Grid code reinforcements for deeper renewable generation in insular energy systems,” *Renewable and Sustainable Energy Reviews*, vol. 53, pp. 163–177, Jan. 2016.

[105] K. Ren, X. Zhang, F. Wang, L. Guo, Z. Wang, and L. Wang, "Grid fault ride through of a medium-voltage three-level full power wind power converter," in *2016 IEEE 8th International Power Electronics and Motion Control Conference (IPEMC-ECCE Asia)*, 2016, pp. 1509–1514.
[106] D. Shi and R. K. Sharma, "Adaptive control of energy storage for voltage regulation in distribution system," in *2013 IEEE International Conference on Smart Energy Grid Engineering (SEGE)*, 2013.
[107] C. Liu, N. Qin, C. L. Bak, and Y. Xu, "A hybrid optimization method for reactive power and voltage control considering power loss minimization," in *PowerTech, 2015 IEEE Eindhoven*, 2015.
[108] H. M. Hasanien, "An Adaptive Control Strategy for Low Voltage Ride Through Capability Enhancement of Grid-Connected Photovoltaic Power Plants," *IEEE Transactions on Power Systems*, 2015.
[109] K. Kawabe and K. Tanaka, "Analytical Method for Short-Term Voltage Stability Using the Stability Boundary in the P-V Plane," *IEEE Transactions on Power Systems*, vol. 29, no. 6, pp. 3041–3047, Nov. 2014.
[110] K. Kawabe and K. Tanaka, "Effect of reactive power control by photovoltaic power generation on short-term voltage stability," in *PowerTech, 2015 IEEE Eindhoven*, 2015.
[111] B. Hoseinzadeh, F. F. da Silva, and C. L. Bak, "Coordination of voltage and frequency feedback in load-frequency control capability of wind turbine," in *IECON - 40th Annual Conference of the IEEE Industrial Electronics Society*, 2014, pp. 5501–5507.
[112] Kundur, "Definition and Classification of Power System Stability IEEE/CIGRE Joint Task Force on Stability Terms and Definitions," *IEEE Transactions on Power Systems*, vol. 19, no. 3, pp. 1387–1401, Aug. 2004.
[113] "Integrated System Plan (ISP)." The Australian Energy Market Operator (AEMO), 2018.
[114] P. Kundur, N. J. Balu, and M. G. Lauby, *Power System Stability and Control*. McGraw-Hill Education, 1994.
[115] W. A. Qureshi, G. Demler, and N. K. C. Nair, "Developing transmission fault ride-through criteria for New Zealand wind farms," in *IEEE Power and Energy Society General Meeting*, 2011.
[116] J. Merino, P. Mendoza-Araya, and C. Veganzones, "State of the Art and Future Trends in Grid Codes Applicable to Isolated Electrical Systems," *Energies*, vol. 7, no. 12, pp. 7936–7954, Dec. 2014.
[117] "Transmission Code 2007. Network and System Rules of the German Transmission System Operators." Verband der Netzbetreiber - VDN – e.V. beim VDEW, Aug-2007.
[118] B. Hoseinzadeh, "A Power System Emergency Control Scheme in the Presence of High Wind Power Penetration," 2015.
[119] S. Lissandron, R. Sgarbossa, L. Dalla Santa, P. Mattavelli, R. Turri, and A. Cerretti, "Impact of non-simultaneous P/f and Q/V grid code requirements on PV inverters on unintentional islanding operation in distribution network," in *Power Electronics for Distributed Generation Systems (PEDG), 2015 IEEE 6th International Symposium on*, 2015.
[120] J. Rodrigues, A. Lopes, L. Miranda, C. Gouveia, C. Moreira, and J. P. Lopes, "The Role of Low-Voltage-Ride-Through Capability of Distributed Energy Resources for the Mitigation of Voltage Sags in Low Voltage Distribution Grids," in *2018 Power Systems Computation Conference (PSCC)*, 2018.
[121] "Technical regulation 3.2.1 for power plants up to and including 11 kW." Energinet, 30-Jun-2016.
[122] "Engineering Recommendation G99." The Operations Directorate of Energy Networks Association, 16-May-2018.
[123] Y. Bae, T. K. Vu, and R. Y. Kim, "Implemental Control Strategy for Grid Stabilization of Grid-Connected PV System Based on German Grid Code in Symmetrical Low-to-Medium Voltage Network," *IEEE Transactions on Energy Conversion*, vol. 28, no. 3,

pp. 619–631, Sep. 2013.
[124] A. Etxegarai Madina, *Compliance verification methodology for renewable generation integration. Application to island power grids*. Servicio Editorial de la Universidad del País Vasco/Euskal Herriko Unibertsitateko Argitalpen Zerbitzua, 2015.
[125] M. Nawir, "Integration of wind farms into weak AC grid," PhD Thesis, Cardiff University, 2017.
[126] A. Jotwani, "An Advanced Investigation on LVRT Requirement in Wind Integrated Power Systems," presented at the 1 st international conference on Large - Scale Grid Integration of Renewable Energy in India, IIT Bombay, India, 2017, p. 7.
[127] J. Martínez, P. C. Kjær, P. Rodriguez, and R. Teodorescu, "Active current control in wind power plants during grid faults," *Wind Energ.*, vol. 13, no. 8, pp. 737–749, Nov. 2010.
[128] M. Nour, A. Ali, and C. Farkas, "Mitigation of Electric Vehicles Charging Impacts on Distribution Network with Photovoltaic Generation," in *2019 International Conference on Innovative Trends in Computer Engineering (ITCE)*, 2019, pp. 384–388.
[129] T. Vo, V. Tran, and H. M. Nguyen, "Impact of Duyen-Hai Wind Farms on Tra-Vinh Power Transmission Systems," in *2018 4th International Conference on Green Technology and Sustainable Development (GTSD)*, 2018, pp. 161–163.
[130] P. R. Kadukar, P. S. Shete, and S. P. Gawande, "Transient Analysis of Distributed Generation AC Microgrid using ETAP," in *2018 International Conference on Current Trends towards Converging Technologies (ICCTCT)*, 2018.
[131] S. Mkattiri and A. Saad, "Islanding operation of an HTA network, Analysis of the impact of decentralized energy generation on the transient stability of an HTA distribution network," in *2018 Renewable Energies, Power Systems Green Inclusive Economy (REPS-GIE)*, 2018.
[132] A. A. Abdou, S. Kamel, M. Abdel-Akher, and F. Jurado, "Voltage Stability Analysis of Distribution Network in Egypt Including UPQC Device," in *2018 Twentieth International Middle East Power Systems Conference (MEPCON)*, 2018, pp. 1115–1120.
[133] P. Demetriou, M. Asprou, J. Quiros-Tortos, and E. Kyriakides, "Dynamic IEEE Test Systems for Transient Analysis," *IEEE Systems Journal*, vol. 11, no. 4, pp. 2108–2117, Dec. 2017.
[134] H. Beleed and B. K. Johnson, "Comparative study on IEEE12 bus system with D-FACTS devices in different simulation tools," in *2017 North American Power Symposium (NAPS)*, 2017.
[135] B. N. Nguyen, L. T. Le, Q. C. Le, T. H. Pham, C. T. Nguyen, and H. T. Nguyen, "Study of FACTS Device Applications for the 220kV Southwest Region of the Vietnam Power System," in *2018 4th International Conference on Green Technology and Sustainable Development (GTSD)*, 2018, pp. 150–154.
[136] A. Annamalai, S. K. Shrivastava, A. Gulati, R. Gera, and S. V. N. J. Sundar, "Development of AC network dynamic equivalents for large scale power system," in *2017 Second International Conference on Electrical, Computer and Communication Technologies (ICECCT)*, 2017.
[137] Johannes Morren, "Grid support by power electronic converters of distributed generation units," TU Delft, S.l., 2006.
[138] A. Swandaru, M. D. Rotaru, and J. K. Sykulski, "The effectiveness of additional reactive current injection from a distributed energy resource unit to mitigate short voltage instability during extreme low voltage ride through," presented at the 2017 International Conference on Modern Power Systems (MPS), 2017.
[139] "DIgsilent PowerFactory User Manual version 15," DIgsilent PowerFatory, Gomaringen, Germany, Jul. 2015.
[140] J. C. Das, *Transients in Electrical Systems.* New York, USA: McGraw-Hill Professional Publishing, 2010.
[141] H.-K. Ringkjøb, P. M. Haugan, and I. M. Solbrekke, "A review of modelling tools for

energy and electricity systems with large shares of variable renewables," *Renewable and Sustainable Energy Reviews*, vol. 96, pp. 440–459, Nov. 2018.
[142] H. Al-Sheikh and N. Moubayed, "An overview of simulation tools for renewable applications in power systems," in *2012 2nd International Conference on Advances in Computational Tools for Engineering Applications (ACTEA)*, 2012, pp. 257–261.
[143] P. Pourbeik *et al.*, "Generic Dynamic Models for Modeling Wind Power Plants and other Renewable Technologies in Large Scale Power System Studies," in *2018 IEEE Power Energy Society General Meeting (PESGM)*, 2018.
[144] "PowerFactory - DIgSILENT licence and installation." [Online]. Available: https://www.digsilent.de/en/licence-and-installation-overview.html. [Accessed: 17-Mar-2019].
[145] H. Saadat, *Power Systems Analysis*, 2nd edition. Boston: McGraw-Hill Higher Education, 2002.
[146] Gerd Balzer, "Short-Circuit Calculation with Full Size Converters According to IEC," 2016.
[147] "IEC 60909-0. Short-circuit currents in three-phase AC systems- Part 0: Calculation of currents," IEC, Technical Report First Edition, 2000-7.
[148] "IEC 60909-0. Short-circuit currents in three-phase AC systems –Part 4: Examples for the calculation of short-circuit currents," IEC, Technical Report First Edition, 2001-7.
[149] B. Tamimi, C. Cañizares, and K. Bhattacharya, "System Stability Impact of Large-Scale and Distributed Solar Photovoltaic Generation: The Case of Ontario, Canada," *IEEE Transactions on Sustainable Energy*, vol. 4, no. 3, pp. 680–688, Jul. 2013.
[150] R. Teodorescu, M. Liserre, and P. Rodriguez, *Grid converters for photovoltaic and wind power systems*. [Piscataway, N.J.] : Chichester, West Sussex ; Hoboken, N.J: IEEE ; Wiley, 2011.
[151] J. Wu, Y. He, and N. Jenkins, "A robust state estimator for medium voltage distribution networks," *IEEE Transactions on Power Systems*, vol. 28, no. 2, pp. 1008–1016, May 2013.
[152] Y. Yang, W. Chen, and F. Blaabjerg, "Advanced Control of Photovoltaic and Wind Turbines Power Systems," in *Advanced and Intelligent Control in Power Electronics and Drives*, vol. 531, T. Orłowska-Kowalska, F. Blaabjerg, and J. Rodríguez, Eds. Cham: Springer International Publishing, 2014, pp. 41–89.
[153] A. Vangari, D. Haribabu, and J. N. Sakamuri, "Modeling and control of DC/DC boost converter using K-factor control for MPPT of solar PV system," in *International Conference on Energy Economics and Environment (ICEEE)*, 2015.
[154] W. R. Issa, M. A. Abusara, and S. M. Sharkh, "Control of Transient Power During Unintentional Islanding of Microgrids," *IEEE Transactions on Power Electronics*, vol. 30, no. 8, pp. 4573–4584, Aug. 2015.
[155] L. S. Czarnecki and P. M. Haley, "Unbalanced Power in Four-Wire Systems and Its Reactive Compensation," *IEEE Transactions on Power Delivery*, vol. 30, no. 1, pp. 53–63, Feb. 2015.
[156] W. Issa, M. Abusara, S. Sharkh, and T. Mallick, "A small signal model of an inverter-based microgrid including DC link voltages," in *Power Electronics and Applications (EPE'15 ECCE-Europe), 2015 17th European Conference on*, 2015.
[157] F. Q. Al-Enezi, "Optimal cost versus efficiency configuration of a grid-connected photovoltaic system exploiting the weighted-sum method with focus on Kuwaiti National Grid," PhD Thesis, University of Southampton, 2015.
[158] R. Kadri, J.-P. Gaubert, and G. Champenois, "An Improved Maximum Power Point Tracking for Photovoltaic Grid-Connected Inverter Based on Voltage-Oriented Control," *IEEE Transactions on Industrial Electronics*, vol. 58, no. 1, pp. 66–75, Jan. 2011.
[159] E. Alizadeh, A. M. Birjandi, and M. Hamzeh, "Decentralised power sharing control strategy in LV microgrids under unbalanced load conditions," *Transmission Distribution IET Generation*, vol. 11, no. 7, pp. 1613–1623, 2017.
[160] V. Blahnik, T. Kosan, Z. Peroutka, and J. Talla, "Control of a Single-Phase Cascaded

H-Bridge Active Rectifier Under Unbalanced Load," *IEEE Transactions on Power Electronics*, vol. 33, no. 6, pp. 5519–5527, Jun. 2018.
[161] H. Akagi, E. H. Watanabe, M. Aredes, and Institute of Electrical and Electronics Engineers, *Instantaneous power theory and applications to power conditioning*. Hoboken, NJ: Wiley-Interscience/ John Wiley & Sons, 2007.
[162] A. Timbus, M. Liserre, R. Teodorescu, P. Rodriguez, and F. Blaabjerg, "Evaluation of Current Controllers for Distributed Power Generation Systems," *IEEE Transactions on Power Electronics*, vol. 24, no. 3, pp. 654–664, Mar. 2009.
[163] "PV array modules - Simulink." [Online]. Available: https://www.mathworks.com. [Accessed: 19-Mar-2019].
[164] A. Ellis, M. Behnke, and R. Elliott, "Generic Solar Photovoltaic System Dynamic Simulation Model Specification," Sandia National Laboratories (SNL-NM), Albuquerque, NM (United States), 2013.
[165] "PWM-controlled three-level converter - Simulink." [Online]. Available: https://www.mathworks.com. [Accessed: 20-Mar-2019].
[166] "250-kW Grid-Connected PV Array - MATLAB & Simulink." [Online]. Available: https://www.mathworks.com. [Accessed: 20-Mar-2019].
[167] "Phase Locked Loop (PLL - 3ph) - Simulink." [Online]. Available: https://www.mathworks.com. [Accessed: 20-Mar-2019].
[168] D. Yang, X. Wang, F. Liu, K. Xin, Y. Liu, and F. Blaabjerg, "Adaptive reactive power control of PV power plants for improved power transfer capability under ultra-weak grid conditions," presented at the 2017 IEEE Power Energy Society General Meeting, 2017.
[169] K. Kawabe, T. Nanahara, and K. Tanaka, "Importance of considering induction motor load for studying impact of photovoltaic generation on transient stability of power systems," in *2017 IEEE Manchester PowerTech*, 2017.
[170] S. M. Alizadeh, C. Ozansoy, and T. Alpcan, "The impact of X/R ratio on voltage stability in a distribution network penetrated by wind farms," in *2016 Australasian Universities Power Engineering Conference (AUPEC)*, 2016.
[171] T. Sarkar, A. K. Dan, and S. Ghosh, "Effect of X/R ratio on low voltage distribution system connected with constant speed wind turbine," in *2016 2nd International Conference on Control, Instrumentation, Energy Communication (CIEC)*, 2016, pp. 417–421.
[172] J. Rocabert, A. Luna, F. Blaabjerg, and P. Rodríguez, "Control of Power Converters in AC Microgrids," *IEEE Transactions on Power Electronics*, vol. 27, no. 11, pp. 4734–4749, Nov. 2012.
[173] DIgSILENT PowerFactory, "Technical Reference Documentation: 'Static Generator.'" DIgSILENT GmbH, 2013.
[174] Ö. Göksu, "Control of Wind Turbines during Symmetrical and Asymmetrical Grid Faults," Aalborg University, Department of Energy Technology, Aalborg, 2012.
[175] L. Wang, R. Yan, and T. K. Saha, "Voltage Management for Large Scale PV Integration into Weak Distribution Systems," *IEEE Transactions on Smart Grid*, no. 99, 2017.
[176] A. Miron, A. Cziker, M. Chindriş, and D. Sacerdotianu, "Impact of distributed generation on weak distribution networks. study case on a Romanian microgrid," in *2016 International Conference on Applied and Theoretical Electricity (ICATE)*, 2016.
[177] J. Miret, A. Camacho, M. Castilla, J. L. G. de Vicuña, and J. de la Hoz, "Reactive current injection protocol for low-power rating distributed generation sources under voltage sags," *IET Power Electronics*, vol. 8, no. 6, pp. 879–886, 2015.
[178] J. Mohammadi, S. Afsharnia, S. Vaez-Zadeh, and S. Farhangi, "Improved fault ride through strategy for doubly fed induction generator based wind turbines under both symmetrical and asymmetrical grid faults," *IET Renewable Power Generation*, vol. 10, no. 8, pp. 1114–1122, 2016.
[179] J. Hu, B. Wang, W. Wang, H. Tang, Y. Chi, and Q. Hu, "Small Signal Dynamics of DFIG-Based Wind Turbines During Riding Through Symmetrical Faults in Weak AC

Grid," *IEEE Transactions on Energy Conversion*, vol. 32, no. 2, pp. 720–730, Jun. 2017.
[180] T. Moger and T. Dhadbanjan, "A novel index for identification of weak nodes for reactive compensation to improve voltage stability," *Transmission Distribution IET Generation*, vol. 9, no. 14, pp. 1826–1834, 2015.
[181] S. L. Lorenzen, A. B. Nielsen, and L. Bede, "Control of a grid connected converter during weak grid conditions," in *2016 IEEE 7th International Symposium on Power Electronics for Distributed Generation Systems (PEDG)*, 2016.
[182] J. Gao, J. Zhao, K. Qu, and F. Li, "Reconstruction of impedance-based stability criterion in weak grid," presented at the 2018 3rd International Conference on Intelligent Green Building and Smart Grid (IGBSG), 2018.
[183] Institute of Electrical and Electronics Engineers, *IEEE guide for planning DC links terminating at AC locations having low short-circuit capacities*. New York: Institute of Electrical and Electronics Engineers, 1997.
[184] "NERC White Paper: Short-Circuit Modeling and System Strength." North American Electric Reliability Corporation, Feb-2018.
[185] P. M. Anderson and A. A. Fouad, *Power System Control and Stability*, 2nd edition. Piscataway, N.J: Wiley-Blackwell, 2002.
[186] Sergio Martinez *et al.*, "CIRED-CIGRE Joint Working Group: Modelling of Inverter-Based Generation for Power System Dynamic Studies." CIRED, May-2018.
[187] S. Peyghami, P. Davari, H. Mokhtari, and F. Blaabjerg, "Decentralized Droop Control in DC Microgrids Based on a Frequency Injection Approach," *IEEE Transactions on Smart Grid*, 2019.
[188] L. Wang, F. Bai, R. Yan, and T. K. Saha, "Real-Time Coordinated Voltage Control of PV Inverters and Energy Storage for Weak Networks with High PV Penetration," *IEEE Transactions on Power Systems*, vol. 33, no. 3, pp. 3383–3395, May 2018.
[189] M. H. A. Bakar, N. M. L. Tan, A. K. Ramasamy, M. R. Othman, and I. Ariffin, "Impact of Active and Reactive Current Injections of Utility-Scale PV Generators during Low-Voltage Ride-Through," in *2018 IEEE 7th International Conference on Power and Energy (PECon)*, 2018, pp. 419–424.
[190] P. H. Divshali and L. Söder, "Improving PV Dynamic Hosting Capacity Using Adaptive Controller for STATCOMs," *IEEE Transactions on Energy Conversion*, vol. 34, no. 1, pp. 415–425, Mar. 2019.
[191] S. Hes, J. Kula, and J. Svec, "Increasing of Renewables Hosting Capacity in the Czech Republic in terms of European Project InterFlex (Case Study)," in *2018 International Conference and Utility Exhibition on Green Energy for Sustainable Development (ICUE)*, 2018.
[192] M. Alturki and A. Khodaei, "Increasing Distribution Grid Hosting Capacity through Optimal Network Reconfiguration," in *2018 North American Power Symposium (NAPS)*, 2018.
[193] G. Lammert, D. Premm, L. D. P. Ospina, J. C. Boemer, M. Braun, and T. V. Cutsem, "Control of Photovoltaic Systems for Enhanced Short-Term Voltage Stability and Recovery," *IEEE Transactions on Energy Conversion*, vol. 34, no. 1, pp. 243–254, Mar. 2019.
[194] C. Grande-Moran, B. Fernandes, D. Feltes, J. Feltes, M. Wu, and R. Wells, "Case Studies on Dynamic Load Modeling," in *2018 Clemson University Power Systems Conference (PSC)*, 2018.
[195] R. J. Bravo and D. P. Chassin, "Fault Induced Delayed Voltage Recovery (FIDVR) model validation," in *2016 IEEE/PES Transmission and Distribution Conference and Exposition (T D)*, 2016.
[196] R. J. Bravo, "Distribution FIDVR Events Analysis," in *Seventh Annual IEEE Green Technologies Conference*, 2015.
[197] R. J. Bravo, "Dynamic performance of residential motor loads," in *2016 IEEE/PES Transmission and Distribution Conference and Exposition (T D)*, 2016.
[198] B. Sparn, D. Krishnamurthy, A. Pratt, M. Ruth, and H. Wu, "Hardware-in-the-Loop

(HIL) Simulations for Smart Grid Impact Studies," in *2018 IEEE Power Energy Society General Meeting (PESGM)*, 2018.
[199] Y. Du, H. Tu, S. Lukic, D. Lubkeman, A. Dubey, and G. Karsai, "Development of a Controller Hardware-in-the-Loop Platform for Microgrid Distributed Control Applications," in *2018 IEEE Electronic Power Grid (eGrid)*, 2018.
[200] A. Nelson *et al.*, "Power hardware-in-the-loop evaluation of PV inverter grid support on Hawaiian electric feeders," 2017.
[201] Y. Huo, G. Gruosso, and L. Piegari, "Power hardware in the loop simulator of photovoltaic plant for smart grid interation analysis," in *2017 IEEE International Conference on Environment and Electrical Engineering and 2017 IEEE Industrial and Commercial Power Systems Europe (EEEIC / I CPS Europe)*, 2017.
[202] C. S. Edrington, M. Steurer, J. Langston, T. El-Mezyani, and K. Schoder, "Role of Power Hardware in the Loop in Modeling and Simulation for Experimentation in Power and Energy Systems," *Proceedings of the IEEE*, vol. 103, no. 12, pp. 2401–2409, Dec. 2015.
[203] S. S. Noureen, V. Roy, and S. B. Bayne, "An overall study of a real-time simulator and application of RT-LAB using MATLAB simpowersystems," in *2017 IEEE Green Energy and Smart Systems Conference (IGESSC)*, 2017.
[204] A. Singh and K. Prabakar, "Controller-Hardware-in-the-Loop Testbed for Fast-Switching SiC-Based 50-kW PV Inverter," in *IECON 2018 - 44th Annual Conference of the IEEE Industrial Electronics Society*, 2018, pp. 1109–1115.